2015

SYSTEMATIC STUDY OF THE BIOLOGICAL EFFECTS OF NITRIC OXIDE (NO) USING INNOVATIVE NO MEASUREMENT AND DELIVERY SYSTEMS

Weilue He
Michigan Technological University, weilueh@mtu.edu

SYSTEMATIC STUDY OF THE BIOLOGICAL EFFECTS OF NITRIC OXIDE (NO) USING INNOVATIVE NO MEASUREMENT AND DELIVERY SYSTEMS

By

Weilue He

A DISSERTATION

Submitted in partial fulfillment of the requirements for the degree of

DOCTOR OF PHILOSOPHY

In Biomedical Engineering

MICHIGAN TECHNOLOGICAL UNIVERSITY

2015

This dissertation has been approved in partial fulfillment of the requirements for the Degree of DOCTOR OF PHILOSOPHY in Biomedical Engineering.

Department of Biomedical Engineering

Dissertation Advisor:	*Dr. Megan C. Frost*
Committee Member:	*Dr. Jeremy Goldman*
Committee Member:	*Dr. Bruce P. Lee*
Committee Member:	*Dr. Xiaoqing Tang*
Department Chair:	*Dr. Sean J. Kirkpatrick*

Dedication

I dedicate my dissertation to my family and friends in China. A special thanks to my parents, Yinghan Liu and Chaoying He, who gave up so many things but always encourage me to fly higher and farther.

I also dedicate this dissertation to my advisor and teachers who spent their precious time and efforts in mentoring me and let me try many different fields.

I finally dedicate this work to all my friends in Houghton MI. It is you that make me feel like I am in a big family full of love and care, so that I can research like a champion every day.

Contents

List of Figures

List of Tables

Preface

All the research described herein was conducted under the supervision of Dr. Megan C. Frost in the Department of Biomedical Engineering, Michigan Technological University, between Sep. 2011 and Aug. 2015.

This dissertation is the result of my work and includes nothing which is the outcome of work done in collaboration, except for SEM imaging, which was carried out by Hao Meng and Connor McCarthy, and one LED-array light source was mainly designed with Andrew DeRouin and manufactured by him.

This work is to the best of my knowledge original, except Fig. 2.6 (authored by Schmidt et al.) and Fig 2.9 (authored by Romanowicz et al.) are directly from two previous publications and used with permissions (see Appendix C), which are used to more clearly state and support my point of view.

The material included in this dissertation has not been submitted for a degree or diploma or any other qualification at any other university. Part of Chapter 3 has already been submitted to *Nitric Oxide* for publication. The work described in Chapter 4 is going to be prepared to an individual paper for publication in the near future, which is under preparation now. Part of Chapter 2, Chapter 5 and part of Chapter 6 will be written to another individual paper for possible publication, which is also

under preparation currently.

Weilue He

Oct. 2015

Acknowledgments

I would like to thank all those who gave me their love, understanding and trust and all those who stop by and leave quickly but give me something to learn for my rest of life.

I would like to especially thank my advisor Dr. Megan C. Frost, who is definitely more than an excellent advisor in my heart but also good friend, mentor and research partner. Without her help, belief and support, I don't think I can even finish my first year in Michigan Tech. I learned many great things and little things from her. Her attitude to work, person, and life always encourages me to be a better me.

I also want to thank my previous advisor Dr. Wan Jin Jahng, who opened up a totally different and interesting world for me. His diligence, sense of objectivity and enthusiasm to science make him a noble example for me.

Besides, I would like to thank my dissertation committees: Dr. Jeremy Goldman, Dr. Bruce P. Lee and Dr. Xiaoqing Tang, for their valuable advice and unreserved support.

I thank those wonderful teachers, who show me respectful attitude and sincere teaching, Dr. Michael R. Gretz, Dr. Eunice Carlson, Dr. Robert Keen, Dr. Lynn R.

Mazzoleni, Jerry L. Lutz and Andrew Galerneau.

I thank all my current and previous labmates Sean Hopkins, Connor McCarthy, Genny Romanowicz, Dr. Matthew Nielsen, Julie Osborne, Elizabeth Ohnstad, Dr. Srinivasa Sripithi, Beth Elledge and my graduate fellows in MTU Jun Tao, Dr. Kefeng Li, Ben Wang, Dr. Tianle Cheng, Dr. Jie Zhou, Dr. Jingtuo Zhang, Mu Yang, Zichen Qian, Hao Meng, Yuan Liu, Andrew DeRouin, Patric Bowen, Yu Wang, Dr. Ramana Pidatala and Dr. Ee Lim Tan for their kind help and sincere suggestions.

Dept of Biomed at MTU is a rocking family. I really want to thank Dr. R (Rupak Rajachar), Dr. JJ (Jingfeng Jiang), Dr. Feng Zhao, and Dr. Keat Ghee Ong for their kind help and wonderful ideas, especially Dr. Sean Kirkpatrick and Dr. Martyn Smith for throwing interesting questions to me in the presentations. I sincerely thank Mrs. Judy Schaefer, Mrs. Stacey Sedar, Mrs. Cory Dompier and Mr. Michael LaBeau for giving me various support.

I sincerely thank all my collaborators, Dr. Qi Xing, Dr. Haiying Liu, Dr. Giri Vegesna, Emily Shearier, Caleb Vogt and Margaret Brunette for your hard work, which promoted me to be as motivated and productive as you are.

My family and friends give me great support and love, especially my parents and my two aunts Ying Zhang and Haiyan He, and my best friends Chi Xu, Li Song and Ji Liu. Wherever I am, I know I'm loved and supported.

I would like to especially thank my previous landlord Mick Chambers and his wife Anne Chambers for giving me so much love and care.

My sincere thanks also goes to My friends in Wonton-group, Jun Ma, Jianyang Li, Liang Qu, Boyi Hao, Huahua Shi, Ye Zhang, Chong Fu, Chao An, Fan Yang, Pei Hou, Yao Li, Tongfeng Wang, Yan Yang, Dr. Xin Zhao, Dr. Yong Meng Shua, Dr. Hui Wang, Dr. Fengde Ma, Dr. Peng Zhou, Yifei Li, Birong Tao, Xiao Sun, Hang Zhang and all my other friends who gave me various supports in my life and working during this wonderful PhD journey.

Last but not the least, I would like to thank Mrs. Feifei Qiang, my middle school English teacher who encouraged me to pursue my PhD degree in US, and Dr. Ke Liu in School of Life Sciences, Sichuan University, for giving me the first chance of doing independent research. Those wonderful memories will alway in somewhere in my heart.

Abstract

Nitric oxide (NO) is recognized as the most important small signaling molecule in the human body. An imbalance of NO is closely associated with many serious diseases such as neurological disorders, cardiovascular diseases, chronic inflammations and cancers. Herein two chemiluminescence-based devices (a real-time NO measurement device and a controllable NO delivery device) were developed to facilitate the NO quantitative study and obtain information for NO related drug design.

The first device used for real-time measuring NO(g) flux from living cells was developed and validated. The principle was to use a two-chamber design, with a cell culture chamber and a gaseous sampling chamber separated by a selective PDMS-based (polydimethylsiloxane-based) membrane. The membrane was polydopamine coated to improve the cell adhesion and growth. The signal response of the devices was validated by using the controlled NO releasing polymer SNAP-PDMS (S-Nitroso-N-acetyl-D-penicillamine covalently linked to PDMS). The real-time NO generation profiles of the macrophage cell-line RAW264.7 stimulated by lipopolysaccharide (LPS) and/or interferon-γ (IFN-γ) were successfully measured. Data also shows that the change of NO generation by different exogenous factors can also be tracked in real-time by the device. The maximum NO flux characterized by the device varies from approximately 2.5 to 9 pmol/10^6cell/s under 100 ng/ml LPS and 10 ng/ml IFN-γ

stimulation depending on different culture conditions, indicating the current NO reporting method by using one single NO flux value is not sufficient to represent the dynamic character of NO in biological samples. By using the similar principle and device characterization processes, an innovative cross-membrane delivery system was developed to successfully deliver NO to the cultured cells in a dose and temporally controlled manner. Different levels and durations of NO were delivered to the smooth muscle cell line MOVAS cultured in the device to validate the controllability of the NO delivery. The device characterized an NO flux of 1.0×10^{-10}mol/cm^2/min as a threshold level, above which NO may cause MOVAS death, and the effect of this lethal level was also duration and cell-type dependent. To further show the utilization of the two devices, the NO measurement device was used to systematically study different NO donors' potencies. It is suggested that measuring the real-time NO profiles of specific NO donors in specific biological conditions can help us avoid generating confusing data and understand the potencies of NO releasing drugs.

Current methods for NO quantitative experiment lack the means to understanding the time-related aspects of NO in biological environment and controlling the actual NO level and duration that cells experience. The two innovative devices solved these problems in cell culture models, achieving quantitatively studying the behavior of NO in the biological conditions and potentially assisting the design of the NO releasing drugs/materials.

Chapter 1

Introduction

Nitric oxide (NO) was first prepared and characterized by Joseph Priestley in 1772 by the chemical reaction of metals and diluted nitric acid [1]. NO is a highly reactive free radical, with an odd number of valence electrons, allowing it to readily undergo autoxidation to form NO_2 in the atmosphere.

Before NO was clearly identified in a variety of mammalian physiological processes in 1980's, NO was only considered to be an significant air pollutant or bacterial metabolite. In 1818, Prout W. reported a significantly different level of nitrogen in urine samples between healthy people and diabetic patients [2]. Unfortunately at that time no indication of NO's involvement was noted and no progress was made in the NO field until 100 years later. Mitchell et al. [3] discussed nitrite/nitrates origin in detail

in their 1916 paper, pointing out that nitrate in human urine might be not only from food, indicating the existence of potential nitrite/nitrate synthesis pathways in the human body. To prove this hypothesis, two papers were published by Tannenbaum's group in 1981 to explore this speculated pathway [4, 5]. They controlled human volunteers' daily nitrate intake and found that nitrate in urine greatly exceeded the intake. Data from $^{15}NO_3^-$ tracking showed the majority of nitrate in urine was from endogenous biosynthesis. They further used germ-free/conventional rats to run the similar nitrate balance experiment, strongly supporting the existence of a certain nitrate source in our body [5]. In 1985 Stuehr and Marletta then further identified the LPS (lipopolysacharide) activated macrophage as the nitrate biosynthesis unit, which was responsible for the elevated nitrate in urine, by using LPS-treated mice model [6]. By studying blood and vascular relaxation and contraction, Furchgott et al. reported the relationship between smooth muscle cell (SMC) mediated vascular relaxation and the acetylcholine (ACh) concentration-dependent relaxation reported in the 1950s [7, 8], and further pointed out this effect is dependent on the endothelial cell resided at the surface of intima. This demonstrated the long sought after endothelium-derived relaxing factor (EDRF) was not ACh itself, but more likely to be certain downstream factors derived from endothelium cells [9]. In 1987, Hibbs et al. elaborated the L-arginine-dependent pathway with L-citrulline and nitrite generated in cytotoxin activated macrophage mediated tumor cell metabolic inhibition [10]. Also in 1987, Palmar et al. and Ignarro et al. characterized it is NO from L-arginine that plays the

role as the EDFR [11, 12]. Since then one of the most important and classic molecular pathway, NO-cGMP mediated vasodilation was fully unveiled. In 1998, the discovery of NO's regulating cardiovascular conditions earned the 3 scientists who elucidated this the Nobel Prize, which greatly inspired NO work and caused an explosion in research related to NO and the related health problems, especially chronic diseases [13, 14, 15]. It is interesting that the two opposite effects of this signal molecule, one to maintain vascular system health, the other to kill cells, were discovered at almost the same time! From this history, it is important to always remember that NO is a double-edged sword, as both beneficial agent and the cause of pathological conditions.

Another interesting question might be raised here, that is, why it took us over 200 years to realize this extremely simple molecule turned out to be so essential that it constitutively functions throughout our body every day? There might be some historical reasons, for example, the lack of molecular and cellular biology in the 18th century, and NO is more related to chronic diseases and multiple-factor diseases, which are not the primary, or life threatening problems for people living over one hundred years ago, who may have had to fight against bacterial infection and scurvy at that time, which are the types of conditions modern medicine has essentially solved. Other reasons also include the preconception of the cytotoxicity of NO and the limitation due to the detection challenges. The detection and quantification method can greatly facilitate the development of certain field and good measurement method helps us explain and integrate controversial results. This chapter will briefly introduce NO's

chemical and biological basis and how NO is quantified and controlled in actual experiments.

1.1 NO and biological functions

Free radical NO is a multiple-functional molecule prevalently existing in almost all the organs in the human body. Its main functions include vascular tone regulation [16], inactivation of platelet adhesion [17, 18], feedback regulation of synaptic processes [19], cell cycle manipulation [20, 21, 22], angiogenesis [23], and immune response [24]. The underlying basis of all those biological events is the biochemical characteristics of NO and the molecules that react with it. The unpaired electron on NO makes it very reactive. It potentially reacts with other free radicals[25], hemeproteins [26], species with thiol groups [27], oxygen[28, 29] and lipids [30]. However, the specific reaction(s) NO will undergo depend on the chemical kinetics, redox microenvironment, and availability of substrates and cofactors.

1.1.1 NO generation in the human body

Like all other signaling molecules in the human body, NO levels are precisely controlled. This control is multiphasic, including the rate of generation, NO consumption,

and localization. EDRF's vasodilation effect was discovered as L-arginine dependent associated with L-citrulline generation. This dependency was very specific, "not D-arginine or other close structural analogues", and can be inhibited by NG-methyl-L-arginine (L-NMMA) [31]. To date NO has been discovered to be synthesized both enzymatically and non-enzymatically. Enzymatic NO generation is the most important and classic NO generation pathway. Three isoforms of nitric oxide synthase (NOS) are responsible for this process (reviewed in [32]). Researchers initially had great difficulties in investigating NOS, since the enzyme lost its activity during purification. The first experiment was reported by Bret and Snyder in 1990 [33]. NOS with arginine to citrulline conversion activity was successfully purified from the cerebellum tissue. And at that time they also pointed out calmoduline as the important moiety for iNOS function, which explained why NOS function was observed as Ca^{2+} dependent. Yui et al. purified NOS from rat macrophage in 1991 for the first time, showing that it was different from constitutive NOS (cerebellar and endothelial NOS), the activity of the inducible NOS purified from macrophage was not calmoduline-dependent [34]. Later Pollock et al. published their work on eNOS purification from bovine aortic endothelial cells [35]. And they claimed that three NOSs share the same chemical reaction as shown in Fig 1.1. The terminal guanidino nitrogen of L-arginine undergoes a 5-electron oxidation to form L-citrulline and the free radical NO [36, 37]. Other reactants include O_2 molecule and NADPH. Co-factors including FAD (flavin adenine dinucleotide), (FMN) flavin mononucleotide, BH_4 (tetrahydrobiopterin), heme

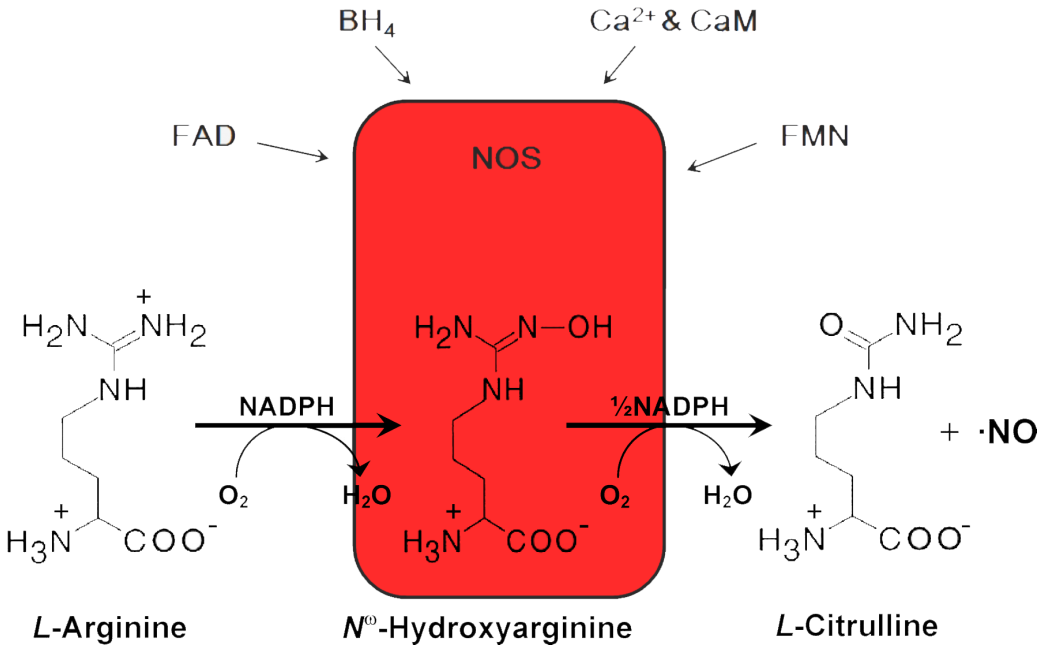

Figure 1.1: NO biological synthesis by NOS

and calmodulin, which helps with electron transference and ultimately activates NOS respectively [36]. The ultimate product is the same, however, we have to keep in mind that different isoforms have their own tissue distributions and produce different quantities of NO, and also NO synthesis by different NOSs can be controlled by different mechanisms in different levels [38]. Initially, NOSs were named according to their tissue distributions, such as brain NOS or hepatocyte-inducible NOS. Molecular clone revealed their sequences and guided the current classification. Immunoblotting and in situ probing greatly enriched our knowledge of the localization of NOS [39].

1.1.2 Biological functions of NO

According to NO's tissue distribution, NO maintains vascular homeostasis, regulates immune responses [24], and participates in nerve stimulation [19, 40, 41]. NO initiates the relaxation of SMCs by responding shear stress and pulsatile blood flow [11, 12], so that to auto-regulate both the overall and local blood flow distributions and regulate vascular and myocardial tones [18, 42]; changes vascular permeability [43]; deactivates platelet and immune cells (more likely a synergistic actions with prostacyclin) [17, 18], prevent cell adhesion to blood vessels and inhibition of thrombogenesis [44]. According to the regulatory regions of iNOS gene and iRNA, iNOS transcription and post-transcription processes are thought to be precisely regulated (reviewed in [38]). One of the most important components in the promoter region is the LPS/IFN $-\gamma$–responsive element, which is directly related to mononuclear leukocytes' foreign infection defense properties, including macrophages and neutrophils [45]; the hypoxia-responsive element lies in -226 to -212 conferring iNOS low-oxygen environment inducibility [46], which is consistent with the observation that iNOS was expressed in infarction tissues and focal ischemia during surgery [47, 48]; different iNOS mRNAs can be generated through alternative splicing in different tissues showing different translational activities; meanwhile the discovery of iNOS mRNA with different a 3' end from RAW264.7 provided important proof for the idea that iNOS

mRNA with different stability produced by alternating splicing might be an important regulatory strategy to control the NO generation profile [49]; additionally, NO participates in immune surveillance over cancer cells [50] and other chronical inflammatory diseases [51], either by inducing immune cell transformation or modulating immune-cell activity and cytokine levels [51]. NO's function as a neurotransmitter is more indirect compared with the traditional neurotransmitter. NO, indirectly generates nerve signals, by modifying those electric signals or changing the intensity it originally elicits, so called LTP and LTD (long-term potentiation and long-term depression) in neuroscience [52], such as altering systemic blood pressure [53], respiration tone [54], and pain thresholds [55], reviewed in [40]. This change of synaptic plasticity might be through NO's diffusion from the postsynaptic cell to the presynaptic cell after NMDA receptor-mediated excitation [41].

The complexity of NO's role is that NO's physiological function is essential but at the same time it was observed to be cytotoxic in many instances. Although NO can sensitize many types of cancer cells to help with cancer treatment [56, 57], NOS within tumor tissue inhibits or even kills T-cells to allow the tumor to escape from the host immune reactions [58], and initiates angiogenesis to assist tumor growth [59]. NO from macrophage can cause tissue damage, apoptosis and necrosis, in immunopathological conditions through nitrosative stress during inflammation [60]. Similar to oxidative stress, nitrosative stress has comprehensive effects on cells, where NO^+ (nitrosonium equivalent) is relatively nonspecifically added to thiols, secondary amines

and hydroxyl groups, modifying structures and functions of lipid [30], protein [61, 62], and DNA molecules [63, 64]. Since NO's effect is broad, able to target both "good" and "bad" molecules, its ultimate consequence becomes hard to predict. For example although high flux of NO indicates its cytotoxicity as a general trend [65], in some tissues with oxidative stress, NO was claimed as a potential anti-oxidative agent [66]. Also iNOS was post-mortem detected in neurodegeneration patients, suggesting that a potential cause-and-effect relationship existing between NO and those diseases [24, 67]. At the same time NO can potentially protect neurons by counterbalancing oxidative stress, and limit calcium level, presumably by restricting the activity of NMDA channel via nitrosation, as a feedback control mechanism [68, 69] (reviewed in [65]).

Dysfunction of NOS is closely related to cardiovascular pathology, immune malfunction, and neurological diseases, including hypertension, reperfusion injury, atherosclerosis, thrombosis, hypercholesterolemia, diabetes mellitus, myocardial depression, various chronic inflammations, and various neuronal degeneration disease such as Alzheimer's disease, amyotrophic lateral sclerosis, Huntington's disease and Parkinson's disease [70, 71, 72].

1.1.3 Quantitative study of NO

Why can this simple chemical can function as such a powerful factor that regulates so many biological processes? Since all the metabolic activities rely on the corresponding biochemical reactions, factors that determine the kinetics and dynamics of NO's chemical reactions determine NO's ultimate biological effects. Physiological status is relatively stable, which means factors such as temperature (normally 37 °C), pressure (normal pressure), and physical state (such as ionic strength in aqueous condition) will minimally affect the biochemistry, while the nature of the reactants (which species NO will react with), concentration (both NO and its targets) and time (when and how long these conditions persist to allow the reactions to proceed) need to be carefully evaluated. One general hypothesis to explain the pleiotropy of NO could be that NO's concentration, timing and duration of its production and the specific cellular environment (or tissue-specificity, where different reactants and reaction conditions such as pH and redox environment may present) determine the ultimate biological effect of the NO. To ensure the correct physiological functions of NO, our body has developed corresponding mechanisms to precisely balance those factors. When our body fails to do so, NO chemistry can be disrupted and diseases can occur. The ultimate goal of this work is to artificially manipulate NO levels (or other factors) within the physiological environment to help the body recover from the pathological NO conditions. To do so, several questions need to be answered:

1. What are the correct physiological NO levels?

2. What are the NO generation patterns in specific cell & tissue?

3. Where, when and how much NO is needed?

4. What kind and how much NO releasing drug is need to achieve specific goals?

Although they appear straight-forward, answers to these questions are not known. A body of experimental data has shown that NO concentrations vary by several orders of magnitude while it serves these different roles (reviewed in [65, 73, 74], generally speaking, lower NO doses ($<$ 400 nanomolar) indicates a certain normal or protective property, while higher doses ($>$400 nanomolar) suggests a potential cytotoxic outcome [65]). However, the quantitative data especially with respect to the time variable information is still missing. Without systematic study, it is hard to draw a general threshold level, above which is dangerous and below which is absolutely safe. For example, it is reported that very low NO level (approximately 1nM) in endothelial cells is able to induce endothelium proliferation, which is very important for vasculogenesis and tissue repair [75]. However if this occurs in cancer tissue, it will bring about serious problems such as angiogenesis which provides more nutrients to cancer cells, and promote the development of vessels with structural defects which leads to the leakage of blood. As a result, it is hard to predict the necessary NO level without systematically studying the NO chemistry present on a case by case basis. The development of NO measurement methods and NO-delivery materials has

contributed greatly to facilitating these studies.

1.2 NO measurement in biological samples

Measuring NO in biological samples is important simply because NO participates in so many diverse biological processes. Without accurately knowing whether NO is present or how much NO is there, it is hard to evaluate NO's contribution to those processes. NO measurement in the biological samples is not easy. The most common problems associated with measuring NO in biological experiment include low physiological NO level, high reactivity and diffusivity of NO, aqueous environment, and biological perturbation caused by the measurement method itself.

1.2.1 Current problems associated with NO measurement

Physiological NO level must be low, because even the micromolar range of NO can be cytotoxic. It is reported that NO's physiological concentration is normally in nanomolar range or even subnanomolar range [65]. Sometimes under nitrosative stress conditions, cells produce high NO fluxes where micromolar NO environment can be formed, causing tissue damages. So the measuring method needs to have both a low limit of detection and a large dynamic range.

NO is a free radicals, which potentially reacts with numerous species including other free radicals, thiol groups, heme, some metal ions, and oxygen, which widely abound in the physiological environment. That means once NO is generated, it can be consumed very rapidly (the half-life of NO is on the order of seconds [76, 77]). So even if a method measures NO concentration accurately, from such result it is still likely to underestimate the total amount of NO generated, because some of the NO is rapidly consumed. This might be acceptable in some cases since NO concentration strongly suggests the likelihood of the occurrence of the specific events, and it is important to determine the relationships between NO concentration and the specific molecular pathways. However, it might be not detailed enough information for pharmaceutical use, because if the total amount of NO that is needed is unknown, insufficient administration of NO could change the molecular pathway and the ultimate metabolic activity of NO.

NO is gaseous under standard temperature and pressure. Under these conditions, reliable and sensitive methods for NO detection have been developed and used for a long time, such as chemiluminascence. Unfortunately NO generated from biological sources always goes into the surrounding aqueous environment that baths cells and tissues, making the conventional gas phase chemiluminescence detection impractical for measuring NO in biological systems.

Different from experiments run under the ideal in vitro case, assays applicable to the

complicated condition is always difficult. For example, NO concentrations in living cells within the aqueous solutions can be well quantified in a sample holder such as a cuvette by using different methods such as an NO probe, colorimeter methods, or chemiluminescence, because we can use deoxygenated buffer, homogenize the sample solution, and pour the sample in and out freely etc.. However, in real biological cases, the NO source is relatively small, and the NO concentration gradient distribution can be very complicated depending on the NO source and the environment. NO also diffuses very rapidly. Successfully measuring NO at one time point becomes relatively meaningless, because there is no way to understand the dynamic NO production. So it is important to achieve real-time NO monitoring for each specific biological condition under examination to truly understand the role of NO in dynamic physiological systems. This requires that the method itself be non-invasive so after NO measurement the same biological sample can be examined by other assays. Any physical probe or chemical reagent potentially brings about contamination and changes to the biological system under investigation, making real-time NO measurement a challenging task.

1.2.2 NO measurement technology

Currently several different assays are used to quantify NO levels in biological samples in different labs. Several recent reviews developed very comprehensive summaries to

those methods [73, 74]. Unfortunately, real-time, commercially available, widely used tools are still limited. Here Table 1.1 shows some commercially available and most commonly used strategies in research to detect NO. Some points must be emphasized here:

1. not all the methods actually quantify NO levels; methods such as Western blot and mRNA real-time PCR only directly indicate the present of NOS enzyme;
2. it is important to distinguish the difference between direct/indirect NO measurement and real-time/instant/cumulative data.

So none of these methods are successful technique for real-time NO measurement for living organelles. The associated problems will be discussed in the following chapters. Some groups successfully estimated the NO levels in living cells, dissected tissues and conscious animals by different NO spin-trapping techniques and EPR (electron spin resonance) spectrometry [89, 90]. However, problems still exist such as complicated calibration and processing steps, bringing about new variables and changes to organelles, resulting in uncertain effects. If we can easily compare NO generated from endothelium cells in health people with hypertension patients with different genetic background, measure NO levels in different tumor tissues during their different development stages, accurately understand the behavior of NO in neuron degeneration cases etc., we could be able to determine and confirm the etiological factors and guide therapeutic strategy decisions. A reliable, accurate method to

Table 1.1
Current commercially available NO measurement methods

Class	Technique	D. M.	RT. M.	Comments	Ref.
NOS assays	Western blot	No	No		
	Real-time RNA	No	No		
Absorbance	Griess assay	No	No	LOD 500 nM whether real-time or not and LOD depend on specific instruments	[78, 79, 80]
	Oxyhemoglobin assay	Yes	No	LOD < 2 nM	[81]
Electron spin resonance	Traps	Yes	Yes	LOD 6 pmol	[82]
Fluorescence	DAF-based fluorophore	No	No	LOD 5 nM Whether real-time or not and LOD depend on specific instruments	[83]
Electrochemistry	Clark-type Pt-Ag/AgCl probe	Yes	Yes	LOD 1 nM	[84, 85]
	Carbon-fiber electrode	Yes	Yes	LOD 10 nM	[84, 86]
Chemiluminescence	$O_3 - NO$ reaction	Yes	Yes	By using NOA LOD 0.5 ppb	[87]
	Luminol-NO	Yes	Yes	LOD 100 fM	[88]

D.M. indicates whether the assay is direct measurement or not; RT. M. indicates whether real-time measurement can be applied; DAF, Diaminofluorescein; Pt-Ag/AgCl, platinum-silver/silver chloride as electrode; LOD, limit of detection.

directly measure NO from cells under physiological conditions is urgently needed to allow a deep understanding of the role NO plays in many health conditions with straightforward principles and experiment procedures.

1.3 NO releasing chemicals

To study NO's effect on different biological conditions, the most straight forward method is to keep other variables unchanged and observe the performance of the organelles under different NO treatment. Currently it is relatively easy to observe NO's biological effect in cases where NO production is eliminated. Several mature strategies such as gene knock-out and knock-down techniques, series of NOS inhibitors (including L-arginine analogs and antagonist such as L-NG-nitroarginine methyl ester (L-NAME), L-NG-monomethyl arginine (L-NMMA), L-N5-(1-iminoethyl)ornithine (L-NIO), Calbiochem) with different specificity and K_i values can been applied to prevent the generation of NO in the living organelles [91]. However, problems on how to deliver known amounts of NO to the biological systems still remain. Since NO is a reactive and dynamic gas under physiological condition, instead of directly bubbling NO into biological systems, chemicals that contain NO generating moiety are used widely for NO delivery.

1.3.1 Small-molecule NO donor

Small drug molecules that releases NO have a long history of use. The most famous example might be glycerin-trinitrate (trinitroglycerin, GTN), which has been used

to relieve the symptoms from angina pectoris and other heart problems for over 150 years. Though at that time the underlying pharmaceutical mechanism was not clear, its potency and ease of preparation procedure still make it the most popular NO drug used to date.

The chemical structure of GTN is shown in Scheme 1.1 (1). It is the most widely used

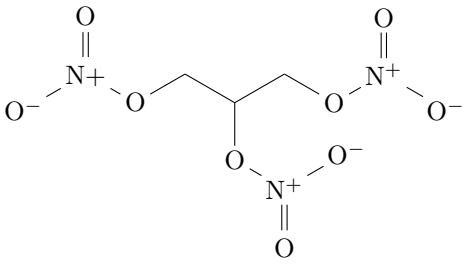

(1)

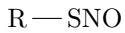

(2)

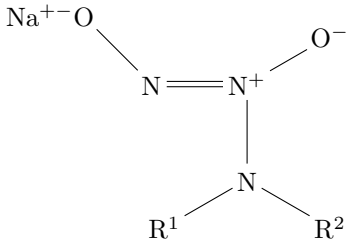

(3)

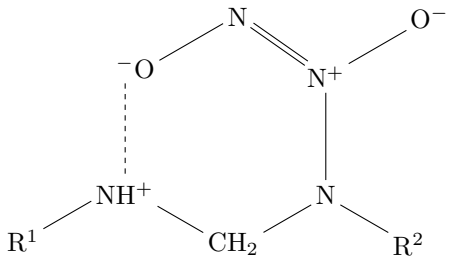

(4)

Scheme 1.1: Chemical Structure of NO releasing molecules.

and best-studied organic nitrate drug, whose NO releasing can be initiated through multiple complicated mechanisms (probably both enzymatically and nonenzymatically), which even today have not been thoroughly described. But after administrating GTN, NO generation in a variety of tissues was positively observed. Three

nitro-oxy ester groups are present in one molecule, but only one group will release NO, generating 1,2-glyceryldinitrate and NO via an S-nitrosothiol or nitrite intermediate pathway [92]. It is believed that GTN needs to be bio-activated in vivo by certain agents before it actually functions. Identification of those bio-activators has been a challenging work for some time. In Miller & Megson's paper [93], they reviewed the work regarding to the most suitable bio-activator identified to date, mitochondrial aldehyde dehydrogenase (mtADH) [94]. Though contradictions and some other problems still exist, on the broad level, we know that the potency of organic nitrate as an NO releasing drug depends on multiple intracellular and extracellular pathways. Dysfunctions of those molecular/cellular pathway brings about nitrate tolerance, which is one of the most common and series problems associated with organic nitrate drugs. Though by supplying ascorbate, low-molecular-weight thiols, folate and L-arginine, nitrate tolerance can be reversed to some degrees, other limitations, including lack of selectivity, adverse hemodynamic effect, and inducing oxidative stress in vasculature still exist.

New generations of NO releasing donors have been developed including other organic nitrates, iron nitrosyls, inorganic nitrate, s-nitrosothiol drugs, diazeniumdiolates (NONOates) reviewed in [93]. S-nitrosothiols and diazeniumdiolates are the most popular NO generators in current NO studies (Scheme 1.1 (2)–(4)). Both classes have relative clear NO generation mechanisms and stoichiometry. S-nitrosothiols, innately present in the human body as physiological NO stabilizers, reservoirs and

transporters, is an attractive class of NO donor to be developed for NO delivery [93, 95]. The NO moiety connects with the adducts through an S-N bond, which can be broken by a variety of controllable factors such as temperature, visible light, presents of transition metal irons and other biological molecules such as ascorbic acid and other thiols [95]. The main reaction schemes are summarized in Scheme 1.2.

$$RS-NO \xrightarrow[\text{or irradiation}]{\text{heat}} RS^{\bullet} + {}^{\bullet}NO$$

$$2RS-NO \xrightarrow[\text{or irradiation}]{\text{heat}} RSSR + 2NO$$

$$2Cu^{2+} + 2RS^{-} \longrightarrow 2Cu^{+} + RSSR$$

$$Cu^{+} + RS-NO \longrightarrow Cu^{2+} + RS^{-} + NO$$

Scheme 1.2: S-nitrosothiol NO generation mechanisms.

Another aspect of S-nitrosothiols' pharmaceutical effects that needs to be pointed out is that in addition to directly generating NO, S-nitrosothiols participate in other reactions such as nucleophilic substitution and transnitrosation, whose effects should be distinguished from NO's effect. Also while S-nitrosothiols undergo heterolytic cleavage, NO^{+} and NO^{-} will be generated. As a result, S-nitrosothiols has been widely used as NO generator and even as NO probe calibration reagents, but its pharmacological application is limited compared with organic nitrates.

NONOates are a relatively new class of NO drugs compared with other NO donors.

NONOates are normally highly soluble in aqueous solution, spontaneously undergo decomposition reactions in the aqueous environment (physiological condition) to release NO, generating a nucleophile and 2 mol equivalent of NO per mol of donor. The reaction rate is pH dependent, suggesting the nucleophilic reaction property. This property makes NONOates easy to store in alkaline stock solution. And for applications, the stock solution is mixed with excessive physiological buffer to form desired concentrations and at the same time the basic storage buffer will be neutralized.

By introducing NO generating groups (normally nitrate esters and S-nitroso groups) to conventional drugs, these drugs can possess NO releasing property, improving the potencies and reducing drug's side effect. NO-releasing aspirin and NO releasing diclofenac have been shown to have both anti-inflammatory and anti-thrombotic properties [96].

1.3.2 NO releasing polymers

To this point, there are no ideally functionalized NO releasing drugs. Serious problems such as NO payload, control over the rate of release, targeting properties, and potential cytotoxicity still exist with all the current NO donors. To overcome these problems or offset some of their negative effects, the most common strategy employed is to bind the NO donors to special scaffold molecules, either physically or chemically,

to obtain control over specific properties such as NO generation rate, targeting abilities, ease of administration and biocompatibility. Scaffolds employed can be diverse, such as relatively large molecules or even polymers, allowing scaffold properties to be tuned for specific NO delivery applications.

The concept of non-covalently blending of small NO donors within polymers is straightforward. Blending small NO donor with a polymer base has been used to increase the bio-compatibility of materials [97]. For example NONOates diethylamine (DEA/N2O2) and diazeniumdiolated-spermine (SPER/N2O2) were blended with hydrophilic biodegradable polymer base polyethylene glycol (PEG) and polycaprolactone [98, 99]; S-nitrosothiol GSNO and S-nitroso-N-acetylcystein SNAC were blended with PEG or PEG/PPG (poly propylene glycol) copolymer to introduce controllability over NO release rate and administration site [100, 101]. Applying the NO releasing material produced from blending the NO donor SPER/N2O2 with a biodegradable polymer has been shown to reduce neointimal hyperplasia [99, 102]. Also instead of applying discrete NO donors, even gaseous NO can be encapsulated and applied as a whole macromolecular vesicle to increase the available NO payload and reduce spontaneous loss of NO. The major drawback of this strategy is the uncontrollable leaching of the NO drugs, resulting in a very high local NO concentration or a generation of high level of by-products such as nitrosamines, a well known carcinogen class [103]. To limit this leaching process, several strategies can be applied such as increasing hydrophobicity of the NO donors (introducing alkyl groups) which reduces

leaching when incorporated into relative lipophilic polymers base and developing bio-safe NO donors, which themselves do not form carcinogenic by-products and can be easily metabolized [103, 104].

To completely solve the leaching problem, NO donors were covalently link to the polymer backbones. Because of their chemical structures and the controllability of NO releasing mechanisms, NONOates and S-nitrosothiols became the most popular choices for such work.

Polymers with secondary amine are potentially available for preparing stable N-diazeniumdiolates once a second basic residue (either exogenous cation or unreacted amine species within the polymers) is present and available. Meanwhile polymers with thiol groups are potentially good candidates for introducing S-nitroso groups. For example polyethyleneimine PEI microsphere and fumed silica particles with alkylamine were reacted to form N-diazenimdiolates respectively by Pulfur and Zhang, obtaining NO generating vehicles that can be further embedded with other matrix [105, 106].

Also by targeting cysteine, an important mammalian amino acid abounding in our body, NO releasing materials through incorporation of S-nitrocysteine sites were synthesized. Backbone materials include PEG hydrogels, BSA [107] and silica particles [108]. Both primary/secondary RSNOs and tertiary RSNOs have been formed on these different backbone materials that produce NO with different rates [108].

By embedding the NO releasing particles in different polymer bases (PU and SR), Frost et al. observed that the NO triggering mechanisms can differ greatly (reviewed in [102]), which suggested that NO release could be significantly controlled by choosing proper scaffold properties and manipulating the triggering factors. By chemical design of the scaffold molecules, NO payload can be greatly enhanced. Stasko et al. [109] designed polypropylenimine dendrimer based N-diazeniumdiolates, showing a prolonged NO releasing pattern (up to 16 h releasing) and high NO storage capacity (up to 5.6 μmol NO/mg). NO generation properties reduced platelet adhesion onto those materials, and significantly improved the biocompatibility of this material [109]. By surface treating of function implantable biomedical devices with NO generation coating, for example pH, oxygen, carbon dioxide and glucose sensors, devices can function longer in the body because of NO's anti-thrombosis properties [102, 110]. Meanwhile NO release has been shown not interfering with devices' original functions.

1.4 Statement of purpose

A quantitative understanding of NO and its role in biological systems is crucial to understanding the functions NO plays in normal physiology and pathology. Real-time NO measurement and the control of the level of NO delivered are essential in this field. The development of tools and methodologies to accurately measure and deliver NO will allow the therapeutic potential of NO to be achieve.

Work presented here is focusing on straightforward and universal means to understanding and achieving better control over factors that related to NO research, i.e. developing and validating real-time NO measurement device and controllable NO delivery device for cell culture work. Chapter 2 describes the principle of how the measurement and delivery devices function and the mathematical basis. This real-time NO measurement device is the first method ever report to achieve direct measurement of NO gas generated from living cells without influencing normal cellular activities or introducing new variables into the original biological system.

To validate and show the usefulness of the new devices, a series of biological experiments were designed including, measuring NO generation profiles of macrophages after LPS and IFN $-\gamma$ stimulation that are presented in Chapter 3 and the real-time measurement of NO profiles generated by different NO donors at different biological conditions is presented in Chapter 4.

By using similar principles, an innovative NO delivery system that achieves dose, temporal and spatial control of NO delivery for culturing cells is presented in Chapter 5. SMCs line MOVAS cells was used as the biological model. The effective diffusion distance of NO and its decay with the diffusion in different buffer were measured and visualized by experiments using the real-time NO measurement device. Conclusions and preliminary work on quantitatively investigating NO kinetics in different biological reactions and the potential use of the two devices for cancer research are

introduced in Chapter 6.

Chapter 2

Theoretical Description of the Devices[1]

2.1 Principles of the NO measurement device

2.1.1 Challenges of NO measurement in biological systems

Biological samples are normally fragile, making almost all the measurement operations difficult. There is a great need and desire to quantitatively measure cellular derived proteins and signaling molecules in order to better understand many physiological

[1]Part of the content in this chapter will be submitted to a journal for possible publication in the near future.

processes. In general, the method itself needs to properly sample objects of interest and correctly evaluate the homogeneity of the biological systems. The quantification method also should not damage the system of interest. An even stricter requirement would be that the quantification method itself should not introduce changes to the sample of interest, and keep tracking the individual trend of each sample in real-time, which are very challenging.

2.1.2 Basic concept of the two-chamber system

The question that we are facing now is how to measure NO generated from the living cells. Collecting NO (which will also be in other forms such as NO_2^-, S-NO, hemoglobin-NO) is a must. The desire is that the sample collection process itself will not affect the original cell growth, not introduce new variables to the cells or change cellular NO production. If the sampling process can be a continuous process, it is possible to develop corresponding measuring processes for real-time measuring. If we consider a cell layer is the source of NO, an NO gradient will be generated around the cells. The strategy applied here is to sample a part of NO passing through a certain surface area around the NO source, measure this NO, and determine the relationship between the amount of NO measured and the total amount generated. To realize this, NO production must be examined.

Cultured cells form a cell layer attached to the bottom of the culture dish and produce NO, which diffuses into the media within the dish and also decays because of the auto-oxidation of NO (Fig. 2.1 A). If the dish were removed, NO produced from the cell layer would diffuse to both direction (as shown in Fig. 2.1 B).

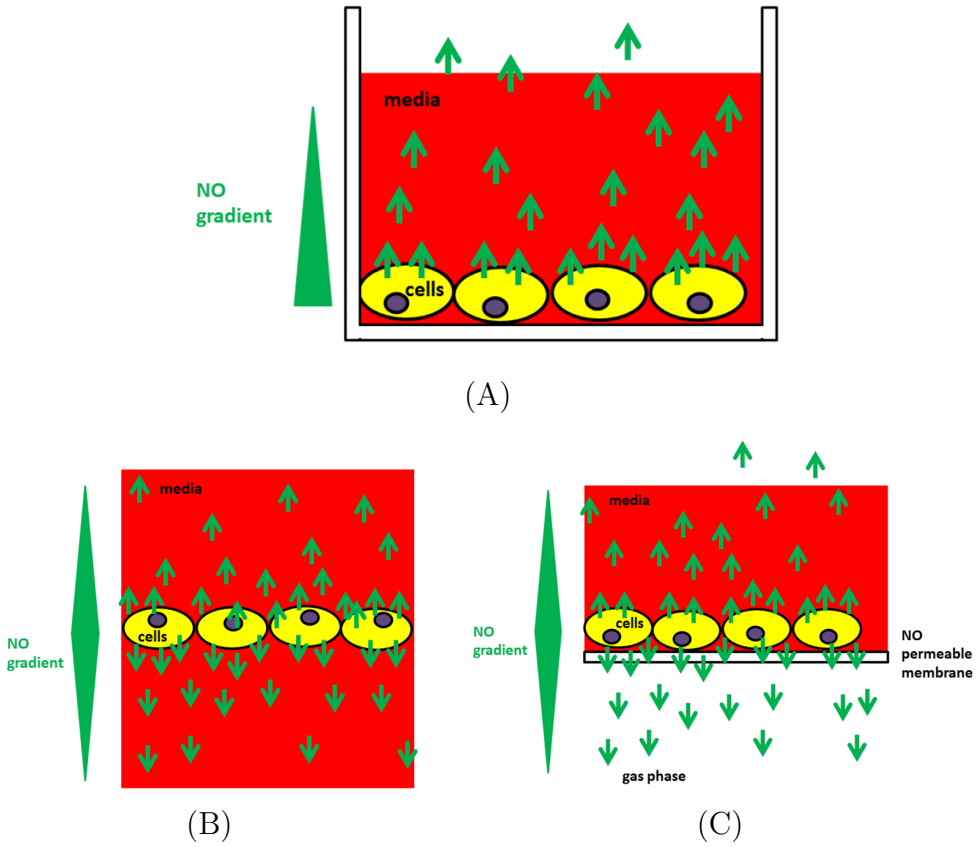

Figure 2.1: NO generated from cells in different cell culture models can potentially form different NO concentration gradients. (A) adhesive cells in the cultured vessel; (B)an imaginary cell culture environment without cell substrate; (C)cells cultured on the NO permeable membrane.

By placing an NO permeable but media impermeable membrane at one side of the cell layer (as shown in Fig. 2.1 C), two relatively separated compartments will be

created (a liquid part with culturing cells and a gas phase). Once NO diffuses across the membrane and enters the gas phase chamber, NO can be collected and swept to the chemiluminescent nitric oxide analyzer (NOA) for quantification. NO generation, diffusion and sweep gas sampling are all continuous processes, based on which real-time NO measurement can be achieved. And if the correct relationship between the sampled NO signal and the total NO signal can be determined, the total amount of NO production can be calculated.

This concept is not new in other biological field and has been widely applied to investigating cell signaling. Boyden co-culture chamber is one good example that has very similar design concept. Boyden chamber was initially used for investigating "the relative chemotactic effect of soluble substances" [111]. In brief, the cell culture chambers are separated by a semipermeable membrane which has a defined pore size allowing for free chemical diffusion of soluble signaling molecules, but not allowing cells to pass through unless the cells actively migrate. Cells, normally leukocytes, are seeded in the upper chamber and the chemical of interest is dissolved in the low chamber. Because of the chemotactic signaling, cells will migrate through the membrane and into the lower chamber. And the chemotactic effects of different soluble substances can be quantitatively compared and analyzed by examining the cell migration (cell number in the lower chamber). Currently Boyden chambers are also used in studying cell-cell interaction. In this case, instead of applying soluble chemicals in the lower chamber, another cell type is seeded in the lower chamber.

Different cell types do not directly contact each other, but they can interact with each other through soluble factors that they produce. When cell Type 1 receives a chemical signal generated from Type 2, cell Type 1 undergoes a series of biochemical activities (Fig. 2.2 A). This allows interaction between different cell types to be investigated by setting up proper controls.

In the NO measurement device, cell Type 2 was replaced by NO measurement methods (specifically, a chemiluminescent analyzer here). Once NO is produced by cell Type 1 and passes through the semipermeable membrane, it will be continuously detected, which can be used to calculate the real-time cellular NO generation profile if the relation between this measured value and the total NO can be found (Fig. 2.2 B).

Over all, cells cultured in media and attached to certain substrate in the measurement device for growth and proliferate (except for some suspending culture cell), and NO production in real-time can be quantitatively measured. The following assumptions are made:

1. NO will be generated by this cell layer, entering the aqueous environment as soon as it diffuse out from cells. And it is reasonable to assume this NO generation is homogeneous if all the cells are cultured and treated under the same conditions.

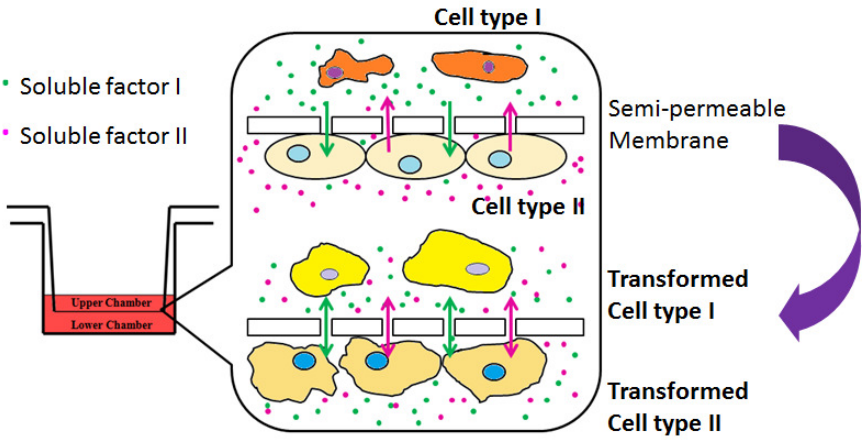

(A)

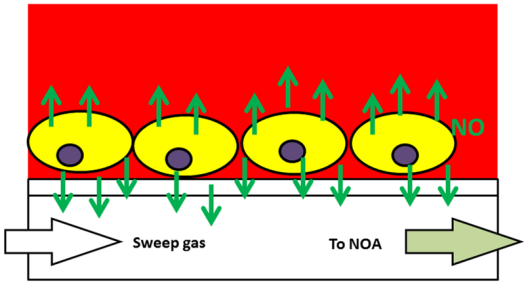

(B)

Figure 2.2: Cross-membrane measurement method inspired from Boyden Chamber (A) design of Boyden chamber, applied to study cell-cell interaction by free diffusion of the soluble molecules secreted by cell; (B)adapted from Boyden chamber, NO can be filtered out for chemiluminescent assay by NOA

2. After generation, NO diffuses homogeneously in only two directions in the one dimension model (Fig. 2.1 B). So part of the NO generated remained in media solution in the form of its oxidation product, while the other part will diffuse into the lower chamber.

3. The NO that diffuse into the lower chamber can be quantified in real-time by NOA sampling.

4. During NO diffusion, it undergoes chemical reaction because of the presence of O_2 under physiological conditions, meaning there is NO signal loss during the traveling of NO.

So in theory, as for NO quantification, as long as we can determine the correct way to guide NO out from the cultured cell layer and measure its flux from the gaseous side and determine the mathematical expression of NO distribution (the relation of NO in upper chamber and lower chamber), then the measured value can be used to calculate the total NO generated.

2.1.3 Cellular NO measurement device design

Because real-time NO measurement should be feasible, detailed operation procedures will be discussed focusing on:

1. What material is appropriate to be used to separate the upper culturing chamber from the lower gas-phase measurement chamber?

2. How to quantitate NO diffusion in real-time?

3. How to use the detected NO signal to determine the total NO emission?

The design constraints for the filtering material used to separate the chambers is first considered. To selectively allow specific molecules to pass through a certain surface is not easy, especially when there is phase discrepancy (extract gas molecule from the aqueous environment). Materials that are hydrophobic and gas permeable are of interest, since the hydrophobicity can sustain the aqueous solutions to ensure correct cell culture conditions and gas permeability allows NO passing through the polymer layer. According to Mowery et al. [112], NO has the highest transfer rate (diffusion coefficient D, as high as 3.0×10^{-5} cm^2/s) within silicone rubber compared with other polymers (polyurethane, polyvinyl chloride, and plasticized cellulose triacetate). Other properties also make this candidate attractive including high hydrophobicity, which prevents media from leaking, good biocompatibility, which allows for normal cell culture, and readiness for manufacturing. Many medical grade silicone rubbers for lab use are commercially available (such as SYLGARD®and RTV-3140 silicone rubber, Dow Corning).

Since we are directly targeting NO gas, this problem becomes relatively easy. Chemiluminescence is a well characterized and robust method to quantitate gaseous NO production. Gaseous NO is continuously swept into a reaction chamber, where ozone will react with NO generating light signal that can be detected by photomultiplier tube (PMT). The detection limit is generally 0.5 ppb, which corresponds to around 0.5×10^{-13} mol/sec (or 30×10^{-13} mol/min). According the existing simulation estimation and EPR data, NO generation from endothelium

is 1×10^{-10} mol/cm^2/min [113] and $8.3 \pm 2.1 \times 10^{-12}$ mol/cm^2/min [82] respectively, which means the chemiluminescent system is sufficient to allow the NO flux to be directly determined (Detailed calculation and experiment will be discussed in Chapter 3 3.4.2.).

The third aspect of developing this device that must be considered is the fact that other molecules present in the biological environment affect NO chemistry. NO will be consumed during the diffusion process via reaction with O_2, and to use the measured value of NO detected in the lower chamber of the device to calculate the total, it is necessary to account for these relations. To mathematically express this behavior, Lancaster et al. [77] established a model describing the NO gradient generated from a point NO source in biological system expressed by using Fick's law and NO's oxidation chemical rate term. Laurent et al. [114] used similar hypotheses to simulate NO concentration gradient made from a plane source (homogeneous cell layer).

According to Fick's second law, which describes the molecule concentration gradient development against time due to the diffusion,

$$\frac{\partial [NO]_{x,t}}{\partial t} = -D \frac{\partial^2 [NO]_{x,t}}{\partial x^2} \tag{2.1}$$

where D is the diffusion coefficient; t represents diffusion time; x stands for distance from site of interest to the source; [NO] is the concentration of NO. In physiological

condition, the NO diffusion coefficient can be roughly approximated to NO diffusion in DMEM media 4.5×10^{-5} cm^2/s [115]. Other groups have used similar values such as 3.3×10^{-5} cm^2/s [116], and 3.0×10^{-5} cm^2/s [117], which are very close to the value of diffusion coefficient of O_2 in PBS at 25°C, which is 2.0×10^{-5} cm^2/s [118].

The distance NO travels is restricted by its chemical consumption. To simplify this problem, only auto-oxidization of NO, which is the main reaction of this process, is taken into consideration. It is an overall third-order chemical reaction.

$$\frac{d[NO]}{dt} = k_1[O_2][NO]^2 \tag{2.2}$$

where k_1 is the oxidation reaction rate constant, and $[O_2]$ presents the oxygen concentration. To simplify this equation, the treatment of Laurent et al.[114] was used. Since in the cell culture system, the culture device will be exposed to air in the incubator, O_2 concentration in culture media is relatively stable (0.22×10^{-3} M) [119]. So by using $k_1 = 6 \times 10^6$ M^{-2}/s [120], then the following pseudo-second order reaction expression was used to replace Eqn(2.2)

$$\frac{d[NO]}{dt} = k_0[NO]^2 \tag{2.3}$$

where k_0= 1.32×10^3 M^{-2}/s is the effective reaction constant.

Then assuming the source has a NO generation rate of v, the following equation was generated:

$$\frac{\partial [NO]_{x,t}}{\partial t} = v - D\frac{\partial^2 [NO]_{x,t}}{\partial x^2} - k_0 [NO]^2_{x,t} \tag{2.4}$$

which takes NO generation, diffusion and consumption into consideration to express NO level at any given site and given time.

To show the NO status in the cell culture model, NO concentration was calculated according to Eqn(2.4). The following assumptions were made:

(1) homogeneous thin cultured cell layer is the only NO source, where $x = 0$, with a constant NO generation rate $v = 1.7 \times 10^{-8}$M/s [77], while $t > 0$;

(2) while $x > 0$, it is an aqueous media environment; and while $x < 0$, there is no NO diffusion;

(3) NO diffusion is driven by concentration gradient and the time-dependent diffusion according to Fick's second law described as Eqn(2.1):

(4) NO diffusion is hindered by NO's chemical consumption, and here only auto-oxidization of NO was considered, which is the third-order chemical reaction overall shown as Eqn(2.2):

(5) The whole process is continuous without instantaneous change or other boundary effects.

Only considering at source x= 0, the term expressing NO's x diffusion is eliminated

and the equation becomes an ordinary differential equation as:

$$\frac{d[NO]_{x,t}}{dt} = v - k_1[O_2][NO]^2_{x,t} \tag{2.5}$$

Buy solving the equation, NO concentration at x= 0 is expressed as:

$$[NO]_t = \sqrt{\frac{v}{k_0}} \times \frac{e^{2\sqrt{vk_0}\times t} - 1}{e^{2\sqrt{vk_0}\times t} + 1} \tag{2.6}$$

indicating while t increases, NO concentration levels reach a steady-state, where

$$[NO]_{ss} = \sqrt{\frac{v}{k_0}} \tag{2.7}$$

and half-life of the reaction $\left(t_{\frac{1}{2}}\right)$ is:

$$t_{\frac{1}{2}} = ln\left(\frac{3}{2\sqrt{k_0 v}}\right) \tag{2.8}$$

According to this mathematical model, Laurent et al.'s work was reproduced by using FlexPDE 6 finite element builder for partial differential equation to calculate Eqn(2.4). Results were summarized in Fig. 2.3 B. Good agreement was observed with their results [114], suggesting that:

(1) the maximum NO concentration is immediately next to the monolayer;

(2) maximum value occurred in the steady-state, where NO concentration gradually reached a plateau and no longer changed with time;

(3) small changes of distance to the source plans can cause significant change of NO concentration;

(4) steady-state level of NO can be reached quickly when NO generation is constant (around 10 min).

This information is important in indicating how awkward the current methods of NO data report are. By using probes, such as electrochemical sensors, different positions (x value) from the cell layer as well as the time point when the probe is placed for measurement will greatly affect the final result. Reporting the average value of NO produced ignores the natural inhomogeneity of the NO concentration. An instant measurement overlooks NO's temporal change information, so the value can mislead researchers and the data is not very meaningful unless the accurate distance between the probe, the source, and time variables are precisely controlled. Moreover, it is noticed that even tens of micrometer of deviation can cause great changes in the NO concentration. Without robust spacial control, current probe operation methods can be very problematic.

When looking at the NO measurement from the proposed two-chamber device shown in Fig. 2.2 B and 2.4 A, rather than calculating NO concentration only, NO flux was also determined according to Eqn(2.4). Using similar assumption as Laurent et al. [114]:

(1) homogeneous culturing cell layer is the only NO source in my system, at $x =$

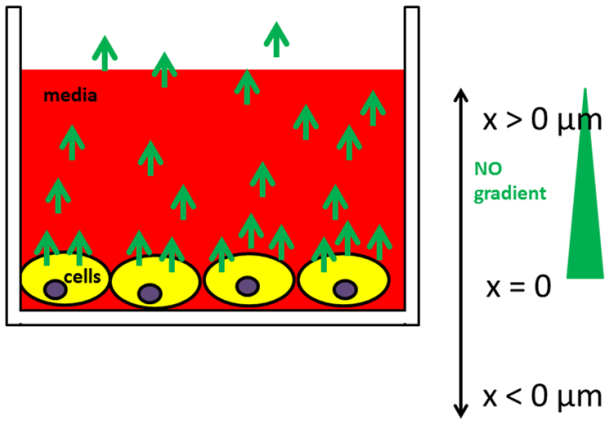

(A)

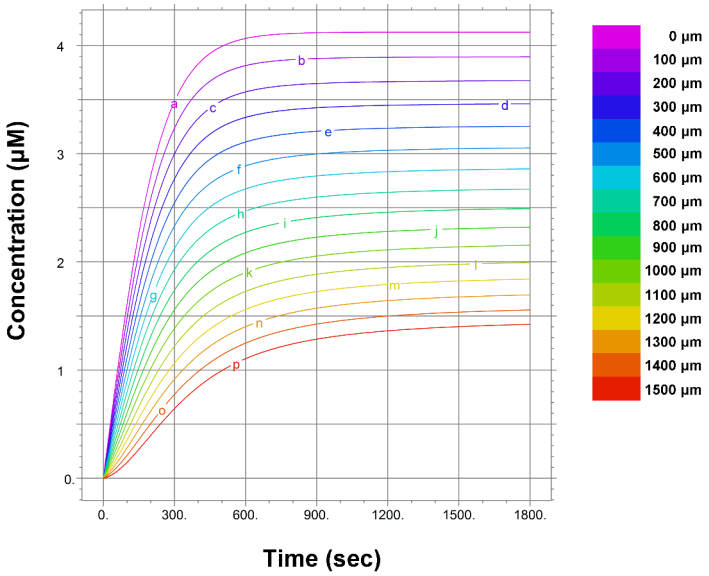

(B)

Figure 2.3: Repeating Laurent et al.'s work, modeling the formation of the NO concentration gradient generated by a single cell layer in the culture plate. (A) illustration of NO generation by cells cultured in the culture plate. (B) the simulation result, showing how NO concentration changes with distance x and time t.

0, with a constant NO flux rate out from the source plane of 5 pmol/cm^2/sec (a physiological NO flux level, which will be mentioned again in 3.6.2) while $t > 0$;

(2) while $x > 0$, it is an aqueous media environment, while $x < 0$, the diffusion media is PDMS; net NO diffuse only in x direction but not paralleled to the cell layer; so this question becomes a one dimension problem;

(3) NO diffusion is driven by concentration gradient expressed by Fick's second law as Eqn(2.2);

(4) NO diffusion is hindered by NO chemical consumption as Eqn(2.2);

(5) The whole process is continuous without instant change or other boundary effect.

Results were summarized in Fig. 2.4. These results suggest that:

(1) the maximal NO concentration and flux is right next to the mono cell layer; meaning that by measuring NO close to NO source is important, because NO loss is minimized and the measurement method will be more sensitive, which is beneficial for detection and calculation;

(2) maximum values of NO concentration and flux occurred in the steady-state as well; the value in the steady-state might be the most valuable information, because the detection method shows the highest sensitivity here and less fluctuation can provide high quality signal;

(3) small changes of distance to the source plane can cause significant changes in the NO concentration and flux; controlling how long the molecule travels (affecting the extent of NO consumption) before it is sampled or detected is important;

(4) steady-state (both concentration and flux will become relatively stable) can be

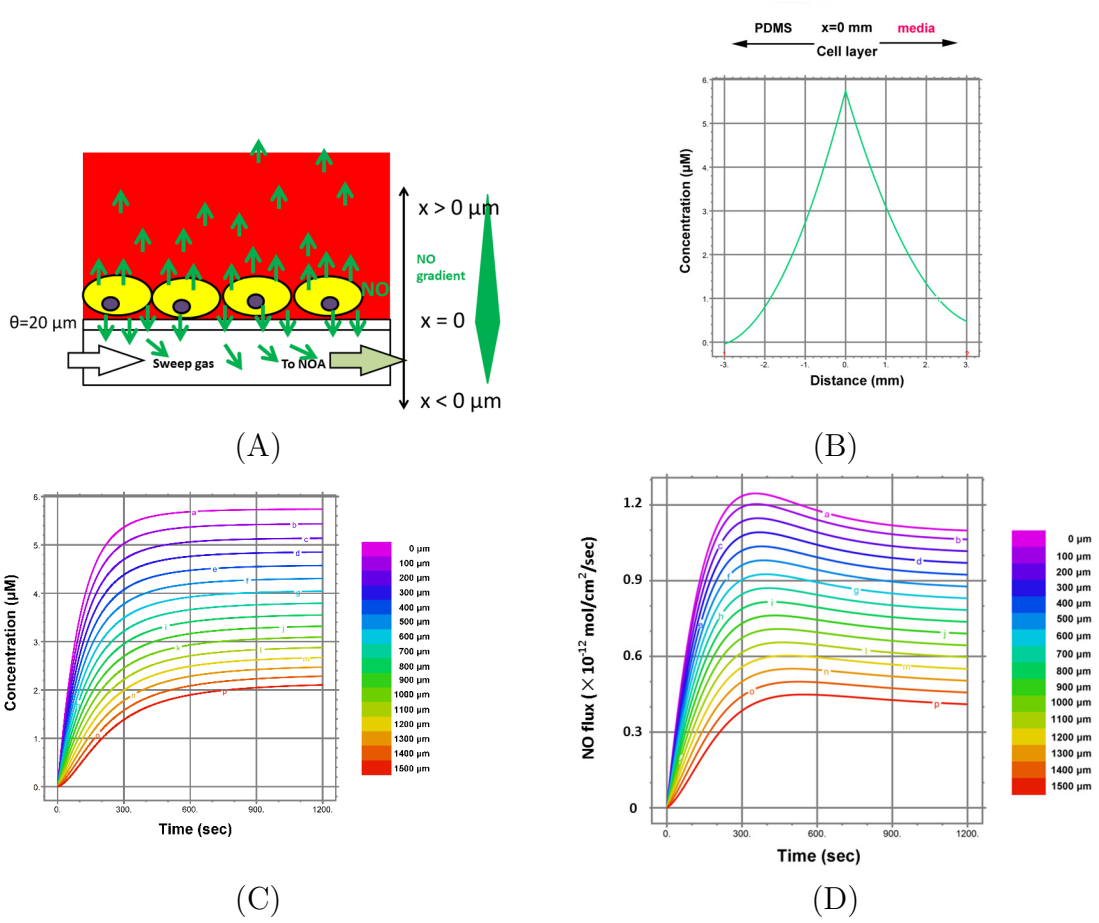

Figure 2.4: Modeling the formation of the NO concentration gradient generated by a single cell layer in the NO measurement device. (A) illustration of NO generation by cells cultured in the NO measurement device; (B) NO concentration gradient at the steady-state in the two phase (media and PDMS) model; the simulation results show that the measured NO concentration (C) and NO flux (D) change with distance x and time t.

reached quickly (around 10 min); this directly determines the correlation between the measured value and the actual value, and is changeable depending on the specific environment which will be discussed later in 2.2.

The proposed advantages of the new detection method include:

(1) by precisely controlling the property of PDMS layer which NO needs to migrate

through for NO sampling, the distance between the NO detection method and NO source can be controlled, greatly reducing the variation because of uncontrollably placing probes at different locations;

(2) the same as NO generation, diffusion and consumption, the whole measurement method is continuous, NO data will be reported as surface flux-time curve, tracking NO change with time;

(3) experimental operation is easy and will not influence normal cell behavior, which is totally biocompatible.

These results suggest by using chemiluminescent to cross-membrane measure NO flux generated from the cultured cells in real-time is feasible. However, it is noted that this measured value is not the total NO generated by cells. Since it is depending on the NO cross-membrane diffusion, the measured value only represents a part of NO generated by the cells. The next question is what this part of NO means to the total level of NO produced. The ultimate goal is to estimate the total NO generated from the cells, which requires the correlation of the measured value to the total. To solve this problem, simulations on how much NO will diffused out from the membrane were performed.

To do this, culture media-PDMS model was used again. By plugging into different total NO generation rates (physiologically relevant level), NO flux measured by cross-membrane measurement and NO concentration at source ($x = 0$) were calculated (by

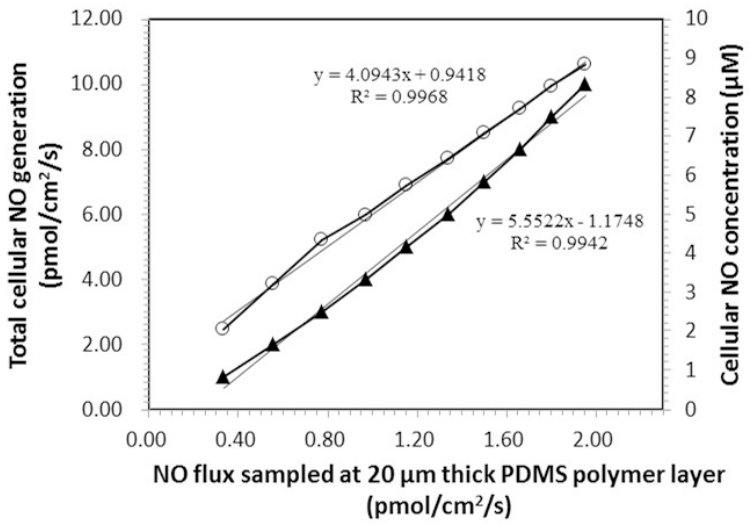

Figure 2.5: Simulation of the different NO generation rates from the single layer NO source ($x = 0$) result in different measured results (NO concentration at x= 0 μm is represented by circles; measured NO flux is represented by solid triangles) at x= 20 μm at steady-state.

finite element analysis software FlexPDE) to determine the relationship between the measured NO value and the total NO generation. Conditions used include:

(1) different NO generation rates (from 1 pmol/cm^2/sec to 10 pmol/cm^2/sec) were repeatedly set as the NO generation rate from the monolayer cell source (where $x = 0$);

(2) it is assumed that the PDMS NO permeable membrane has a thickness of 20μm; so the NO flux value calculated at x = 20 μm was used to represent the measured value by NOA;

(3) all data points were only collected at steady-state;

(4) the system is a continuous system so there is no boundary effect or interface effect.

The result was summarized in Fig. 2.5. Linear regression analysis clearly showed that at steady-state the NO flux (solid triangles) was directly proportional to the total NO generated, and NO concentration at $x = 0$ was also directly proportional to the total NO generation. The theoretical measured NO flux through a 20 μm PDMS membrane was shown to be only 18% of the total. This indicates that by testing NO flux through a specific thickness of PDMS polymer total NO generation can be calculated by simply multiplying a factor to the measured values.

However, in practice, this is difficult to achieve. This is related to some characters of the device membrane including:

(1) membrane was manually cast from PDMS organic solution, which may introduce variations between each different membrane;

(2) instead of using perfectly even, thin polymer layers as the cell substrate, the ultimate membrane in use has a sponge-like structure (see 3.4.1.), which differs a little from the calculation assumption above but ending up with a better experiment result;

(3) the assumption that NO only undergoes auto-oxidation in the culturing system and O_2 concentration is a constant during the whole culture processes may not be true;

(4) a real cell system is not a homogeneous single phase system but with other different phases (culture media, cell, polymer layer and gas phase sampling chamber) and interfaces, creating a noncontinuous system, potentially causing the ultimate experiment results differ from the calculation.

So to use the NO measured from the lower gaseous chamber to estimate the total NO flux, precisely calibration of each specific device/membrane is essential. The detailed operation processes will be introduced in Chapter 3 (Session 3.3 to 3.6).

2.2 Principle of the NO delivery device

To investigate the effect of certain chemicals on biological systems, the most important step is to achieve variable control and precisely adjust the parameter of interest and scientifically evaluate the data. For NO research, manipulating NO level that biological subject experiences is a critical step. However, because NO is a gas and so reactive, control of the NO level that cells experience in the experiment has long been a significant challenge. The most commonly used method of NO delivery is to use soluble NO donors. Depending on the specific chemistry of each donor, NO generation ability (duration time, rate, and stoichiometry) will be different. In general, NO donors release NO through different decomposition mechanisms.

$$\frac{d[NO]}{dt} = k_D[D]e_{NO} \tag{2.9}$$

where $[D]$ is the donor's concentration and e_{NO} represents the mole(s) of NO released per mole of donor. In case of soluble NO donors, k_D mainly determines the NO generation of the specific donor and concentration that is applied. After NO is released, it

goes into the surrounding environment and is consumed by reacting with the species in the solutions. Eqn(2.2) expresses its consumption. Only the main reaction, auto-oxidation, is considered at this point. Considering the high reactivity of NO, it will be consumed and generated at nearly the same time. So combining Eqn(2.9) and Eqn(2.3), to estimate NO status within an oxygenated solution, the model can be approximated as:

$$\frac{d[NO]}{dt} = k_D[D]e_{NO} - k_0[NO]^2 \tag{2.10}$$

Schmidt et al. [121] showed changes in the NO level when the using NO donor DEA/NO by plotting NO concentration according to simulation and experimentally measuring DEA/NO phosphate buffer solution as shown in Fig. 2.6.

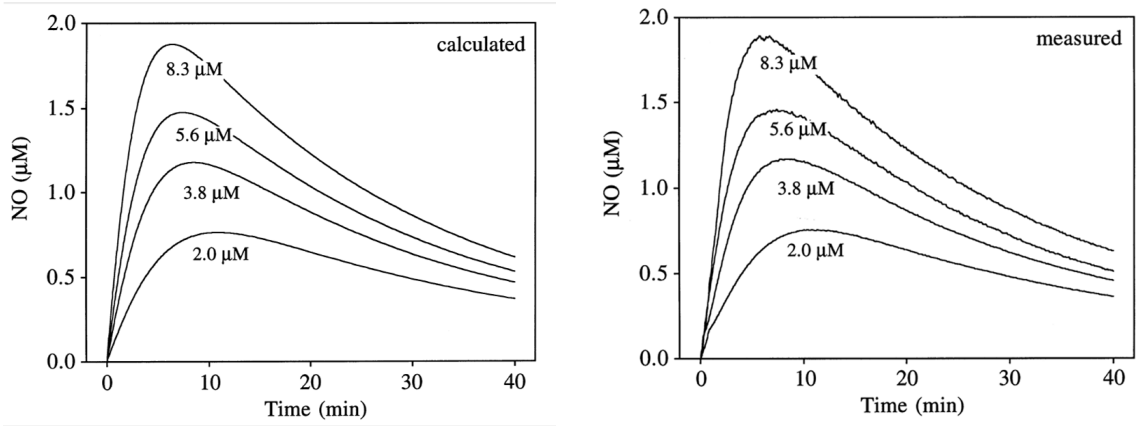

(A) (B)

Figure 2.6: NO concentration profiles of DEA/NO solution. (A) the calculated value by using $k_D = 1.4 \times 10^{-3} s^{-1}$, $e_{NO} = 1$, $k_0 = 1.932 \times 10^3 M^{-1} s^{-1}$, (B)the measured value by using different concentrations of DEA/NO indicated in the figure in 100 mM phosphate buffer (pH 7.4, 25°). Direct photocopy from [121]. The right of using the original images was kindly granted by Springer, see Appendix C.

Results showed that by using the NO donor, the NO level is variable and can be determined by the initial donor concentration and time. In phosphate buffer solution, this simulation prediction is accurate.

Applying this method to deliver NO to biological objectives, NO concentration varies with time. The NO donors' concentration alone does not directly reflect the real NO level within the solution, since the NO level is highly depending on the generation rate k_D, (which can be very complicated since some NO donors have multiple and uncontrollable NO generation mechanisms), as well as consumption routes (will prove this statement in 4.2 and 4.3). So that by using soluble NO donors, it is hard to maintain and track NO level during cell work in the actual biological conditions and it is almost impossible to precisely manipulating NO level and duration. This demonstrates the need to have a well controlled system that can provide cells more controllable NO environment.

Again the simulation illustrating NO concentration changes with time and distance to the source plane in a monolayer NO source model done by Laurent was inspiring (Fig. 2.3). Is it possible to use a plane to generated NO? If the cells can be directly cultured on this material, NO can be delivered to the cells directly (as shown in Fig. 2.7). More importantly, Compared with the traditional NO administration method, this method overcomes several shortcomings.

First, NO level in traditional soluble NO donor system changes sharply with time,

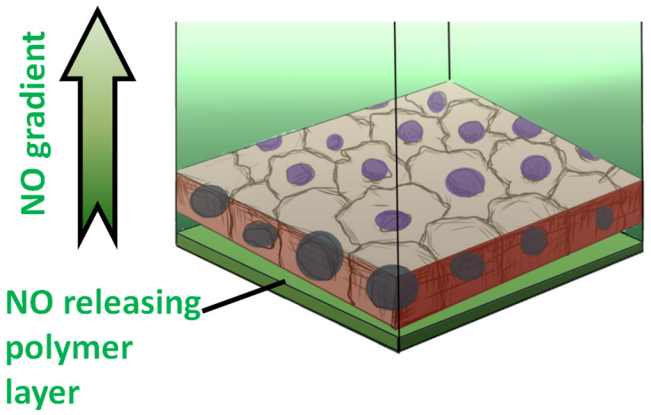

Figure 2.7: The confluent cell sheet is cultured directly on top of an NO generating material, which allows NO produced from the polymer layer to enter the cells directly, making this NO amount quantifiable.

while because of the steady-state, this new method can create a stable NO environment as long as the NO generating flux is constant.

Second, half-life of soluble NO donor in different buffer conditions widely varies so that estimations in the level of NO are difficult ([122] and will be shown in 4.3). However, in our system, cells directly adhere to the NO generation materials, if no other initiators can be accessed by NO releasing group, uncontrollable NO generation from the source can be limited and NO delivered to cells will be relatively stable, so that a desirable NO environment can be created for substantial longer time.

Third, the NO flux experienced by cells cultured in the vicinity of NO source layer can be directly adjusted by introducing control over NO generation rate from the source.

Fourth, by using some materials where the NO donor was chemically cross-linked to scaffold backbone, no other chemical components or side products are likely to be

introduced to cells as is the case when using soluble NO donors. This limits complicating the biological effects caused by other agents and mechanisms which may confound analysis.

This new delivery strategy appears to be an excellent approach to satisfy all the requirements needed for an ideal NO delivery system. One additional aspect of this device that needs to be investigated is the time resolution of the NO delivery. According to Fig. 2.3 B and 2.4, steady-state conditions are reached, and the NO concentration can change greatly within the first 5-10 min of the delivery, which brings about large variation into the biological system. So in the initial stages of the delivery process, is the NO accessible to cells controllable or not? It is noted that in our previous simulation, all the calculation is base on "auto-oxidation only" model, which might not be true in the real case. This led to investigation of a more complicated model. Besides the reaction with O_2, other NO consumption route may exist in the real biological system. The following equation expressing that NO is consumed by both oxygen and superoxide.

$$\frac{\partial [NO]_{x,t}}{\partial t} = v - D\frac{\partial^2 [NO]_{x,t}}{\partial x^2} - k_1[O_2][NO]^2_{x,t} - k_2[O_2^-][NO] \qquad (2.11)$$

where $k_2 = 5 \times 10^9 \mathrm{M}^{-1} \bullet \mathrm{s}^{-1}$ representing the reaction constant between NO and superoxide [123]. By using the average superoxide concentration (70 nM in different vascular cells, a general number is not found; this number is an average of [124, 125, 126]),

k_2 and $[O_2^-]$ are combined to k_3= 350s^{-1}, and NO concentration at steady-state while $x = 0$ became:

$$[NO]_{ss} = \frac{\sqrt{k_0^2 + 4k_3 v} - k_0}{2k_3} \tag{2.12}$$

and the reaction half-life is expressed as:

$$t_{\frac{1}{2}} = \frac{1}{\sqrt{k_0^2 + 4k_3 v}} ln \left(\frac{k_0 + 3\sqrt{k_0^2 + 4k_3 v}}{k_0 - \sqrt{k_0^2 + 4k_3 v}} \right) \tag{2.13}$$

To illustrate the effect of this extra term, simulations were performed by using the same assumptions and parameters previously described. The simulation result was shown in Fig. 2.8. Compared with result in Fig. 2.4, it is obvious to see that if more complicated NO consumption routes was considered, with the same total NO generation rate from source, maximum NO concentration in this system was much smaller, and the time needed to reach the steady-state NO levels became much shorter (within several seconds).

The NO concentration gradient turned out to be much sharper as well (decreased to less than half within 100 µm for both concentration and flux). This result indicated that compared with auto-oxidation model, the high chemical reactivity of NO can delivery stable flux of NO to cells without time delay once the NO flux is a constant. So it is concluded that adjusting the total NO generation from the NO source plane can achieve the change of NO flux/NO concentration that cells experience. New delivery methods also have good time resolution. The high reactivity of NO limits

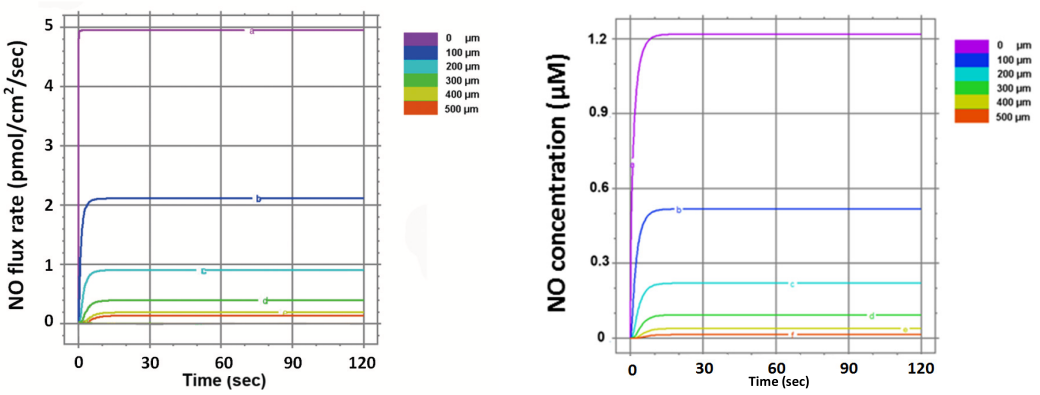

(A) (B)

Figure 2.8: Modeling of the formation of the NO gradient close to NO generating plane. According to Eqn(2.11), which is derived from Fick's second law and chemical reaction rate with the following parameters: $D_{DMEM} = 4.5 \times 10^5 cm^2/s$, $k_0 = 1.32 \times 10^3 M^{-1}/s$ and $k_2 = 5 \times 10^9 M^{-1}/s$ [77, 114, 115, 117]. (A) the calculated theoretical NO flux value at different distances away from NO source; (B) the NO concentration gradient formation against time and distance.

NO diffusion in static culture condition. Other cases such as irreversible reactions and dynamic body fluid may either elongate half-life of NO or facilitate its consumption, but those factors have a small influence to the static system developed here and will not be discussed in this dissertation.

2.2.1 Controlled NO releasing polymer SNAP-PDMS for development the devices

To develop the controllable NO delivery system, an NO plane source that generate NO homogeneously and controllably is needed. As mentioned before NO(g) is hard

to be bubbled directly into the culture cells. NO releasing material becomes a good candidate to deliver NO.

There are many NO releasing materials developed for fundamental research and biomedical applications. Several recent reviews summarized their chemical base and related practical use [102, 107]. One of the most popular application is for wound healing, since the proper NO level can promote endothelial cell proliferation and modulate inflammation processes. NO releasing tissue engineering scaffold, especially hydrogels have been proved to be good tools to study NO's effects on wound healing [107, 127, 128]. For example Amadeu et al. [128] used a NO releasing material Pluronic F-127 hydrogel, which was physically blended with 100μM GSNO, to treat rat cutaneous wound every day till wound healing was achieved, showing a better wound closure compared with hydrogel only treatment (S-nitrosoglutathione-containing hydrogel accelerates rat cutaneous wound repair). Another paper introduced the same material to the same animal model but at different wound healing phases, they concluded that NO is important and has beneficial effect to wound healing at both inflammatory and proliferative phases, indicating a minimum of 7-day long NO interference after injury can be applied to promote injury healing [129]. This is also a good example of temporal study of NO's effect. However, for more detailed quantitative study, NO levels need to be carefully controlled when using NO incorporated cell scaffold which will be discussed in detail in Chapter 5.

Both nitrite with acid and NO alone were shown to have broad anti-bacterial efficacy [130, 131, 132]. NO releasing materials have be used to fight against bacterial infection. One collaboration work of our lab with Dr. Zhao, Michigan Tech, Houghton MI, showed a SNAP chemically incorporated NO releasing gelatin nanofibrous matrix, with a highest NO flux of 20 pmol/g/s, inhibits the growth of *S. aureus* and in this process copper ion within the environment is preferred because it is contributing to a higher NO flux [133]. A more quantitative analysis was shown by Friedman et al. [134]. They took the advantages of the features of trehalose glassy matrices and hydrogels, developed an innovative nanoparticle that releases long-lasting therapeutic levels of NO in phosphate buffer by reducing nitrite to NO through reducing sugar within the glassy matrix. The NO releasing rate was tuned by preparing particles with different PEG size. Then this material was applied to a study looking for the minimum NO level that is needed to treat superficial skin infection [135]. The minimum working concentration for NO to inhibit methicillin-resistant SA (MRSA) strains and methicillin-sensitive SA (MRSS) strains infection were found to be different (ranging from 3.125 to 37.5 nM for MRSA and from 3.125 to 18.75 nM for MSSA).

Overall, for NO delivery, materials with long term and constant biologically relevant level of NO releasing and the controllability of the NO releasing rate are of interest. A large NO reservoir is also preferred to allow long term effects to be studied. Meyerhoff's group reported the first tunable NO-releasing microparticles (100-200 μm) [136]. The polymethacrylate-based polymer with different degree of secondary

amine groups was converted into N-diazeniumdiolates with different NO storage under sodium methoxide. So that the NO releasing from the polymer with different amine contents would be different (ranging from 0.64 μmol/mg to 1.99 μmol/mg). By incorporating different contents of such NO releasing particles with other polymer matrix and using different alkylamines for the base of diazeniumdiolate, NO flux provided by the final material can be further tuned [102, 104]. However, normally the limitation of NO releasing material is that once it is synthesized, the NO generation rate cannot be further tuned under physiological condition. Romanowicz et al. did some pioneering work developed a light triggered controllable NO releasing polymer SNAP-PDMS (Fig. 2.9), whose NO releasing rate can be further tuned by exposing the material to different light intensity [137].

The highly hydrophobic material PDMS was used as the backbone and NO donor SNAP was chemically linked to the cross-linked PDMS through the reaction between self-protected NAP and the PDMS cross-linker (3-aminopropyl)trimethoxysilane. The primary amine on 3-aminopropylmethoxisilane provides important reaction site. The detailed synthesis protocol was introduced in Romanowicz's paper [137]. In brief, 1.6 g of silanol-terminated PDMS dissolved in 4 ml of toluene was mixed with 2 ml of 0.15 g/ml (3-aminopropyl)trimethoxysilane toluene solution (the cross-linker). Then the mixture was vortex-mixed with 1.0 ml of dibutyltin dilaurate stock solution (25 mg of dibutyltin dilaurate in 20 ml of toluene). The PDMS mixture was continually

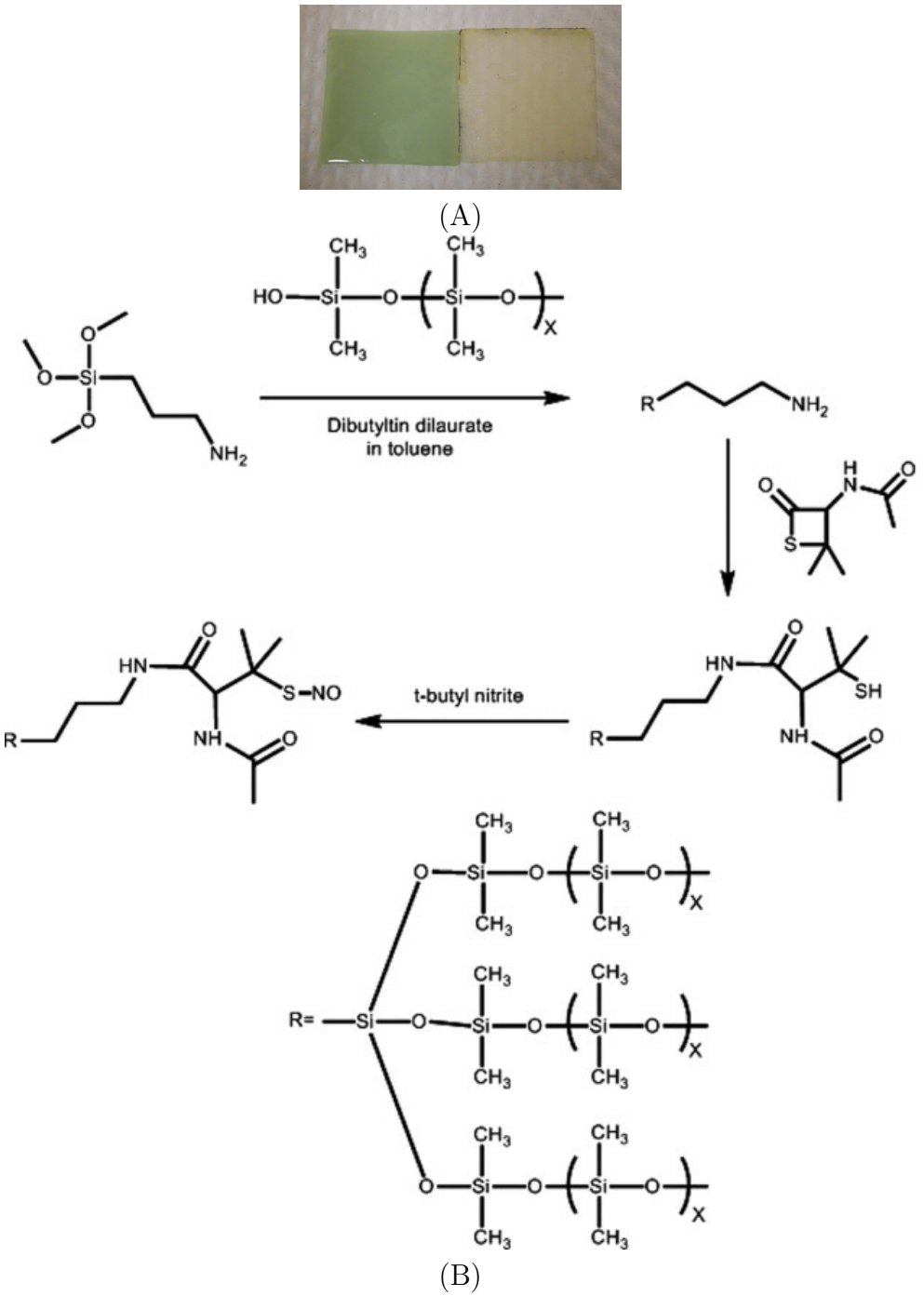

Figure 2.9: SNAP-PDMS polymer and its chemical structure. (A)green SNAP-PDMS and the control NAP-PDMS; (B) synthesis and chemical structure of SNAP-PDMS. Those are direct photocopied from [137]. The right of using these materials was kindly granted by Elsevier; see Appendix C.

stirred at room temperature for 24 h to allow for cross-linking. Thiolactone was synthesized according to the method developed by Moynihan and Robert [138]. Then 50 mg of self-protected thiolactone, 1 ml of toluene, and 2 ml of the cross-linked PDMS solution were mixed together and stirred for 24 h reaction. Thiol groups were then nitrosated with 1 ml t-butyl nitrite, which was cleaned by repeatedly extraction with 30 mM aqueous cyclam. The mixture was shaken for 40 min for reaction to form a dark green colored SNAP-covalently linked PDMS polymer. SNAP-PDMS solution and RTV-3140 solution were manually cast layer by layer to form RTV-3140 encapsulated 200-400 μm thick SNAP-PDMS film. Polymer was stored in dark at 4 °C until use. Fig. 2.9 shows the produced polymer (A) and SNAP-PDMS chemical structure (B). The maximum NO flux can reach around 5×10^{-10} mol/cm^2/min under $40 \times \mu$W/cm^{-2} light stimulation at room temperature.

Light emitting diodes (Mouser C503B-BAN-CY0C0461, peak wavelength 470 nm) were used as the modulator, where light energy impinged onto the polymer is proportional to the NO releasing flux from the polymer film (Fig. 2.10).

SNAP-PDMS can be cast to thin films and shaped to the needed dimensions or dip-coated to other materials or implants to release NO.

SNAP-PDMS has many advantages compared with conventional NO generation materials. PDMS has good biocompatible and has been widely used in biomedical field. Since SNAP is chemically linked to the backbone, this prevents the leaching of small

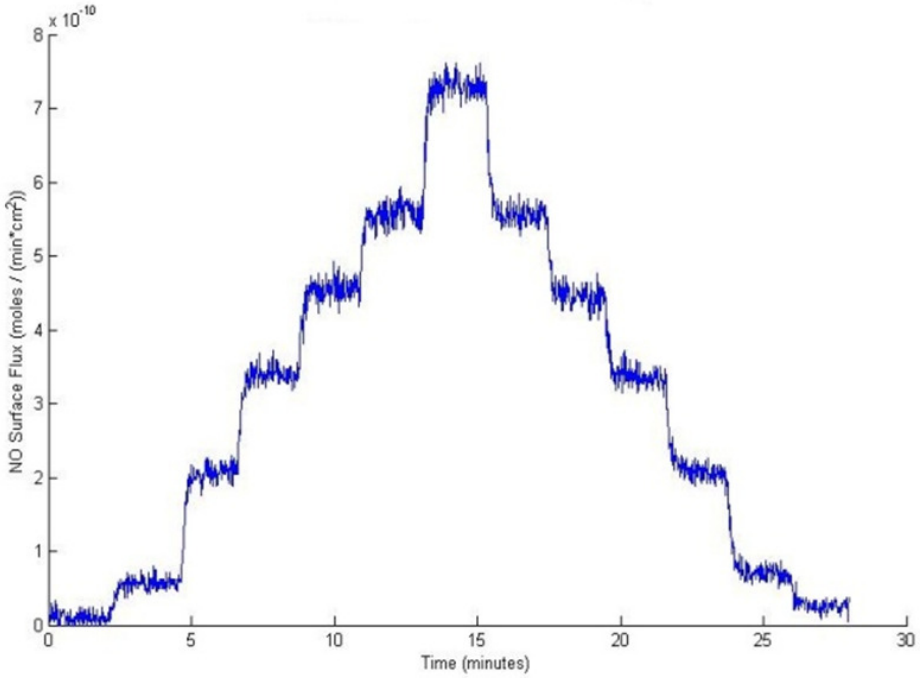

Figure 2.10: Measurement of NO surface flux from a 4.0 mm diameter, 100 μm thick film when drive current of the white LED (C503C-WAN-CBaDb152) was varied to change the light impinged on the film. Different steps correspond to different driven currents (in the order of 1 mA , 5 mA, 10 mA, 15 mA, 20 mA ad 30 mA).

SNAP molecule. High hydrophobicity of PDMS base protected SNAP, from contacting with other species that may initiate the cleavage of S-NO bond. It is noted that SNAP can readily generate NO once it is exposed to the decomposition triggers such as metal ions in aqueous solution, reducing agents, thiols, etc. [95]. While SNAP-PDMS is in the air, this potential passive NO release is essentially none. However, when the whole structure is immersed into a complex aqueous solution, ions within the solution is likely to attack the SNAP residues exposing to the surface of SNAP-PDMS polymer and initiate great uncontrollable NO release. To avoid this, another layer of PDMS was cast on top of SNAP-PDMS for encapsulation, which can block

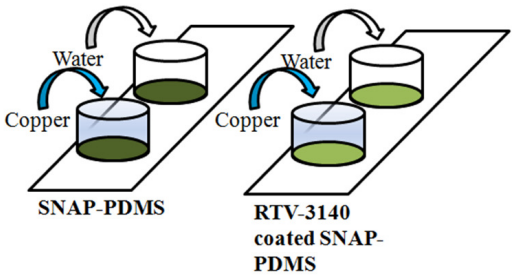

(A)

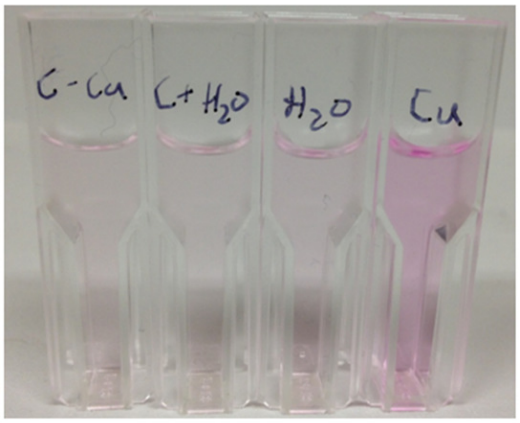

(B)

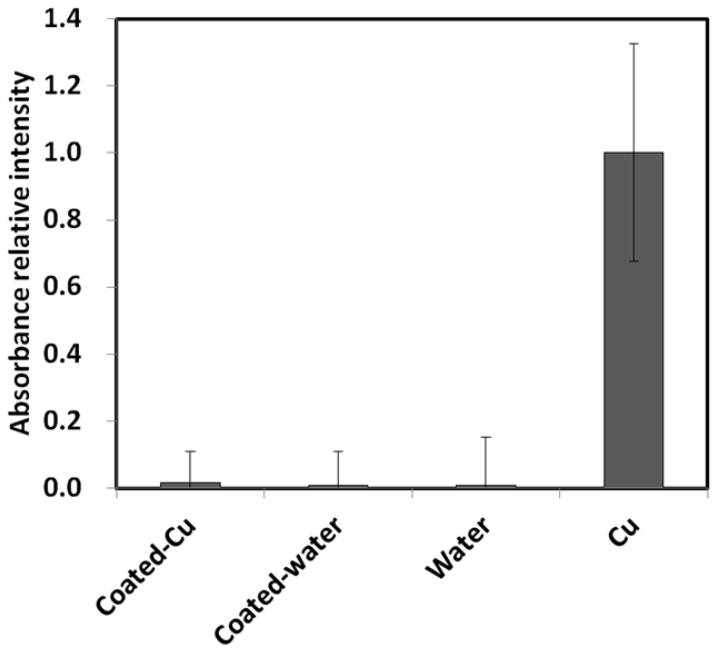

(C)

Figure 2.11: RTV-3140 coating prevents copper ion from attacking SNAP residues in SNAP-PDMS bulk proved by Griess assay. (A) Experiment design, water and 100μM $CuCl_2$ solution were used to immerse the polymers to trigger the NO release; (B) the result of Griess assay; (C) Relative absorbance of each sample.

the reactive ionic environment. In this case even in complex cell culture media environment NO release from SNAP-PDMS will be severely restricted (only thermal degradation will trigger NO release).

To prove that with the extra PDMS layer coating uncontrolled NO release can be eliminated, the Griess assay was applied (development of the dark pink color indicates that NO decomposition products are accumulating). $CuCl_2$ (100 μM) solution was used to treat SNAP-PDMS film and RTV-3140 coated SNAP-PDMS film at 20 °C as shown in Fig. 2.11 A. Deionized water was used as the control. After 90 sec solution was removed and applied to Griess assay.

As shown in Fig. 2.11 B and C, without RTV-3140, copper initiated significantly NO releasing, while the RTV-3140 coating eliminated this effect greatly to almost the same level compared to the controls. Result clearly showed that without other initiator, PDMS coated SNAP-PDMS will not deliver NO in a uncontrolled matter. Now that other species in biological conditions are not likely to change the release of NO, introducing light becomes a very efficient method to adjust the NO flux coming out from the polymer surface, making SNAP-PDMS an ideal choice for NO delivery.

2.2.2 PDMS surface modification

PDMS has high hydrophobicity, which makes it a poor substrate for growth of cells. To make surface more favorable to cell adhesion, growth and proliferation, the PDMS surface needs to be modified.

There have been many techniques used so far for material surface modification. Some of them need UV or high temperature or other harsh conditions (reviewed in [139]), which is not suitable for SNAP-PDMS. Since S-NO bond is very weak, such conditions may lead to the cleavage of the bond causing great NO loss before actual use. For example, temperatures higher than 50 °C may lead to a very fast NO releasing rate, resulting in huge NO loss from the polymer reservoir (data not shown). To achieve surface modification under mild condition, an intermediate polydopamine layer newly developed by Lee et al. was applied [140].

Dopamine, the essential component of mussel adhesion proteins, undergoes auto-polymerization on the targeting materials when oxygen is present in slightly basic environment. This self-assembling dopamine coating is compatible with a wide range of materials including inorganic metals, oxides and organic materials, even very hydrophobic materials like polytetrafluoroethylene (PTFE). The treatment procedure is very easy, just simply dipping the materials of interest into the dopamine solution.

The polymer does not chemically react with the materials, but forms a very thin (up to 50 nm thick after 24 h) and stable polydopamine layer strongly attaching onto the surface. The thickness of this polydopamine layer can be controlled by the immersion time. And this layer is very sticky and can be readily further modified. The polydopamine layer is very stable. Even in 1 N hydrochloric (HCl) acid [140] and 0.1 N sodium hydroxide (NaOH)[141], this sticky layer still remains. Envision, one side of this intermediate layer is attached to the PDMS surface, and the other side can be further stick to the other layer, conferring good biocompatibility if ECM (extracellular matrix) was applied. This is extremely helpful for cell culture. The modification strategy was illustrated in Fig. 2.12. Polydopamine layer has been proved to be non-toxic, which is very important for biological application too.

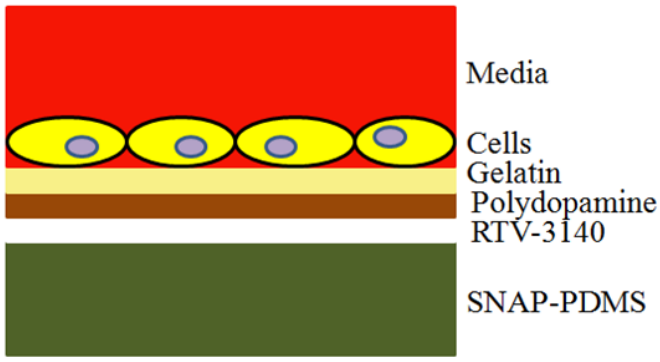

Figure 2.12: Illustration of cells cultured on polydopamine and gelatin treated PDMS/SNAP-PDMS.

To accomplish this, SNAP-PDMS was soaked in 2 mg/ml of 10 mM Tris buffer with a pH of 8.5 for 48 h (according to [140], around 50 nm thick of polydopamine layer will

be generated). After treatment sonication was used to remove the discrete polymer particle aggregates attached on the surface. Then the polymer was sterilized by 70% ethanol submersion for 20 min. Polydopamine layer was further soaked into 2 mg/ml gelatin solution for 1 h. Then cell adhesion assay was applied. Since the layer that directly interacts with polydopamine is RTV-3140, cover-slips cast with RTV-3140 were used in the assay first. The result is shown in Fig. 2.13 A-G. To quantify the cell number per unit surface area, calcein-AM (2 μM) was used to stain the cells. Cell counting was performed by Image-J software. The relative cell numbers are shown in Fig. 2.13 H. Without dopamine treatment, cells can hardly grow on PDMS (B), even with the gelatin treatment (C). However, after polydopamine treatment, cell adhesion was improved (D). And with both polydopamine and gelatin treatment, cell adhesion was significantly improved (E). Further controls were tested with this treatment to confirm its utility for improving over all +cell adhesion for culturing cells on NAP-PDMS as well (the material that has the same chemical structure with SNAP-PDMS except for nitrosating -SH, so no NO release capacity). Data showed that there was no statistic difference between the control and NAP-PDMS with polydopamine and gelatin treatment. Overall, smaller cell number and cell size was observed in all these groups compared with the control (glass cover-slip), it is suspected that the stiffness of the material may also influence the cell growth. To minimize this effect other adjustment was used in my research and will be discussed in 3.3.3.

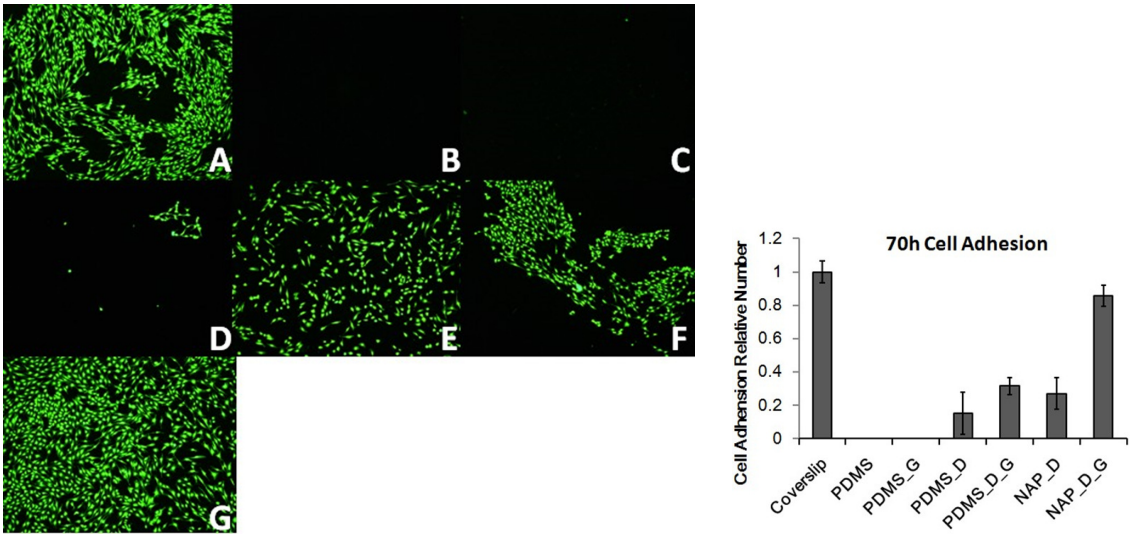

(H)

Figure 2.13: Cell adhesion to different surfaces. (A) to (G), MOVAS was seeded on different substrates and cultured for 24 h. Then cells were stained by 2 μM calcein-AM. Cells were cultured on (A) cover-slip coated with gelatin, (B) PDMS, (C) PDMS treated with gelatin, (D) PDMS coated with polydopamine, (E) PDMS coated with polydopamine then treated with gelatin, (F) NAP-PDMS coated with polydopamine, (G) NAP-PDMS coated with polydopamine then treated with gelatin; (H) shows the relative cell numbers of each group; result obtained from the control, cover-slip treated with gelatin, was arbitrarily set as 1; D stands for polydopamine and G for gelatin treatment; ANOVA and Tukey HSD test were applied, showing no significant difference exists between control and D-G-NAP group

2.2.3 Cell culture assay device for selecting proper SNAP-PDMS concentration range

In order to establish the useful range of NO delivery for cells, a means was developed to assess the general level of NO to be investigated. SNAP-PDMS synthesis was performed according to the protocol introduced in 2.2.1. At 37 °C the newly prepared

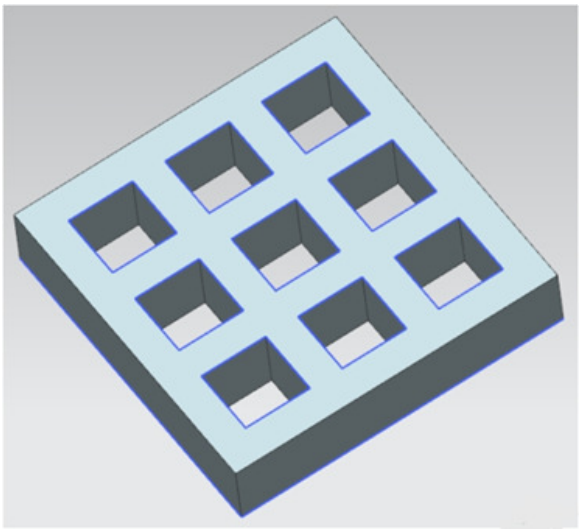

Figure 2.14: Multiple compartments Teflon mould for SNAP-PDMS casting. Each well is $1 \times 1 \times 1\text{cm}^3$

polymer will generate NO in a much higher (up to a flux of 100×10^{-10} mol/cm^2/min) than physiological level in the initial several hours, which is hard to control. This high NO flux may bring about permanent cell damage. So it is necessary to find a point (proper range of NO release) where cell can easily attached to the polymer layer and at the same time SNAP-PDMS has enough NO storage for the future NO administration and level adjustment.

To do this, SNAP-PDMS of different concentration was used for cell experiments. Different SNAP-PDMS concentrations were prepared by diluting the produced SNAP-PDMS solution with RTV-3140 solution with different ratio. Then the final polymer mixture was cast into a device as shown in Fig. 2.14, so that a cell culture vessel with different NO flux gradient grids can be established.

Then RTV-3140 was cast onto the SNAP-PDMS layer as a top coat again to prevent ion-initiated NO generation. After surface modification, cells (MOVAS cell here for device test) were seeded into the device. Fig. 2.15 shows how cells grow on the SNAP-PDMS with different concentrations, indicating 10% SNAP-PDMS may be a good NO releasing polymer for NO delivery experiment. Further intensive and accurate experiments can be designed according results obtained from this rough estimation.

This grid design can be used to investigate NO's effect on different cells by casting same concentration of SNAP-PDMS and seeding different cell types, which may have different sensitivity to NO (will discuss more in 6.4.2).

2.2.4 Cell culture on SNAP-PDMS

Since the multiple compartment device suggested proper SNAP-PDMS concentration for cell culture, cells were cultured on 10% SNAP-PDMS again. To eliminate the effect from other unpredictable factors that may influence final result, a NAP-PDMS polymer with the same surface treatment processed was used as the control. Fig. 2.16 shows after dopamine and gelatin treatment, MOVAS cell succeeded in adhering and growing on SNAP-PDMS.

Statistic analysis showed no significant difference between NAP-PDMS and SNAP-PDMS group. The hypothesis is that if initiators (light) that can be used to trigger NO release from SNAP-PDMS polymer, NO's effect on MOVAS cells can be studied. The result and the detail procedure will be shown in 5.1.

2.3 Conclusion

NO real-time measurement and controllable NO delivery have been an on going research challenges. In this chapter, the importance of comprehensive NO data presentation and the critical role of real-time NO monitoring was described. A theoretical treatment of the tow-chamber concept was presented. The mathematical models showing that how NO flux generated from the culture cells can be real-time measured by cross-membrane measuring and how total NO generated from cells can be calculated by using the two-chamber system was also presented. The problem of uncontrolled NO delivery was also examined with the current NO administration method (using NO donor). It is proposed the new method to control NO level during experimental practice by using NO generating materials. Mathematical models were introduced, showing how the new method is helpful for NO quantification study and how this method may be able to control NO that cells experience in cell culture experiment in terms of both NO level and duration. To achieve those concepts, the components needed to fabricate the measurement and delivery devices were tested.

This includes growing cells on hydrophobic PDMS substrate, which has very poor cell adhesion normally. It was demonstrated that by using polydopamine as an interfacial material, a gelatin layer could be formed on PDMS surface to allow cells to grow and proliferate. NO measurement and NO delivery devices will be fabricated using this information.

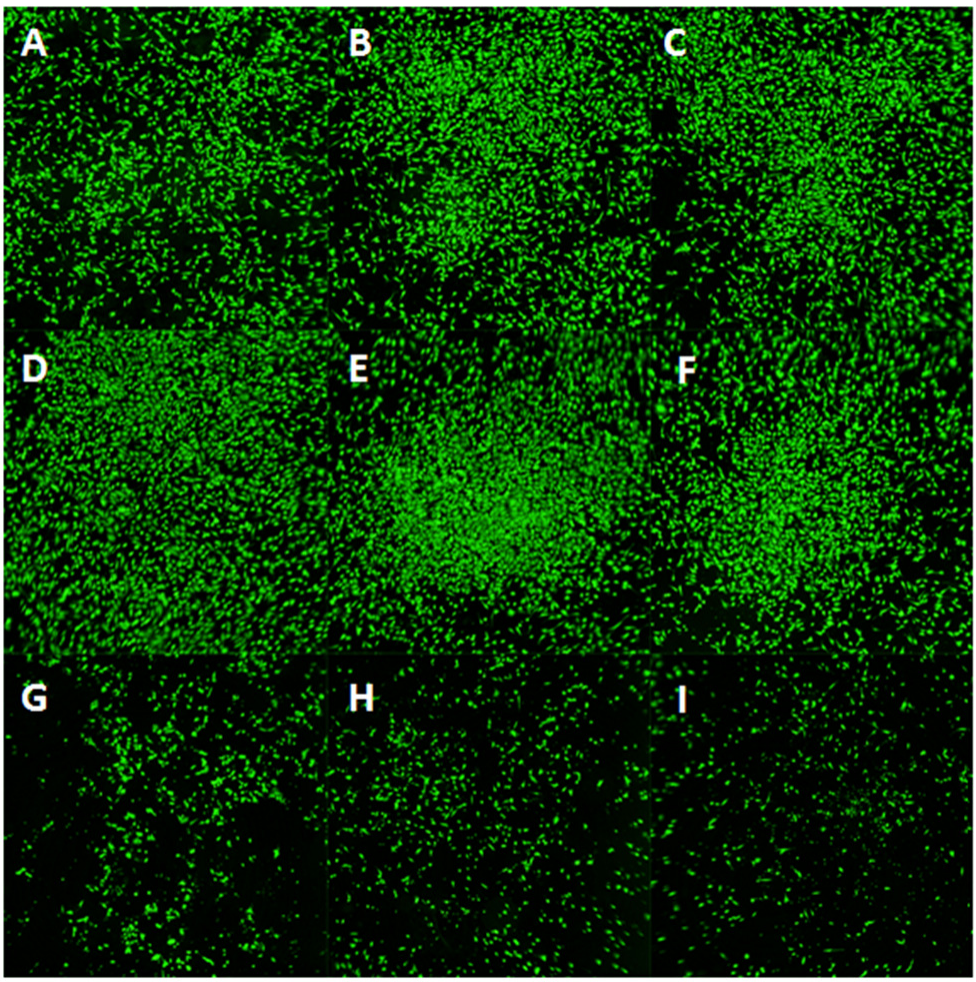

Figure 2.15: MOVAS cell was seeded onto different concentrations of SNAP-PDMS then cultured for 17 h. Cells were stained by calcein-AM and examined at 40× magnification. 300 μl of SNAP-PDMS polymer cast in (A) and the rest of the wells were 300 μl diluted SNAP-PDMS with RTV-3140 in a wt/wt ratio. (A) RTV-3140, (B) NAP-PDMS, (C) 1.5625% SNAP-PDMS, (D) 3.125% SNAP-PDMS, (E) 6.25% SNAP-PDMS, (F) 12.5% SNAP-PDMS, (G) 25% SNAP-PDMS, (H) 50% SNAP-PDMS, (I) 100% SNAP-PDMS. All the wells were top coated with another RTV-3140 layer then treated with polydopamine and gelatin.

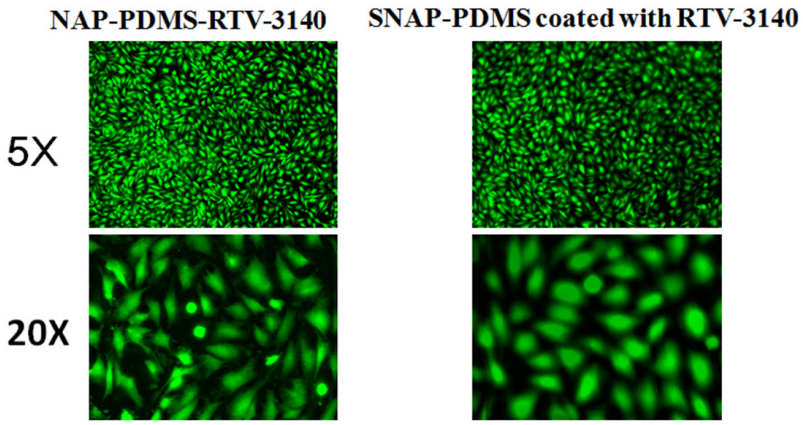

Figure 2.16: MOVAS cell was successfully cultured on SNAP-PDMS substrate. MOVAS was seeded onto different gelatin treated substrates and cultured for 24 h in dark. Cell was stained with 2μM calcein-AM; no significant difference of cell numbers was observed between NAP-PDMS and SNAP-PDMS group.

Chapter 3

Real-time NO Flux Measurement from Living Cells[1]

The measurement of NO is not a new idea. Many methods with excellent specificity and limits of detection have been developed for NO measurement in the controlled laboratory experiments. However, similar success for the measurement of NO in biological samples has not been attained. Measurement data has shown that NO concentration varies several orders of magnitude while it functions in different roles (many reviews have very detailed explanations on those methods [73, 74, 142, 143]). In the human body NO synthesis is a precisely controlled process. Three isoforms of nitric oxide synthase (NOS) are responsible for NO synthesis [32]. Different NOSs

[1]This chapter has be submitted to *Nitric Oxide* for possible publication in the near future.

have their own tissue distributions [39] and may produce different quantities of NO [38]. This free radical signaling molecule is extremely difficult to measure owing to its high reactivity and diffusivity and the large number of biological molecules present with which NO will react rapidly. The half-life of NO is on the order of seconds to minutes in oxygenated solutions [76, 77], and is substantially shorter in the presences of molecules such as hemoglobin [144, 145]. This chapter will present the design, fabrication and validation of a two-chamber NO measurement device that achieves real-time NO measurement in biological samples.

3.1 Background of NO measurement

Figure 3.1 illustrates the three work horse methods of measuring NO in biological solutions. The colorimetric Griess assay, which measures the accumulation of nitrite in oxygenated aqueous solution [142, 146], electrochemical detection, which measures NO by recording the change of electric current due to the oxidation reaction of NO dissolved in aqueous solution occurring on a probe surface [147, 148], and chemiluminescence detection of NO in the gas phase after its reaction with ozone [146, 149].

Each of these methods has significant limitations in quantitative measurement of

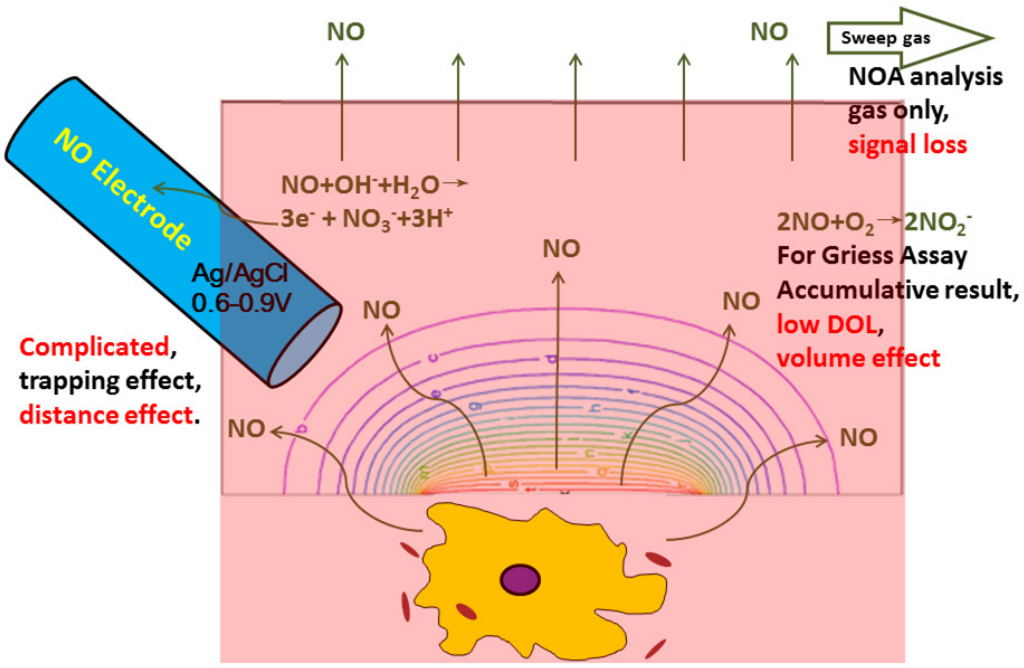

Figure 3.1: Illustration of the 3 most common methods for detection of NO in biological media.

NO from cells grown in culture. The Griess assay measures the accumulation of nitrite/nitrate over time and attributes the elevated levels to total NO generation. In a study to determine accuracy of this method with a standard NO donor, Hunter, et al. [146] reported that the Griess assay resulted in 30% less total NO detected in phosphate buffered saline than the theoretical amount predicted by the concentration of PROLI/NO used. Different biological media that were also tested including serum, plasma, and DMEM, with which there was even greater variation introduced. Importantly, the level of variation was also dependent on the total volume of solution used, making the offset in detection very difficult to calibrate. Another improper part is in the assumption is that the elevation of nitrite/nitrate is only resulting from NO

production, which might not be true. Meanwhile, there are some other absorbance based methods too, such as oxyhemoglobin assay and NO trapping reagents, however, neither can achieve real-time NO flux measurement.

Electrochemical detection relies on the electron transfer during the redox reaction. This is a concentration based detection method and the results for quantitating the highly reactive NO molecule depend on a number of factors including distance between the electrode and the cell surface (distance effect shown in 2.1.3), trapping effect resulting from the size of the electrode, and stirring rate [150, 151]. Besides, the calibration procedure is very time consuming and labor intensive, so that results from using these probes can be skewed.

Chemiluminescence detection relies on the gas-phase reaction of NO with ozone to generate an excited state NO_2 molecule that relaxes to release a photon that can be counted [149, 152, 153]. This is a highly sensitive method of direct NO detection but is

$$NO + O_3 \longrightarrow NO_2^* + O_2$$

$$NO_2^* \longrightarrow NO_2 + hv$$

limited by the requirement that NO has to diffuse out from the culture media and enter the head-space above the cell culture dish and be swept into the chemiluminescence analyzer. The bathing solution in this experiment ideally needs to be purged by an inert bubbling gas in order to force NO out from the solution phase before it reacts with molecules such as oxygen presenting in biological environment. So none of these

current techniques have provided satisfactory results for determining the level of NO that cells actually produce or experience in a real-time manner.

The method developed has made full use of the current chemiluminescent method, manufactured a special cell culture vessel and guided NO out from the aqueous environment, so that gaseous NO can be sampled for standard chemiluminescence quantification. In addition to accurately knowing the level of NO cells produce or experience, it has become abundantly clear that temporal aspects of when NO is released by cells and under what circumstances it is produces, as well as what the duration of NO production that cells achieve are critical to understanding the roles NO plays in normal and pathological processes. As an example, Thomas and co-workers published a paper that demonstrated that the duration over which a dose of NO is delivered to cells has a profound impact on the protein expression of the cells [154]. They showed that the time frame over which NO was delivered to MCF7 breast cancer cells impacted the level of $HIF-1\alpha$ and phosphorylation of p53-Ser-15. A single, large bolus dose of NO (1000 nmol) administered at time 0 showed increased production of p53-Ser-15, which indicates apoptosis. While a larger dose of NO delivered from time 0 and continued over a 9 hours period (4000 nmol), showed a significant production of $HIF-1\alpha$. When the NO dose (5000 nmol) was introduced later in the culture period, such that the maximum NO was experienced by the cells at Hour 5, the ratio of $HIF-1\alpha$ and p53-Ser-15 was markedly different. The data clearly shows that protein expression was affected by the amount of NO delivered and the timing of this

delivery, highlighting the importance of understanding the temporal variable involved in when cells experience NO as well as the duration over which a specific dose of NO is delivered. Fortunately, the chemiluminescent method itself relies on continuously sampling the gas and provides real-time NO flux information. Currently the fastest commercial available NOA's sample rate reaches 32 time/sec, which in theory can track NO time variable accurately.

3.2 Experiment set-up I–preliminary design

Only considering a homogeneous cell layer that homogeneously produces a steady-state level of NO, diffusion and consumption described by Eqn(2.4), intuitively the NO gradient generated around the cell layer can be roughly described as Fig. 3.2 A. The maximum concentration is in the vicinity of cell layer and it gradually decreases along the z-axis. It is easy to see in the real case, where adhesive cells cultured at the bottom of the culture vessel and covered by culture media, the NO gradient can be modeled as Fig. 3.2 B.

Once NO escapes from the media and enters the headspace air phase, NO can be chemiluminescently quantified by NOA sampling. According to this concept, a simple experimental set-up (Fig. 3.3 A) was tested to measure the NO flux coming out from a 100 ng/ml LPS and 10 ng IFN $-\gamma$ stimulated mouse macrophage RAW264.7 cell

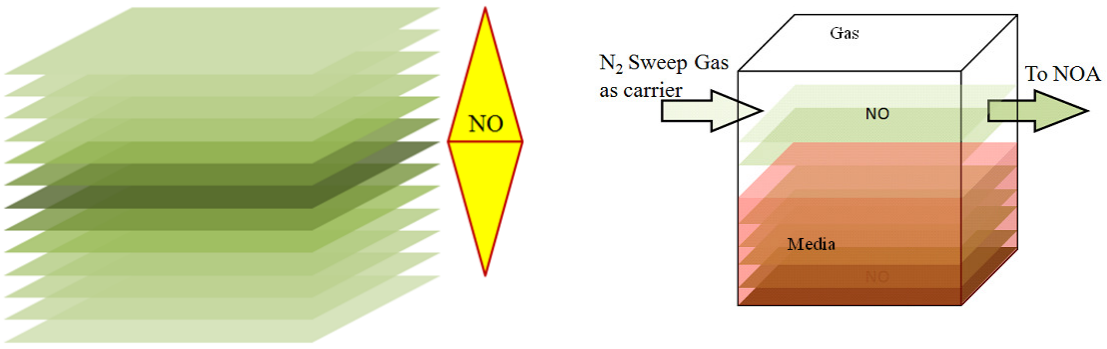

(A) (B)

Figure 3.2: Illustration of NO gradient generated by the NO releasing cell layer. (A) imaginary NO concentration gradient in an infinite big space; (B) NO concentration gradient in the cell culture vessel.

line. The T-25 cell culture flask was directly concatenated within NOA sampling line. Air in the headspace of flask was continuously sampled by NOA using air in the incubator as the sweep gas and zero gas. And result was obtained as shown in Fig. 3.3 B. This was the first real-time NO flux profile representing cellular NO production due to the free diffusion of NO and measured by directly sampling NO using chemiluminescent detector.

RAW264.7 is a good model for NO study, which produces very high levels of NO (up to μM [65]) after endotoxin from bacterial and/or cytokine stimulation (so that it can be used as positive controls in many circumstances) [155]. The NO generation time variable has also been investigated by many other methods such as iNOS Western blot and electrode [28, 29, 156]. For example Noda et al. showed that iNOS appeared 4 h after LPS treatment, which is well correlated with data obtained [156].

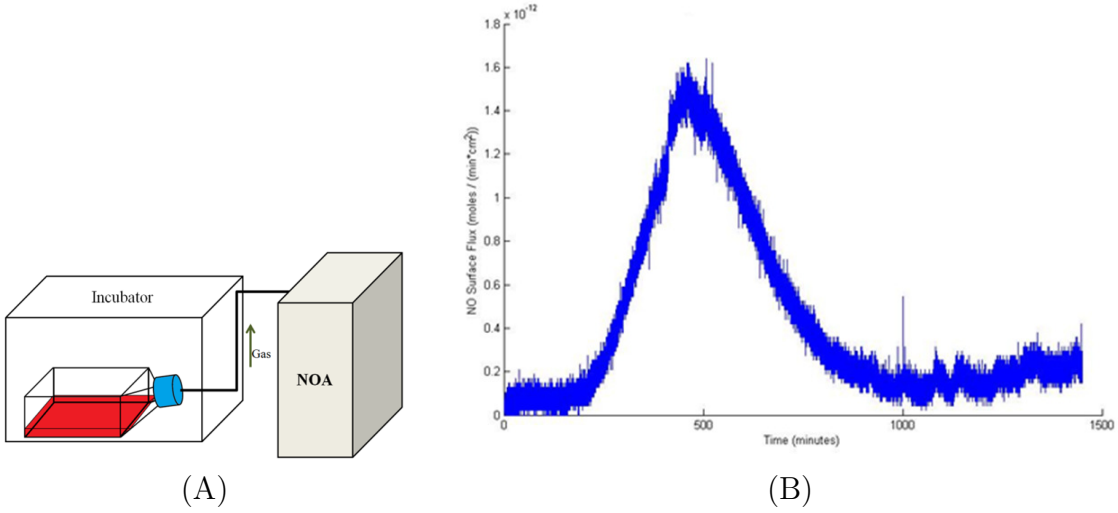

(A) (B)

Figure 3.3: Illustration of measuring NO flux from the cultured cells in T-25 culturing flask. (A) the experiment set-up; (B) real-time NO releasing profile of 100 ng/ml LPS and 10 ng IFN $-\gamma$ stimulated mouse macrophage cell line RAW264.7.

This method achieved real-time NO monitoring (gaseous) with high time resolution, introducing minimum interference to cells during measurement. And compared with the current data [156], the produced NO profile trend is consistent with the reported time-dependent behavior, suggesting directly measuring NO (gaseous) from the living is feasible.

However, question came out when more quantitative analysis was applied. RAW264.7 has be reported to produce NO at an average rate of 2.6 pmol/10^6cell/s under conditions of bacterial infection [29]. The Sievers 280i NOA utilized has a calibration constant of around 0.1 pmol/PPB/s and should therefore have sufficient detection limit to monitor NO production in RAW264.7. However, assuming a confluent RAW264.7 cell layer has a cell density of 5×10^5 cell/cm^2, experimentally determined values

were around 1000 time smaller than the reported value! What could be the reason?

As introduced in 2.1.3, NO diffusion is free and can be in any directions, but it is driven by concentration gradient; in a homogeneous model (Fig. 3.2 B) the net NO moving is only considered in z direction; so to capture the NO signal, NO generated by the cell layer needs to pass through the media layer and enter the head-space, then be sampled by sweep gas; diffusion in aqueous solution is significantly slower than in air, which takes a longer time for NO to be captured by the NO detector.

The net time needed for NO to pass through the media layer can be calculated by Einstein-Smoluchowski equation [76], which describes the net molecule displacement, Δx, versus time (t) as:

$$(\Delta x)^2 = 2Dt \tag{3.1}$$

where D represents the diffusion coefficient. NO reacts with different species during diffusion. So with longer diffusion time t, a more complicated environment is not favored for NO sampling, simply because NO will have more opportunity to be consumed per unit time. To decrease such signal loss, one method is to minimize the depth of the media and thereby reduce the diffusion distance (Δx) of NO before it enters the gaseous environment. If so, the question would be how to accurately control the media depth and how to keep it constant during the hours long gas sampling. However, it is almost impossible to do this because too small an amount of media is not favored by cell culture and sampling process itself inevitably removes moisture,

gradually drying and concentrating the media, which is both bad for cell growing and NO measurement.

Over all, this experiment can successfully capture gaseous NO signal from the cultured cells and do rough semi-quantification, and obtain cellular NO temporal information with good resolution. But this method may interfere with normal cell growth and cannot achieve absolute quantification due to the difficulty in estimating signal loss during the sampling.

3.3 Experiment set-up II–two-chamber design

After evaluation of the short comings of the initial experimental design, the two-chamber system introduced in 2.1.2 was fabricated and tested.

Recall that in Eqn(2.4), the cell layer generated NO creates an NO gradient. If the bottom of the culture is replaced by a layer that is NO permeable but water impermeable, NO will pass through the layer and enter a solution free space below, where NO gas sampling can be carried out (Fig. 2.2 B). This idea shares the same principle with Boyden chamber (Fig. 2.2 A). To realize this idea, an NO permeable material is the essential components. And to minimize NO diffusion distance within this material so that to minimize NO loss and increase the NO signal, it is needed to

control and minimize the thickness of the NO permeable material (a consistent and small diffusion distance) and find out the relationship between the detected NO and the total NO to achieve absolute quantification.

3.3.1 NO permeable membrane fabrication

As mentioned in 2.1.3, PDMS was chosen for manufacturing the NO permeable, water tight membrane. PDMS used in the beginning was room-temperature vulcanized PDMS RTV-3140. RTV-3140 was dissolved in toluene (1 g/10 ml toluenen) and fully vortex-mixed. The produced solution was manually cast (72 μl/cm^2) on the top of glass-fiber filter paper (with 0.2 μm pore size), and air-dried to let the organic solvent evaporate in a chemical hood. This process was repeated 3 times then the produced membrane composite was left at room-temperature for overnight curring. To understand the actual structure of the membrane, the membrane was cross-sectioned for SEM imaging (Fig. 3.4).

From the image, it is observed that PDMS polymer layer was formed on the top of the filter paper, and both the thickness and surface are very even. However, PDMS itself is not a very good cell adhesion substrate. So its surface needs to be further treated to support cell growth. One method is polydopamine treatment [157]. To do this, the composite membrane was soaked in 1 mg/ml dopamine solution (in Tris-HCl

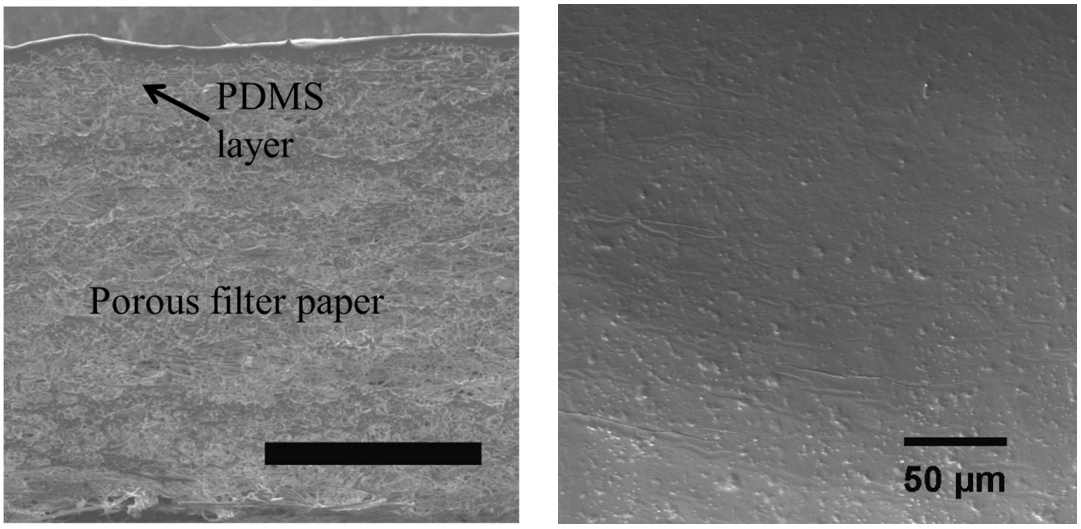

(A) (B)

Figure 3.4: SEM image illustrating the structure of the semi-permeable membrane. (A) cross-section of PDMS coated glass-fiber filter paper; (B) topographic image of PDMS coated glass-fiber filter paper

buffter pH=8.5) for 24 h. Then the product was sterilized by soaking in 70% ethanol for 10 min and UV treatment for 30 min. Then the sterile membrane was top-coated with 2 mg/ml gelatin solution (in PBS) for 1 h to further facilitate cell adhesion onto the surface. Polydopamine is a novel bioadhesive layer, which acts as an intermediate sticky layer so gelatin can easily attach to the substrate. Then cells can adhere to the gelatin layer. The modified PDMS composite membrane will be ready for cell culture.

More quantifiable examinations were applied shown in Fig. 3.5. SEM reveals polymer layer thickness as 17.3 ± 3.2 μm, which is good for NO diffusion according to Einstein-Smoluchowski equation and the previous simulations. AFM quantified the surface roughness, root mean square (Rms) as 63.51 nm $\pm$ 19.60 nm, indicating a suitable

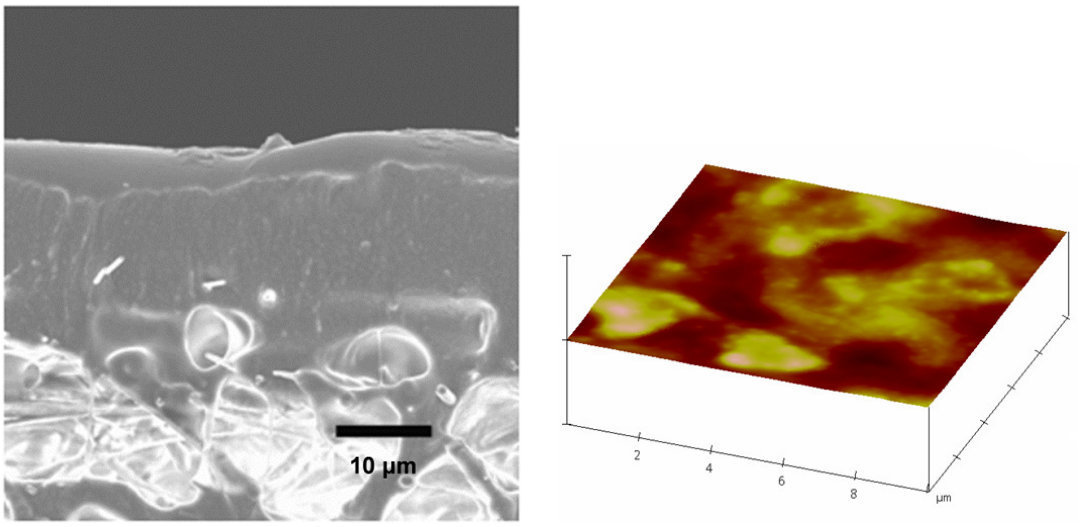

(A) (B)

Figure 3.5: Membrane characterization. (A) cross-section of PDMS polymer layer by SEM; (B)topographic image of polydopamine and gelatin treated PDMS coated glass-fiber filter paper by AFM.

surface roughness for cell culture [158]. Different cell types were cultured on the membrane to test whether cells will grow and proliferate normally on the membrane. Fig. 3.6 showed the growth of, ARPE-19, primary tenocyte, fibroblast, and HAEC on the produced membrane.

3.3.2 NO permeable membrane characterization and validation of time resolution

To validate the feasibility of the cross-membrane NO measurement and whether there is enough time resolution by sampling NO in the lower chamber of the device, NO release profile from controllable NO releasing material SNAP-PDMS were measured

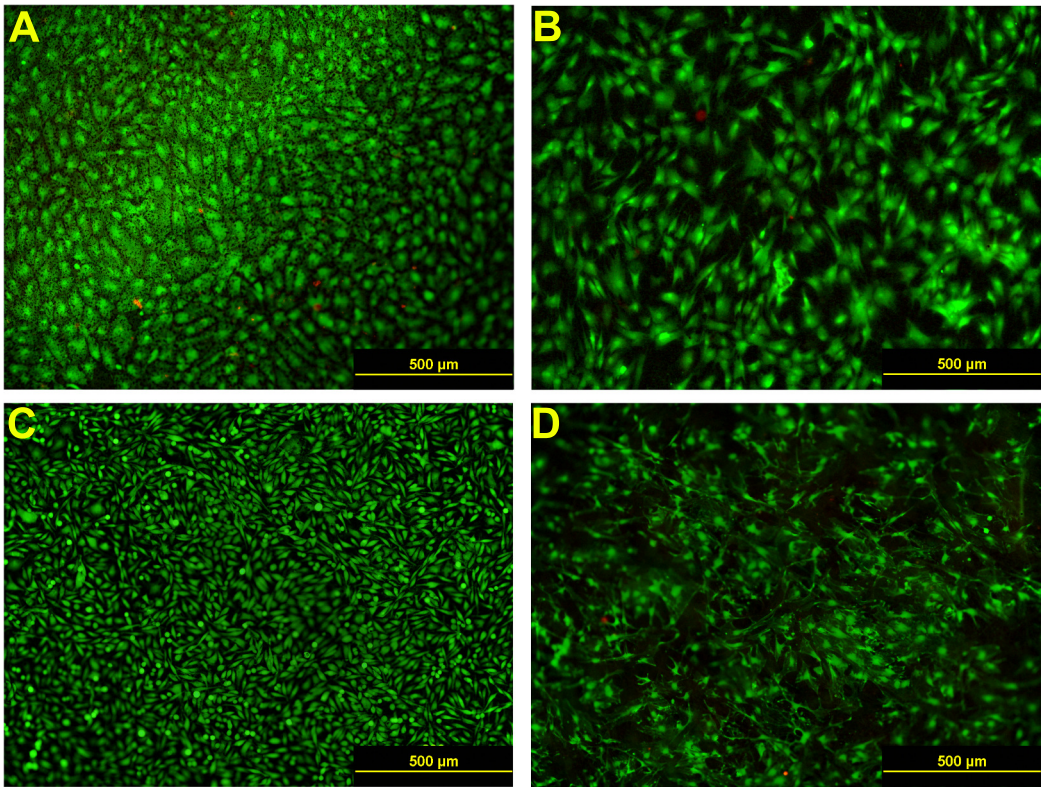

Figure 3.6: Membrane biocompatibility test by culturing different cell types on the polydopamine and gelatin treated NO permeable membrane. (A) ARPE-19, (B) primary tenocyte, (C) fibroblast, (D) HAEC. Cell was stained with 2μM calcein-AM

cross-membrane. The experiment set-up is shown as Fig. 3.7.

A piece of prepared PDMS composite glass-fiber membrane (with dopamine treatment) was fixed in between co-culture Kube chambers; a 4 mm diameter, 0.1 mm thick SNAP-PDMS film was placed on the membrane in the upper chamber (as shown in Fig. 3.7); LED light (VAOL-5GSBY4, Mouser electric, Mansfield, TX) was applied to the polymer to trigger NO releasing. By simultaneously sampling NO from both the upper and lower chambers using two identically calibrated chemiluminescence

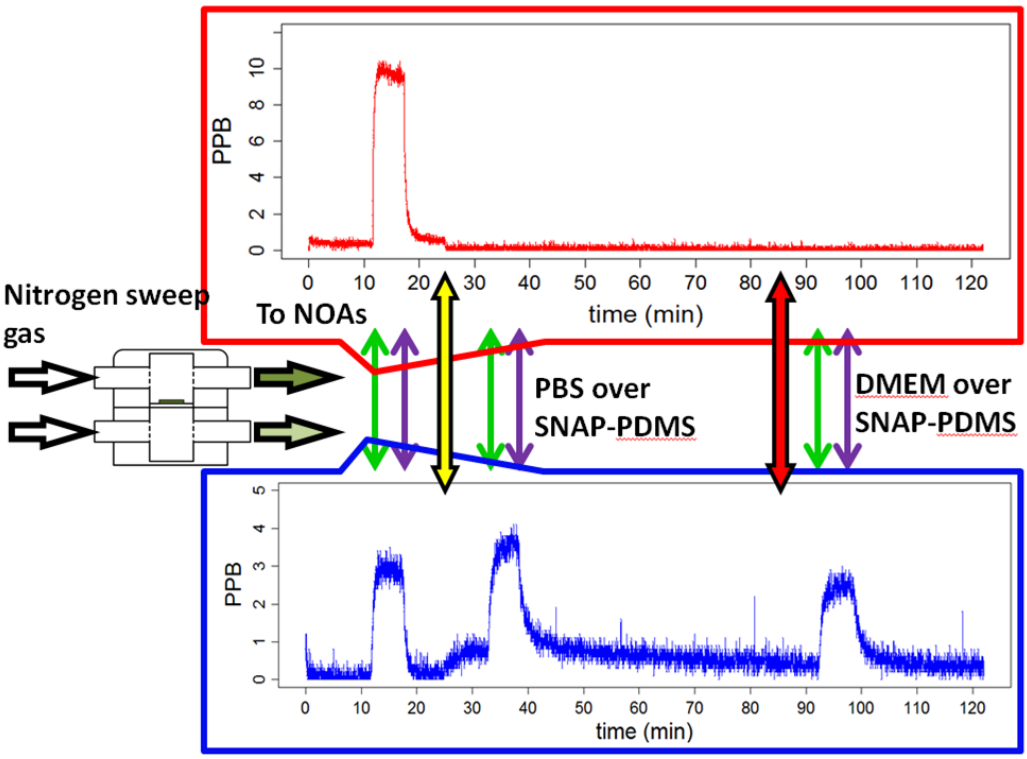

Figure 3.7: Lower chamber's quick response towards NO generation in the upper chamber. Bathing solution in the upper chamber damped NO signal but will not have significant impact on the lower chamber signal. 4 mm diameter 200 μm thick SNAP-PDMS disc was placed on the PDMS coated filter paper, which separated Kube into two different chambers; LED light was used to initiate the controllable NO releasing. Green arrows indicate light-on, purple off. NO surface flux from both upper chamber and lower chamber was monitored by two identically calibrated NOAs. 100 μl PBS solution or DMEM cell culture media were applied onto SNAP-PDMS top one after another. The polymer interface was fully immersed by the bathing solution.

detectors, the NO signal change with time was obtained from both chambers. Once NO releasing was triggered by light, the NO flux was detected (first increase, in both blue and red line) at the same time from both chambers, indicating no time delay in the cross-membrane NO measurement.

To further compare direct measurement (sampling over the bathing solution) with cross-membrane measurement when bathing solution is present, the same light intensity was applied after PBS solution and DMEM media were added to the upper chamber over the SNAP-PDMS disc with NO sampling continuing in both chambers (solution height $>$ 5 mm). The addition of the bathing solutions dramatically hindered the gas phase measurement of NO flux in the upper chamber, while the NO signal measured from the lower chamber remained relatively stable compared to the initial measurement with no bathing solution as the light was turned on and off (second and third increase in blue but not in red). Of particular importance, the NO measured in the bottom chamber showed release that exactly corresponded to the light being turned on and off, demonstrating that we maintained excellent temporal resolution for the tracking of the production of NO in the lower chamber, regardless of the addition of solution over the SNAP-PDMS disc in the upper chamber. From these data, it is suggested that by applying cross-membrane measurement to cultured cells we should be able to obtain NO signal and record the temporal aspect cellular production of NO.

3.3.3 Control over membrane properties

Since increasing the sensitivity of the NO measurement method relies on restricting the thickness of PDMS layer, it is necessary to manufacture membranes with consistent thickness (the thinner the polymer layer, the better for NO permeability without allowing water leakage). Meanwhile, cell growth requires certain level of stiffness. If a material is too soft cell migration and proliferation will be affected, which may introduce significant variability in behaviors of standard cell-line models [159, 160]. So it is necessary to control and optimize the properties of PDMS layer.

To control the thickness of PDMS layer, different repeats of casting or different concentration of PDMS solution were applied. Still using different RTV-3140 solutions (1 g/10 ml toluene and 1.25 g/10 ml toluene) and applying different numbers of layers cast, NO permeable composite membranes with different thicknesses of PDMS were generated (Fig. 3.8 shows the control over the PDMS layer thickness imaged by SEM; B to E have different PDMS layer thicknesses, 17.3 $\pm$ 3.2 μm, 39.4 $\pm$ 4.7 μm, 53.8 $\pm$ 6.2 μm, 162.3 $\pm$ 9.5 μm, respectively.).

To control the stiffness of PDMS, Sylgard PDMS was used. Different from RTV-3140, the PDMS polymer base and the curing agent are supplied separately. By using different base to curing agent ratio and different curing temperature, silicone

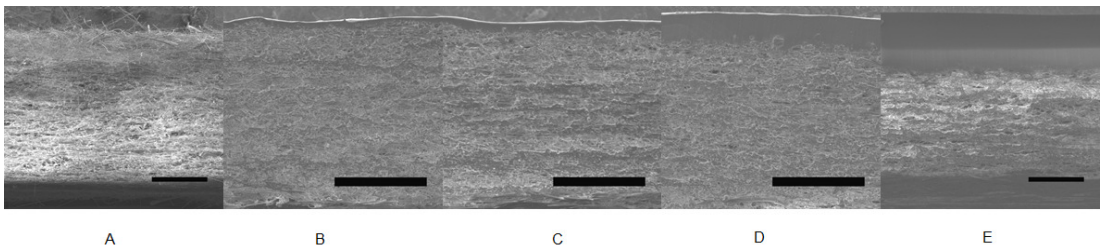

Figure 3.8: The control over PDMS layer thickness on glass-fiber filter paper. Cross-section SEM image of different thicknesses of PDMS membrane by multiply casting different concentrations of PDMS solutions (for each cast, 72 μl/cm^2 solution was applied), scale bar: 150 μm. (A) glass fiber filter paper; (B) 3 repeat of 1 g /10 ml RTV-3140 PDMS cast; (C) 1 cast of 1 g /10 ml RTV-3140 PDMS and 2 repeat of 1g / 8 ml RTV-3140 PDMS cast; (D) 1 cast of 1 g /10 ml RTV-3140 PDMS and 3 repeat of 1g / 8 ml RTV-3140 PDMS cast; (E) 1 cast of 1 g /10 ml RTV-3140 PDMS and 4 repeats of 1g / 8 ml RTV-3140 PDMS cast.

elastomer with different stiffness can be produced [161]. For the following adhesive cell culture, a base : curing agent = 10 : 1 (w/w) was used, and the curing condition was set to 52 °C overnight.

3.3.4 Measurement device manufacture

The whole purpose is to create two chambers that are separated by the gas-permeable membrane as shown in Fig. 3.9. To do this, the bottom of 100 mm dia. × 20 mm deep or 60 mm dia. × 15 mm deep commercially available polystyrene cell culture dishes were removed, leaving a 2.5-3.5 mm wide rim around the bottom of the plate (Fig. 3.9 A). The PDMS-glass-fiber filter paper composite membrane was adhered to the culture dish, creating a PDMS/glass filter paper bottom. A second culture dish

was attached under the PDMS-bottomed dish and two holes for NO sampling were drilled in the wall of the lower chamber, creating a cell culture dish with two chambers (Fig. 3.9 B). After liquid leakage examination, upper chamber was filled with 2 mg/ml dopamine solution for 24 h for polydopamine coating (in 10 mM Tris buffer, pH=8.5). For sterilization, the whole device was sterilized through ethylene oxide for 24 h and then the polydomapomine surface was treated with a 2 mg/ml gelatin solution for 1 h, after which the device is ready for cell culture (Fig. 3.9 C). Device was placed within a cell culture incubator and the lower chamber was connected to the chemiluminescence NO analyzer sampling line for real-time continuous NO measurement (Fig. 3.9 D).

3.4 Validation of two-chamber NO measurement device

3.4.1 Investigating membrane NO permeability

Since all the fabrication work was manually completed in the lab and it has been shown that NO enters the gaseous sampling chamber right after it was generated in the culturing chamber, it is necessary to understand if NO gas is consumed in the membrane and how consistent the fabricated gas permeable membrane is.

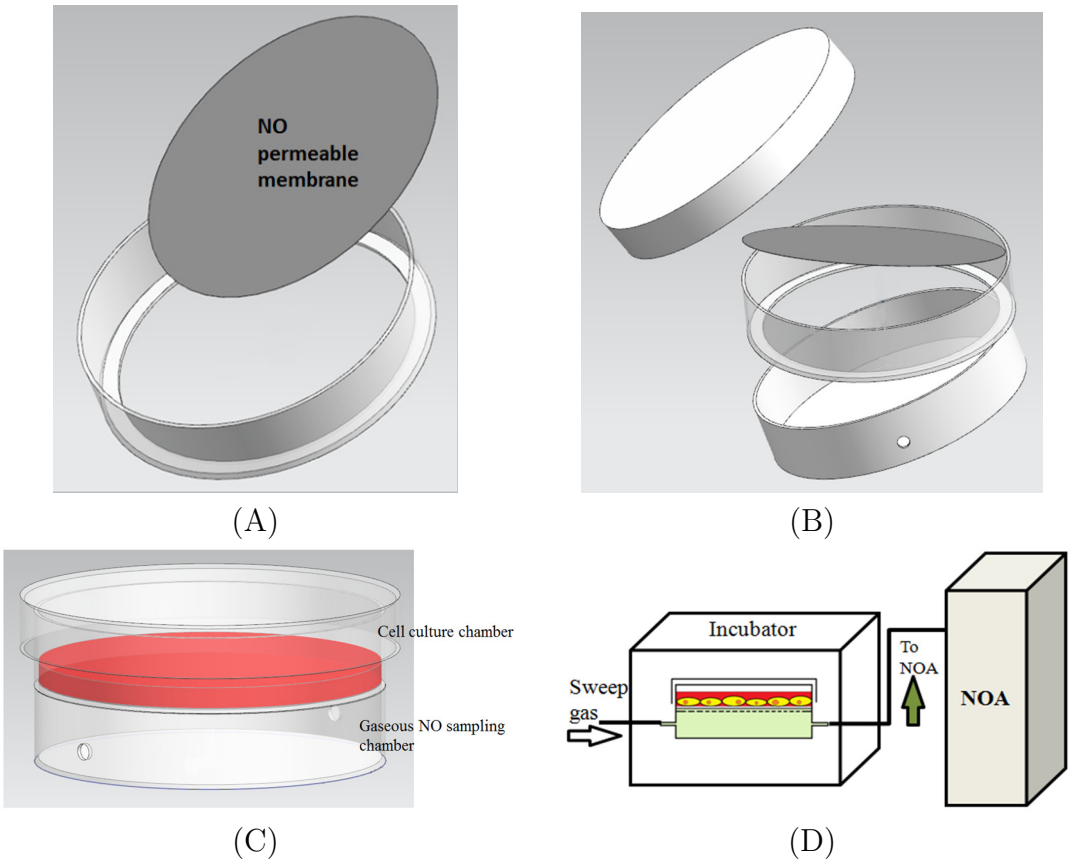

Figure 3.9: NO measurement device build-up. (A) PDMS coated glass fiber filter paper was adhered to the bottom-removed conventional polystyrene cell culture dish. (B) The main components of a single device, including the dish cover, selective-permeable membrane and the upper and lower chambers. (C) and (D) Cell culture experiment set-up. Cells were seeded within the upper chamber (C) and the device was placed into culturing incubator for normal cell culture and can be hooked up into sampling lines connecting to NOA (D). NO sampling can be initiated and stopped at any time point during cell culture according to specific needs.

First it is necessary to define an NO permeability for quantitative study. This is depending on the experiment design shown in Fig. 3.10.

Assuming a source produces NO with a constant flux of J_p and NO diffusion is only in the z direction. NO diffuses across the membrane, during which it might react with

oxygen dissolved in the polymer layer. The final detected value is J_{Tr}. Membrane relative NO permeability η was defined as:

$$\eta = \frac{J_p}{J_{Tr}} \times 100\% \tag{3.2}$$

To achieve this, controllable NO releasing polymer SNAP-PDMS was cast on a cover-slip and top coated with RTV-3140 PDMS layer. This SNAP-PDMS piece releases NO at a certain constant rate at specific temperatures (due to thermal degradation). By measuring NO flux when polymer layer faces up from the upper chamber, the original NO flux coming out of the polymer (J_p) was obtained and facing down (polymer needs to be tightly attached to the semi-permeable membrane), the NO diffusing across the membrane was detected (J_{Tr}) (Fig. 3.10 upper and lower panels). At the edge of SNAP-PDMS piece, water was applied to prevent NO from leaking.

By using NO measurement device with different polymer layer thickness (membranes examined in Fig. 3.8 were used to manufacture the NO measurement device), it is obvious to see that with thicker PDMS layer and the same J_p, J_{Tr} decreased (Fig. 3.11). This result also directly proved the conclusions from the simulation in 2.1.3.

So now the task would be to manufacture a membrane with the highest NO permeability (where $\eta = 1$). The total PDMS amount applied onto the membrane was reduced in the subsequent steps by decreasing PDMS solution concentration to 0.5 g/10 ml

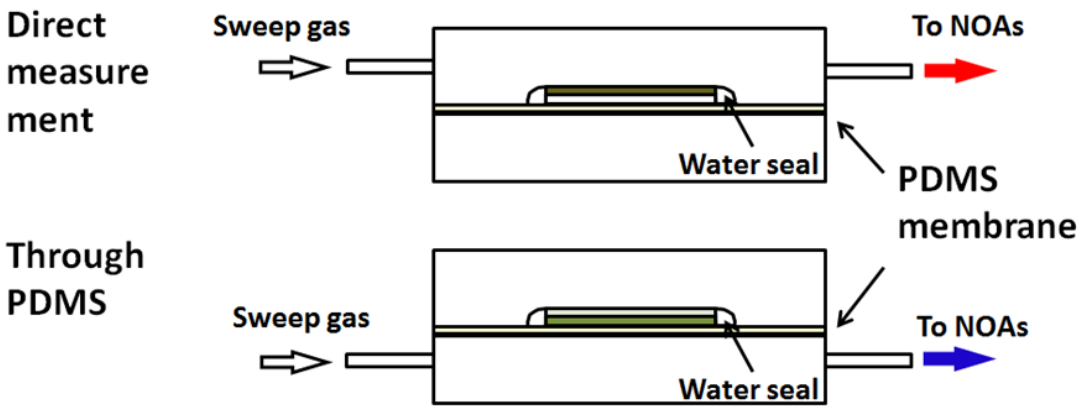

Figure 3.10: Experiment design of the evaluation of NO cross-membrane signal dampening. Controllable NO releasing polymer SNAP-PDMS cast on glass cover-slip was placed face-up and face-down in the NO measurement device; the NOA was connected to the upper chamber or the lower chamber to measure NO flux coming out from the polymer at 37 °C or NO flux measured across the membrane while the same polymer was applied, respectively.

toluene. Three layers were cast (72 μl/cm^2). After 52 °C heating for overnight, membrane was examined by both SEM and permeability test again.

Fig. 3.12 shows the cross-section and the surface of the new membrane. Compared with previous membranes (Fig. 3.8), the new membrane does not have distinguished polymer layer on top of the glass-fiber layer, instead the polymer coated the glass-fibers, increased fiber diameter and formed a foam-like structure. The whole membrane was homogeneous. After mounting this new composite membrane onto the two-chamber device body, liquid leakage test shows no leaking of water. Permeability test was run according to Fig. 3.10. The result is shown in Fig. 3.13.

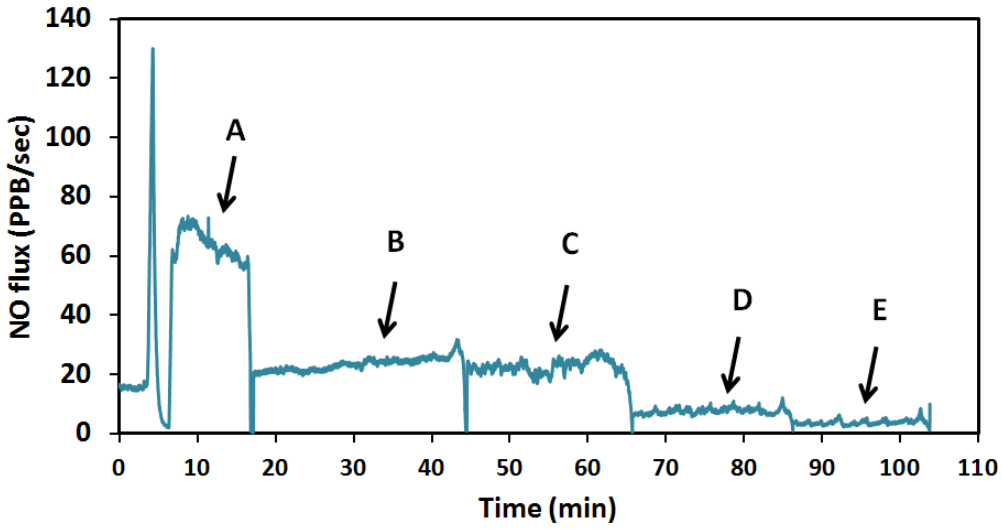

Figure 3.11: NO flux measurement influenced by the thickness of the NO permeable membrane. SNAP-PDMS disc was used to release NO at a specific flux rate, arrow A; then different NO measurement devices manufactured from different membranes was used to measure the trans-membrane NO. Arrow B to E correspond to the membrane shown in Fig. 3.8 B to E (with a thickness of 17.3 $\pm$ 3.2 μm, 39.4 $\pm$ 4.7 μm, 53.8 $\pm$ 6.2 μm, 162.3 $\pm$ 9.5 μm, respectively).

Direct NO measurement and cross-membrane measurement produced almost identical NO releasing profiles. After 5 repeats, the NO flux value in steady state (after 1 h, the state where NO flux from SNAP-PDMS reached a plateau) were averaged. Values were applied to paired t-test. Data showed that no detectable difference exists between using these two methods, indicating that when NO passes through the membrane that was manufactured, there is no detectable signal loss. So that the relative NO permeability η can be considered as 100%. This is important for later NO calculation. Since the main idea for the NO real-time sampling method is to estimating the total NO generation by accurately measuring a part of NO flux. So

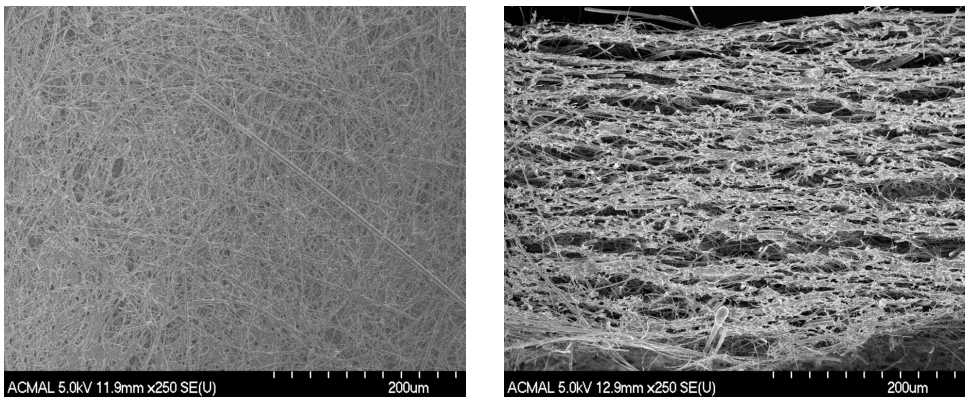

(A) (B)

Figure 3.12: Foam-like structured semi-permeable membrane manufactured by casting Sylguard PDMS solution on the glass-fiber filter paper. (A) surface (B) cross-section.

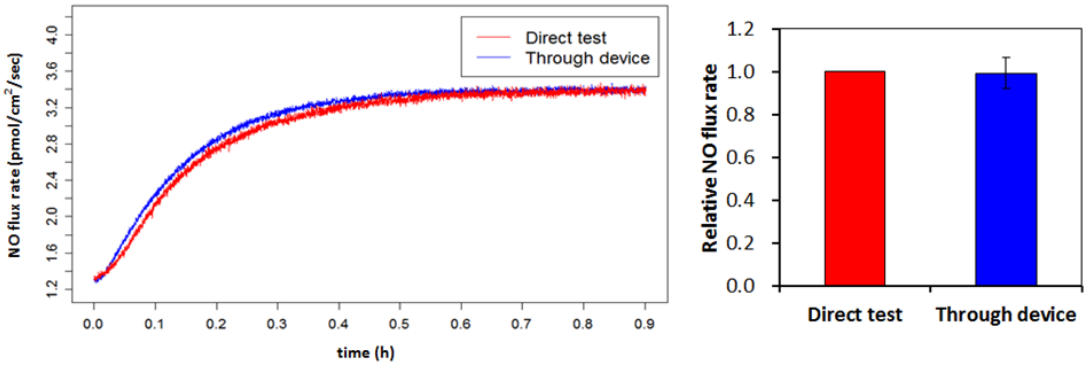

Figure 3.13: Permeability examination on foam-structured membrane. (A) real-time NO flux data of both J_p and J_{Tr}; (B) comparison of direct measurement and cross-membrane measurement. After 5-time repeats, the average NO flux at steady-state (defined as the NO flux from time 60 min -70 min after polymer was applied for measurement, where NO signal became almost stable) was calculated; NO flux at steady-state measured by direct measurement was arbitrarily set as 1 and the corresponding cross-membrane NO flux was normalized to this value; P $>$ 0.9 according to t-test.

precisely understanding the relationship of the detected NO and the total NO is important. Then it is necessary to understand NO's fate and the consumption routes.

Since there is almost no NO loss during NO crossing the membrane, the calculations for the model become easier.

3.4.2 Quantifying NO coming out from the cultured cell layer

Since preliminary experiments have proved that NO can be measured by cross-membrane measuring and the measurement result is not likely to be influenced by the solution added above the NO source attaching to the gas-permeable membrane, it is necessary to understand what the measured value actually means. What is the relationship of this measured value J_{Tr} and the total NO J_0 generation by the source? The next task is to find a mathematical expression $J_0 = F(J_{Tr})$ to describe this relation.

A series of experiments were designed to find the relationship between the detected NO and the total amount of NO generated. PDMS coated SNAP-PDMS films were used as the NO source again; the polymer disc (15 mm diameter SNAP-PDMS film) was attached tightly on the prepared semi-permeable membrane, where different LED drive currents were used to adjust the rate of NO generation; NO was sampled in both the upper and lower chambers by using identically calibrated NOAs (Fig. 3.14 A). Since there is negligible NO loss when passing through the membrane, total NO released from NO source was calculated as the sum of the total amount of NO

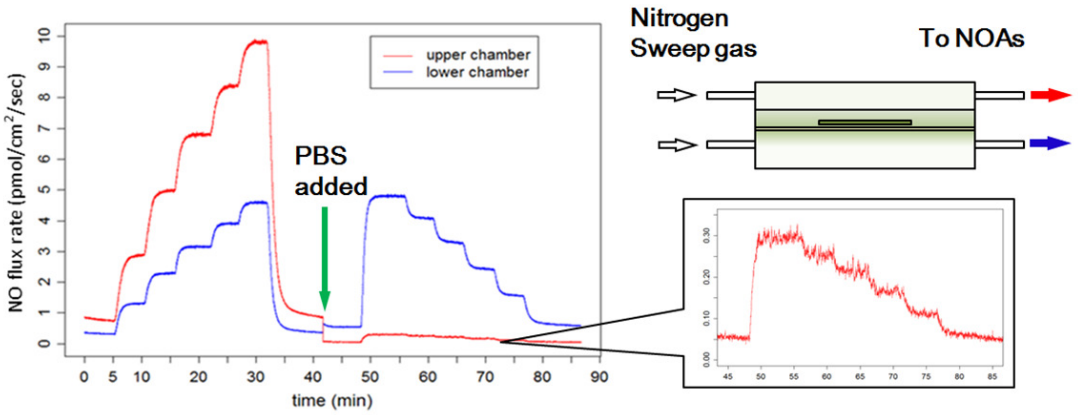

(A)

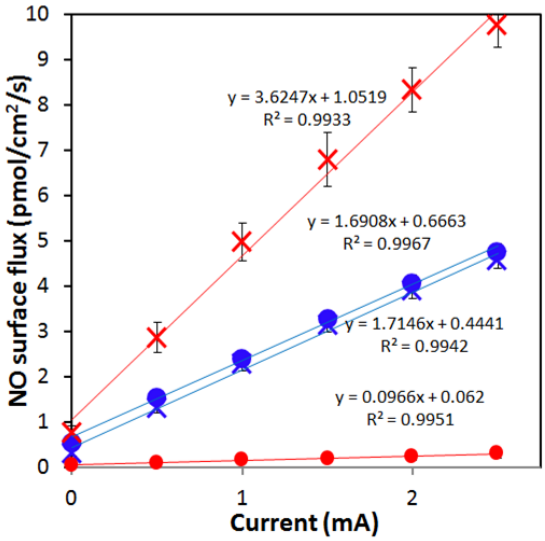

(B)

Figure 3.14: Linearity of the detected NO signal over the total NO generated in both gas-gas and gas-liquid chamber condition. (A) test set-up and NO flux data. 0.2 mm thick, RTV-3140 top-coated SNAP-PDMS was placed within the NO measurement device; NO fluxes in both upper and lower chambers were measured by two identically calibrated NOAs simultaneously; different NO fluxes were controlled by changing the drive current through a position fixed LED light; to assess the effect of bathing solution on top of NO source, PBS was applied and the same current intensity values were repeatedly applied. The damper of NO flux signal due to bathing solution was shown in the bubble; three independent experiments were run. (B) Linear regression analysis. The slope reflects the detection sensitivity. Red refers to the signal from the upper chamber, blue the lower chamber; $\times$ corresponds to before adding bathing solution, $\bullet$ after.

measured from both upper and lower chambers, as determined by integrating the area under the NO release curves. Data showed clearly that the tested NO flux across the membrane (Fig. 3.14 A blue line before green arrow) changed in the same way the NO flux change in the upper chamber (Fig. 3.14 A, the red line before green arrow), indicating the NO flux tested in the lower chamber also changed the same way as the total NO change. More importantly, after PBS was applied on top of the NO source and the same LED driven current was used (same light energy was used to initiate the same NO release), NO flux through the membrane remained constant (Fig. 3.14 A blue line after green arrow). However, the NO signal sampled from the upper chamber decreased dramatically (Fig. 3.14 A red line after green arrow). This is expected since thick PBS layer slowed down NO diffusion such that NO auto-oxidation has more time to occur, which also explained why the device membrane needs to be thin. Linear regression analysis (Fig. 3.14 B) further demonstrated that the bathing solution on top of NO source will not affect the NO flux into the lower chamber (Fig. 3.14 B, blue slope remained after PBS addition), although it greatly decreased the detection sensitivity from the top chamber (Fig. 3.14 B, red slope declined after PBS addition). It is also worth pointing out that although the signal detected in the upper chamber dramatically decreases, the NO production still increases linearly with increased LED drive current (Fig. 3.14 B).

This data proved again the feasibility of cross-membrane measurement, and suggested that NO signal measured from the lower chamber is linearly related to the total NO

generated from the source, which is particularly important for later calculation, that is, the measured NO value is directly proportional to the total NO. So $J_0 = k \times J_{Tr}$, where k is a factor determined by system parameters (including membrane properties, source properties and states, will be discussed later).

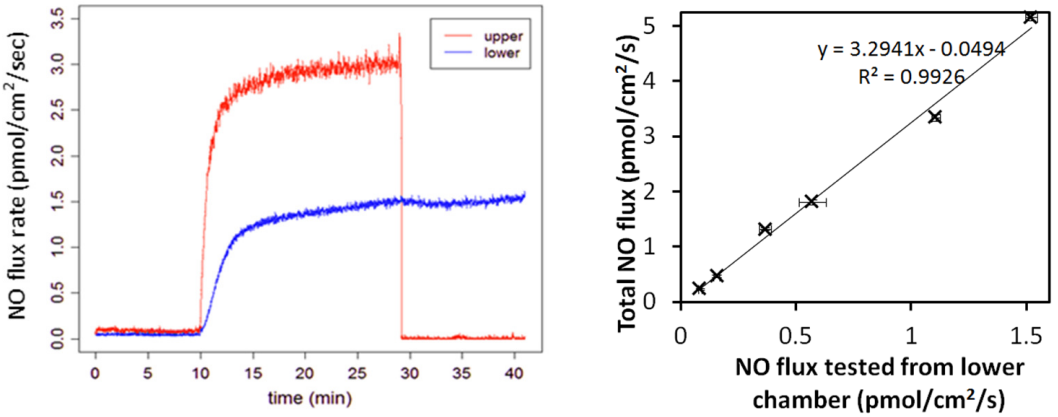

(A) (B)

Figure 3.15: Linearity of the detected NO signal over the total NO generated in culture conditions. (A) experiment procedure was the same as in Fig. 3.14; complete culture media was used as the bathing solution in the upper chamber; (B) linearity test of the detected NO signal to the total NO. Media NO_2^- levels quantitated by Griess assay were used to estimate the total NO fluxed into the upper chamber, and the total NO generation was represented by the sum of the total NO_2^- cumulation in the upper chamber and the total NO sampled by the NOA in the lower chamber.

To examine whether a linear relationship still exists in real cell culture conditions and culture media above the NO source will influence the NO measurement by sampling form the lower chamber, the PBS bathing solution was changed to normal complete DMEM. As shown in Fig. 3.15 A, NO diffusion into the lower chamber and cross-membrane measurement were not influenced by the applied culture media. Linear

correlation of total NO generated and the NO sampled from the bottom was also examined. Once the upper chamber was filled with media solution, the NO signal cannot be directly measured by the NOA at this point. To quantify how much NO entered the bathing solution, after NOA sampling the media was collected and applied to Griess assay to calculate the cumulative NO_2^- level. So that the total NO generated was calculated as the sum of NO measured from the lower chamber and the total NO_2^- quantified from the media sample. Result was shown in Fig. 3.15 B, showing that when the upper chamber was filled with media, the NO signal obtained from the lower chamber is also linearly related to the total NO generation.

3.5 Real-time measurement of NO from cultured living cells

3.5.1 NOA calibration

The calibration process for measuring cellular NO requires slight modification compared with measuring NO coming from a specific NO donors or NO releasing materials. For chemiluminescent detection, NO is continuously sampled into the reaction chamber of NOA, where it reacts with excessive ozone (O_3), converting sampled NO into NO_2^*. The relaxation of NO_2^* to its ground state results in the release of energy in

the form of light (red and near-infrared, [87]). The final quantification is dependent on the counting of light energy. However, if NO is consumed before entering the reaction chamber, the NO results will be underestimated. To avoid this, the sampling process needs to be carefully controlled. Once NO is generated, it needs to be carried by the sweep gas immediately for the chemiluminescent reaction and the sweep gas needs to be inert to minimize NO loss during sampling (usually several seconds depending on the set-up). So before NO measurement occurs, the whole sampling line needs to be swept by N_2 for 10 min. However, this is not feasible for the NO measurement from cell layers, because cells need a continuous supply of CO_2 and O_2 with their aqueous environment. A dry sweep gas leads to changes of those parameters and cell dehydration.

To prevent the potential oxygen tension reduction within cells media, ambient air (air drawn from the cell culture incubator with 5% CO_2 and high moisture) was used as the sweep gas to carry NO into the NOA and zero calibration gas for the NOA in all cell experiments. To investigate how different it is when using ambient air compared with house nitrogen as the sweep gas, the NO flux from SNAP-PDMS films were measured by using both pure nitrogen and ambient air.

Fig. 3.16 A shows the representative NO releasing profiles tested using nitrogen and ambient air, respectively. Linear regression analysis showed linearity was good for both experimental conditions (R=0.9999 and 0.9998, while the slopes obtained were

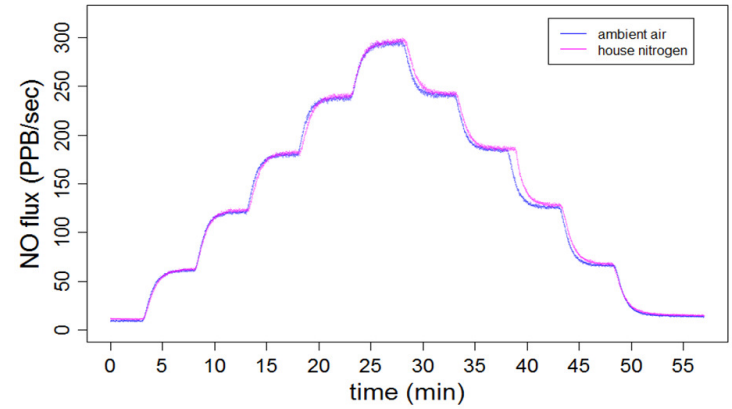

(A)

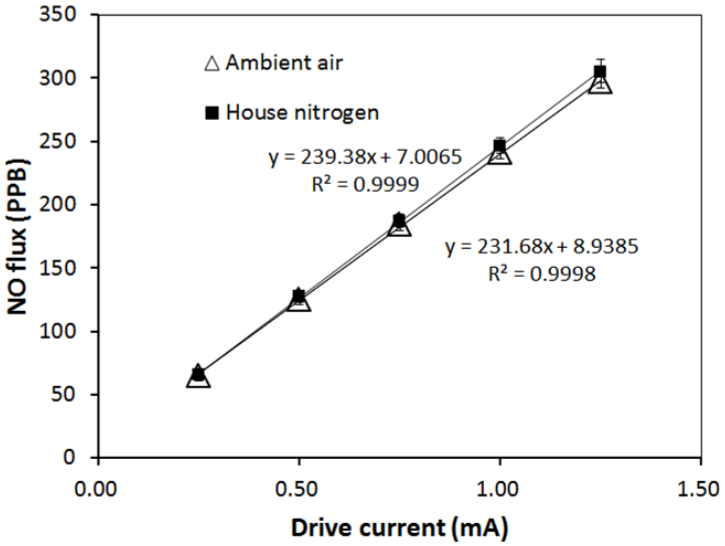

(B)

Figure 3.16: The effect of ambient air as sweep gas to NO signal. 15 mm diameter, 0.2 mm thick RTV-3140 coated SNAP-PDMS was exposed under different LED light intensities by changing the LED drive current. House nitrogen and ambient air were used as sweep gas for independent experiments. (A) Representative curves of NO surface flux detected through nitrogen and ambient air by the same NOA. Three independent experiments were run. (B) Linear regression analysis of NO flux vs. LED drive current by two different sweep gases. Though the slope values indicate around 3% loss of signal by using ambient air, paired student t-test applied to each value obtained at different drive current shows no significant difference between the two groups.

239.38 PPB/mA and 231.68 PPB/mA for N_2 and ambient air, respectively); a slight decrease of detection sensitivity (slope in Fig. 3.16 B, 3.2% decrease) was observed in ambient air group. This is an indication that there is a tendency of losing some NO signal by sampling with ambient air because of the autoxidation of NO. And this effect might be more obvious if a trap (for collecting condensed water in the sample line) was added. However, by paired student t-test there is no statistically significant difference between the two groups (P=0.1926), indicating the feasibility of using ambient air as the sweep gas for NO measurement. To obtain accurate NO signal, it is highly recommended to run NOA signal constant calibration. 100 μl of 500 μM $NaNO_2$ standard was injected in freshly prepared acidified Lugol solution (acetic acid/Lugol solution 5:2 v/v).

$$2NO_2^- + 2I^- + 4H^+ \longrightarrow 2H_2O + I_2 + 2NO$$

Scheme 3.1: NOA calibration.

The total NO signal (PPB) was calculated through integrating NO profile curve. The constant was calculated through:

$$Calibration \quad constant = \frac{100\mu l \times 500\mu M}{TotalPPB}(mol/(ppb.sec)) \tag{3.3}$$

3.5.2 The enhancement of NO signal by using new measurement device

Direct NO sampling from the culture flask led to great NO loss, (explained and proved in 2.1.1). The signal damper of NO generated from the cultured macrophage cell line RAW264.7 has also be shown in 3.2. The reported average rate of NO production following LPS and IFN-γ stimulation was 2.6 pmol/10^6cell/sec [29]. So RAW264.7 cells were used again to test whether the new design can achieve real-time NO measurement and the signal sensitivity can be improved.

RAW264.7 cells were cultured within the device (to 0.5-1$\times 10^6$cell/cm^2) and stimulated with both 10 ng/ml IFN-γ and 100 ng/ml LPS. Right after stimulation, the device was connected to the NOA sampling inlet which was mounted in the cell culture incubator and connected to the NOA (Fig. 3.9 D). Collection of continuous NO release data lasted for 24 h.

Figure 3.17 shows the NO profile measured by both directly sampling from the culture flask (blue) and the lower chamber of the two-chamber system (red). From the raw PPB data and the surface flux data (normalized to culture surface area, this will be discussed in detail in 3.5.3), both methods achieved real-time NO measurement and the NO generation trends are similar (NO flux peak occurred at around t=8 h),

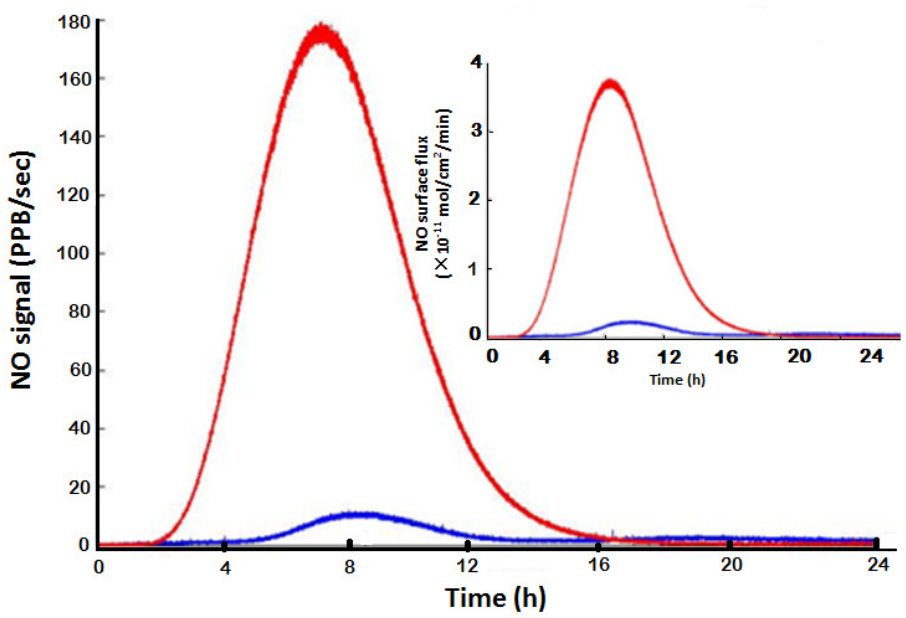

Figure 3.17: Validation of measuring NO generated by cells in real-time by using the two-chamber system. Blue line represents directly sampling NO from the T-25 flask; red shows data collected from the two-chamber device.

but the two-chamber system greatly increased the sensitivity of the measurement. One obvious advantage is that when NO level is low at the initial stage (t=2 to 4 h), the two-chamber system still captured the signal and was able to track the NO level change more readily. This is because of the thin NO permeable layer (<20 μm) minimally inhibited NO diffusion, therefore it experiences significantly fewer consumption reactions compared with passing through the culture media (which is normally at least several mm thick).

3.5.3 NO flux calculation and NO data report

In most NO work, NO is normally described by its overall equilibrium concentration mol/l, which is very useful to study its chemical properties. However, the duration over which cells experience NO is important in determining the ultimate effect the NO will have physiologically. But much NO research fails to discuss this variable because such information is hard to obtain. This new chemiluminescent method achieves both absolute NO quantification and tracking NO change with time. The raw data is given by X PPB or PPM (volume ratio). Depending on the sampling rate, it is reported as PPB/sec or PPB/min etc.

After calibration by known amount of NO_2^- (mentioned in 3.5.1), the PPB (or PPM) number can be convert to x_1 mol/sec, where $x_1 = X \times calibrationconstant$ (constant mol/PPB/sec). When cells form a homogeneous layer, the culture surface will be A cm^2. It is noted that this is not the surface area of the cells themselves, and is used (for more convenient and reproducible normalization) to calculate the NO flux as $\frac{X \times constant}{A}$ (mol/cm^2/sec) or further converted to pmol/cm^2/sec or mol/cm^2/min, which is a more widely used surface flux unit in characterizing NO generating materials. The use of this dimension with time parameters more accurately and comprehensively describes the NO status of the system. And this dimension is useful in calculation as well, because this makes the measured value and the simulation result

and NO delivery data comparable.

Another more practical dimension is pmol/10^6cell/sec for investigating cellular NO production. It is easy to understand that his dimension is more useful in when discussing NO and cell behavior. Cell number needs to be determined to obtain such values. For example a batch of cells produces X PPB NO per sec; this time using calibration constant to get X $\times$ constantmol/sec and normalized to cell number (N cells) by $\frac{X \times constant}{N}$ mol/cell/sec. Considering the calculated value will be very small when only discussing one single cell, and also our measurement method does not target one single cell, instead, it measures an overall fashion of all cells under investigation, pmol/10^6cell/sec is used in the end, which may be more meaningful.

3.5.4 Repeatability examination of the new device

It is necessary to understand how different batches of manufactured devices affect the final measured result. Is manual casting controllable enough to produce device with consistent properties? To test the repeatability, RAW264.7 cells were cultured within the different batches of device (for 1-2 days to allow the cells to be confluent to form a relative uniform cell layer so that cell density could be relatively stable, normally to 0.5-1$\times 10^6$cell/cm^2) and stimulated with both 10 ng/ml IFN- γ and 100 ng/ml LPS. Recording of continuous NO release lasted for series of time duration depending on

specific cases (usually 17-48 h for RAW264.7).

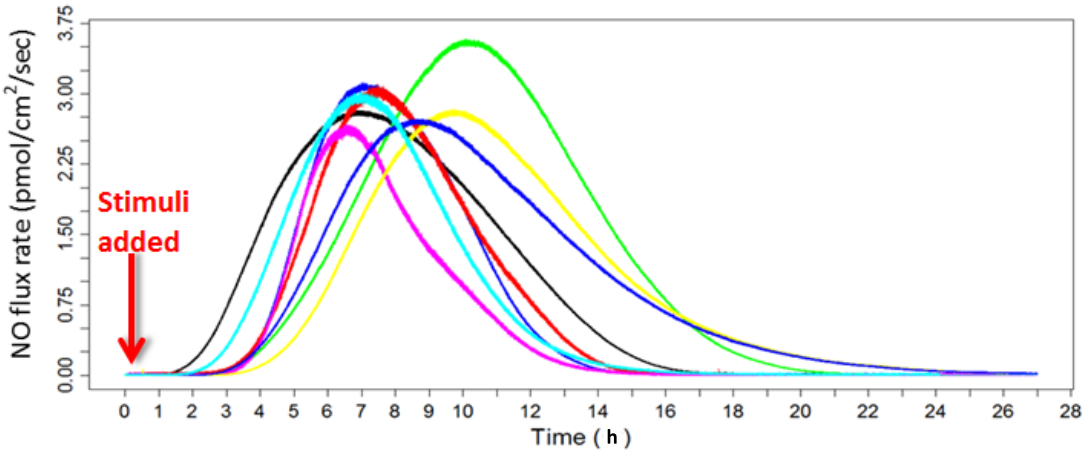

Figure 3.18: Macrophage cell-line RAW264.7 real-time NO releasing patterns. Different colors show different repeats; data was collected by using different batches of devices to culture RAW264.7 cells.

Fig. 3.18 (each color represents one culture replicate) summarizes real-time NO releasing profiles, with similar peak shape, especially the time when the maximum NO production occurred. Experimental data from the NOA was recorded as PPB/sec. Then PPB raw data was converted to pmol/cm^2/sec according to the method introduced in the previous section. To further evaluate the repeatability of this method, different sizes of device were also used for culturing cells. Normally the NO signal started to appear between 2-3 h. The decrease of NO generation rate after 8 h might be because the cell death rate increased significantly at hour 8 (according to the live-dead assay). So that cells gradually lost NO generation ability. Overall,

by using different devices manufactured through manually casting PDMS on glass-fiber filter paper, the measured NO profiles showed very consistent results and good repeatability.

3.5.5 NO generation rate normalized to cell number

To more precisely understand how much NO was produce by cells the rate of NO generation was normalized to cell number. One of the drawbacks of the cell measurement device is that although the cells can be observed through fluorescent labeling, the current membrane is not compatible with conventional visible light microscopy. However, by fluorescent staining, the number of cells that actively generate NO can be determined and counted by applying NO staining.

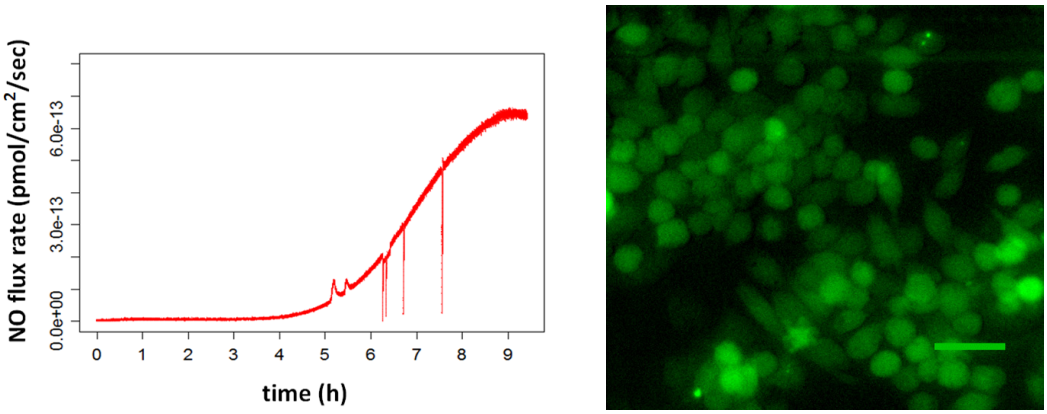

(A) (B)

Figure 3.19: Normalization of NO releasing rate to cell number. (A) cell NO releasing rate was measured by the NO measurement device, (B) NO releasing cells were stained by NO staining DAF-FM-AD (5 μM) and cell number was counted under microscope, scale bar: 30 μm.

To do this, after specific NO measurement operation (Fig. 3.19 A), cells were removed from incubator and stained with the NO dye DAF-FM (or Calcein-AM and EthBr); then cells were counted under the microscope (Fig. 3.19 B). DAF-FM diacetate is very sensitive to low NO concentration and can passively diffuse across cellular membranes and be deacetylated in cells so that the turned-on probe's leaching from cell is limited [162]. DAF-FM directly indicated which cells produce NO and was used to determined the NO positive cell number.

Table 3.1
RAW264.7 cell NO generation rates stimulated by 100 ng/ml LPS and 10 ng/ml IFN-γ

	Average	St.d.	95% Confidence area
AVG Flux rate (pmole/10^6cell/sec)	1.73	0.63	1.73± 0.72
Max. flux rate (pmole/10^6cell/sec)	3.48	0.95	3.48±1.08
Adjusted AVG Flux rate (pmole/10^6cell/sec)	2.23	0.81	2.23±0.92
Adjusted Max. flux rate (pmole/10^6cell/sec)	4.47	1.22	4.47±1.38

Table 3.1 Row 1 and 2 summarize this data. This number only represents NO detected from the lower chamber. To back calculate the total NO released, culture media was collected from the upper chamber after NO sampling for analysis with the Griess assay.

Since the total NO flux (n_{total}) is directly proportional to the measured NO value in the gas phase (n_{NO}), it is needed to determine the ratio k (explained in 3.4.2). To do this, NO entering the upper chamber ($n_{NO_2^-}$, remained in the media as the form of NO_2^-) was determined by measuring cumulative NO_2^- through Griess assay. The

constant k is calculated through.

$$k = \frac{n_{NO_2^-} + n_{NO}}{n_{NO}} \tag{3.4}$$

Then

$$n_{total} = k \times n_{NO} \tag{3.5}$$

In theory, with the same device quality and cell culture condition, this constant should be the same among different devices. However, it was noticed that some variations still exist between different devices. So each and every sample was applied to this method to calculate a specific k to calculate the total NO production. The total NO generated by the cells should be presented as in Table 3.1 Row 3 and 4, which is very consistent with the previous report [28, 29, 156].

3.5.6 Factors that may influence observed NO distribution

In our system where NO is generated from the source plane, NO will only have two routes, it will be trapped in the solution in the upper chamber or sampled by NOA from the lower chamber. Source dimension (thickness of NO source), attachment and membrane properties were studied to investigate how those factors influence NO distribution. For quantifying NO entering the lower chamber, the NO release curve obtained from the NOA was directly integrated, while for NO remained in upper

chamber, the ultimate oxidization product of NO in the solution in upper chamber was estimated through the Griess assay. Their relationship was presented in Fig. 3.20 (open circles), showing that more than half of the generated NO can be sampled by NOA by using the device, while only 21.8% was trapped in the media.

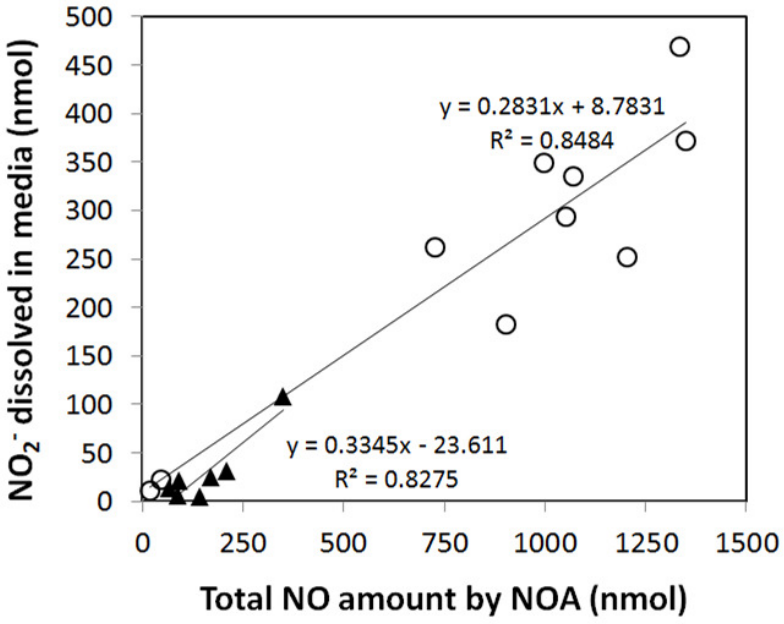

Figure 3.20: Linearity test between NO captured by NOA and NO dissolved in the media. The total NO signal was calculated through integrating the area under the curve. NO trapped within the media was quantitated using Griess assay. Data points were plotted in the hallow circles. 35 μl of SNAP-PDMS solution was dissolved within 1 ml toluene and cast onto the 60 mm NO measurement device and top-coated by 1 ml RTV-3140 solution, which generated around 25 μm (by calculation) thin SNAP-PDMS layer as the NO source, which mimicked the cell layer. Data points were represented by the dark triangles.

This is contradictory to the previous observation, the result shown in Fig. 3.14 B, where only 23.4% of NO were detected by the NOA, 76.5% remained in the media when using SNAP-PDMS for device validation. It is suspected that the main reason is

the thickness of the NO source. Compared with cell layer (for RAW264.7, less than 15 μm thick), the SNAP-PDMS film used was much thicker (over 200 μm). The effect of a thicker film on the device membrane may influence the final distribution of NO (i.e., retarded NO diffusion into the lower chamber by effectively increasing the thickness of the membrane through which NO will diffuse). So a thinner SNAP-PDMS layer (up to 25 μm by calculation) was directly cast on the device and top coated with RTV-3140 to mimic cell generating NO from a thin cell layer. PBS solution was applied on top. Still NOA recorded the NO flux in the lower chamber across the membrane and Griess assay tested the NO that entered the bathing solution. Then NO amount in each repeat was summarized in Fig. 3.20 dark triangles. In this case similar NO distribution to the cell culture experiment was observed (with 25.07% trapped in bathing solution and 74.93% NO went to NOA), proving our hypothesis that the thickness of the NO source can affect the final NO distribution during measurement by using the device. Also this data validated the measured cellular NO result and indicated that our method samples the majority of NO generated by the cells.

It was also noticed that when using NO releasing films, tighter attachment to the device membrane resulted in higher measured value in the lower chamber. This is easy to understand since the tighter attachment created larger concentration gradient between the NO source and the NO permeable membrane, which is favored by faster diffusion.

Thicker device gas-permeable membrane can make the distribution ratio more complicated. Since there might be significant consumption reactions taking place within a thick membrane and thereby changing the fate of NO, NO's fate changes. It not only affects upper/lower NO distribution, but also changes the calculation to obtain the total NO produced. So in our cellular NO experiment, we only use membrane with 100% relative permeability.

Understanding the NO distribution ratio can be useful for understanding the quantification principles and fate of NO within our measurement system. The result can also be validated roughly by this ratio to avoid potentially serious errors.

3.5.7 More data validation by using Griess assay

To verify the NO results obtained by this new method, we also ran the Griess assay, a conventional NO measurement method, to measure the accumulated NO at different time points in cultured media and compared these results. RAW264.7 cells were cultured in both 6-well cell culture plate until confluent (around 10^7cell/well) and our device (60 mm diameter, $1.07 \pm 0.65 \times 10^7$cell/device). Then old media was removed and 2 ml new DMEM media with 100 ng/ml LPS were applied to the wells and 5 ml to the devices. The device was connected to NOA for real-time measurement. The cumulative NO calculated from integrating real-time NO profile from

the NOA was plotted in Fig. 3.21 (circles). While for the 6-well plate, samples of the media was collected at different time points and tested with Griess assay. Fig. 3.21 squares show the time-dependent cumulative NO_2^- within the 100 ng/ml LPS stimulated media. Results show a similar trend, that is before t=4 h, NO_2^- accumulation is mild (0.35±0.51 nmol/10^6cell by Griess assay, 2.46±0.12 nmol/10^6cell by NOA); there is a sharp increase of NO_2^- from 4 h to 11 h (to 17.23±1.95 nmol/10^6 cell by Griess assay and 30.32±4.50 nmol/10^6cell by NOA); after 11 h, NO_2^- signal changed slowly, suggesting a slow-down of NO generation rate from 11 h to 16 h (to 17.51±3.52 nmol/10^6cell by Griess assay and 33.30±3.30 nmol/10^6 cell by NOA), which suggests the time response of our method is reliable. However, the total NO generation determined by Griess assay were significantly lower (around 50% of the result obtained with the two-chamber device). This is consistent with Hunter's report [146], indicating underestimation problem associated with using the Griess assay to estimate the NO generation in biological application.

The reaction of NO in biological condition might be complicated and it is also not safe to assume all produced NO and NO oxidation product is trapped in the media. Our data showed directly that NO can escape from the media. Meanwhile, chemiluminescence has much smaller limit of detection compared with Griess assay and provide time variable information directly.

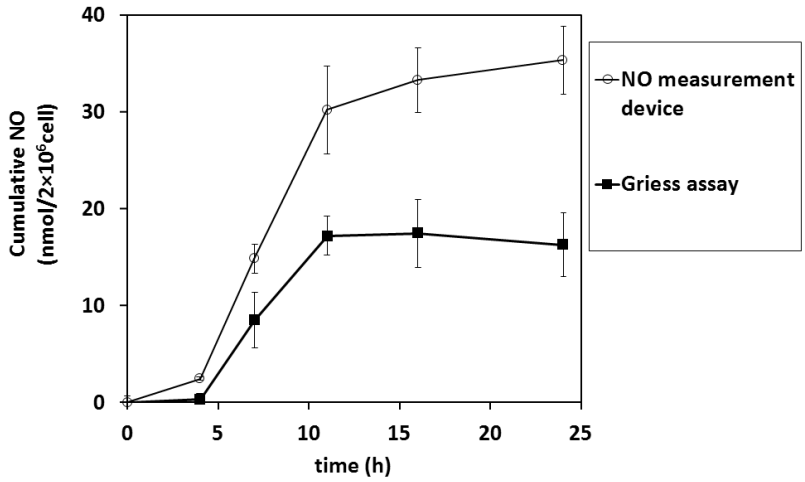

Figure 3.21: Validation of the new NO measurement method by comparing our result with the result obtained by Griess assay using 100 ng/ml LPS stimulated RAW264.7.

3.6 Investigation of the temporal profile of NO production from RAW 264.7 cells

It has been shown that by using the measurement device the dose-dependent biological effects of NO can be efficiently studied, but we still lack data that shows how the temporal effect of NO plays a significant role in determining the ultimate biological response. Here we demonstrate three examples showing how this NO measurement device can help us understand the timing of NO generation, which can potentially provide extra dimensional (time variable) information to NO studies.

3.6.1 Investigating temporal aspect of NO production under different stimuli

IFN-γ and LPS can stimulate NO in a synergetic manner because the total accumulation of NO end-products is greater when both agents are used [156]. To understand this statement, different combinations of stimuli (IFN-γ and LPS) were applied to the same passage RAW264.7 cells. Right after adding the stimuli, cells were applied to NOA sampling line for NO measurement.

Fig. 3.22 shows the real-time NO releasing profiles from the same batch of RAW264.7 stimulated by 10 ng/ml IFN-γ alone, 100 ng/ml LPS alone, and both added at time zero. Fig. 3.22 B-D focus on the initial stage of NO profile after stimulation, showing that in all the groups, NO generation started at around 2 h after stimulation, indicating that both pathways need at least 2 h to respond the stimuli to produce NO (the NOA has a detection limit of 0.5 PPB, a 1 PPB increasing of the average rate was considered to be the start of cellular NO generation; no significant difference among groups in regards to time required to initiate NO production was observed).

Noda et al. [156] reported the 24 h iNOS expression pattern after stimulating RAW264.7 by 100 ng/ml LPS using Western blot. Though this is an indirect NO quantification method, iNOS catalyzes NO production in a Ca^{2+}-independent way,

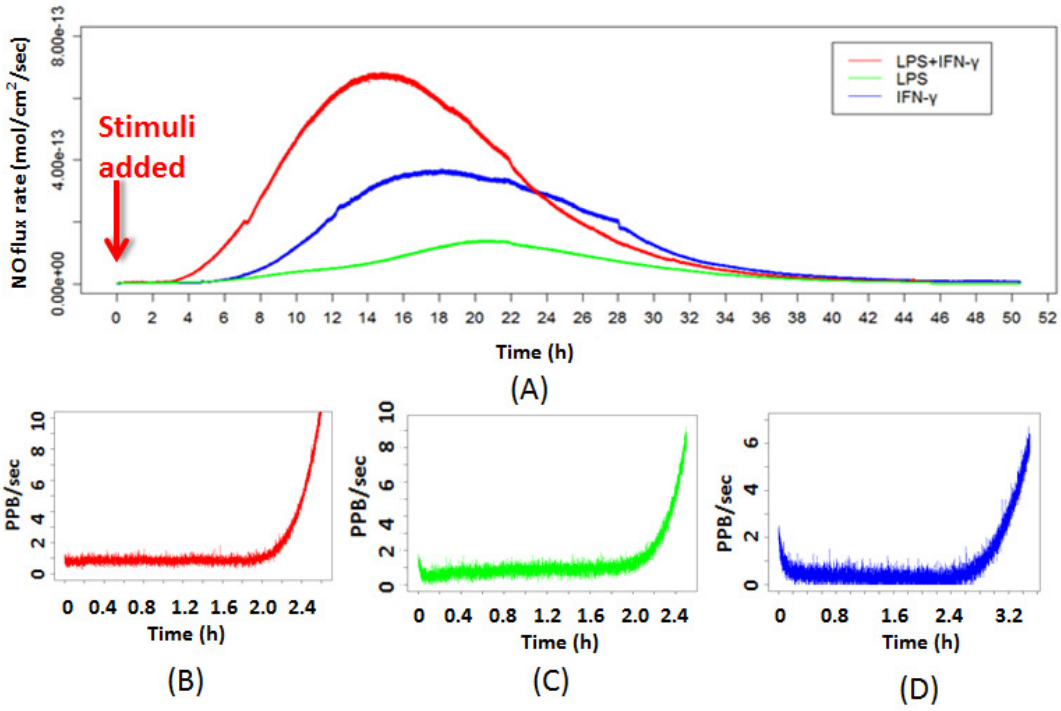

Figure 3.22: Synergetic effect of LPS and IFN-γ to RAW264.7 NO generation. NO flux was normalized to surface area. (A) Representative profiles of RAW264.7 NO releasing under different stimuli. 100 ng/ml LPS , 10 ng/ml IFN-γ or a combination of the two were applied to stimulate the cells. The experiment and analysis were run by groups. The same group means the same cell passage, the same seeding density, the same prepared PDMS-coated filter paper and the same culturing time. (B)-(D) larger culture dishes (100 mm dia.) were used to increase the signal strength, showing the time point when NO signal starts to be detectable is almost the same among groups.

so it is agreed that the presence of iNOS means the presence of NO. The earliest immunoblotting band was characterized at 4 h. But it was not clear whether there was actual NO production before 4 h after LPS stimulation due to their lack of sampling points and maybe detection limits. However, using much simpler experimental operation procedures, it is proved here that the NO signal appeared 2 h after stimulation. This method clearly showed how soon the stimulated cells begin to produce

NO, the rate of NO production, the maximum level of NO produced by each stimuli individually and how long the NO production persists under static culture conditions (without media change after treatment).

More detailed quantification can be carried out according to the NO profiles as well. For example, IFN-γ and LPS alone initiated NO production with maximal surface flux reaching 2.4×10^{-11}mol/cm^2/min after 18 hours and 1.2×10^{-11} mol/cm^2/min after 22 h, respectively (measured value from the lower chamber only). When the same amount of IFN-γ and LPS were added together, NO production reached a maximal surface flux of 4.2×10^{-11}mol/cm^2/min (measured value from lower chamber) after only 15 h. Real-time, experimental data directly showed the increase in NO production when LPS and IFN-γ are added together is greater than either of them used separately. Integrating the area under the NO release curves allows the total dose of NO released to be calculated. Table 3.2 summarizes the integrated data from the NO releasing curve, Row 1-3.

Compared with Noda's report [156] (around 400 nmol/10^6cell and 100 nmol/10^6cell for LPS with and without IFN-γ within 24 h respectively), these numbers (around 50 nmol/10^6cell and 35 nmol/10^6cell for LPS with and without IFN-γ within 24 h respectively shown in Table 3.2) are far smaller. Cell viability tests indicated that in our system cells started to die at a high rate after 8 h of stimulation; the pH indicator in cell media also showed the pH changed greatly between 8 to 12 h after stimulation.

Table 3.2
Total NO generation of RAW264.7 cell 24 h after treatment by using different NO inducing agents.

	Total NO release (nmol/10^6cell)	**Std.**
100ng/mL LPS	35.37	2.90
10 ng/mL IFN-γ	30.29	14.4
100ng/mL LPS + 10 ng/mL IFN-γ	52.77	16.9
100ng/mL LPS + 10 ng/mL IFN-γ (Low cell number) $\star$	405.6	54.7
100ng/mL LPS + Arg at 4 h Δ	199.4	63.1
100ng/mL LPS + Arg at 8 h	63.10	17.3
100ng/mL LPS + Arg at 12 h	70.30	22.7
100ng/mL LPS + nor-NOHA at 8 h	45.20	8.41
101ng/mL LPS + L-NAME at 8 h	33.57	2.51

Result is from the integration of the NO releasing time-flux curve. NO generation was normalized to cell numbers (10^6 cells). One way ANOVA and Tukey's test were run by R program. $\star$, $P < 0.05$, compared with all the rest groups. Δ, P is close to 0.2, compared with all the other groups. Others are > 2.

It is suspected that in current system, the relative cell number might be too high compared with Noda's model, which affected cell normal growth and suppressed NO generation. So next, cell density was reduced and the measurement experiment was repeated.

3.6.2 Investigating NO production tempo change due to different cell density

Initially to obtain enough NO signal, high cell densities (to 5-10 $\times 10^5$ cell/cm^2) were used in all experiment. High cell density led to fast cell death after NO stimuli were added. This might result from a combination of fast nutrient consumption and too high concentration of NO and other metabolic products which leads to fast change of media pH. Since it is noticed that in low cell density environment, after the same stimuli treatment, cell survived for longer periods of time, a systematic study on the relation of cell density and NO profile was carried out. RAW264.7 were seeded and cultured to 1-2 $\times 10^5$cell/cm^2. Then media with 100 ng/ml LPS and 10 ng/ml IFN-γ was used to treat the cells. Right after LPS administration, cells were applied to NOA sampling line for NO measurement.

Fig. 3.23 showed that using the same stimulants with a lower cell density $1.24 \pm 0.18 \times 10^5$cell/cm^2 compared to $5.56 \pm 0.33 \times 10^5$cell/cm^2 in Fig. 3.23), NO release profile can be greatly altered. Compared with results in Fig. 3.18, NO signal also started between 2-3 h, but the NO release profile was elongated. Additionally, the rate of NO generation continued to increase until up to 18 h (red). Compared with the high cell density groups, NO flux per unit cell in the lower density groups was significantly increased (the maximum flux was 7.65$\pm$1.3) and the total NO generation

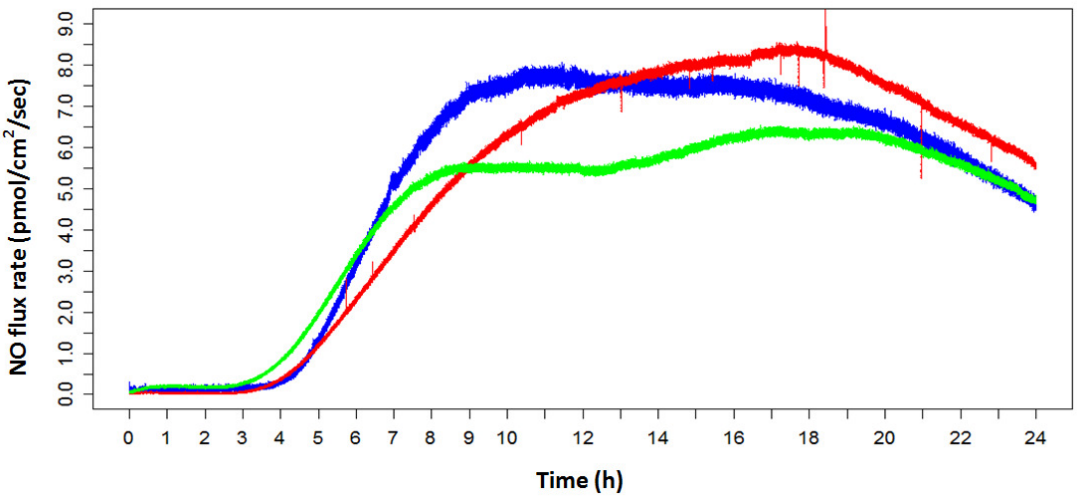

Figure 3.23: Real-time NO releasing profiles of low cell density RAW264.7 cell culture. Cells were cultured within the NO measurement device (60 mm diameter) to a total of $1.24 \pm 0.18 \times 10^6$ cell/cm^2. Cells were stimulated by 100 ng/ml LPS and 10 ng/ml IFN-γ at time zero. Three different colors represent 3 repeats.

per unit cell (by integrating area underneath the curve from 0 to 24 h) also increased greatly (summarized in Table 3.2). This phenomenon is important, because this data directly shows how flexible NO production can be due to the change of one single factor such as different cell densities. In this case the ultimate NO generation are two times larger than Noda et al.'s report [156] but within the same order of magnitude. Note that, parameters such as the on-set time, total NO generation, maximum NO flux and signal duration of NO signal are dependent on cell numbers cultured in the device and media conditions. Static culture may associate with great environment changes especially after 24 h. So to study the on-set time, it is recommended to use high cell density model that shown in Fig. 3.22 B to D. To study NO levels, defining specific conditions is needed. Obtaining such information and discussing NO profiles

need more precise control over the experiment conditions mentioned before, which is beyond the scope of this study.

This might be one of the reasons why there were significant variations of NO generation rate reported by different groups. Cellular NO production rate can be very sensitive to the cellular environment. This highlights the importance of real-time measurement of every experiment and controlling the culturing conditions to obtain consistent results in NO generation from these cells otherwise results from different replicates or methods are not comparable.

3.6.3 Tracking the change of cellular NO production due to administration of other chemicals

Modulating the NO level to recover normal biological functions is the ultimate goal of all NO research. Currently, there is no standard method to test and quantify the potency of certain drugs. Drug's time-dependent potency and how much change in NO levels can be introduced by those drugs are hard to evaluate. Since the new device directly targets the measurement of NO and provides quantitative and temporal information, it may be a very useful tool to study the modulation of NO level.

Since arginine is the most important substrate for NO generation, we examined the

relationship between NO generation and the arginine pathways. In RAW264.7 in vitro cultures, high doses of NO were produced, consuming large amount of Arg. Also, as a competing pathway, arginase catalyzes the urea cycle reaction which consumes arginine to form urea [163], thereby shunting arginine away from the NO production pathway. The arginine concentration might be an important limiting factor for NO production. In our study, exogenous arginine (an additional 1 mM) was added; the arginase specific inhibitor nor-NOHA (20 μM), and iNOS inhibitor L-NAME (50 μM) were added to 100 ng/ml LPS stimulated RAW264.7 cells (cell density used was 0.5-0.7$\times 10^6$cell/cm^2) to show the ability of monitoring real-time NO generation changes of the device.

One advantage of the two-chamber measurement system is that the cell culture and NO measurement can be carried out independently but simultaneously. Treating cells and sampling can be processed simultaneously without losing data or generating confusing noise, so that the change in NO generation introduced by condition changes can be tracked in real-time. After RAW267.4 cells were stimulated with 100 ng/ml of LPS and applied to the real-time NO measurement system, arginine was added at different time points into the cell culture media. Fig. 3.24 A-C show that, right after Arg addition, the rate of NO production underwent a sharp increase. Considering time as a factor, the degree of increase in NO production upon the addition of Arg was significantly different at different time points of stimulation. When arginine was added at 4.5 h after stimulation, NO production increased slightly from 0.46 to 0.57

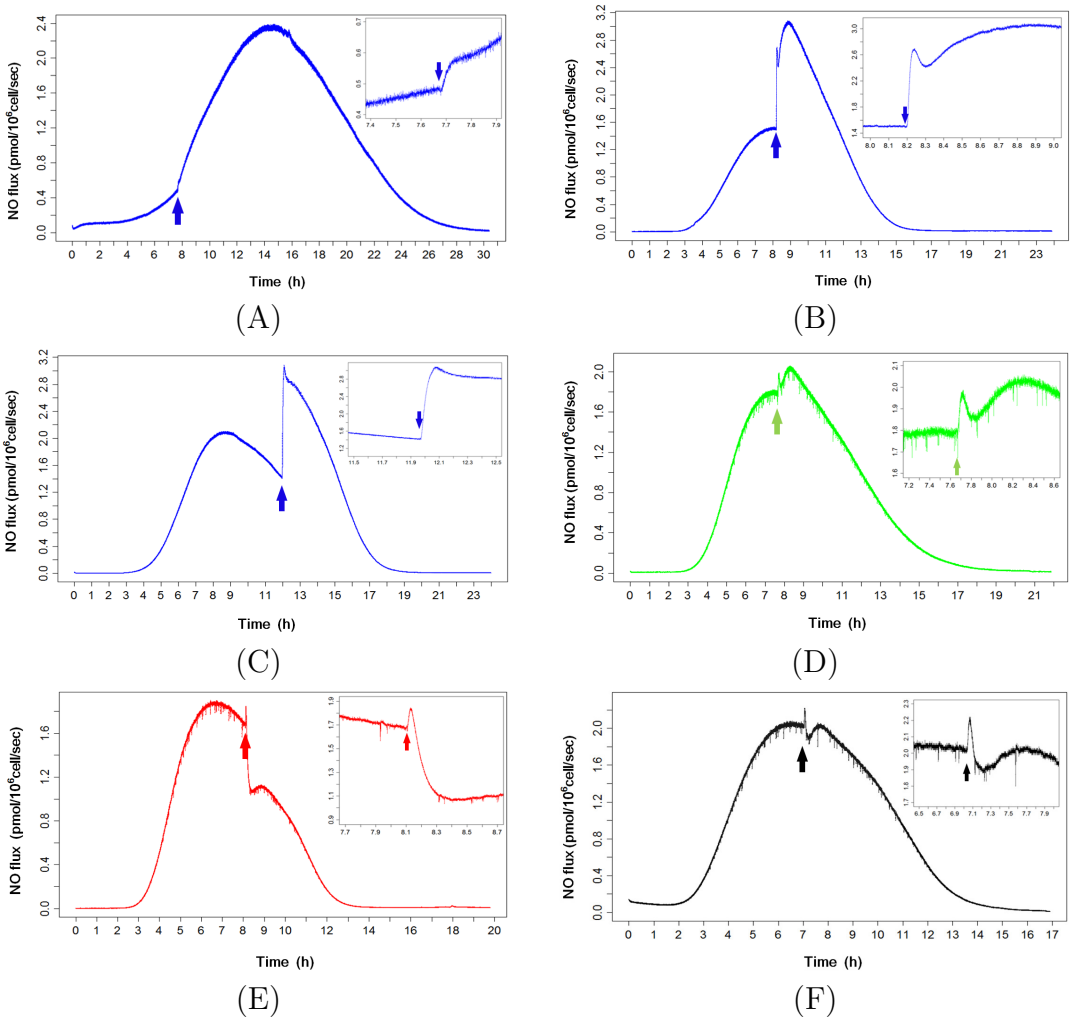

Figure 3.24: Change of NO generation profile monitored by NOA under different chemical treatment. 100 ng/ml LPS was used to stimulate RAW264.7. The curves at the up-right corner of each plot are the expanded plots focusing on the change. (A)-(C) 500 mM Arg stock solution was added into the media at different time points (indicated by blue arrows) during cell culturing (resulting in 1 mM exogenous Arg in the culture media). (D) Nor-NOHA (final concentration of 20 μM) was applied to the culturing media (indicated by green arrows). (E) L-NAME (final concentration of 50 μM) was applied to the culturing media at about 8 h (indicated by red arrows). To allow a homogeneous distribution of the chemicals, device was gently shaken after chemical addition. To eliminate the possibility that the experiment procedure itself may alter cellular NO production, control (F) was run by adding PBS and shaking device gently (indicated by black arrows).

pmol/10^6cell/sec (Fig. 3.24 A, by 28.9±4.1% on triplicates average), however, after 8 h and 12 h, NO production increased by 85.2±2.3% and 97.6±7.5%, respectively (from 2.16 to 4.37 pmol/10^6cell/sec and from 1.12 to 2.37 pmol/10^6cell/sec, in Fig. 3.24 B and C). This could be explained by different limiting factors that occurred relative to different points of stimulation. With the consumption of Arg in static culture, after 8 h, the concentration of Arg might become the main limiting factor. So replenishing the Arg substrate for NO production might significantly change the NO producing profile. While at the initial stage, arginine was sufficient.

To further directly show that arginine accessibility determines the rate of NO production can be easily observed by our device, arginase specific inhibitor nor-NOHA, (which may potentially make more arginine accessible for iNOS), was applied. Fig. 3.24 D shows 20 μM of nor-NOHA was applied to RAW264.7 after 8 h of stimulation, the NO production rate was increased from 1.99 to 2.30 pmol/10^6cell/sec (by 13.64.0%, based on triplicate average), but not as potent as supplying arginine, which is around 1 fold. L-NAME's hydrolysis product inhibits NO production by binding with iNOS with high affinity. Fig. 3.24 E showed that after supplying 50 μM of L-NAME, NO production indeed decreased from 1.68 to 1.07 pmol/10^6cell/sec (by 34.94.0%, based on triplicate average) within 20 min (see Table 3.2). To eliminate the influence brought about by the experimental processes such as opening the incubator, adding exogenous chemicals and shaking, 10 μl of PBS was applied to the cells as well (shown in Fig. 3.24 F). Shaking will potentially increase the NO concentration

gradient in the vicinity of the membrane and change the NO profiles. In fact, a small sharp peak was observed in the real-time NO profile of the control group. The quick increase and decrease of the NO signal might be because of the NO concentration gradient was quickly changed but return to the previous status again after the application procedure. The total NO releasing after 24 h stimulation was summarized in Table 3.2.

Definitely more work need to be completed to fully understand which factors are responsible for the changes in NO production in LPS stimulated RAW264.7 cells when those chemicals are added. But this devise successfully demonstrated the degree and time aspect of NO change introduced by different chemicals, which will be a good example for NO pharmaceutical study and will allow the molecular biology to be linked to direct NO measurement data, permitting the temporal aspect of NO release to be investigated.

3.7 Discussion

NO has multiple biological functions, which may be both deleterious and benevolent. The ultimate biological effects of NO might depend on many parameters, including NO concentration, duration, and NO responding mechanisms within individual cells. Many of the contradictory roles that NO has been reported to play may be in part

rooted in failing to record the different temporal NO generation profiles caused by variable environmental conditions (e.g. different cell densities). Because of the lack of knowledge regarding the dose and duration of NO cells experience, attempting to understand the roles NO plays is complicated.

Although attempts have been made to quantitatively determine the level of NO produced by cells or that cells experience, the problem remains unsolved because of the drawbacks within the measurement methods themselves. Western blot directly shows status of NOS isoforms, which have been used to indirectly indicate an increase or decrease in overall NO production. But this cannot be carried out in real-time and the actual NO level can be greatly affected by various things such as enzyme modification levels, Ca^{2+} level (for nNOS and eNOS), cofactors, NO consumption rate, competitive reactions and levels of substrates and inhibitors, too. Immunohistochemitry or immunocytochemistry reveals NOS subcellular localization, which may be indicative and interesting in suggesting localized NO production, but in fact does not directly represent the level or NO production or for what duration NO is actually generated.

Currently, immunohistochemical studies use NOS antibodies to evaluate NO's role in tumor development, which has been pointed out by many researchers as an indirect method [22, 65], as the final NO production is not solely dependent on the enzyme level. An interesting finding by Mehibel et al. [164] is that iNOS, instead of generating NO in HT1080 and HC116 tumor tissue under hypoxic condition, may function as

a reductase that activates the pro-drug into a topoisomerase inhibiter, showing how important it is to target NO directly rather than focusing on NOS level alone while discussing NO's effect in cancer cell. NO fluorescent dyes such as DAF can hardly reflect NO real-time status and most NO dyes reflect NO accumulation in subcellular localization based on solubility, partition coefficients, structures of the dyes, and even some less specific side-reactions. Other indirect measures of NO such as the Griess assay measure oxidized products, which are very likely to underestimate the amount of NO produced due to the escape of NO into cell culture vessel head-space and reactions with other biomolecules [28, 146]. NO electrochemical microprobes have been used to record NO concentration measurement and can achieve real-time measurement but there is a great deal of variability in results when using probes of different sizes and results are heavily influenced by how close the probe is placed to the actual surface of cells under investigation [147].

It is necessary to improve the current measurement method. One interesting thing is that currently the most sensitive electrochemical microsensors are able to detect NO concentrations to as low as 1×10^{-12} M [123], but NO measurement and data report is still problematic. Instead of focusing on increasing detection limit, the new method is trying to directly target NO itself, creating a biology-friendly interface, and making full use of the current detection means. In the system presented here, due to the biocompatibility and gas-permeability of PDMS based substrate, cells were able to be seeded, grown, and tested in the same device without deviating from standard

cell culture protocols. Dissolved NO was guided into gaseous phase and the flux was directly recorded. This only relies on the correct calibration of the instrument and the device. Different from measuring concentration, our signal can be enhanced by increasing the sample size. Though NOA has its own detection of limit (0.5 PPB), this limitation can be simply overcome by using larger device and higher cell number, which makes this method very economic. With proper normalization calculation, the final result will not be changed but the apparent resolution and sensitivity can be improved.

Our goal is to standardize NO data presentation, obtaining as much information as possible from the testing systems and making NO data from different laboratories comparable. Some pioneers' work reported NO generation rate in cytokine/LPS stimulated RAW264.7 cells. Normally the calculation is based on monitoring the change in NO and O_2 concentration and assuming no other NO consumption routes exist other than certain specified chemical reactions [28, 29, 96]. The range differed from 2.6±0.1 pmol/10^6cell/sec to 6.0±0.4 pmol/10^6cell/sec, which is close to but generally a little less than our result. One reason could be the calculations only considered the oxidation of NO by oxygen and superoxide, while in fact there are additional side reactions that potentially affect the overall reaction too. We highly recommend that NO quantitative data should be reported with the time variable and the specific conditions if possible, so that NO data from different labs can be more comparable.

One main problem of those results is that they reported only a single average value. It is almost impossible to extract information on time related NO level change or track the process of NO change due to the change of the factors (such as culture condition, exogenous chemical) from that data. As shown in Fig. 3.23, NO generation may be very variable. One single value may not be enough to describe this complex process, over simplified data may in fact mislead researchers. The power of the device developed in this work makes it overcome this problem, providing comprehensive time related data covering the whole experiment. So that other results can be analyzed based on the specific time points and NO status.

Wang et al. mentioned NO oxidation in the PDMS membrane of their NO delivery system [165], which potentially could be one source of NO loss in our system too. However, their membrane was around 500 μm thick, which is much thicker than the membranes used in this system. To prove that in our system, NO loss during sampling is negligible, we used controllable NO releasing polymer SNAP-PDMS to release NO with a constant rate. NO rate was measured directly and across the membrane. Result shows that there was no statistically detectable signal loss within the membrane. In this method, close measurement is a key concept, which is achieved and well controlled by fabricating the NO permeable membrane. So that NO undergoes the lowest level of chemical consumptions between its generation and being captured after across the thin PDMS layer.

Any extra treatment to cell during measurement (such as stirring, probe placement, adding extra chemicals and dyes) may potentially bring about contamination, cell damage, or alter cell behavior. Our method was able to maintain cell sheet integrity and cell growth condition during NO sampling. Cells were also easily treated with stimulants and inhibitors (such as substrates and drugs), and the resultant changes to NO generation were able to be monitored in real-time. It is clear that NO production from cells depends on a series complex of factors. But it is unclear how much each parameter contributes to this process. If all the cell work to date related to NO generation had the corresponding direct, real-time NO measurement levels to accompany the elegant molecular biology that has been completed in an effort to understand how various factors influence NO production, our level of understanding of the normal and pathological roles NO plays in health and disease would be staggering. By accurately measuring both the dose and timing of NO production in cells and tissues, we will be able to accelerate our understanding of the diverse and sometimes apparently contradictory effects of NO in normal and pathological states.

3.8 Conclusions

A two-chamber NO measurement device that is capable of measuring the level of NO produced by living cells in a continuous, real-time manner was fabricated. The design of the device was inspired by Boyden chamber. NO generated by the cells

diffuses through a hydrophobic, gas permeable membrane that serves as the bottom of the culturing dish into a gaseous lower chamber that allows NO to be swept to a chemiluminescence detector, thereby quantitating the level of NO produced by cells in real-time. The measuring ability was validated by using NO-releasing polymer (SNAP-PDMS) films that generate NO in a highly controllable manner, which allowed the functional characteristics and potential utility of this device to be investigated. The device was successfully used to measure NO generation profiles from macrophage cell line RAW 267.4 and investigate NO production changes because of different stimuli and inhibitors. However, the application should not be limited to measuring NO generated from the macrophage. Since the design is compatible for general adhesive cells, different NO releasing cells/tissues can be studies by this device too.

This is the first device to be reported that truly achieved real-time cellular NO flux measurement without disturbing the cells under investigation or deviating from standard cell culturing protocols. This device may open up a huge potential for increasing our understanding the role NO plays in both normal and pathological conditions in a variety of tissues and could potentially accelerate our ability to design NO releasing and generating therapeutic interventions by allowing quantitative understanding of both the dose and temporal aspects of NO production in cells.

Chapter 4

Understanding Soluble NO Donor by Using the Novel NO Measurement Device[1]

The great potential of the two-chamber NO measurement device relies on taking the advantage of free diffusion of NO to guide dissolved NO out from the aqueous environment to gaseous space for chemiluminescent detection, making a gas-based NO measurement possible from a solution. Moreover, this sampling process only uses the molecule's free diffusion, and minimally influencing other parameters in the solution (i.e., the cellular culturing environment is not altered) This chapter will discuss the

[1]This chapter will be submitted to a journal for possible publication in the near future.

application of the two-chamber device to monitor NO levels in different solutions, and elucidate the NO environment cells actually experience when cells are treated with soluble NO donors.

As mentioned before, NO is a very common immune regulator [24], critical neurotransmitter [19] and the most potent vasodilator [15]. NO abnormities can cause a series of diseases in a varieties of tissues. NO deficiency is closely related to chronic cardiovascular diseases such as hypertension, coronary heart diseases, and arterial thrombotic disorders [75]. To restore the correct NO level, NO releasing chemicals (NO donors) have been widely used for more than one hundred years. Currently GSNO has been clinically used to prevent the formation of thrombosis [166]. Additionally SNAP derivatives have also shown considerable potential to maintain vascular tone [167, 168]. However, caution needs to be exercised when using NO as a drug, since NO potentially brings about fatal side-effect such as shock. Different labs have their own requirements when choosing NO releasing chemicals according to their specific needs and expertise. Considering the wide range of different biological models, in vitro or in vivo studies, different target cell types, and different animal species potentially, observed results are at a minimum complicated but also contradictions abound.

Some critical concepts associated with using NO donor molecules that need to be recognized include:

1. Regardless of using an in vitro or in vivo biological system, the NO donor's analytical concentration does not represent NO level that cells or tissues experience;

   This can be explained by Eqn(2.4) or (2.10). It is easy to see that the ultimate NO level is determined by the NO generation rate, NO consumption rate and the distance between the NO source and site of interest if is not in a homogeneous system. The half-life of NO donor determines the generation rate and greatly affects the ultimate NO level. Using NO donors' half-lives, NO level may be estimated in a very rough way [121].

2. NO level that cell experiences is not determined only by the NO donor, but also by species present within the buffer solutions and culture media;

   NO is highly dynamic and reactive and biological systems are complicated, species within the biological system react with NO to a significant extent. For example in Eqn 2.12. the effect from both O_2 and O_2^- increased the consumption as a result of oxidation, may significantly reduce NO that can eventually reach cells.

3. NO donor treatment time does not accurately represent the true NO exposure time, because the NO donor moiety must decompose to deliver NO, which can be released within a shorter time period; (i.e. the donor molecule is not itself NO)

NO's chemical properties make it impossible to always maintain its level once it is generated in biological conditions. In different biological environments, the half-life of NO varies from less than a second to minutes depending on its concentration and specific environment. This means different from other stable drugs, NO's level is mainly determined by the generation process. So once the generation process is over, there will be no further NO exposure.

4. NO donor's biological effects should not be considered as equal to the effect of NO.

   NO donors contain not only the NO moiety but various functional groups and residual by-products remaining after release. Additionally some chemistry that affects cellular response may not be through NO such as direct S-NO transfer [169]. These effects can easily be confused with the effect of NO, since these two effects can be very similar and it was hard to observe the underline mechanisms. Normal experimental conditions were unable to discern this difference, until Singh et al. reported a method to detect the generation of free thiol radicals in different RSNO decomposition mechanisms by using EPR [170].

Considering the aspects of NO donor behavior mentioned above, there is a great need to understand how much NO is actually present at the cell layer during in vitro culturing to fully understand NO's roles and the factors that may affect NO levels. It is necessary to reiterate here that NO related data needs to be accurately and

comprehensively reported to avoid misunderstanding and misinterpreting data. The new chemiluminescent-based NO measurement device described in Chapter 3 can directly monitor NO level within solutions and also NO levels that cells experience during the entire duration of experiments in real-time. The NO generation profiles of different commonly used NO donors were directly measured and analyzed. Different factors that influence these profiles including cell culture conditions, pH, free thiol levels, oxidative stress and solution volume were examined in detail by using the device.

Also presented is a demonstration of using this device to illustrate the potencies of different NO donors in inhibiting MOVAS cell proliferation and observing the real-time NO level that cells experience.

4.1 Definition and quantification of cell NO level

When soluble NO donors are applied to aqueous buffer or cell culture media, donors begin to release NO. Once NO is generated, its consumption also begins. To describe the NO level in the aqueous environment when using NO donors, Schmidt et al. presented a straightforward method to calculate NO concentration by considering the NO generation rate and NO auto-oxidation [121]. The detailed method has been introduced in Chapter 2.2.

The issue associated with this method is the calculation was only applicable to solutions with simple compositions (NO consumption routes were limited), making its application to real biological environments largely inaccurate. Herein, an NO flux method is introduced, in the dimension of mole per surface area per time (or pmol/cm^2/sec or 10^{-10}mol/cm^2/min), which can be easily calculated by using the two-chamber system introduced in 3.5.

As illustrated in Fig. 4.1, the upper chamber serves as a conventional cell culture environment to which drugs (including NO donors) can be directly applied to cells through using normal cell culture protocols. While NO is present in the cell environment, NO diffuses in all directions, and most importantly, through the gas-permeable membrane into the lower chamber. Since the lower chamber is relatively independent from the upper chamber, gas in the lower chamber can be sampled by sweep gas for NOA quantification without influencing activities in the upper chamber. So that once a solution with a specific NO donor is applied into the upper chamber, the NO generation profile of this particular donor can be tracked in real-time through chemiluminescent NOA .

Previously, measuring NO flux in aqueous solution was a conundrum, preventing the wide-spread of using this in NO research. This system takes the advantage of biocompatible polymer PDMS to guide dissolved NO within the solution out into a gaseous chamber, making long-term real-time NO monitoring possible. The NO

signal obtained from the lower chamber (the measured value) directly pointed to NO level in the cell culture chamber.

The key question is what this measured value (NO level) means to cells cultured in the device? To illustrate this, two models were shown below. First, assume a tightly attached intact mono layer of cell is attached onto the device membrane to obtain the cell sheet model (see Fig. 4.1 A):

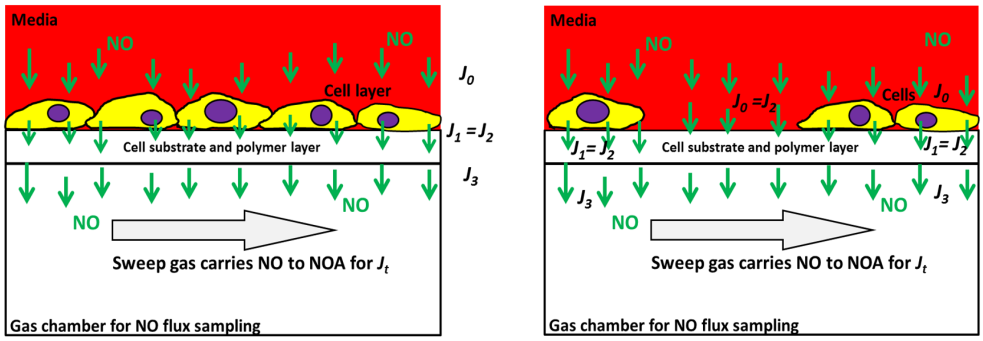

(A) (B)

Figure 4.1: NO quantification in the confluent mono cell layer model (A) and the nonconfluent cell culture model (B). Cells were cultured in the two-chamber system device to either total confluent or a specific percentage of confluency. The parameters used are labeled in the figures including: NO flux entering the cell as J_0; NO flux exiting from the cell as J_1; NO flux entering the semipermeable membrane as J_2; NO flux exiting from the semipermeable membrane as J_3; NO signal measured by NOA as J_t.

Suppose J_0 is NO flux entering the cell;

J_1 is the NO flux exiting the cell;

J_2 is the NO flux entering the semipermeable membrane;

J_3 is the NO flux exiting the semipermeable membrane;

and J_t is the NO signal measured by the NOA.

NO will be consumed through each interface such as J_0 to J_1. The decay is represented as J_c, so:

$$J_0 = J_1 + J_c \tag{4.1}$$

Predicting NO flux (J_t) at time (t) relative to J_0 or J_1 will allow the actual NO level around cells to be known.

Because cells tightly attach to the membrane, J_1 and J_2 were considered to be equal, so:

$$J_1 = J_2 \tag{4.2}$$

Also since sampling process by sweep gas in the lower chamber is a continuous and very fast process, it is considered that right after NO travels through the membrane, the signal can be detected by the NOA, regardless of the sweep gas (N_2 or air) used, such that:

$$J_3 = J_t \tag{4.3}$$

The foam-structured PDMS treated glass-fiber membrane has a relative NO permeability (η) of 100% (shown experimentally in 3.4.1), meaning the NO flux coming out from the NO releasing polymer (J_p) showed no significant difference from the measured NO flux across the membrane (J_{Tr}) (Fig. 3.13 A). So it is concluded that:

$$J_1 = J_2 = J_3 \tag{4.4}$$

In this model, from Eqn(4.2), (4.3) and (4.5), it is reasonable to use J_t to represent J_1. So the NO level that is measured by the NOA is equivalent to the NO flux coming from the cell sheet.

In the second model, if cells are not confluent (assume $k\%$ is the fractional area covered in Fig. 4.1 B), since Eqn(4.3) and Eqn(4.5) are still valid here, it is easy to obtain the following relationship to represent J_t:

$$J_t = J_1 \times k\% + J_0 \times (1 - k\%) \tag{4.5}$$

In addition, while the cell coverage ratio is very low and considering that the thickness of cell layer might be very small (around 0.5 μm thick for endothelial layer), NO can quickly diffuse across the cells (<sec, estimated by Einstein-Smoluchowski equation [76]) with negligible reaction occurrence (i.e. a very small J_c), such that J_t and J_0 might be considered as equal in very low cell density model.

In summary, there is a theoretical basis to describe the two-chamber system's utility to measure NO diffusing out from the upper chamber. Once an adhesive cell is cultured in the device, this measured NO flux J_t accurately reflects the NO coming from the cell layer (J_1) in cell layer model or a value that is closely related to J_0 and J_1, represented by Eqn(4.5). And this value is the average NO flux experienced by many cells growing on a relatively large area scale (cm^2). In this chapter, this NO

flux is used to reflects the NO level that cells actually experience (related to J_0 and J_1) when exposed to NO donors in solution.

4.2 NO generation profile study

Different NO donors generate NO with different rates and stoichiometry. It is also believed that NO generation from NO donors can be very sensitive to different buffers. This section will focus on showing how different NO profiles generated by different soluble NO donors were directly measurement and how the NO profile of a specific NO donor differs in different buffer conditions. The hypothesis is that because of the high reactivity and diffusivity of NO even using the same NO releasing chemical with the same concentration actually results in different NO levels at the cell layer when different solutions were used.

NO generation profiles of four different commonly used NO donors were examined by using the NO measurement device. In order to elucidate the NO level in real biological conditions, all the experiments were run at 37 °C in PBS buffer or complete cell culture DMEM media. The same effective concentration of NO donors (i.e. such that the same number of moles of NO were in theory generated) was used for easier comparison.

Biologically irrelevant concentration was avoided, so 50 μM of donor was used in most of the following experiments. While PBS (pH=7.4) was used as the buffer, 10 ml PBS with 50 μM of CySNO, SNAP and GSNO and 25 μM of DETA NONOate was applied to NO measurement device (manufactured from 60 mm diameter dishes). The lower chamber was sampled with atmospheric air as the sweep and zero gas. Considering the reported NO donors' half-lives [76, 171], it is estimated that these soluble NO donor systems should not have an NO level that is likely to last days. Therefore we only reported NO releasing profiles for the initial 24 h after adding donors, though GSNO and DETA NONOate continued releasing detectable amounts of NO after 24 h under these conditions.

Fig. 4.2 A to D (blue traces) show their NO release profiles. According to the real-time data, we detect the NO releasing duration and average/maximum NO generation rates of each donor. By integrating the area under the release curve, the total NO released in moles can be calculated. All those results were summarized in Table 4.1.

The reported half-lives of each NO donor are also summarized in Table 4.1 [169, 170, 172, 173]. Although half-life and NO generation duration are different concepts, the overall trend can still be suggestive. Combining these two pieces of information, CySNO did show the most rapid NO release, while GSNO and DETA NONOate generated a gradual and long-term releasing pattern. However, both the reported SNAP half-life and the NO generation duration measured by the device showed large

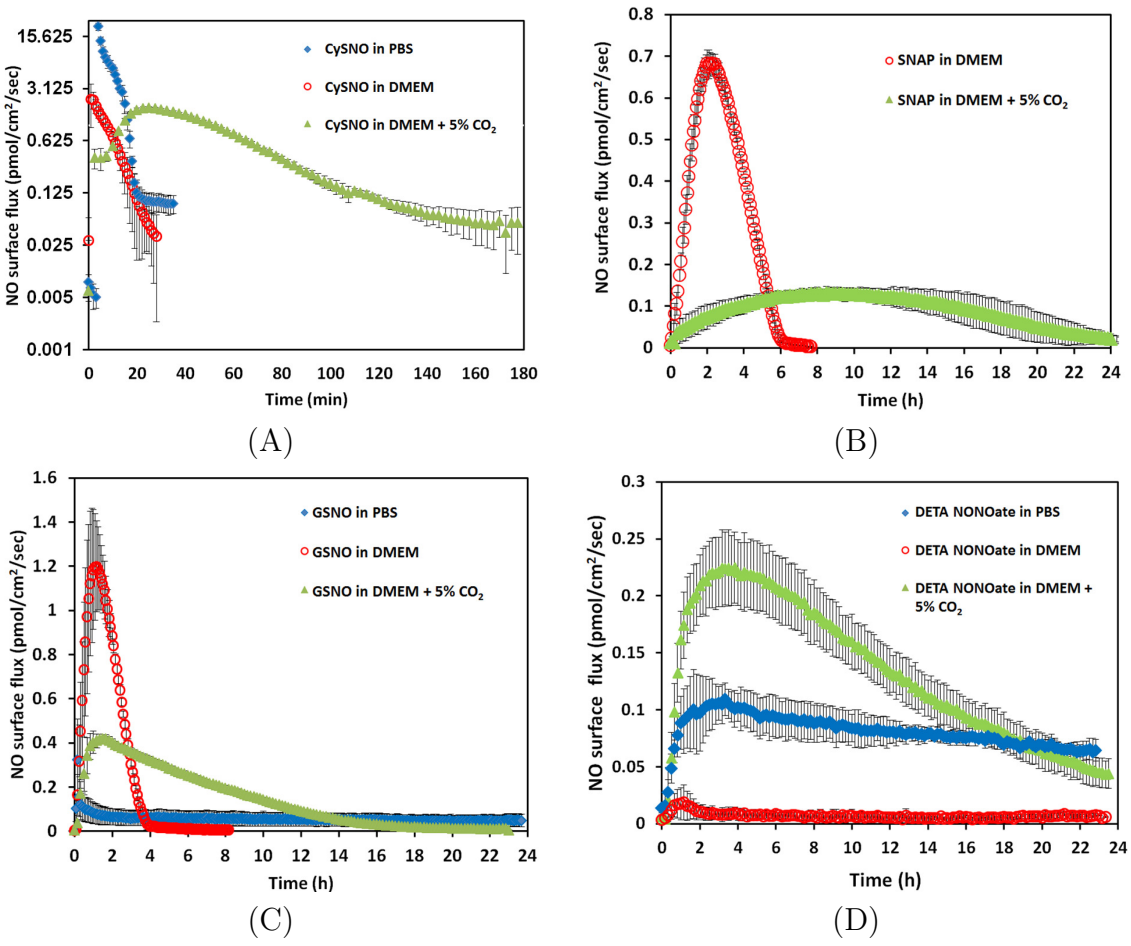

Figure 4.2: NO releasing profiles of three different RSNOs and DETA NONOate in different buffer conditions. 10 ml of 50 μM CySNO, SNAP, GSNO and 25 μM DETA NONOate prepared in PBS or DMEM was applied to NO measurement device for NO flux real-time monitoring (A) CySNO, (B) SNAP, (C) GSNO, (D) DETA NONOate. Under each condition, triplicate experiments were run independently. Data was presented as the average value of the three independent repeats; error bar represents the standard deviation of the three values.

variations. Fig. 4.3 shows each individual repeats, which differs greatly from other donors' consistent and repeatable releasing profiles (see Fig. 4.2).

The inconsistencies of the release from SNAP also leads to the question:

Table 4.1
Quantitative analysis of the NO releasing profiles of different NO donors

			CySNO	SNAP	GSNO	DETA NONOate
reported $t_{1/2}$ (in PBS or PSS, h)			0.023	1.15, 4.6, up to 6	159	20
PBS	**W/out CySH**	**total NO (mol)**	7.37E-08 (4.76E-09)	8.87E-08 (4.87E-08)	1.09E-07 (6.30E-08)	9.30E-08 (1.30E-08)
		Average flux (mol/cm^2/sec)	2.49E-12 (1.61E-13)	4.89E-13 (2.92E-13)	9.06E-14 (5.21E-14)	8.11E-14 (1.14E-14)
		Max flux (mol/cm^2/sec)	2.12E-11 (1.89E-12)	1.11E-12 (6.72E-13)	4.36E-13 (4.80E-13)	1.19E-13 (1.32E-14)
		Duration (h)	0.62 (0.024)	4.04 (2.76)	more∗ than 24 h	more∗ than 24 h
DMEM	**W/out CO_2**	**total NO (mol)**	1.38E-08 (8.88E-10)	1.18E-07 (2.96E-09)	1.36E-07 (2.70E-08)	8.44E-09 (3.94E-09)
		Average flux (mol/cm^2/sec)	5.76E-13 (3.70E-14)	6.96E-13 (2.86E-14)	5.68E-13 (1.25E-13)	7.22E-15 (3.30E-15)
		Max flux (mol/cm^2/sec)	2.65E-12 (1.08E-12)	3.05E-13 (7.67E-15)	1.24E-12 (2.22E-13)	2.55E-14 (1.14E-14)
		Duration (h)	0.45 (0.056)	6.42 (0.12)	4.48 (0.80)	more∗ than 24 h
	with CO_2	**total NO (mol)**	7.43E-08 (1.14E-09)	1.10E-07 (2.78E-08)	1.64E-07 (4.94E-09)	1.55E-07 (2.30E-08)
		Average flux (mol/cm^2/sec)	5.07E-13 (1.49E-14)	7.11E-14 (8.50E-15)	1.44E-13 (6.42E-15)	1.32E-13 (1.96E-14)
		Max flux (mol/cm^2/sec)	1.73E-12 (6.81E-14)	1.25E-13 (1.41E-14)	4.31E-13 (1.59E-14)	2.33E-13 (3.39E-14)
		Duration (h)	2.44 (0.46)	more∗ than 24 h	22.01 (0.83)	more∗ than 24 h

Effective concentration of all NO donors is 50 μM and the solution volume is 10 mL; the total mole of NO was calculated through integrating area under NO releasing curves; maximum NO flux was directly read from the NO releasing profile; average NO flux refers to averaging the flux during the lasting time; $t_{1/2}$ is the half-life of donors; $*$ duration is longer than 24 h, however we only examined the initial 24 h. Data was presented as average (Std.)

how rational it is to use half-life of each NO donor measured in phosphate buffer as the references to predict NO level in real biological conditions?

NO donors were dissolved in 10 ml freshly prepared complete DMEM (with FBS and pen/strep) and applied to the device at 37 °C incubator for real-time NO monitoring. 5% CO_2, which is a common condition for real cell culture, was considered as

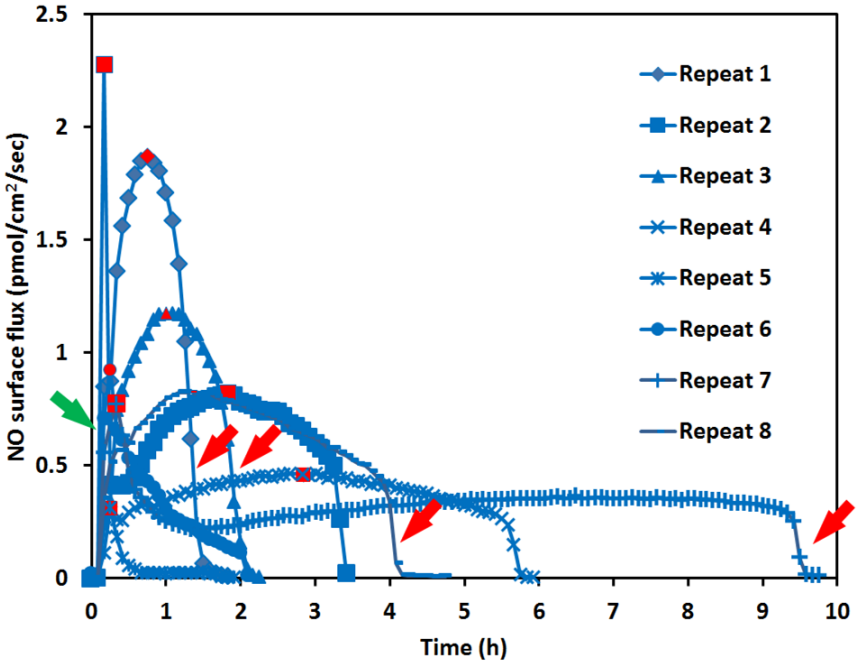

Figure 4.3: NO releasing profiles of 50 μM SNAP in 10 ml PBS. SNAP was prepared by either dissolving SNAP crystal by diH_2O to 2 mM stock and further diluted by PBS obtaining the 50 μM solution (1-4), or direct dilution from SNAP stock collected from the nitrosated N-acetylpenicillamine solution without recrystallization (5-8). Since the profiles showed big variation among repeats, all repeats are presented for readers' reference. Red marks indicate the highest flux values, red arrows show sharp decrease of the NO flux, green arrow, sharp increase.

an additional variable (since CO_2 might potentially affect solution pH and carbonate concentration). Fig. 4.2 shows that NO profiles of each NO donor differs greatly in DMEM (red traces) in terms of both NO release rate and duration. At this specific concentration (50 μM), NO release profiles of all NO donors differed greatly in PBS from in DMEM (without CO_2). In DMEM, the total NO that was captured by the sweep gas was 5.4 times and 11.0 times lower for CySNO and DETA NONOate respectively, while SNAP and GSNO both showed more (1.3 and 1.2 times, respectively) NO passed through the membrane compared with in PBS group within 24 h (Table

1). The change of NO flux rate also diverged; reduced in CySNO, SNAP and DETA NONOate but increased in GSNO groups (Fig. 4.2 blue traces vs. red traces and quantified in Table 4.1). Those results clearly demonstrated that different buffers do significantly affect NO generation of all four NO donors examined.

In the presence of CO_2, making the condition more representative to the real case, NO generation patterns were further affected. In the presence of 5% CO_2, all the RSNOs showed longer NO generation duration compared with DMEM without CO_2 (around 2 h longer release for CySNO and more than around 20 h longer for SNAP, Fig. 4.2 B, red and green traces), while DETA NONOate released NO in a significant faster fashion (Fig. 4.2 D, red and green traces). The results might be explained by the lower media pH brought about by CO_2. GSNO and DETA NONOate no longer constantly released low level NO for over 24 h but released faster in the initial stage, and after 24 h, the NO level became very low that can be barely detected. That might be one of the reasons why the reported GSNO's half-life is much longer than SNAP's but in some study their potencies did not follow away with this trend [169, 173]. All the quantified results were summarized in Table 4.1.

4.3 Factors that may affect NO generation profiles of NO donors

Because a great difference of NO release profiles exists between using PBS and DMEM, this complicated system was investigated by manipulating a single factor at a time. As previously described, the NO level created by NO donors is determined by both the NO generation and the NO consumption reactions. In first order kinetics model, NO generation can be expressed by Eqn(2.9). And in NO auto-oxidation model, NO level can be influenced by consumption described as in Eqn(2.2). Any factors that can change generation, consumption or introduce other consumption mechanisms will change the NO level obtained. Several mechanisms that can initiate the generation of NO from RSNO have been proposed, including transition metal ions mediated NO releasing, photocleavage, and ascorbate initiated NO release [95]. In addition to decomposition, RSNO can undergo transnitrosation reactions with nucleophiles and other thiols without generating any NO, which produces new RSNOs which may affect the NO generation profiles as well [95]. The influence of pH on DETA NONOate decomposition was also investigated. The redox states of the solution environment was also examined to determine how ROS molecules affect the final NO that cell may experience.

4.3.1 The effect of transition metal irons

10 mM EDTA PBS solution was used as the NO donor buffer to eliminate the effect of low level of transition metal ions that are ubiquitous contaminants in buffer salts. Using the same experimental set-up and conditions, SNAP's NO generation profile under ion-free condition appeared to be significantly slower and more repeatable (red traces in Fig. 4.4 A). This result suggested that transition metal ions mediated NO releasing is the main releasing mechanism for SNAP decomposition in PBS, and without transition metal ions, SNAP may be preserved for much longer time. (After SNAP was placed in 37 °C incubator for 48 h in 10 mM EDTA PBS, 1 mM ascorbic acid was applied to initiate NO release, which produced a huge amount of NO in a very rapid fashion, indicating the stability of SNAP in solutions without transition metal ions (data not shown)).

When transition metal ions were removed in CySNO and GSNO solutions, similarly, significant decrease in NO generation was observed in both groups (blue and green traces respectively in Fig. 4.4 A). After 1 h, NO generation in both CySNO and GSNO became almost undetectable, but after adding ascorbic acid, NO generation also recovered (one example was shown in Fig. 4.4 B). We then quantified how much NO was generated in the initial 10 min by these three RSNOs in both normal PBS and PBS with 10mM EDTA.

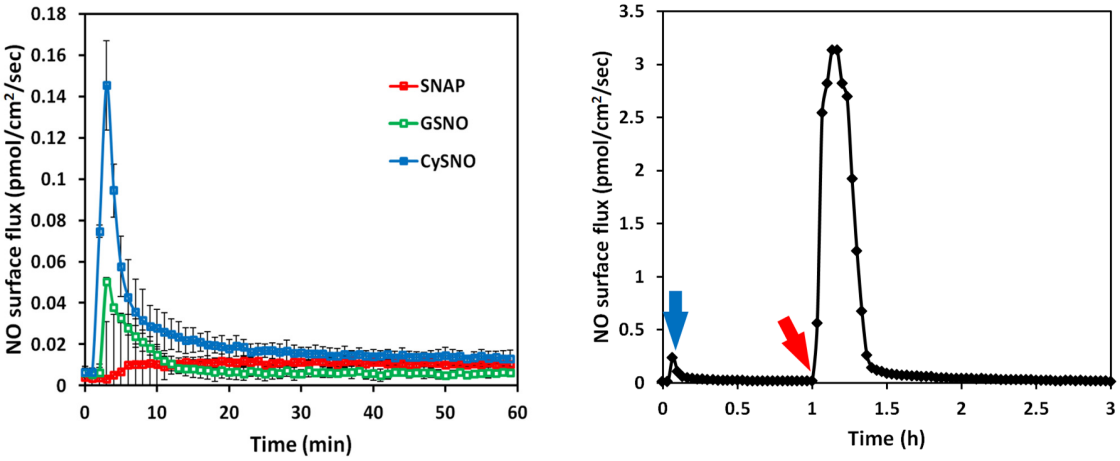

Figure 4.4: NO releasing profiles of 50 μM three RSNOs in 10 ml PBS with 10 mM EDTA. (A) Real-time NO releasing profiles of RSNOs; three independent experiments for each RSNO were run and data was presented as the average of the three, error bar representing standard deviation. (B) 50 μM CySNO in 10 mM EDTA PBS applied to NO measurement device from time 0 and NO releasing was real-time measured from time 0 to 1 h (blue arrow shows the signal peak); at 1 h, 1 mM ascorbic acid was applied (red arrow) and right after that rapid NO releasing was initiated.

Table 4.2 summarized that with transition metal ions RSNOs' NO generation increased to different degrees, where CySNO generated over 140 times more total NO in the initial 10 min in normal PBS compared with PBS with EDTA , whereas the total NO generation only increased by around 50 times and 10 times respectively in SNAP and GSNO groups. This demonstrates that CySNO is more sensitive to transition metal ions than SNAP and GSNO. Removal of the transition metal ions from RSNOs environment (even CySNO, which is normally considered to be highly reactive), can make RSNOs much more stable, which is consistent with Singh et al.'s statement that SNAP's stability can be significantly longer in transition metal ion

Table 4.2
Quantitative analysis of transition metal ions effect on RSNO's NO generation

		CySNO	SNAP	GSNO
PBS	**First 10 min NO releasing (mol)**	6.64E-08 (4.12E-09)	4.69E-09 (2.32E-09)	2.13E-09 (2.07E-09)
PBS with EDTA	**Total NO (mol)**	1.12E-09 (2.41E-10)	1.53E-09 (5.97E-10)	3.53E-11 (7.80E-12)
	Average flux (mol/cm^2/sec)	2.97E-14 (6.75E-15)	8.88E-15 (2.06E-15)	5.43E-14 (2.84E-14)
	Max flux (mol/cm^2/sec)	1.64E-13 (2.42E-14)	1.46E-14 (3.22E-15)	8.99E-15 (1.71E-15)
	Duration (h)	1.5 h sample time	6 h sample time	1.2 h sample time
	First 10 min NO releasing (mol)	4.74E-10 (1.07E-10)	8.24E-11 (2.49E-11)	2.05E-10 (1.47E-10)
Ratio (with TIs/without TIs)		140.1	56.9	10.4

Effective concentration of all NO donors is 50 μM and the solution volume is 10 mL; NO mole was calculated through integrating area under NO releasing curve between 2 specific time points; first 10 min was chosen because CySNO's NO releasing in PBS solution and all RSNOs' releasing in 10 mM EDTA PBS became very low. Data was presented as average (Std.)

free solutions [170]. The NO generation from RSNOs may be mainly through the transition metal ion mediated mechanism at 37 °C.

4.3.2 The effect of free thiols

GSH and CySH as free thiols were added to NO generating solutions to examine their effect on the overall NO level cells experience. It is noted that high concentration

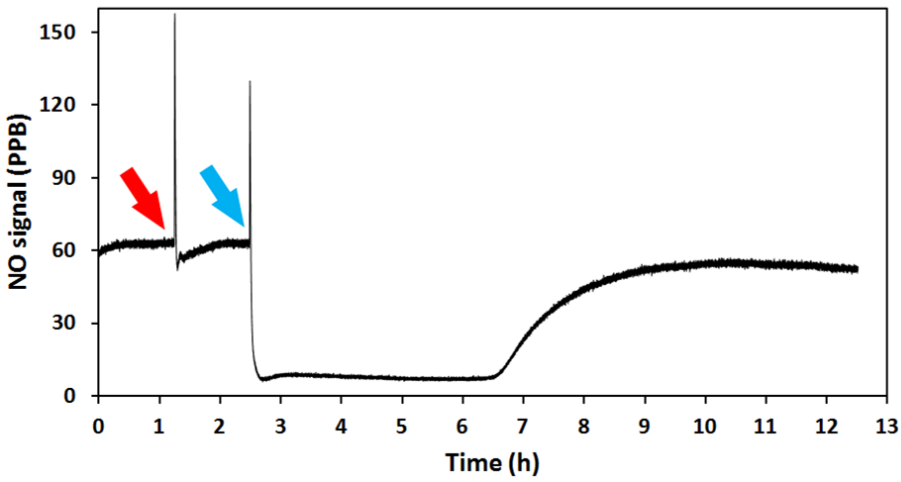

Figure 4.5: NO level change by introducing GSH. 10 ml 100 μM DETA NONOate solution was applied to the device for NO flux measurement until signal reaches steady states. NO flux increase right after introducing shaking but reduced sharply to normal level(as controls, red arrows), or plummet significantly and stayed there for around 4 h and returned slowly to normal (200 μM GSH added, blue arrows).

of thiol (mM rage) should be avoided, because it may change the system pH. So we used a maximum of 500 μM CySH and GSH in the following experiments.

When GSH was directly added to a solution of DETA NONOate in PBS, which releases NO in a continuous and near constant rate fashion at 37 °C, a significant NO drop was observed (Fig. 4.5), suggesting the existence of NO-GSH or DETA NONOate-GSH interaction. However, after approximately 4 h, the NO level started to return to original levels, suggesting this inhibition of NO release was reversible. To further show that thiol groups may indeed affect other donor's NO generation profiles, GSH was added to SNAP PBS solution, but no significant profile change was observed (data not shown).

But when CySH was added instead of GSH, there was a significant reduction in total NO and average flux (Table 4.3). Obviously different total NO generation duration and the pattern of releasing curves was observed (Fig. 4.6).

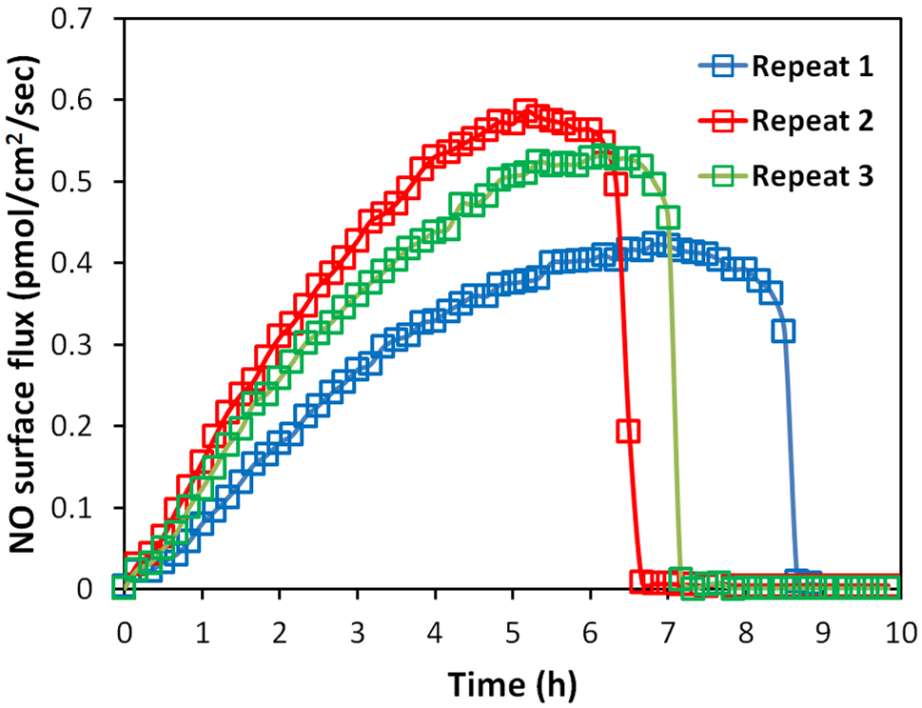

Figure 4.6: NO releasing profiles of 50 μM SNAP in 500 μM CySH PBS. As mentioned before SNAP's NO releasing profiles showed big variations among repeats in PBS, to show the results more clearly three independent repeats are directly shown here.

In PBS, one of the most noticeable NO release pattern from SNAP can be summarized as rapid initial release and quickly diminishing level, meaning that all NO donors' maximum release flux was detected at a relatively early stage, and in the last stage of the releasing NO signal plummets to a very low level quickly. For example, the

Table 4.3
Quantitative analysis of free thiols' effect on RSNO's NO generation

			SNAP
PBS	**normal PBS**	**Total NO (mol)**	8.87E-08 (4.87E-08)
		Average flux (mol/cm^2/sec)	4.89E-13 (2.92E-13)
		Max flux (mol/cm^2/sec)	1.11E-12 (6.72E-13)
		Duration (h)	4.04 (2.76)
	CySH or CO_2	**Total NO (mol)**	1.26E-07 (2.30E-9)
		Average flux (mol/cm^2/sec)	3.39E-13 (4.56E-14)
		Max flux (mol/cm^2/sec)	5.38E-13 (9.02E-14)
		Duration (h)	7.54 (0.97)

Effective concentration of SNAP is 50 μM and the solution volume is 10 mL; NO mole was calculated through integrating area under NO releasing curve. Data was presented as average (Std.)

maximum NO flux of the SNAP sample in examination (red traces in Fig. 4.3) normally appeared within the first two hours except one outlier, then dropped sharply in the last stage (red arrows in Fig. 4.3). However, in PBS with CySH, the maximum flux was reached gradually and after that the NO flux plummeted immediately, characterized as slowly increasing release with rapid decline.

Table 4.3 summarized the flux parameters, clearly showing that instead of greatly changing those numbers -SH significantly reduced the variations, making results more repeatable. Interestingly, in DMEM, NO generation of SNAP is normally observed to be more repeatable and the profile increases slowly and decreases slowly, indicating that thiols may be a factor that account for this slowly increasing NO release.

Free thiols are important NO reactants in body. They can elongate the effective NO release and help with NO transportation [174]. They also serve as important

regulators of protein nitrosation [120]. Understanding the relationship between NO and thiols can help us understand the underlying mechanisms affecting NO levels present in biological systems. This real-time tool can potentially help us separate NO's effect from RSNO, for example with GSH, NO generated by DETA NONOate was low in the first several hours, during which NO's effect might be limited and the observed biological effect might be contributed to RSNO or –SH not NO.

4.3.3 The effect of pH and CO_2

Different tissues have different pH levels, which may make NO generation profile different [175, 176]. The device was used to directly investigate how different NO levels generated by the same NO donor can be affected by different pH environments. To do this PBS with different pH was prepared as the buffer solution to run the experiment.

Fig. 4.7 showed 25 μM DETA NONOate's releasing profile changed greatly in different pH. At pH=6 although total NO that cells might experience was only around 1.4 times larger (within 24 h), the maximum NO flux was increased around 4.6 times and NO release duration was shortened significantly to around 16 h. Considering the biological effect of NO is determined by the level and duration of NO that specific cells experience, this data indicates that different NO releasing drugs may have different

potencies in different tissues or cell compartments based on the pH of the target tissue and the structure of the NO donating moiety.

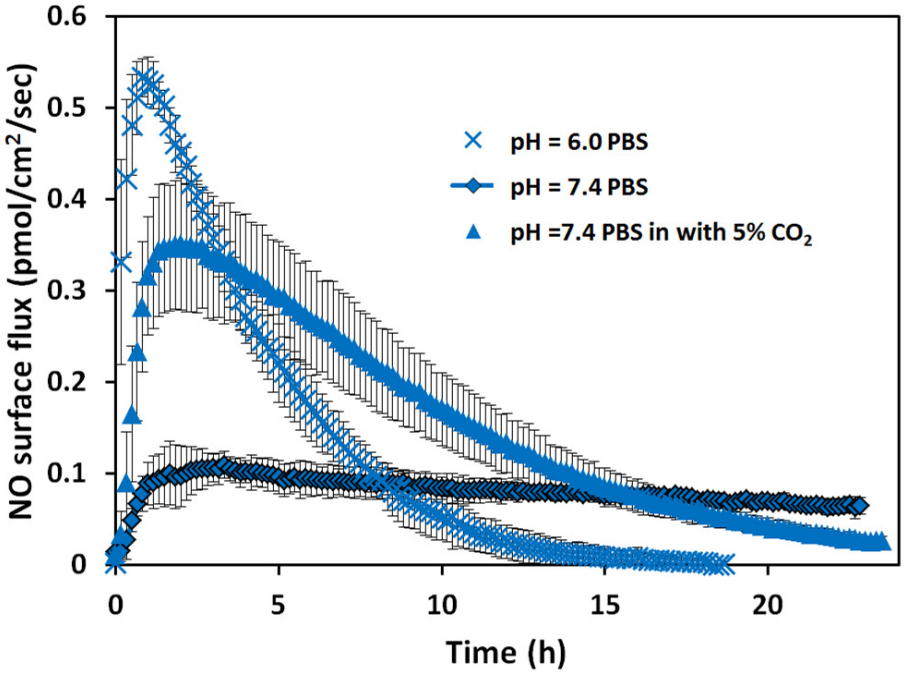

Figure 4.7: NO releasing profiles of 25 μM DETA NONOate in pH=7.4 and 6.0 PBS and pH=7.4 PBS with 5% CO_2; three independent experiments under each different conditions were run and data was presented as the average of the three, error bar representing standard deviation.

Because blood is a pH buffered system that relies on the balance between CO_2 and HCO_3^-, it is hypothesized that 5% CO_2 within the incubator may exert similar effects on the NO level by changing pH of the solution. To test this hypothesis, PBS buffer was added into the device and placed into the cell culture incubator with 5% of CO_2. Result from VWR sympHony pH meter shows that the solution pH decreased to around 6.6 within 90 min. Using pH=7.4 PBS buffer to prepare 25 μM DETA

NONOate with 5% CO_2, result is shown in Fig. 4.7 demonstrating that CO_2 has a significant effect on the NO generation profiles. One fold increase of total NO flux and almost 3 times greater maximum flux rate compared with without CO_2 were observed (Table 4.4). After 24 h, only barely detectable NO signal remained.

Table 4.4
Quantitative analysis of pH's effect on DETA NONOate's NO generation

			DETA NONOate
PBS	**pH=7.4 PBS**	**Total NO (mol)**	9.30E-08 (1.30E-08)
		Average flux (mol/cm^2/sec)	8.11E-14 (1.14E-14)
		Max flux (mol/cm^2/sec)	1.19E-13 (1.32E-14)
		Duration (h)	more than 24 h$*$
	pH=6.0 PBS	**Total NO (mol)**	1.31E-07 (1.81E-08)
		Average flux (mol/cm^2/sec)	1.69E-13 (2.63E-14)
		Max flux (mol/cm^2/sec)	5.48E-13 (2.59E-14)
		Duration (h)	15.86 (1.19)h
	pH=7.4 PBS with CO_2	**Total NO (mol)**	1.86E-07 (3.76E-08)
		Average flux (mol/cm^2/sec)	1.47E-13 (2.96E-14)
		Max flux (mol/cm^2/sec)	3.62E-13 (7.37E-14)
		Duration (h)	more than 24 h$*$

The concentration of DETA NONOate is 25 μM and the solution volume is 10 ml; NO mole was calculated through integrating the area under NO releasing curve; $*$ duration is longer than 24 h, however we only examined the initial 24 h. Data was presented as average (Std.)

The decomposition of diazeniumdiolates to generate NO has been shown to be pH dependent [177]. The release of NO from diazeniumdiolates through the decomposition to their parent diamine compounds and NO in aqueous solution is spontaneous. Factors that affect the dissociation rates include pH, its concentration and the presence of metal ions [178, 179]. Protonation is necessary for the decomposition reaction and depending on the pH, protonation can be single state or dual states, which makes the

underlying mechanism very complicated and NO release hard to control [180]. However, at physiological conditions, NO generation from DETA NONOate is mainly determined by the protonation of the secondary amine nitrogen [180].

These results pointed out that more careful re-evaluation is needed when using DETA NONOate as the NO donor for the biological study. The statement that DETA NONOate releases NO in a long-lasting fashion might be true only in conventional buffer conditions. The micro-environments of many inflammation situation and tumor masses can achieve relatively low pH value in vivo (even lower than pH=6 [176]), which is very likely to greatly change the effective NO delivery duration. Although diazeniumdiolates' release duration can be shortened in lower pH, RSNOs are more stable in lower pH [181], which should be considered when choosing the proper NO donors for specific applications.

4.3.4 The effect of redox environment

Once NO is generated, oxidative condition may heavily influence the NO levels obtained. It has been reported by many groups that elevated ROS levels suppressed NO's biological potency. The underlying mechanisms might be complicated. Some ROS directly react with NO, decreasing the NO that cells can access and some are through other mediators [182, 183].

The interaction of NO and the ROS (peroxide and superoxide) by real-time monitoring of the NO flux was investigated using DETA NONOate solution. Different peroxide sources were used (H_2O_2 and di-tert-butyl peroxide(DTBP)) to complete this examination.

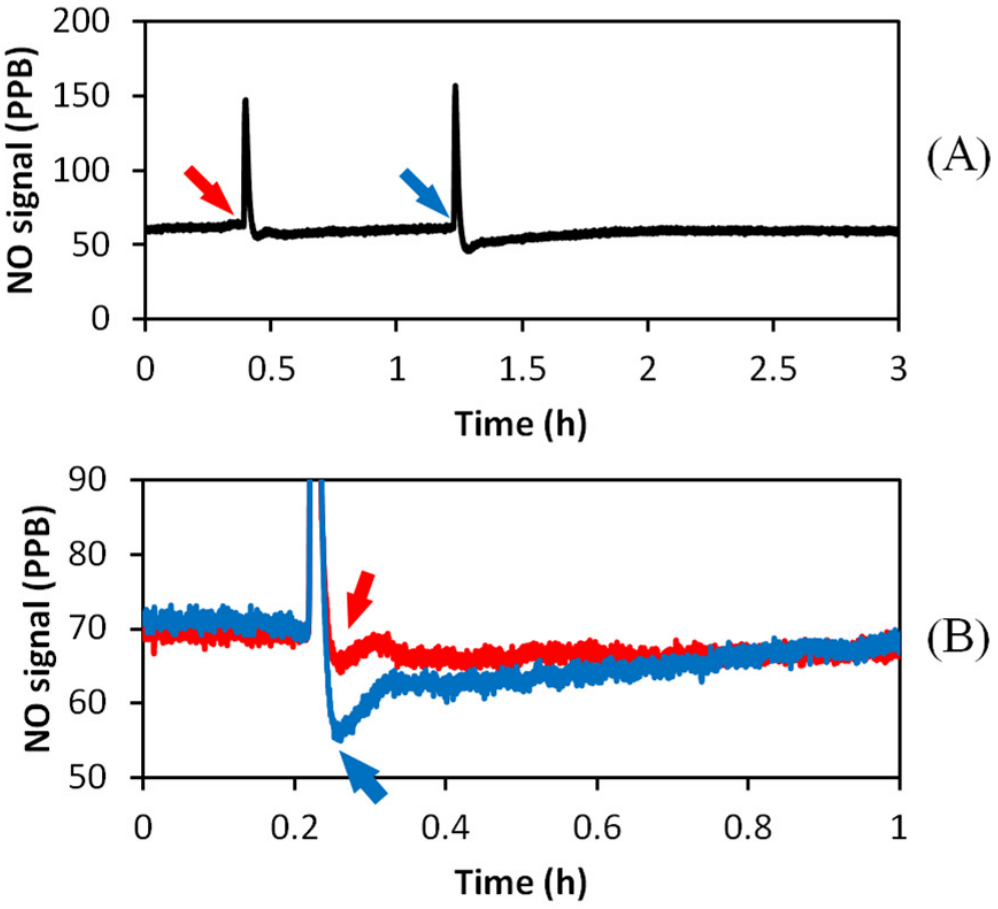

Figure 4.8: NO level deceasing by introducing peroxide. (A) NO level changes in accordance with the addition of peroxide (blue arrow) and PBS shaking as the control (red arrow); (B) blue curve represents with peroxide, red one the control. 10 ml 100 μM DETA NONOate solution was applied to the measurement device for real-time NO flux measurement. Once NO flux reached the steady state, t-butyl peroxide was added into the solution (to the final concentration of 1 mM). All experiments were run at 37 °C.

No significant NO level decrease was observed when H_2O_2 was applied (data not shown) and only very mild NO decrease was observed when up to 1 mM DTBP was applied into 100 μM DETA NONOate solution (Fig. 4.8). And NO level returned to normal after around 0.5-1 h, indicating only a mild interaction of peroxide and NO might exists.

Using the same principle, superoxide was applied to DETA NONOate solution by using hypoxanthine-xanthine oxidase (HX/XO) system [184].

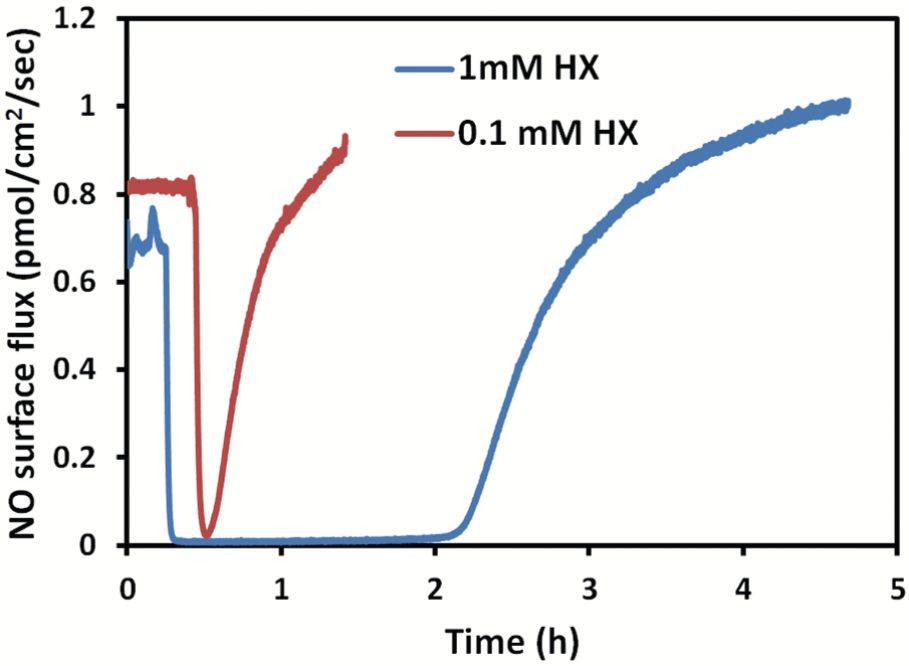

Figure 4.9: NO level deceasing by introducing superoxide. Hypoxanthine (1 mM in blue and 100 μM in red) was added into 10 ml 100 μM DETA PBS solution pH=7.4 (with 10mU/ml xanthine oxidase). All experiments were run at 37 °C.

Superoxide generation relies on the availability of the substrate HX. Different concentration (100 μM to 1 mM) of substrate was applied to the system to modulate the amount and duration of superoxide. Data shows that immediately after applying superoxide, the NO signal quickly decreased, indicating that superoxide greatly suppressed the resulting NO level (Fig. 4.9). The NO level could recover gradually to the original level later, and the time needed for this recover is correlated to the amount of hypoxanthine added, further confirming that superoxide and NO are involved in certain reactions. And the present of superoxide in biological system can greatly affect the NO level experienced by the cells.

4.3.5 The effect of solution volume

In in vitro experiments, quantitative study of NO is normally run through applying media with specific concentration of NO donor. However, the volume applied to a culture well may differ from each other. The hypothesis is that different solution volume (different bathing solution height) may lead to different final NO flux experienced by cell layer at the bottom of the culture vessel due to the diffusivity and reactivity of NO.

To investigate whether this hypothesis is true, 5, 10, 15 ml of 50μM CySNO DMEM solution was applied to the device. Fig. 4.10 A showed the NO releasing profiles of all

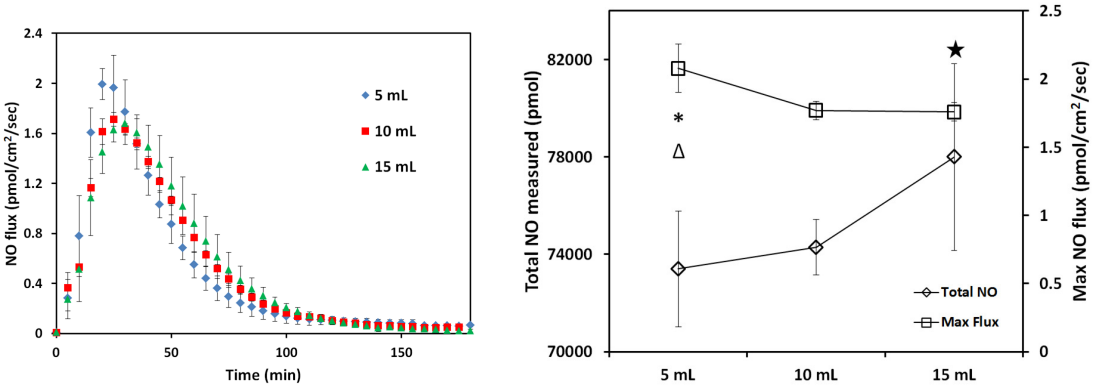

(A) (B)

Figure 4.10: Media volume's effect on NO level experienced by cultured cells. (A) NO releasing profiles of different volumes of 50 μM CySNO in DMEM with 5% CO_2; three independent experiments of each volume were run and data was presented as the average of the triplicate, error bar representing standard deviation among different repeats; (B) the change of total NO and NO flux experienced by cells along with the change of the media volume. From ANOVA and Tukey-test, significant difference of maximum NO fluxes that will be experienced by cells between 5 ml and 10 ml, and 5 ml and 15 ml is indicated by $*$ and Δ respectively, while significant difference of total NO that will be experienced by cells between 5 ml and 15 ml is indicated by ★.

different volumes. Under exactly the same other conditions, 5 ml solution generated the highest NO flux (P=0.023, 0.022 to 10 ml and 15 ml group respectively shown by $*$ and Δ, $P > 0.05$ between 10 and 15 ml by Tukey-test). There is a decrease in NO flux with increasing solution volume. But in terms of total accumulated NO that cell experienced, the trend is reversed, summarized in Fig. 4.10 B (P=0.0370 between 5 and 15 ml groups shown by ★, $P > 0.05$ in other groups in Tukey-test).

These results directly proved that by using the same concentration of soluble NO donor, but different total media volume applied into cell vessels resulted in different NO level and total NO that cell ultimately experienced. And this trend can be

generalized as the stretching of the NO releasing profile curve with increasing bathing solution volume, i.e. less media (larger surface to volume ratio) higher NO flux (in the initial states) but shorter duration time when cell may experience NO, and vice versa. One explanation might be due to the gradual consumption of the NO donors and the different reservoir capacities, the NO flux goes down faster in the larger surface area to volume ratio group. So to strictly use consistent volumes of media in cell culture vessels is important in NO experiments when treating cells with soluble NO donors.

4.4 Connecting NO profiles with cell work

After gaining a general understanding of factors that influence the flux of NO cells experiencing with the four NO donors in DMEM under different conditions (37 °C and 5% CO_2), the potencies of different NO donors in biological applications was examined. The effect of NO donors on smooth muscle cells was investigated, where NO was reported as an important inhibiting signal of cell proliferation [185, 186, 187].

4.4.1 Different NO donors have different ultimate effect on MOVAS cells

A more precise way to understand how different NO donors determine the final biological effect of NO is to analyze each situation according to the corresponding NO real-time profile. In the previous section, NO release profiles of the four NO donors in real culture conditions (DMEM at 37 °C with 5% CO_2) have been measured. With information regarding predicted NO fluxes, MOVAS cell proliferation was studied.

Those four NO donors with the same effective NO concentration (50 μM for RSNOs, and 25 μM for DETA NONOate) were used to treat MOVAS cells. After 24 h both cell number and cell proliferation ratio were examined as shown in Fig. 4.11. Result shows that DETA NONOate treatment had the least potent effect on restricting cell numbers after 24 h treatment. All three RSNOs showed significantly greater inhibitory effect on cell growth and proliferation as indicated by ANOVA ($P<0.05$ between CTRL and all three RSNOs and DETA NONOate between all three RSNOs by ANOVA), however ANOVA did not suggest any statistic difference existed among the three RSNO groups. This is difficult to explain in DMEM media. With CO_2, DETA NONOate did not show the lowest NO flux rate or the total cumulative NO. Meanwhile cell proliferation assays indicated that after 24 h only SNAP treated cell proliferation ratio differed significantly from the control group ($P=0.0565$ by ANOVA

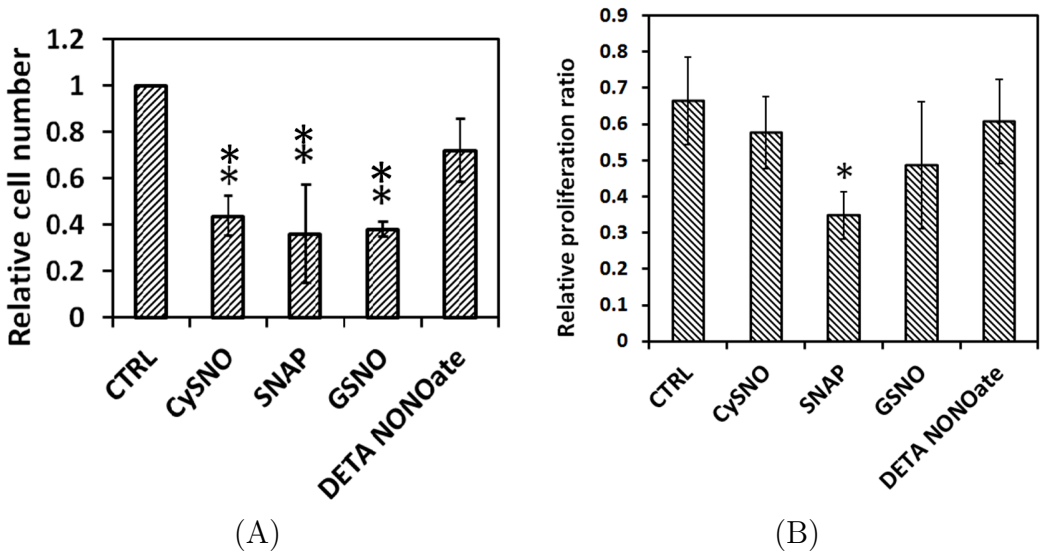

(A) (B)

Figure 4.11: Different NO donors' effect on MOVAS cell proliferation. Cell starting density was 10,000 cell/cm^2 and before applying NO donors cells were cultured overnight to allow recovery; 24 h after treatment, cells were applied for live-dead assay and proliferation assay (A) Relative living cell number. ** represents P<0.01 by ANOVA and Tukey-test compared with the control (CTRL). (B) cell proliferation ratio. * represents P=0.0565 by ANOVA and Tukey-test but P<0.05 by t-test compared with the control (CTRL). Data represents the average of the 3 independent repeats and error bar represents standard deviation among repeats)

and P<0.05 by t-test), while cell proliferation ratios of all other groups were slightly smaller but close to the control group (P>0.2 by ANOVA), meaning cell number and cell proliferation rate did not match at 24 h.

Compared with CySNO, neither GSNO nor SNAP showed significant better potency, which also does not correlate directly with the NO flux profile. Because from the measured NO profile, CySNO showed significantly shorter releasing duration. And DETA NONOate produced relatively larger flux compared with SNAP and similar flux to GSNO (Table 4.1), but the ultimate cell number appeared significantly higher

in DETA NONOate group (though t-test, compared with control, shows $P<0.05$, ANOVA shows P is between 0.2 to 0.3). At this point, the real-time NO profile in DMEM media with real culture condition does not fully explain different potencies of NO donors in real biological cases.

However, considering NO generation from those NO donors is very sensitive to experimental conditions, it is suspected that adding cells, is just like adding other variables into the NO donor solution and may therefore change the NO releasing profiles of the donors.

4.4.2 Real-time monitoring NO level that cells experience during NO donor treatment

Because the pattern of measured NO release profiles did not align with the observed effects on cell levels, the real-time NO release profile was recorded during cell culture experiment. The device was used for cell culture, and at the same time real-time NO measurement was made to obtain cell proliferation data that corresponded with real-time NO data.

Cells were cultured using standard cell culture protocol in the two-chamber system. Dissolved NO donors solutions were added to the culture media and real-time NO

flux was recorded. Result and quantification analysis were summarized in Fig. 4.12 and Table 4.5. It is clearly showed that GSNO did not release NO in low and long-lasting fashion as people normal think under actual cell culture conditions, but DETA NONOate did. Instead GSNO's release was more similar to CySNO, which released most of its NO in the initial 4 h of the experiment.

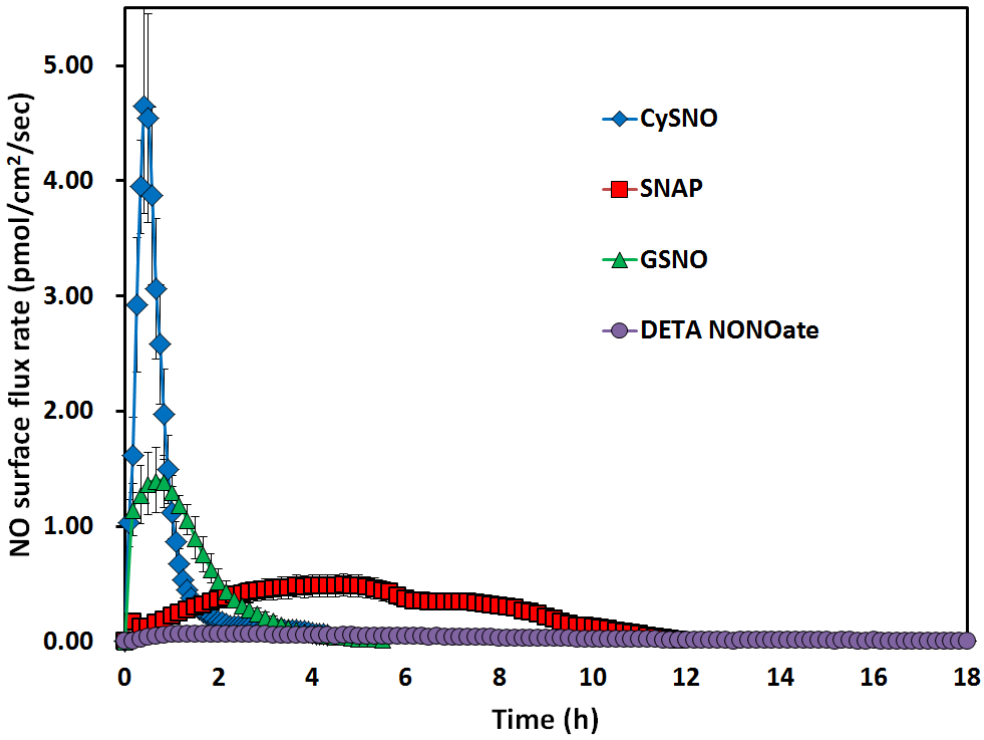

Figure 4.12: Real-time measuring the NO levels that cells experienced when cultured in the device and treated with NO donors. 10 ml media was used to culture cells in the device with 50 μM CySNO, SNAP, GSNO and 25 μM DETA NONOate respectively. Under each condition, triplicate experiments were run independently. Data was presented as the average value of the triplicate; error bar represents the standard deviation of the three values.

Compared with media only condition, the average and maximum flux of all RSNOs increased significantly (around 2, 4, and 9 times more for CySNO, SNAP and GSNO respectively), though the total accumulated NO experienced by cells did not change too much (a little over 1 fold for CySNO and only 50 % more and 20 % less for SNAP and GSNO). However, both NO flux rate and total NO diffusing to and through the cell layer greatly decreased in the DETA NONOate treatment group (only 30% and 15% compared with media only conditions).

This data clearly proved that during actual cell culture the NO donors may release NO in a very different manner than predicted from the release profile obtained from the controlled experimental conditions. Simply knowing that different NO donors have different NO releasing profiles is important but not enough to explain some of their biological outcomes. It is also important to remember that a donor's NO delivery behavior is highly changeable, and may result in a totally different profile when experimental conditions are changed slightly. For example, CySNO and GSNO are normally considered as very different in stability. But actually both of them released NO rapidly in the initial stage with a very high flux ($>$ 1 pmol/cm^2/sec, Fig. 4.12), and no NO flux was detected 24 h after treatment. This result explained data shown in Fig. 4.11 as to why cell number and cell proliferation ratio in CySNO and GSNO group were very similar, and DETA NONOate's least potency may be resulting from the very low NO level generation during actual cell culture. SNAP has intermediate NO level in real cell culture condition (around 0.4 pmol/cm^2/sec)

and lasted a significant longer time compared with other RSNO (more than 9 h), this might be one of the reason why after 24 h the smallest cell proliferation ratio was observed in the SNAP group. But overall, the SNAP group did not show significantly smaller cell number after 24 h compared with CySNO and GSNO. This observed inconsistency between cell number and cell proliferation ratio may result from the fluctuation of cell proliferation ratios within 24 h because of the changing of the NO level. To better understand NO's effect on MOVAS, instead of doing one single end-point examination on cells, cells need to be examined at multiple intermediate time points during the course of the 24 h experiment.

4.4.3 NO profile and cell proliferation at different time points

From the statement above, it is clear that the end-point test time point chosen for biological assays needs careful evaluation, otherwise it may produce inconclusive or contradictory data. To avoid this, the cell number and cell proliferation ratios were examined at different time points. According to the NO profile data showed in Fig. 4.12, CySNO and GSNO's NO release lasted for around 3-4 h, and at 11-12 h SNAP finished its releasing, this lead to the examination of cells at 4 h and 12 h and 24 h.

Cell number data clearly showed that even though at 24 h cell numbers in three RSNO groups were similar, the change of cell number/proliferation ratio was very different

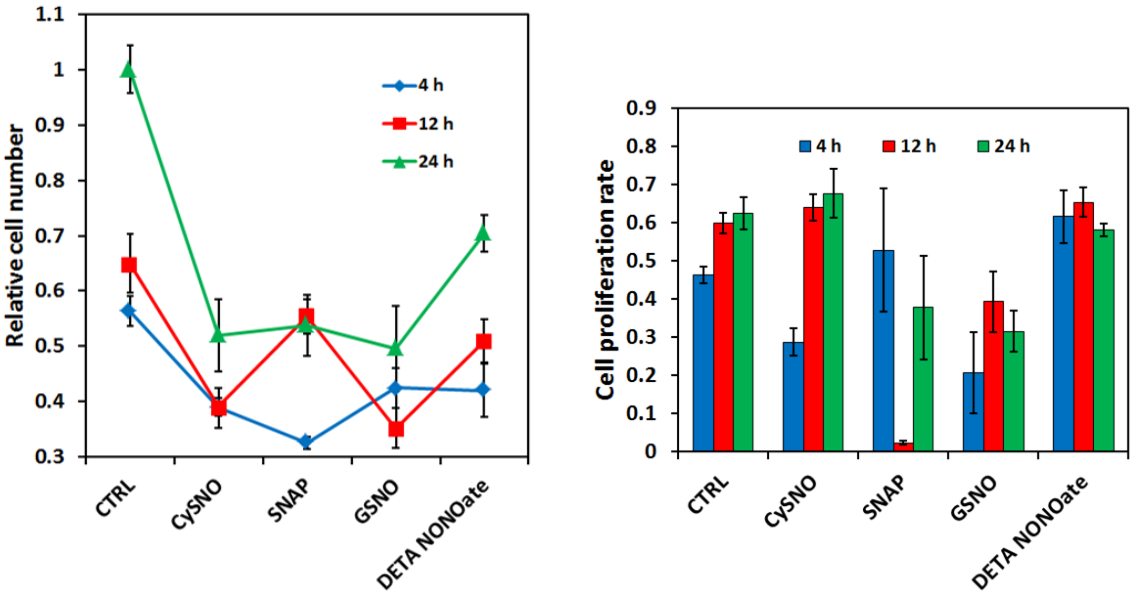

(A) (B)

Figure 4.13: Different NO donors inhibit MOVAS cell proliferation in different degrees at different time points. (A) relative cell numbers normalized to cell number of control groups at 24 h. (B) MOVAS's cell proliferation ratio under different NO donor treatment at different time points. Cell starting density was 10,000 cell/cm^2 and before applying NO donors cells were cultured overnight to allow recovery; 4, 12 and 24 h after treatment, cells were strained for life-death assay and proliferation assay. Data represents the average of 3 independent repeats and error bar represents sample standard deviation.

at the intermediate time points(Fig. 4.13 A). The increase of cell number in CySNO and GSNO groups was mainly after 12 h and between 4 to 8 h the increase is low, however, SNAP showed a totally inversed pattern, where the increase was mainly in the first 12 h. DETA NONOate has relatively stable and slow increase of cell number. And these results are also consistent with the cell proliferation ratio data (Fig. 4.13 B), where in CySNO and GSNO treatment the smallest proliferation ratios were observed at 4 h, and in SNAP the value was at 12 h. DETA NONOate showed

consistently high cell proliferation ratio, but the resultant cell number was still a little smaller than the controls (Fig. 4.13 A). By using the device, it is shown that a flux of around 0.4-1 pmol/cm^2/sec on average showed good inhibition of smooth muscle cell proliferation. A constantly high flux (around $>$ 1.5 pmol/cm^2/sec lasting for over 2 h) may kill the cells, which is very consistent with data presented in 5.4 of this dissertation.

It has now been clearly illustrated that the actual NO status experienced during the culture experiment is critical, not the empirical values determined or measured under other conditions (for example, it is not recommended to use half-lives of NO donors' measured in PBS or DMEM even with 5% CO_2). The results presented here directly show the significance of tracking the actual NO level generated by NO releasing drugs in biological experiments and how useful the real-time measurement device is in such studies.

To further show that different culture conditions did change the NO status cells experience greatly, we tried different coating methods for cell culture. Dopamine-gelatin treatment was used to surface-coat the device membrane; then cells were cultured in those devices and the same NO donor treatment was applied.

Fig. 4.14 and Table 4.5 show that although the overall trend is similar to using the collagen I treated device, difference still exists, such as when using polydopamine coating SNAP showed much shorter releasing profile and around 1.2 and 1.4 time

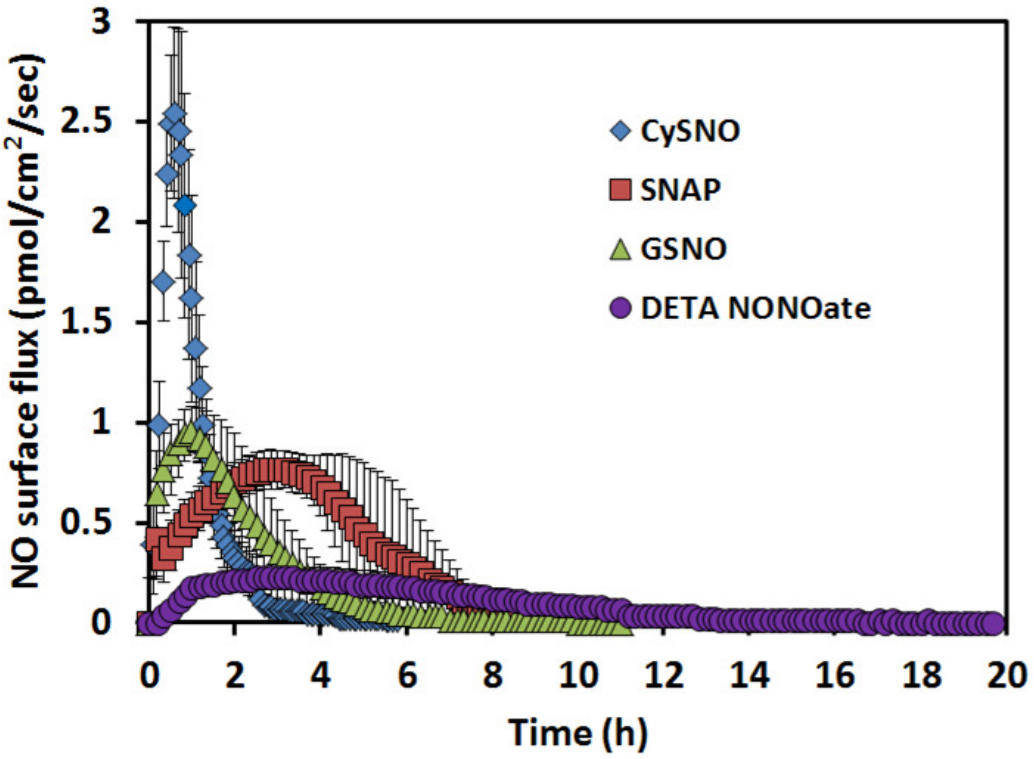

Figure 4.14: Real-time measuring NO levels that cells experienced when cultured in the dopamine-gelatin treated device and treated with soluble NO donors. 10 ml media containing 50 μM CySNO, SNAP, GSNO and 25 μM DETA NONOate respectively was used to treat cells cultured in the device. Under each condition, triplicate experiments were run independently. Data was presented as the average value of the triplicate; error bar represents the standard deviation of the three values.

higher NO average and maximum flux; DETA NONOate has around 4.2 and 3.4 times higher NO average and maximum flux, proving that only monitoring NO in specific experiments is meaningful for specific analysis.

Table 4.5
Quantitative analysis of the real-time NO generation profiles of different NO donors under cell culture conditions

			CySNO	SNAP	GSNO	DETA NONOate
Complete media with cells	Collagen I coating with cells	Total NO (mol)	1.67E-07 (5.17E-08)	1.71E-07 (2.39E-08)	1.32E-07 (2.15E-08)	2.54E-08 (4.21E-09)
		Average flux (mol/cm^2/sec)	1.07E-12 (2.56E-13)	3.77E-13 (8.33E-14)	4.70E-13 (3.35E-14)	3.21E-14 (1.05E-14)
		Max flux (mol/cm^2/sec)	4.96E-12 (1.18E-12)	5.92E-13 (7.42E-14)	1.80E-12 (3.58E-13)	7.38E-14 (3.40E-15)
		Duration (h)	3.15 (0.98)	9.46 (2.55)	4.44 (0.43)	14.60 (3.12)
	Dopamine coating with cells	Total NO (mol)	1.30E-07 (3.15E-08)	1.87E-07 (4.92E-08)	1.31E-07 (2.60E-08)	9.30E-08 (3.20E-08)
		Average flux (mol/cm^2/sec)	6.86E-13 (4.68E-13)	4.61E-13 (9.00E-14)	5.95E-13 (1.05E-13)	1.38E-13 (7.42E-14)
		Max flux (mol/cm^2/sec)	2.67E-12 (5.46E-13)	8.40E-13 (2.94E-14)	1.24E-12 (3.85E-13)	2.48E-13 (9.03E-14)
		Duration (h)	2.76 (0.19)	5.33 (2.20)	4.06 (0.64)	13.15 (1.06)

Cells were cultured in collagen I top-treated device and dopamine-gelatin treated device respectively. Effective concentration of all NO donors is 50 μM and the media volume is 10 mL; NO donors were dissolved into media to 2× equal volume media to original cell culture media and applied to the cultured cells. Data was presented as average (Std.)

4.5 Implications

Though NO's biological roles became much clearer during the past several decades, many controversies and enigmas still exist. One problem is that NO's effect on cells in cell culture is hard to be separated from the behavior of the NO donors. One systematic study on biological effect of different RSNO donors was reported by Mathews et al.[169]. Considering the general idea that RSNO's effect was through NO released from the cleavage of S-NO bond, they designed gas-purging experiment which showed that removing NO had negligible influence on smooth muscle relaxation, suggesting

that at least other activation pathways to sGC exist. They also showed that the correlation of RSNO decomposition first-order half-life and the degree of the smooth muscle relaxation to be low. However, the half-life values they used were measured within 0.5 mM physiologic saline solution, while the biological assays were in more complicated systems. Wink et al. [188] showed NO's cyto-protective effect on hydrogen peroxide stressed V79 cells and no protective effect on superoxide stress, even after SOD was added. However, in the same paper they also showed different NO donors of the same working concentration had very different potencies in counteracting peroxide mediated cyto-toxicity, showing that choosing the proper NO donor is critical. Using a system with both XO-HX and RSNO showed more complicated behavior according to Trujillo et al. [189], where peroxynitrite might form and stress cells when simultaneously using these two chemicals in the same system. SNP was shown to be cytotoxic because of the synergetic effect of peroxide and the release of other ions such as CN^- and iron complex [190], and SIN-1 may facilitate the accumulation of H_2O_2 for cell cancer cytotoxicity [191, 192]. So tracking NO status is a key critical step which will help researchers evaluate the net effect of NO in complicated systems. Instead of using new NO donors, some groups developed NO delivery systems that can directly deliver only NO(g) into the biological systems [165, 193, 194]. Though problems still exist such as the controllability, consumption of NO through the biological system, biocompatibility and cyto-toxic effect of NO's oxidative products, the use of NO releasing polymer and device is still promising.

A huge number of potential biological species can react with NO, including ROS [182, 183], thiols [27], lipid [30], DNA [63, 64], and proteins [62, 195, 196], which makes the actual NO level present in cellular environments hard to predict. For example, the effect of free thiol to NO is complicated. On one hand, thiols may react with NO forming new RSNOs, which may increase the effective half-life of NO but decrease the effective NO level. On the other hand, free thiols can facilitate RSNO decomposition resulting in a more rapid NO generation [197]. And these processes are very likely to be pH dependent. For RSNOs, lower pH potentially generates more HNO_2 and NO^+, which are strong nitrosating agents, preventing NO generation [198], while for diazeniumdiolates NO releasing is through protonation, which favors lower pH [180]. In biological system, cases can be more complicated because of different environment such as ion strength [178], making final NO level difficult to predict. By using our real-time NO measurement device, which directly showed that free thiols may significantly affect the NO level, has provided the direct evidence showing the correlation between thiols and NO exists. Although more complex experimental design is needed to thoroughly study the underlying mechanism and determine the optimal NO generation and effective NO level in the body.

4.6 Conclusions

This chapter introduced an application of the two-chamber real-time NO measurement device, to monitor NO levels in biological solutions and cell culture conditions. This information allows the direct correlation of NO level (not NO donor concentration or NOS level) with the observed biological response. This device was used to measure the NO generation profiles of different NO donors (CySNO, SNAP, GSNO and DETA NONOate) at physiological relevant levels in different buffer conditions, proving that NO generation profiles of all NO donors can be very dynamic affected by their specific environments. It was shown that this measurement device can detect the NO level change due to the introduction of free thiols, oxidative states, pH and volume of the solution. In the end, cells can be directly cultured in the device so that NO experienced by cells during the whole culture can be tracked; and the result showed that NO experienced by cells cannot be simply predict or estimated by the NO donor half-life or from a measured value obtained in PBS. To precisely study NO's biological effect, it is highly recommended to monitor and report real-time NO level of each specific experiment to eliminate the reporting of complicating circumstances that lead to inaccurate results. The different effects of NO shown by different NO donors on inhibiting MOVAS proliferation was studies by using this device, highlighting the importance of choosing correct examination time points and tracking NO duration of release.

Chapter 5

Highly Controllable NO Deliver System[1]

It has been established that, there is a need to develop a means to precisely deliver specific and known levels of NO at defined times to study the potential treatment of disease with NO. The chemical properties of NO and the aqueous environment of biological systems make controlling how much NO cells experience very problematic. Bubbling NO into a solution is not practical. A more viable approach was to exploit chemicals that produce NO in vivo, both enzymatically and non-enzymatically. More than 100 years ago, people began using glyceryl trinitrate (GTN) to relieve angina pectoris [38, 123]. However, in addition to drug tolerance issues, NO delivered in

[1]This chapter will be submitted to a journal for possible publication in the near future.

this manner is not precise and controllable and is very dependent on the individual's metabolism. Though using soluble NO donor is still one of the most widely used methods to expose cells to exogenous NO, this method may produce confounding and contradictory data. The information on the actual NO level and time variable is almost impossible to trace. A third approach used is gene therapy to control NOS level expressed in cells. NO levels in mammals relies on the normal function of NOS, restoring NOS or knocking-down/out NOS gene expression can change cellular NO level in such a way as mimics the normal biological events. However, this method is costly, and more seriously, altering gene expression is hard to control so the dose-dependent effect of NO, which is the most distinguished characteristic of NO, is difficult to study systematically in this manner.

Then researchers started to develop NO delivery systems specifically for biological research. Wang et al. [165] developed a gas-to-media NO delivery system for the culture study. The idea is that NO is highly diffusible and can pass through gas permeable polymers such as PDMS. So they submerged 500 μm thick PDMS tubes with outer diameter of around 0.2 mm into culture media solution, flowed NO gas into the tubes, stirred the solution with a magnetic bar within the culture solution to generate a homogeneous system. This device achieved control over NO concentration of the culture media. The NO level modulation depends on several factors, primarily the partial pressure of NO and O_2, which was supplied by a second PDMS loop. The major NO consumption occurs close to the tube edge, the so-called the boundary

layer, where excessive NO reacted with O_2 to form N_2O_3. The problem with this system is the potential of introducing high level of other nitrogen oxides and the stirring process significantly affects the cell activity in the culture system.

Since 1990's, S-nitrosothiols (RSNOs) have drawn more and more researchers' attention as NO donors. S-nitrosothiols are endogenously produced and labile molecules that are involved in NO delivery, storage and metabolism in vivo [93]. S-nitrosothiols can achieve wide distribution within organelle systems as long as there is thiol-containing substrate such as cysteine, glutathione and albumin. S-nitrosothiols function as the NO reservoir in vivo and there is great pharmacological potential of S-nitrosothiols for the treatment of vascular diseases. The mechanism of NO release from RSNOs is also relatively clear. In general, RSNO decomposition in physiological condition can be both enzymatic and non-enzymatic. The related enzymes include glutathione peroxidase, γ-glutamyl transpeptidase and xanthine oxidase [95], while the non-enzymatic factors includes thermal and photochemical decomposition, Cu^+ initiating decomposition, and ascorbate initiating decomposition [198]. Different from other NO donors, such as diethylamine NONOate (DEA/N2O2), which decomposes spontaneously in a nucleophile, pH dependent way in solution [93], and GTN, which requires a series of enzymes and factors [199], S-nitroso-N-acetylpenicillamine (SNAP), a commonly used RSNO, may be able to decompose in a regulated manner through controlling the decomposition triggering factors. And this control was

improved even more by covalently grafting SNAP onto hydrophobic polydimethylsiloxane (PDMS) [137]. It was clearly shown that by excluding transition metals and other reducing equivalents, NO release can be well controlled using light to trigger the decomposition of the RSNOs. This material will be used as the essential NO resource and calibration tool of the following research.

In order to accomplish the goal of developing a robust NO delivery system, several constraints need to be addressed: the NO delivery system should only deliver NO, not NO generating chemicals or NO reaction products; some means to easily modulate NO level is required; the structure of the system itself needs to be simple so that it can be easily sterilized and applied to cell culture.

In this chapter, a cell culture system that is able to deliver NO in controllable levels with temporal and spacial control is designed. The principle and calculation process, the detailed validation techniques and its application are also presented. Achieving delivering NO and the controllability relies on the controlled NO delivery polymer and the two-chamber coupled to the NOA. The system is applied to real cell work, that does not require deviation from the current cell culture protocols.

5.1 Localized NO delivery to cultured cell

Fig. 2.4 and 2.8 illustrated how NO concentration and flux changes with time and distance relative to the NO plane, proving that with appropriately increasing t, NO level in the vicinity of source plane can be stabilized and both NO concentration and flux decay to around half of the maximum value at a very small x value (within micrometer range). Especially because biological condition are complex, the high chemical reactivity of NO limits NO's spreading into the static culture environment. This result suggests that by using a plane of NO delivery, NO may be delivered in a very localized fashion since the NO level decreased sharply along with its diffusion pathway.

To experimentally show how localized NO's potency is, two-chamber NO measurement device introduced in Chapter 3 to measure NO flux at different distance away from the source plane (experiment set-up as Fig. 5.1 A).

From our model introduced in Chapter 2, we predicted that NO flux would decrease significantly when NO source was moving away from the measuring plane, and that the amount of NO present will be different in different solutions because of the different competing reactions (Fig. 2.4 and 2.8). Because of this, both PBS and complete culture media (DMEM with 10 % FBS and 1 % pen-strep), were used to measure the

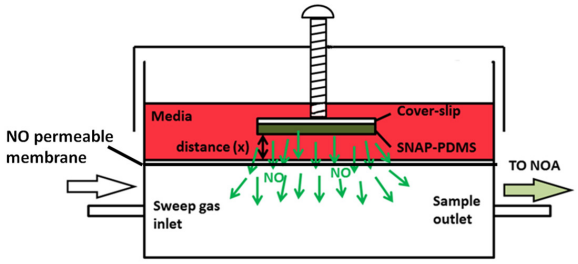

(A)

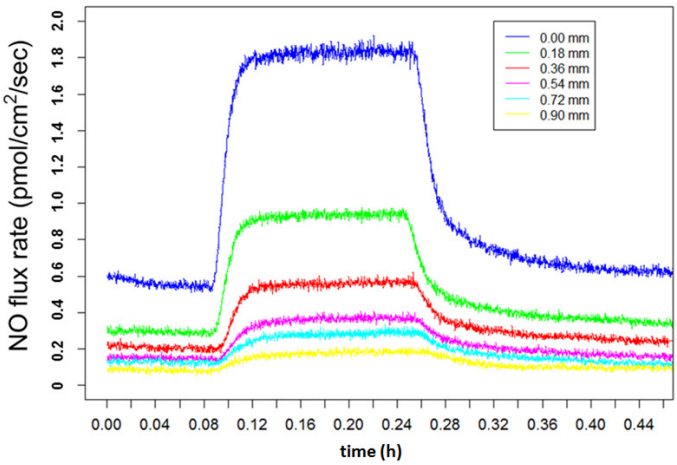

(B)

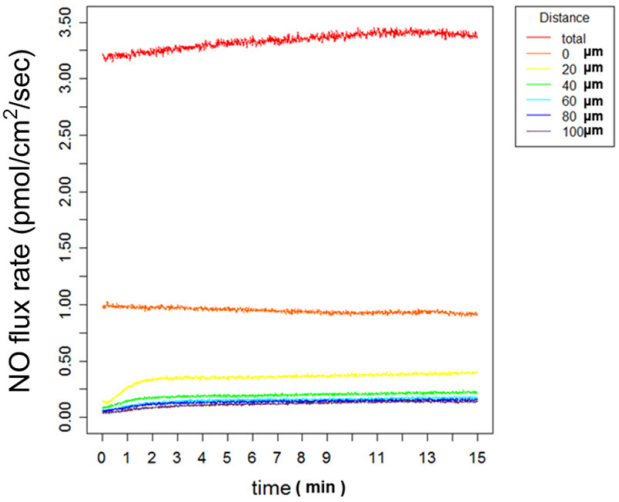

(C)

Figure 5.1: Measurement of NO decay with diffusion in buffer solutions. SNAP-PDMS was cast on a glass cover-slip and top coated with RTV-3140; the cover-slip was fixed at different positions in buffer solutions; NO flux passing through the semipermeable membrane was measured by using the NOA in real-time; all experiments were run at 37 °C. (A) experiment set-up; (B) in PBS solution; (C) in complete DMEM medium.

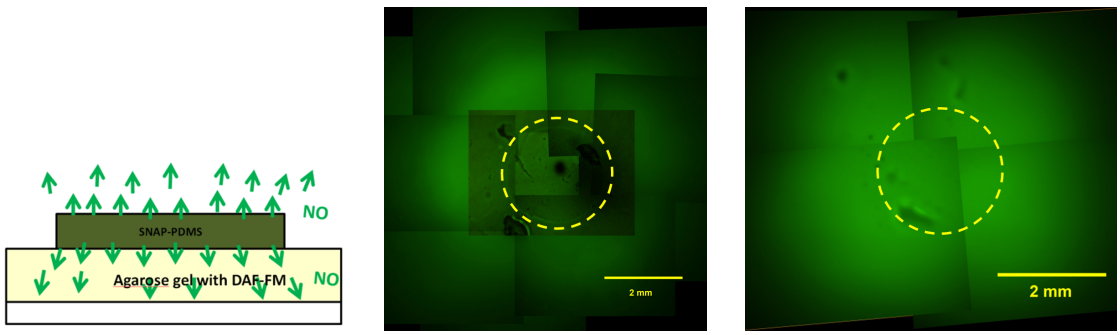

(A) (B) (C)

Figure 5.2: Visualizing NO's localized effect by using SNAP-PDMS films and NO fluorescent dye. (A) experiment set-up; (B) NO released from SNAP-PDMS labeled by DAF-FM was stained to green; yellow dash-line circle indicates where the disc was placed; (C) 2 mm diameter filter paper piece soaked in 5 mM $NaNO_2$ solution was placed on the DAF-FM plus agarose gel (circled by yellow dash-line); NO_2^- diffused out was labeled by DAF-FM as well.

diffusion distance of NO through solution.

In PBS (Fig. 5.1 B), the NO flux decayed to half its original level at a distance of approximately 180 μm away from the source, while in DMEM media (Fig. 5.1 C), NO decay was much more rapidly, to half its original level at about 20 μm. These results validated the modeling result, and also suggested that more complicated consumption routes may exist in complete DMEM (or in the in vivo environment). More importantly, since the source plane produced NO in a constant and stable fashion, the detected NO signal was very stable and continuous, confirming the previous simulation conclusion that by using the polymer NO delivery system, it is possible to create a stable NO environment with spacial control over where the NO is present.

To further test how localized NO's effect can be with the polymer NO delivery system,

a fluorescent dye was used to visualize NO's potential effective range. To do this, a SNAP-PDMS film was cut into 2 mm diameter disks and placed on to 1 % agarose gel with 20μM NO fluorescent dye DAF-FM in 37°C moisture incubator (experiment set-up as shown in Fig. 5.2 A). After 4-6 h, gel relative fluorescent signal was imaged under fluorescent microscope. Fig. 5.2 B showed the relationship between the position of the SNAP-PDMS piece (yellow circle by dash line) and the surrounding fluorescent signal. Fluorescent signal was observed only 2 mm away from the central polymer, suggesting again at aqueous condition NO will not diffuse very far so that its effective will be spatially limited. When the SNAP-PDMS disk was replaced by a piece of 5 mM $NaNO_2$ soaked 2 mm diameter filter paper, the result was very similar (Fig. 5.2 C), suggesting that the fluorescent halo might mainly be due to the diffusion of the activated dye. So that NO's effect might be even more localized than the fluorescent signal indicated.

To confirm this, a SNAP-PDMS film that released a relatively high flux of NO (up to an average of 1.2×10^{-10} mol/cm^2/min for 24 h) was cut into different shapes and placed on top of cultured MOVAS cells for NO treatment (experiment set-up shown in Fig. 5.3 A). Cell status was examined by calcein-AM staining as shown in Fig. 5.3 B to D, which showed sharp edges between NO releasing regions and regions without NO, further proving NO's effect can be very local by using NO releasing materials for NO delivery.

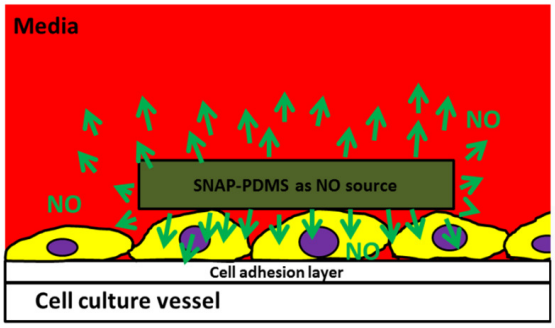

(A)

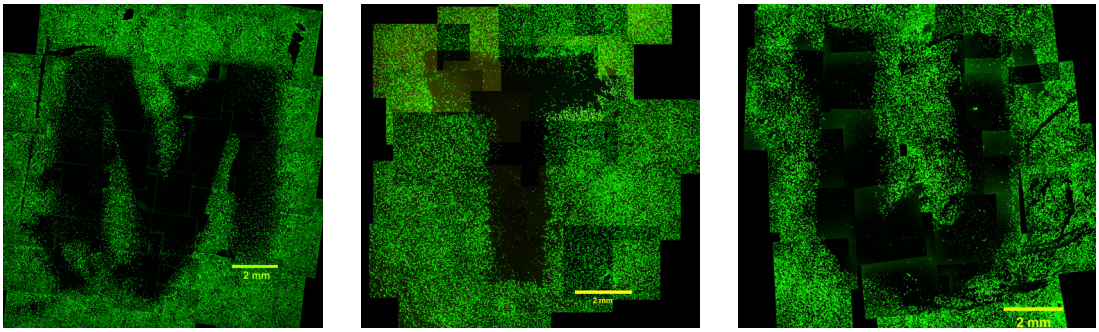

(B) (C) (D)

Figure 5.3: Visualizing NO's localized effect by observing the effect of NO released from SNAP-PDMS to MOVAS cells. MOVAS cells were seeded into the 6-well plate with a starting density of 4.0×10^4cell/cm^2; 4 h after seeding, SNAP-PDMS disks of different dimensions were placed onto the cultured cells; after 24 h culture, cells were labeled with 2 μM calcein-AM. (A) experiment set-up; (B) to (D) cell growth patterns.

5.2 Two-chamber NO delivery device for controllable NO delivery

To ensure that NO delivery can be systematically carried out, a tool that achieves delivering controllable level and duration of NO was developed. Since the real-time NO measurement device introduced in Chapter 3 allows NO generated from the cells

cultured in the upper chamber to pass through the semi-permeable membrane into the lower chamber for NO sampling, thinking of it in a reverse way, it should also be applicable to use an NO source attaching to one side of the NO permeable membrane to deliver NO to the cells cultured on the other side. This new method is based on both SNAP-PDMS and the two-chamber cell culture system, so that NO flux delivered to the cultured cells can be real-time tracked and adjusted according to the real-time NO flux feedback.

Using MOVAS cells, it was demonstrated that the localized effect of NO resulted in different cell fates. The NO level needed for preventing smooth muscle cell from hyperplasia was measured to be around $0.7 - 0.9 \times 10^{-10}$ mol/cm^2/min; and a higher NO flux (2.0×10^{-10} mol/cm^2/min) even for short time exposure (1 h) showed permanent cell damage, which should be avoided when designing SMC related NO releasing materials or using NO donors.

5.2.1 Device design

A new NO delivery set-up was designed to achieve controlled localized NO delivery (Fig. 5.5)

Cells are grown on the membrane of the NO measurement system and NO releasing polymers can be applied to the cultured cells from the other side of the membrane

according to specific needs and then removed so that the NO flux is zero after the defined delivery time. By connecting this system to the chemiluminescence detector, actual NO delivered to the cells can be monitored. Ethidium bromide was introduced to label the dead or dying cells for better understanding the cell status.

However while RTV-3140 and glass fiber filter paper was used to fabricate the NO permeable but water tight gas-permeable NO membrane, it was noted that there were some issues associated with the NO permeable membrane, including NO releasing polymer SNAP-PDMS could not be easily applied to the membrane and the quality of the fluorescent cell image and the stiffness of the produced film need to be improved for adhesive cells. To improve the use of the device for NO delivery, the fabrication process of the NO measurement device was modified.

Sylgard® PDMS replaced RTV-3140 reproducibly generates stiffer composite membrane. Glass-fiber filter paper was replaced by PVDF (polyvinylidene fluoride) membrane (pore size 2 μm). Compared with glass-fiber filter paper, PVDF has finer fiber structure. After PDMS polymer was cast, the produced membrane displayed more homogeneous and smooth surface, which is very important for fluorescent imaging. To manufacture the membrane the mixture of Sylgard® PDMS base and curing agent (10:1, w/w) dissolved in hexane was vortex-mixed to form 1:20 (w/v) PDMS solution. The solution was manually cast onto the PVDF membrane (72 μl/cm^2/cast) and air-dried. Three layers were cast to form a usable membrane. After the organic

solvent was air-dried, the membrane was carefully transported into 52°C heating oven for overnight curing. The micro structure of the produced gas-permeable membrane was examined by SEM shown in Fig. 5.4.

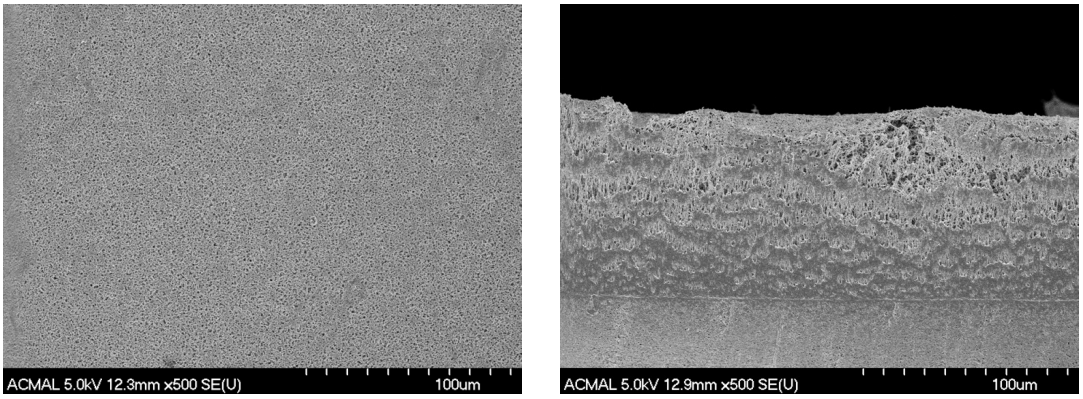

(A) (B)

Figure 5.4: SEM image showing the foam-like structure of the PDMS coated PVDF membrane (A) surface, (B)cross-section.

5.2.2 NO delivery device fabrication

To manufacture the delivery device, a semipermeable membrane was attached to plastic boxes to form the upper chamber of the device for cell culture as shown in Fig. 5.5 A. Dopamine solution (1 mg/ml, in Tris-HCl buffter pH=8.5) was applied into the upper chamber, soaking for 24 h to increase PDMS hydrophilicity; the chamber was ethylene oxide sterilized and top treated with 2 mg/ml gelatin solution for 1 h to facilitate cell adhesion. Then the device will be ready for cell culture. The lower chamber was produced by adding 2 ports onto a plastic box, so that the device

can be easily coupled into NOA sampling line. Once the two chambers were placed together, with the SNAP-PDMS polymer disk attached directly under the membrane, NO was delivered into the upper chamber at a specified flux, which simultaneously being quantified through sampling NO from the lower chamber as shown the Fig. 5.5 B and adjusted by the light source underneath the device.

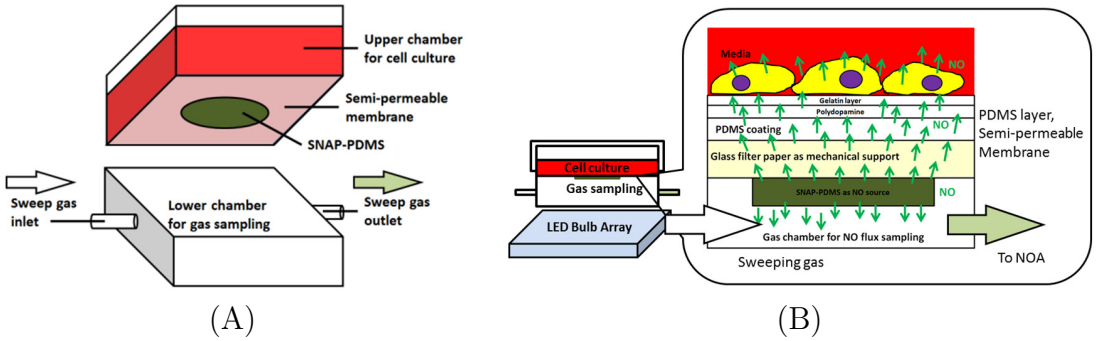

(A) (B)

Figure 5.5: New controllable NO delivery system for in vitro cell culture. (A) two-chamber device build-up, (B) experiment set-up for controllable NO delivery.

Because the actual level of NO being delivered to the cells is monitored in real-time, the NO generating rate can be modulated in real-time by adjusting light energy impinged on the polymer.

Since NO flux will be mainly controlled by light, to create a system that will generate homogeneous NO across the whole NO source plane, a homogeneous light source was needed. With the help of Andrew DeRouin, an 7×7 LED light array by using (VAOL-5GSBY4, Mouser, TX) LED bulb was fabricated. Blue light LED buds (593-VAOL-5GSBY4, Mouser), was tin-soldered onto the printed circuit board (PCB) to form a

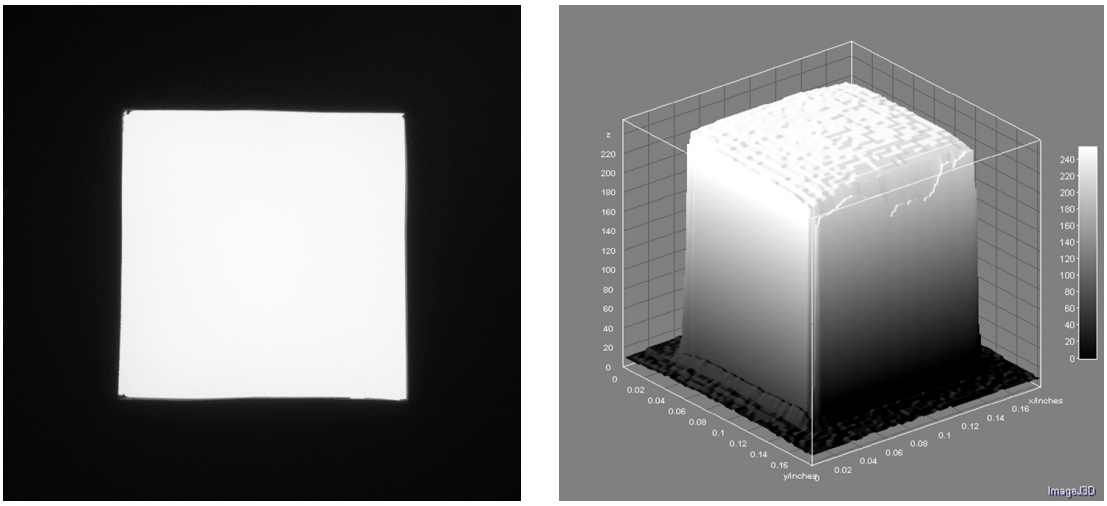

(A) (B)

Figure 5.6: Characterizing homogeneity of the light source. (A) raw digital photo of the light source; (B) analysis of signal intensity of each pixel of light source; the picture was represented by using 8 bits greysacle.

7×7 LED array. LED diffuser kindly provided by Bright View Tech (Morrisville, NC) was placed over the LED array to homogenize the light. To evaluate how homogeneous the light from the source plane was, digital pictures of the light source plane were taken with a black foam board placed on top of the light source to avoid light leaking. ImageJ was used to analyze the digital photo of the light source (Fig. 5.6 A) and the light intensity distribution is shown in Fig. 5.6 B. Signal strength of each and every pixel of the picture indicated a good homogeneity of the light source.

5.2.3 Controllable NO delivery device build-up

To confirm that the NO signal measured in the lower chamber and the NO entering the upper chamber are linearly related and the change was synchronized, two identically calibrated NOAs were simultaneously used to measure NO flux in real-time from both chambers; different LED light intensity was used to manipulate the total NO flux such that different NO levels in both chambers at different time points were recorded in real-time. Linear regression analysis was performed to validate the relationship between the flux levels measured from both chambers.

Note that NO released from SNAP-PDMS film either diffuses into the cell culture device or remains in the lower chamber. The signal sampled by NOA does not actually represent the NO flux experienced by the cells (the idea is the same with the two-chamber NO measurement device). The current question is how to use the real-time NO profile to calculate the NO flux experienced by the cells cultured in the device.

The following experiment was completed to determine the relationship between the sampled NO flux and NO flux that the cultured cells will experience in the upper chamber. The SNAP-PDMS disk (4 mm diameter, around 340 μm thick) was placed under the PDMS membrane as the NO source. SNAP-PDMS film was exposed under linearly changed light intensity by changing LED drive current linearly to generate

different total NO fluxes while NO in both chamber was recorded via two identically calibrated NOAs.

The NO flux pattern was recorded simultaneously (Fig. 5.7 A) and it can be seen from the linear regression analysis that NO signals in both chambers did change linearly with each other, R=0.9999 (Fig. 5.7 B). The difference of NO signals in the upper and lower chamber is observed and the distribution rate is determined by the geometry of NO releasing material, membrane properties and the attachment as explained in Chapter 3 3.5.6. These results suggested that once there is NO generation in the lower chamber by using SNAP-PDMS attached to the NO permeable membrane, cell cultured on the upper chamber can experience NO immediately without time delay, and the NO signal captured from the lower chamber and the actual NO delivered into the upper chamber was indeed linearly related.

To investigate whether the solution within the upper chamber alters the linear relationship, 10 ml complete cell culture media was added into the cell culture chamber and the linearity between NO remained in the lower chamber (integrated from NO profile curves) and the total NO entered the upper chamber (measured by I_3^- test) was examined. SNAP-PDMS was used as the NO source to release NO for a series of different duration (1 h – 24 h); then NO flux measured from the lower chamber and the corresponding cumulative NO products collected from the upper chamber were applied for analysis.

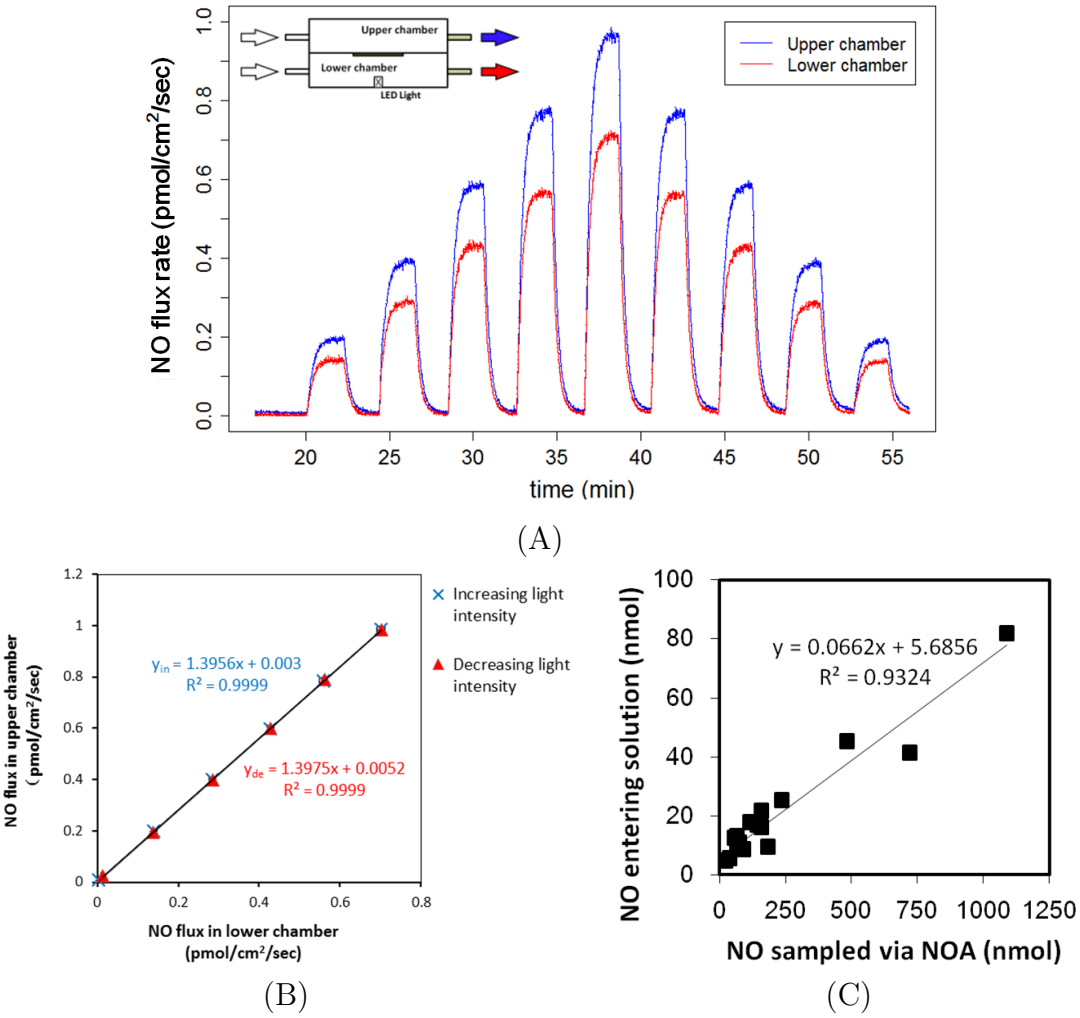

Figure 5.7: Analyzing NO signal in the two-chamber system. (A) NO measured in the upper and the lower chamber when using SNAP-PDMS for NO delivery. Different NO releasing rates were achieved by adjusting LED light intensity every 2 min (2.5 mA, 5 mA, 7.5 mA, 10 mA, 12.5 mA, by using VAOL-5GSBY4 LED); two identically calibrated NOAs were used to record the NO signal simultaneously from both chambers; (B) linear regression analysis of the NO flux signal captured in the upper and lower chambers at different LED drive currents; (C) Complete cell culture media was added to the upper chamber; the total NO entering the upper chamber was quantitated by measuring NO_2^- accumulation in the upper chamber using the tri-iodide assay [200]; total NO in the lower chamber was integrated from the real-time NO profile. The measured NO and the NO delivered to the cell culture chamber were indicated to be linearly related.

After repetitively using SNAP-PDMS to deliver different amount of NO (by different NO flux and time duration), the final result was summarized in Fig. 5.7 C, which also showed a very good linearity between the measured NO value and NO delivered into the cell culture chamber, though the distribution ratio differed greatly from the value obtained without bathing solution.

To summarize:

$$Flux_{upper} \propto Flux_{lower} \quad or \quad Flux_{upper} = a \times Flux_{lower} \tag{5.1}$$

$Flux_{upper}$ and $Flux_{lower}$ represent the NO flux into the cell culture chamber and the NO flux measured through NOA in the lower chamber at each time point, respectively (mol/cm^2/sec). $Flux_{lower}$ can be directly measured by the NOA in real-time. And a is the factor that represents the linearity ratio.

$$n_1 \propto n_2 \quad or \quad n_1 = a \times n_2 \tag{5.2}$$

where n_1 represents the total NO that entered the upper chamber (mol), which can be quantified by NO_2^- assays (tri-iodide assay was used), and n_2 the total NO sampled by NOA, calculated by integrating the NO flux curve:

$$n_2 = \int_0^t Flux_{lower} dt \tag{5.3}$$

So that the factor a can be found from Eqn(5.2)and used in Eqn(5.3), $Flux_{upper}(t)$ at each time point can be obtained. The whole process is illustrated in Fig. 5.8.

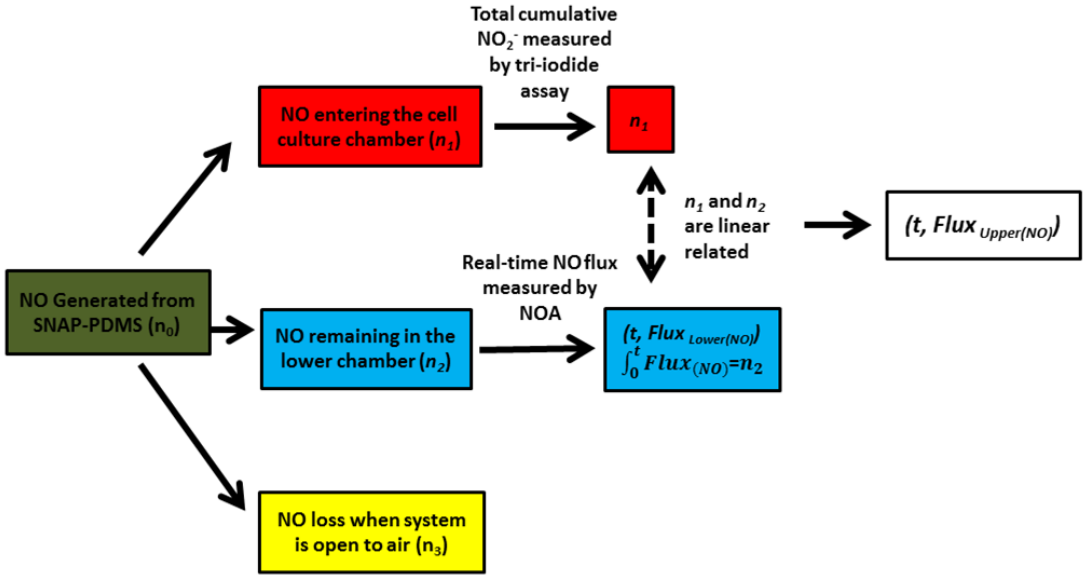

Figure 5.8: An flow chart illustrating how real-time NO flux that cells experience is calculated by using our NO delivery system.

By accurately measuring the NO level in the lower chamber and finding out the ratio of the upper chamber and the lower, the NO flux entered the upper chamber can be quantified and our device can achieve both NO delivery and the real-time monitoring. It is important to understand that the ratio of signal captured in lower chamber to the total accumulated NO in the upper chamber (the factor a) for each device set-up and must be experimentally determined.

5.2.4 Level and temporal control over NO delivery

To experimentally validate the procedure outlining in Fig. 5.8, complete cell culture media was applied into the upper chamber (without cells at this time) and different SNAP-PDMS was used to delivery NO. The SNAP-PDMS films were synthesized and cast from the same batch of polymer (to 340±70μm thick) but NO was pre-released from the polymers to obtain films with different NO fluxes at 37 °C, which are all physiologically relevant NO levels. Then those polymer films were used to deliver NO to the culture media applied in the upper chamber by using the device. Quantification was done according to Fig. 5.8.

Fig. 5.9 A showed their real-time NO delivery patterns. Although NO flux shows a decreasing trend in general, NO flux entering the upper chamber during the whole 24 h was much more stable (with around 30% to 70% decrease depending on the starting flux) compared with commonly used soluble NO donors which release all the NO within 4-16 h at physiological conditions (shown in Chapter 4).

NO releasing from SNAP-PDMS films can be precisely controlled by using light [137, 193]. By using this property, pulsed delivery of NO to cell culture chamber was achieved by applying/removing extra light from the LED array periodically (by using around 180 mA). Fig. 5.9 B showed that NO can be delivered to cells periodically

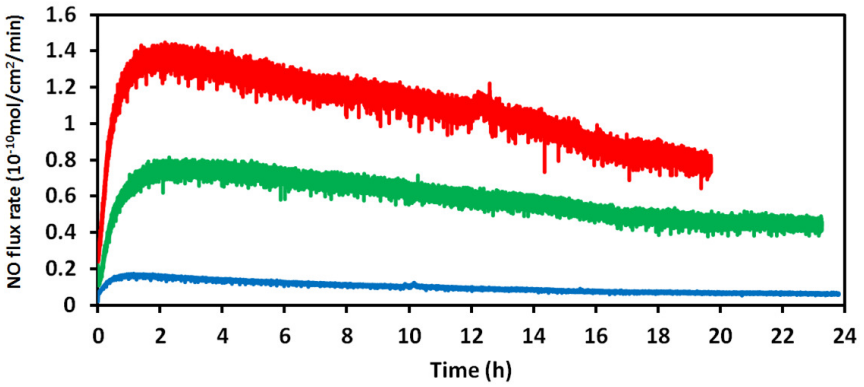

(A)

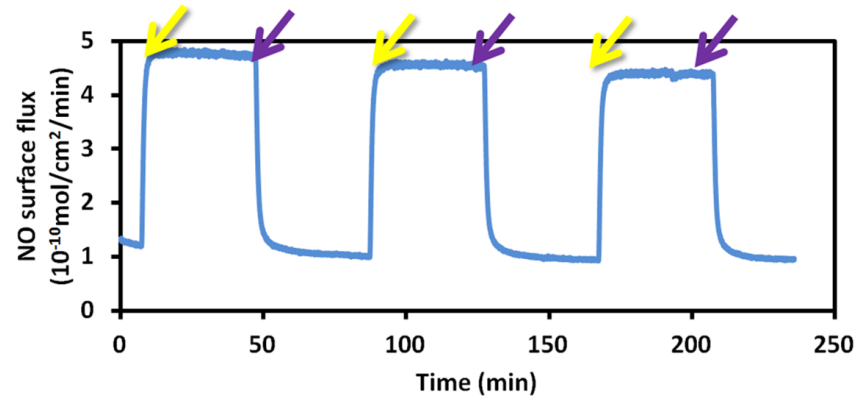

(B)

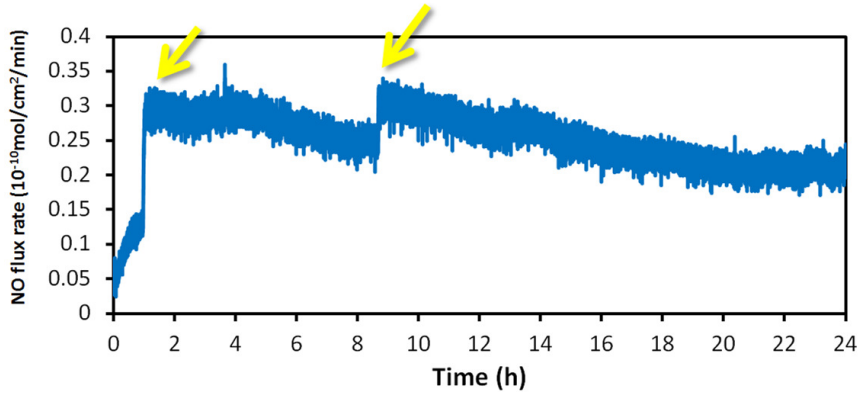

(C)

Figure 5.9: Examples of delivering physiologically relevant level of NO to the cultured cells with both level and temporal control. (A) Examples of overnight (maximum 24 h) NO delivery to the upper chamber; three lines represent SNAP-PDMS films with different passive releasing rates to deliver different levels of NO to cells; (B) pulsed NO delivery by switching on (yellow arrows) and off (purple arrows) LED light (add current/voltage) in very 40 min; (C) the control over NO delivery to cells by timely introducing light (yellow arrows, by increasing forward voltage) to generate a more physiological relevant and stable NO flux level.

with a very controllable pattern. If it is noted that NO level is too low, by applying different light energy onto SNAP-PDMS, desired NO levels may be reached. Fig. 5.9 C showed one example that when NO level was found to be too low, light was applied onto NO releasing polymer (yellow arrows), so that a much more stable NO level can be created during the whole treatment. From our previous work, no side-effect from the light was observed (data not show).

5.3 MOVAS responses to different NO patterns studied by the delivery device

This delivery system was then used to deliver NO to cultured MOVAS cells. Since we have roughly estimated the NO level to inhibit the proliferation of cultured smooth muscle to be 1×10^{-10}mol/cm^2/min [113], we re-examined this system by using our delivery system with real-time monitoring of the NO level experienced by cells during the whole SNAP-PDMS treatment. The SNAP-PDMS film position was indicated in Fig. 5.10 A to C imaged under bright-view light microscope. A 4 mm diameter SNAP-PDMS disc was attached underneath the membrane. The NO real-time profile was calculated according to Fig. 5.8.

Fig. 5.10 showed the relationship of MOVAS cell growing status and the corresponding real-time NO flux profiles. Interestingly, it was found that A compared with

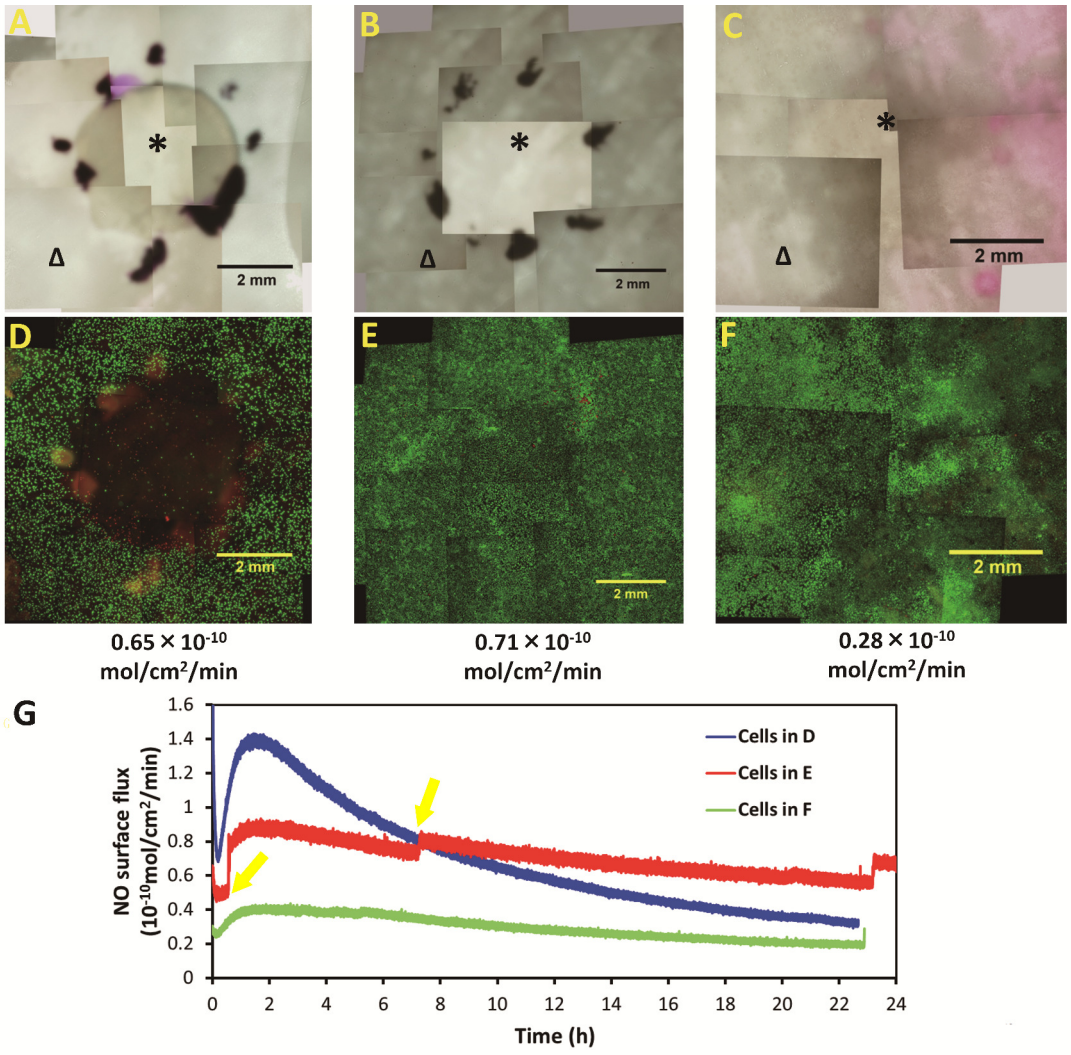

Figure 5.10: Real-time NO monitoring along with NO delivery. (A) to (C) indicate where SNAP-PDMS was placed (∗), Δ indicates regions without NO flux; (D) to (F) cell growth on the membranes, green indicates living cells stained by calcein; red, dead cells by EthBr; (G) represents real-time NO flux delivered to the cells in (D), (E) and (F) respectively; yellow arrows represent introducing light to adjust the NO flux.

B had a slightly lower averaged NO flux for 24 h, but the ultimate cell status was reversed compared with the observations in the previous section. However, from real-time NO flux data (Fig. 5.10 Panels G), it is showed that cells in D (treated

by polymer in A) experienced a maximum level of 1.4×10^{-10}mol/cm^2/min NO flux in the initial stage, without introducing light, NO flux decreased over 60% after 24 h. While cells in E (treated by polymer in B) experienced relatively stable NO flux during the whole 24 h due to the introduction of light (yellow arrows Fig. 5.10 H). Results indicates that the average NO level or total NO that cells experienced during a long-term treatment was not enough to interpolate the ultimate result. NO short-term fluctuation may have profound effect to cells so that it is important to consider the time dependent change of NO level. Overall, while the NO flux was larger than 1.0×10^{-10}mol/cm^2/min, cells that experienced such flux for even a relatively short period of time (4 h in this experiment) may undergo cell death (Fig. 5.10 D). An average of $0.7 - 0.9 \times 10^{-10}$mol/cm^2/min might be a good NO level to inhibit smooth muscle cell over proliferation without killing them (Fig. 5.10 E). These data might be important to develop proper NO releasing materials to prevent hyperplasia of smooth muscle cells, antherosclerosis or thrombogenesis. Because both levels that are too high or too low level ($0.3 - 0.4 \times 10^{-10}$mol/cm^2/min is considered to be low, Fig. 5.10 C, where no inhibition of cell proliferation was observed) were shown to prohibit its anticipated function. One consistent phenomenon is that NO's effect was always shown to be local. There is a good evidence suggesting that by using bulk NO releasing materials in real tissue, it is not likely to introduce NO's deleterious effect to other nearby cells unless those cells are within hundreds micrometers of the NO source.

It was appeared that an NO level higher than 1.0×10^{-10}mol/cm^2/min might bring about permanent damage to MOVAS cells. Using the device an experiment was completed to deliver different levels of NO to cells for the same duration trying to confirm the NO threshold. Currently it is also not clear what dose and duration of NO exposure at the level can cause irreversible damage to the cells.

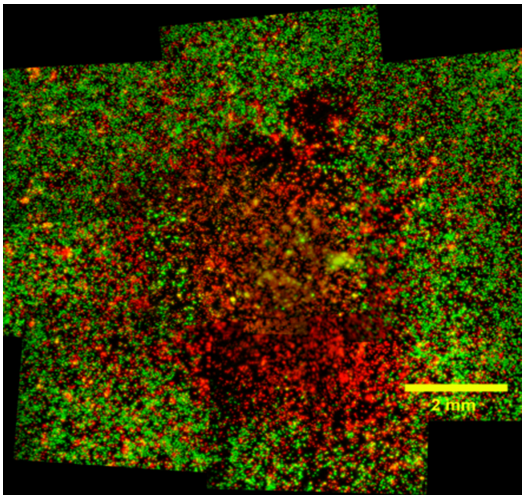

41.9×10^{-10} mol/cm^2/min

(A)

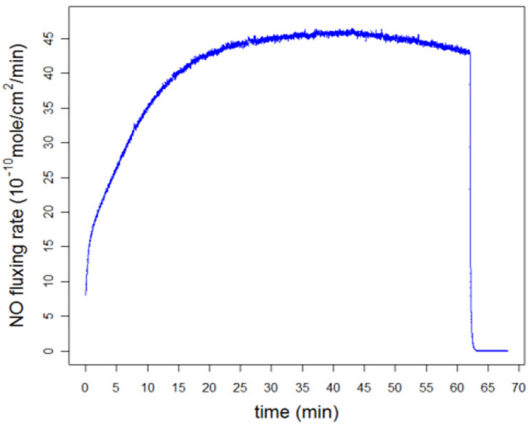

(B)

Figure 5.11: High NO flux for 1 h treatment caused MOVAS cell death. 4 mm diameter SNAP-PDMS disc was attached underneath the device; (A) cell status was examined by using live-dead staining 20 h after NO source was removed and cells were imaged under fluorescent microscope; the average NO flux was summarized under the cell image. The real-time NO flux was shown in (B).

One preliminary experiment showed that high NO flux (up to 45.0×10^{-10} mol/cm^2/min) for 1 h treatment caused cell death (Fig. 5.11). The flux was gradually decreased to below 1.0×10^{-10} mol/cm^2/min (the theoretical NO threshold) but the treatment time was held constant by using our NO

delivery system to search for the threshold flux value. In detail, cells were seeded into two-chamber NO delivery device at a starting density of 2×10^4 cell/cm^2, then cultured for overnight for recovery. Cells were treated with NO from a SNAP-PDMS film for 1 h and NO flux was real-time recorded with the NOA. NO flux was adjusted by changing light energy impinged onto SNAP-PDMS disc using LED light arrays underneath the cultured cells. 23 h after treatment, cells were stained with 2 μM calcein-AM and 5μg/ml EthBr and imaged with Olympus BX51 fluorescent microscope.

As shown in Fig. 5.12 A, cells exposed to high NO level for 1 h underwent cell death, generating an acellular culture region. Once the NO flux was close to 1.0×10^{-10} mol/cm^2/min, cells survive, but the eventual cell number was significantly less than regions without exposing to NO (Fig. 5.12 B). When the flux was further decreased (Fig. 5.12 C), cells showed no response to the NO compared with control cells (both cell morphology and living and dead cell numbers). This indicated that as for MOVAS cells an NO flux of 1.0×10^{-10} mol/cm^2/min might be a critical value. Larger than this value, NO may kill MOVAS for 1 h exposure. See Fig. 5.13 for representative images of replicate culture experiment.

Then different treatment duration was investigated. 1.0×10^{-10} mol/cm^2/min for 30 min (Fig. 5.14 A) and 40 min (data not shown) was used, and cell growing was observed as normal. After less than threshold treatment for 20 min (less than

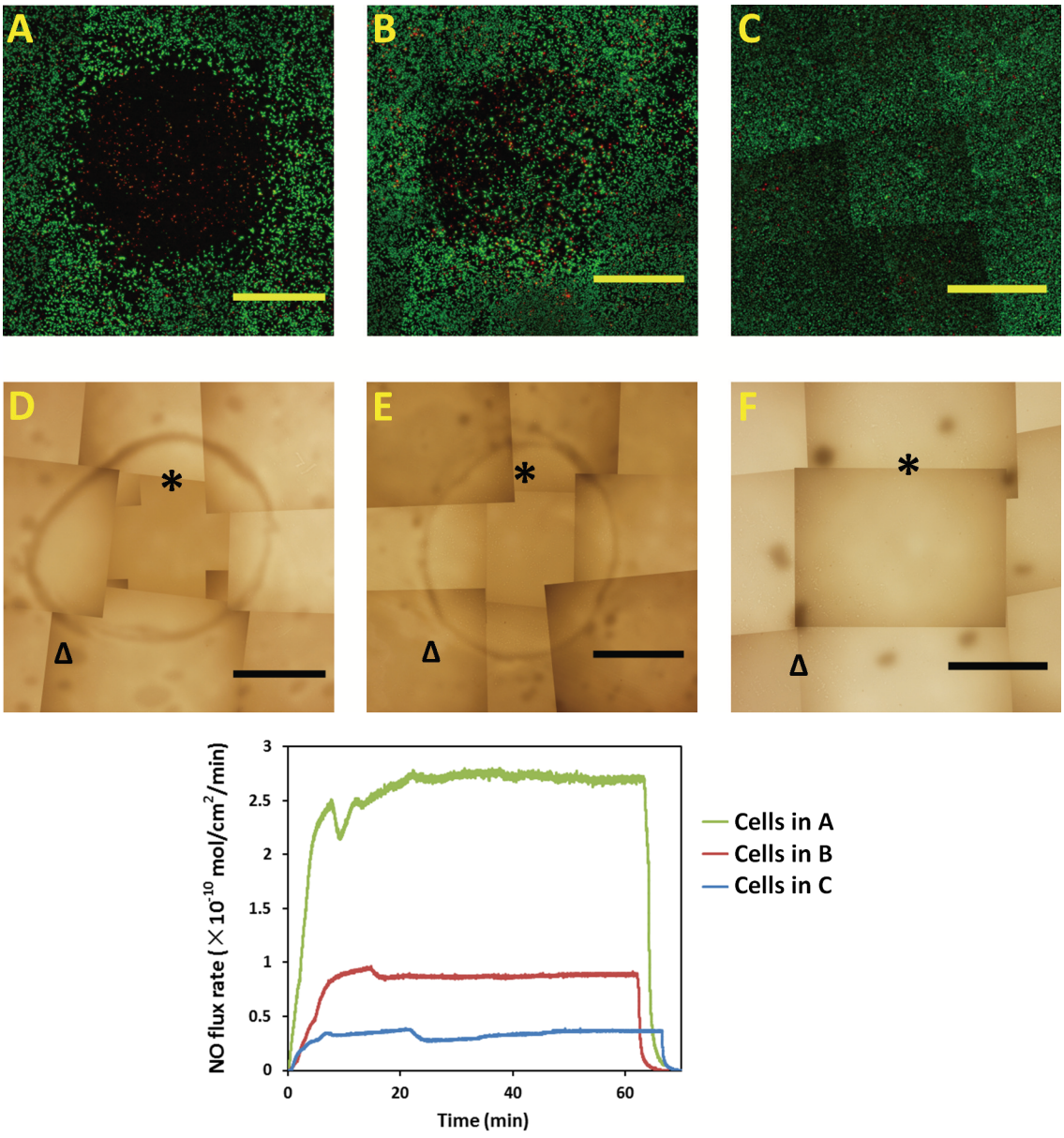

Figure 5.12: Quantitative study of NO flux threshold level that may kill MOVAS cells. Real-time data represents NO profiles of each corresponding sample above; (A) to (C), cell growth on the membranes, green indicates living cells stained by calcein; red, dead cells by EthBr; (D) to (F) indicate where SNAP-PDMS was placed; the location of NO releasing region was indicated by $*$ and regions without NO was indicated by Δ. (G) shows real-time NO flux delivered to the designated cells. Scale bar, 2 mm.

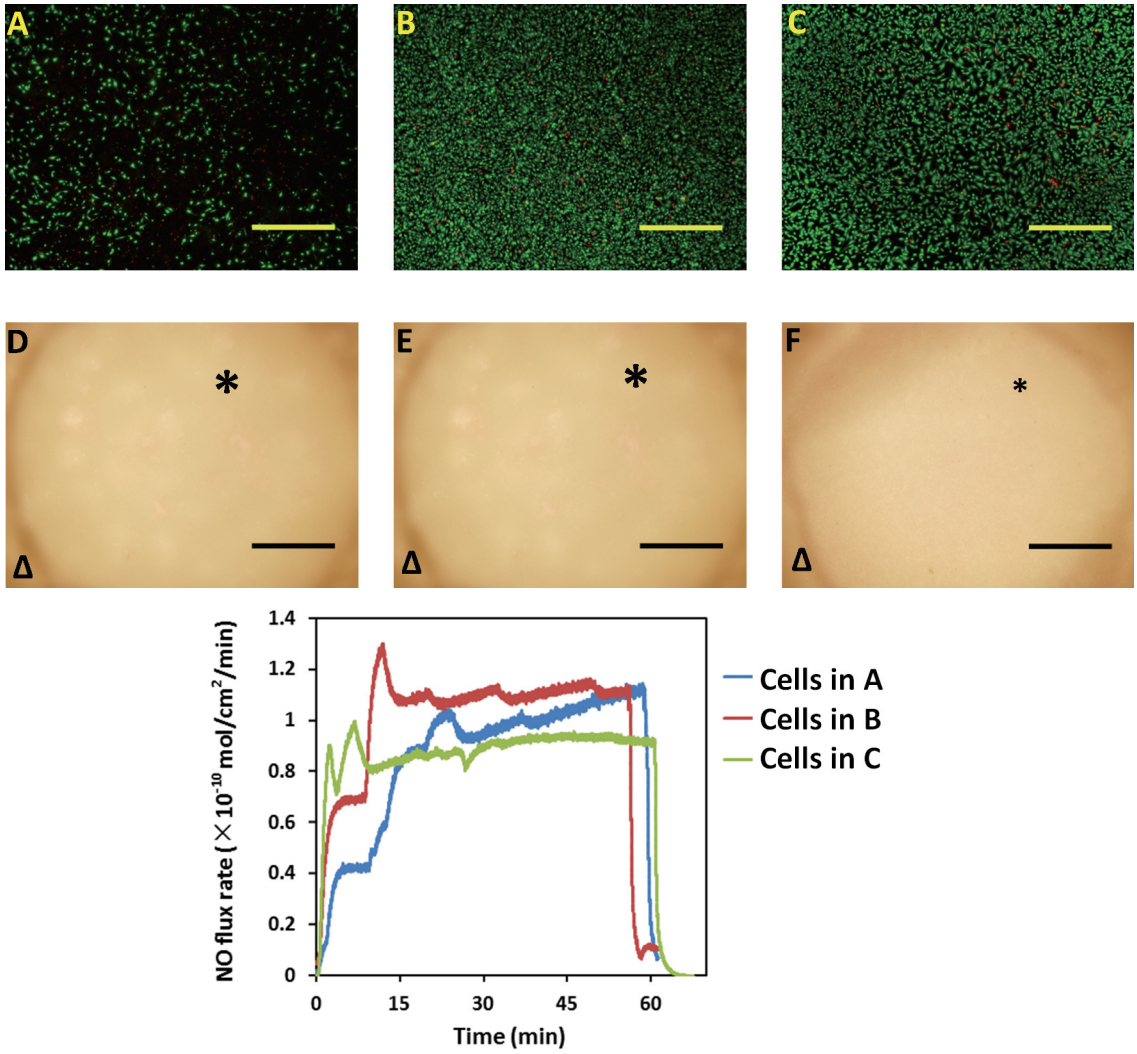

Figure 5.13: Different repeats of around 1.0×10^{-10} mol/cm^2/min NO flux for 1 h treatment to MOVAS cell. (A) to (C), cell growth on the membranes, green indicates living cells stained by calcein; red, dead cells by EthBr; (D) to (F) indicate where SNAP-PDMS was placed; the NO releasing region was indicated by $*$ and regions without NO were indicated by Δ. (G) shows the real-time NO flux delivered to the designated cells. Scale bar, 1 mm.

0.5×10^{-10} mol/cm^2/min), then close to 1.0×10^{-10} mol/cm^2/min treatment for 40 min, cell growth was also shown as normal compared with the control regions (Fig. 5.14 B). However, if the NO flux was increased to very high (average of

50×10^{-10} mol/cm^2/min), for even very short time (10 min), NO exposure also caused cell death (Fig. 5.14 C). It is notice that even the highest NO flux rate goes up to 200×10^{-10}mol/cm^2/min, NO's effect was still shown to be localized.

This data directly proved that both NO level and duration that cell experiences are important to determine the final cell fate. Looking at only one phase of this molecule cannot reveal its role or may even cause data misinterpreting. Neither conventional NO administration methods nor data presentation can achieve detailed understanding in these two dimensions, which limited the application of NO as a therapeutic tool. The new in vitro NO delivery system, integrating the real-time NO measurement device and NOA, and taking advantages of controlled NO releasing material SNAP-PDMS, an unprecedented control of level and temporal-controlled NO delivery has been achieved. Herein a systematical and quantitative study of the relation of NO and smooth muscle cell fate was given as an example, which provided very useful data to develop vascular implants and tissue repairing gels that release physiological relevant NO level.

5.4 Implications

There have been many NO releasing materials developed for fundamental research and biomedical applications. Several recent reviews summarized their chemical base

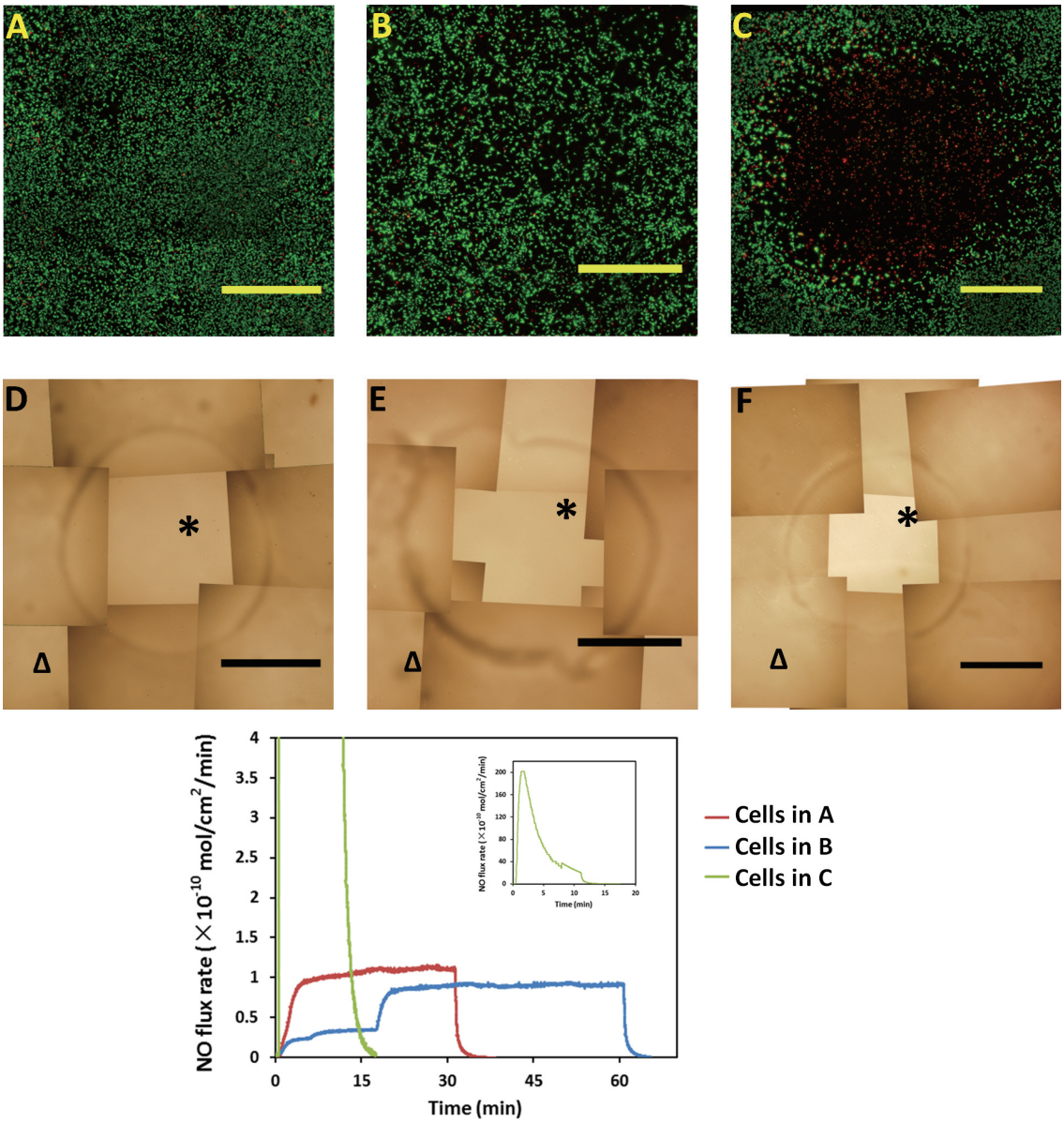

Figure 5.14: NO treatment duration determined the final cell fate. (A) to (C), cell growth on the membranes, green indicates living cells stained by calcein; red, dead cells by EthBr; (D) to (F) indicate where SNAP-PDMS was placed; the NO releasing region was indicated by $*$ and regions without NO was indicated by Δ. (G) shows the real-time NO flux delivered to the designated cells. Scale bar, 2 mm.

and related practical use [102, 107, 201, 202]. One of the most popular applications of these materials is for wound healing, since proper NO level is reported to promote endothelial cell proliferation and modulate the inflammation process. NO releasing tissue engineering scaffolds, especially hydrogels, have been shown to be a good tool to study such NO property and help wound healing. For example, as mentioned in 2.2.1, Amadeu et al. used a wound repairing hydrogel Pluronic F-127 with NO releasing properties by incorporating 100 μM GSNO to treat rat cutaneous wound, indicating that NO is important and has beneficial effect on healing at both inflammatory and proliferative phases [128, 129]. This is a good example of temporal study of NO's effect, although they did not report the actual NO status in the biological system; instead the GSNO decomposition rate was estimated in buffer solutions, which may differ greatly from the actual biological environment (shown in Chapter 4 4.2 and 4.4). The NO level needs to be carefully controlled when using NO incorporated cell scaffold. For instance, Xing et al. developed a SNAP conjugated gelatin hydrogel which releases NO in a fast fashion (up to 30×10^{-10} mol/cm^2/min) in the first 2 h at physiological condition, where this hydrogel inhibited the attachment of the hMSCs permanently [203]. Nablo et al. proposed NO releasing solgels as a coating layer for inhibiting bacterial adhesion [204], and also suggested that the NO releasing rate needs to be carefully controlled since 24 h exposure to NO fluxes to an average of 50 pmol/cm^2/s was cytotoxic to L929 mouse fibroblast [205]. So only if we precisely understand both NO level and temporal parameters, will NO's detrimental effect be

avoided and the beneficial functions can be utilized. Many current NO releasing tissue engineering scaffolds produce high flux of NO in the initial stage due to the properties of the NO generating functional groups used. Now that we understood the burst of NO should be avoided, measures to limit this fast NO generation can be developed. The light controlled NO releasing polymer SNAP-PDMS might be a good example, which avoided uncontrolled NO releasing initiated by other species such as copper ion, and achieves empirically tuning NO flux experienced by cells. And by using the two-chamber system, NO delivery can be more controllable, flexible and measured in real-time.

NO has pleiotropic effects on various physiological reactions. To clearly understand the NO level and time parameters would be a very important step to establish the real underlying cause-and-effect relationship of NO and the corresponding cell responses. NO's highly dynamic and reactive nature makes it difficult to predict and control its level under actual biological conditions. The NO levels discussed herein directly refers to NO flux that cell experiences, which can be calculated and measured by using our modeling and new device.

5.5 Conclusion

A new two-chamber NO delivery device was developed and validated. The delivery system integrated the technologies of controllable NO releasing polymer SNAP-PDMS, cross-membrane NO delivery and NOA chemiluminescent assay to achieve NO local, level and temporal-controlled delivery. The device was used to directly show how localized the effect of NO is in plane source model. By cutting SNAP-PDMS films into different geometries, desirable cell growth pattern can be achieved. The real-time data collected by NOA helped us understand the NO level during the whole experiment. It was demonstrated that both the NO levels and exposure time affect MOVAS cell fate, characterizing 1.0×10^{-10} mol/cm^2/min as the critical value; exposing to such value for more than 1 h may cause MOVAS permanent damages. To show this device is useful to study the importance of both NO level and time aspect, very high NO flux (an average of 50×10^{-10} mol/cm^2/min) and a little higher than 1.0×10^{-10} mol/cm^2/min of NO were applied to MOVAS for different duration, resulting in MOVAS death after short time exposure (10 min) under high NO flux treatment and no cell death was observed while 1.0×10^{-10} mol/cm^2/min was applied for less than 1 h, respectively. NO's double-edged-sword characteristic limited its use in tissue repairing gels, though NO's roles have been shown to be beneficial. This is primarily because we lack the understanding to know at what point good NO may switch from beneficial effect to damaging effect. This novel NO delivery

device will be useful for fundamental research including mimicking physiological and pathological level of NO, and evaluating the effective distance of NO, NO level and temporal dependent aspects.

Chapter 6

Conclusions and Future Direction of NO Quantification Devices[1]

NO is one of the most important signaling molecules that plays a role in nearly every organ. To ensure the balance of NO in the body, the biological level of NO needs to be well regulated on many different aspects such as level, location and activity of nitric oxide synthases (NOSs), accessibility to substrates (O_2 and arginine) and control of the NO environment (especially oxidative states). NO deficiency can cause serious problems such as cardiovascular diseases [75, 206] and neurological disorders [70, 71, 72]. Due to the high reactivity of NO, NO can react with many different species in a very local fashion, which is why this simple molecule is able to serve

[1]Part of the content in this chapter will be submitted to a journal for possible publication in the near future.

so many different biological functions. These different biochemical reactions require different NO levels and localized reactions to ensure the specificity of the reaction at each specific site. The effect of NO was generalized as beneficial to cells at low concentrations and detrimental at higher concentrations, however the reality is in fact far more complicated in different scenarios. NO's biologically relevant concentrations vary greatly from sub-nano molar (such as promoting endothelial cell growing, estimated from DETA/NO concentration [207]) to potentially up to micromolar range (such as inactivation of MMP-9 measured by applying exogenous SPER/NO solution [208], for more detailed review see [65]). It is also important to remember that NO's effective distance is short, otherwise its systemic side-effect would be fatal.

NO releasing materials have shown to be good tools for completing NO fundamental research, especially materials with hydrophobic backbones which limit the materials' interactions with the biological system and introduces more controllability over NO releasing patterns. So the very important hypothesis is that by using such materials to release biologically relevant levels of NO to achieve specific biological functions, the necessary NO levels may be determined. Definitely it requires accurate measurement of NO surface flux and material dimensions. For example Frost et al. estimated the NO level to prevent thrombogenesis on intravascular oxygen sensing catheters to be between round 1.0 to 2.5 $\times 10^{-10}$ mol/cm^2/min by using DACA $-$ 6/N_2O_2 $-$ SR coating [110]. However, such information is still lacking. Our lab did a great deal of research to develop controllable NO releasing materials and NO delivery systems [137,

194]. Currently an adjustment in the required NO levels can be dynamically controlled because of the feedback from the real-time measuring, however, this was still done empirically. One future direction could be combining the NO delivery system with a feedback loop and remote light control system ([193]), so that a programmed smart NO delivery system can be set.

The two devices introduced herein, just like the development of a microscope which can be used to observe many different samples, have great potential to enable many other applications. The ability to track NO in real-time and control the level throughout different experiments can provide us a large amount of useful information. This chapter will show some of the preliminary work and results, and examine how feasible and practical it is to apply the devices for different biomedical studies. Definitely more in depth future work is needed.

6.1 Measuring NO generation from other biological systems

Note that in different tissues, different NOSs generate NO at different rates, producing different local NO concentration environments, which is the basis of the multiple functions of NO. But the details of each situation might be more complicated than

this statement. Is NO flux mainly dependent on types of cells or types of NOSs or types of stimuli? What other biological molecules and conditions may influence the ultimate NO flux? Even with the same NO generation rate, at different physiological conditions such as different pH, oxygen tension, substrate accessibility, will the final NO level change? By using the two-chamber NO measurement device, these questions can be answered. One example was shown as follows.

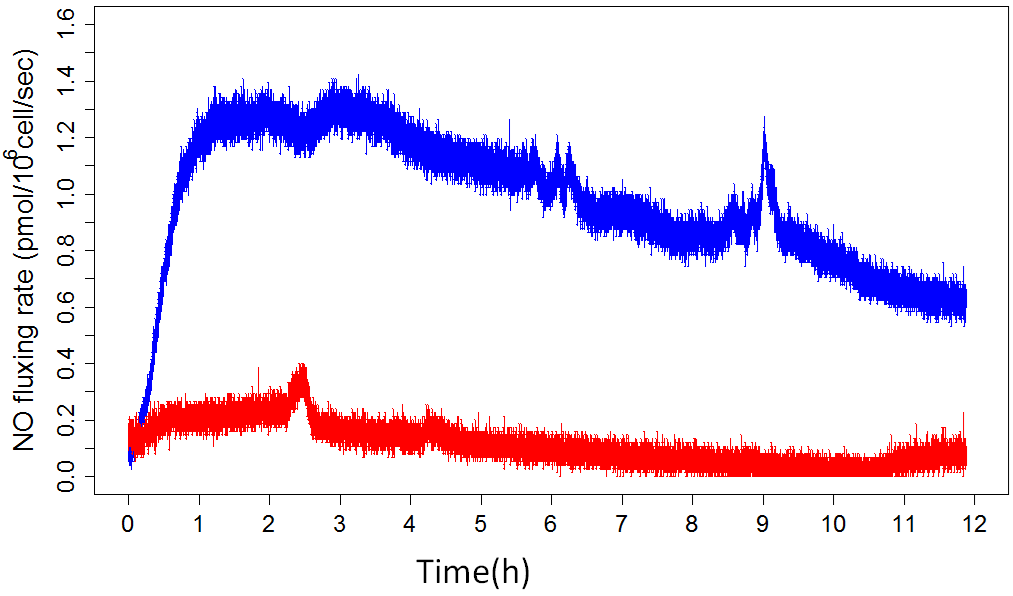

Figure 6.1: NO generation from rat primary tenocyte. Blue tenocyte, red fibroblast as the control.

An increase of iNOS experience has been discovered in the overuse of rotator cuff tendons in a rat model [209] and NO's roles on tendon healing, probably in different tendon healing stages, was summarized in Sharma and Maffulli's review paper [210]. NO generation from primary tenocytes, harvested from rat, were quantitated by the

NO measurement device.

Rat tenocytes were seeded into the two-chamber NO measurement device at a starting density of 8,000 cell/cm^2. Right after seeding, the device was connected to the NOA sampling line for NO real-time NO measurement. The level of NO generated is shown in Fig. 6.1. NO surface flux was calculated as introduced in 3.5.3. The result clearly showed that the NO generation profile from the different cell types differed from each other. Without extra stimulation, tenocyte harvested from the injury site showed inherent NO production, indicating iNOS might have already been induced before measurement. Tenocytes had a maximum of 1.4 pmol/10^6cell/s of NO, which is significantly lower than RAW264.7 cell (shown in 3.5.5). However, further work is needed to unveil the underlying reasons, which cannot be accomplished in this PhD work. But this result indicates that theoretically all the adhesive cells can be possibly applied to this NO measurement method. This simple method can be very useful for understanding different NO levels in different scenarios.

6.2 Monitoring NO status in solutions

Since soluble NO donors are still the most widely used method to supply NO to cultured cells, fully understanding the NO release patterns of those donors under real application conditions can also help us explain previous data and data collected from

different labs, which is also helpful for controlling NO to some extent. It has been shown how the NO measurement device helped us analyze NO data in Chapter 4. Other very useful quantitative studies can also be carried out with the similar principle. One simple example is that to investigate what different donor concentrations mean to cells? By using different concentrations of the donors, different NO concentrations are expected to be generated. So that many dose-dependent behaviors of cell-NO interactions are based on this hypothesis. To examine whether this assumption is valid, SNAP was dissolved in complete DMEM media at different analytical concentrations. Media volume was fixed to be 10 ml. Right after the SNAP solution was added into the measurement device, the device was coupled into the NOA sampling line. All the experiments were run under 37 °C without CO_2.

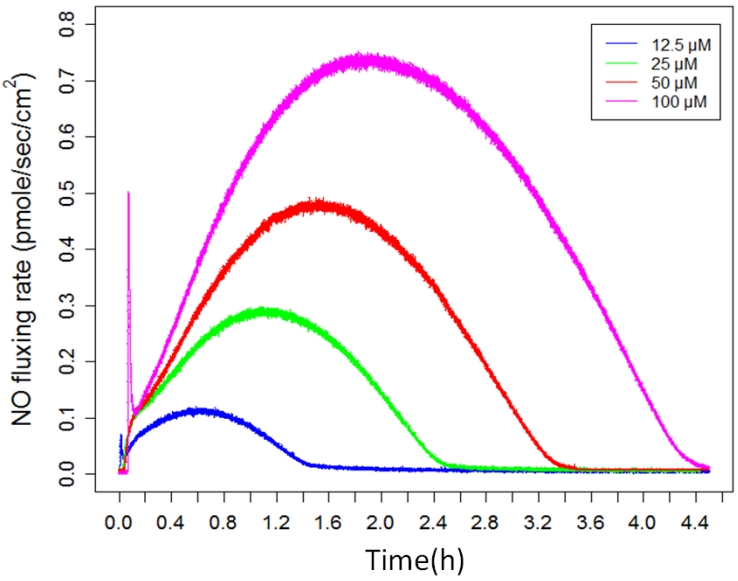

Figure 6.2: Evaluating NO profiles generated by different concentrations of SNAP by using real-time two-chamber NO measurement device.

Fig. 6.2 clearly shows the concentrations of SNAP not only determined the NO level within the solution but also duration of NO present in the solution. It also clearly proved that by using soluble NO donors to apply NO for cell culture, NO is only present in the initial several hours of the incubation. Since it has been shown that the time parameters are important to determine the ultimate cell fate in Chapter 5, to analyze such dose-dependent data needs to comprehensively consider the duration parameters. The data presented in this work directly proves that when analyzing the dose-dependent phenomenon observed through using different concentrations of soluble NO donors may not only result from a dose effect but also from different NO exposure time. This implies that much of the previously reported data may need more careful re-evaluation.

The biological environment of NO is complicated. NO generated from the NO source can be consumed by varies reactions. Without directly tracking the NO level, the study of NO reactions and the pharmaceutical applications cannot be accomplished. In Chapter 4, I showed how oxidative stress, pH and -SH all influence the effective NO level. The power of this measurement device is that it directly and in real-time presents NO information to help us understand NO biochemical reactions. The following example is that the device can be used is to study the relationship between vitamin-c and NO.

The redox level strongly contributes to the NO level achieved. It is clear that NO

reacts with superoxide, generating peroxynitrite. Strategies have been applied to limit the level of superoxide to enhance the NO level. It was also widely believed that applying ascorbic acid is beneficial for raising biological NO levels, because ascorbic acid potentially consumes tissue superoxide so that more NO can be used for other functions.

To examine this statement and for easier analysis, a simple composition buffer (PBS) was used as the reaction system to dissolve DETA NONOate (up to 200 μM). Then DETA NONOate solution was applied to the NO measurement device. Under these particular conditions (PBS buffer pH=7.4, 37 °C, without CO_2) it was shown that DETA NONOate generates relatively low NO level in a continuous and stable manner. If factors that can react with NO or influence NO generation from DEAT NONOate are introduced into the system, the change of the ultimate NO level can be directly observed by NOA. Freshly prepared (0.5 M stock solution) ascorbic acid was added into the device and the device was shaken gently to homogenize the mixture and right after adding ascorbic acid, NO flux started to plummet. To validate this result, different final concentration of ascorbic acid solution was prepared. It is interesting to observe the dose-dependent NO flux drop, directly proving that ascorbic may not increase NO level, instead may decrease NO level (Fig 6.3).

Though the detailed chemistry is not clear, it was observed that with longer time, the NO flux recovered (data not shown). The free radical scavenging property of

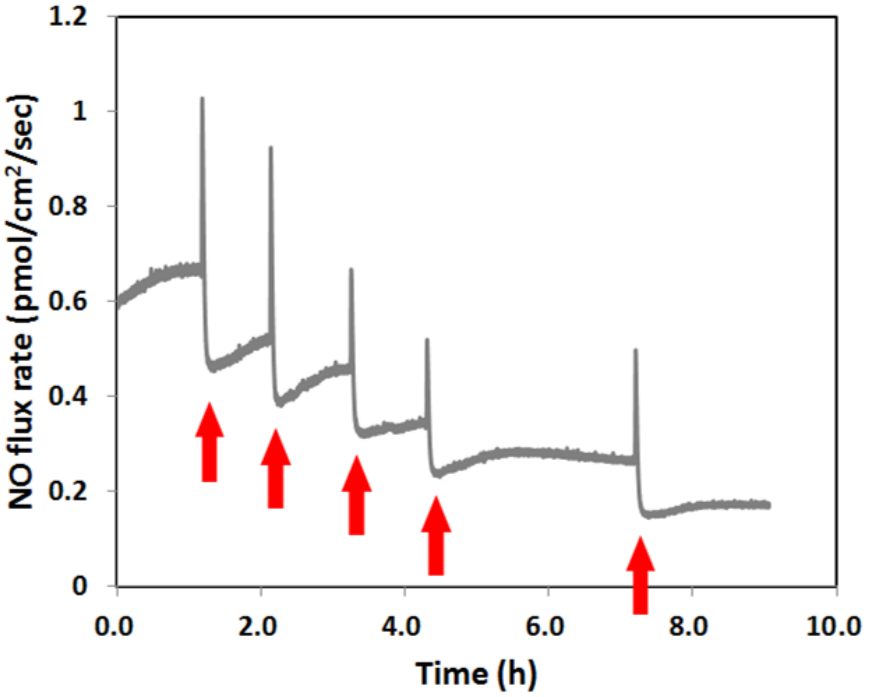

Figure 6.3: NO generation by DETA NONOate influenced by adding different concentrations of ascorbic acid. Red arrows indicate adding exogenous 100 μM of ascorbic acid.

ascorbic acid is widely known, bearing the brunt of the active and stable oxygen radicals in the human body [211]. The ultimate NO level has also been shown as ROS level dependent (shown in Fig. 4.8 and 4.9). Increasing the superoxide level by manipulating SOD was shown to increase the effective concentration of NO [212]. However, from the current data, to restore the correct NO level, there is still great need to more carefully evaluate whether taking extra ascorbic acid is a good strategy. To further unveil the mechanism of this reaction, other assays in different biological models are necessary. But from this device, the conclusion can be drawn that using ascorbic acid might not be helpful for restoring the correct NO level in our body,

which is also consistent with the report from Jackson et al. [213].

6.3 Assisting cancer staging and investigating the background NO within tumor tissues

The general trend is that high NO levels cause cytostasis and cytotoxic effects to cancer cells, while low NO levels may assist tumor development through angiogenesis and blood flow adjustment. To facilitate NO therapy, it is critical to find the threshold values and understand how to clearly differentiate between NO that promotes tumor growth from NO that inhibits tumor growth. Another on-going research project in our lab utilizes the NO measurement and delivery devices is to use specific NO levels to assist cancer killing without damaging the surrounding health normal cells. Different from MOVAS (a threshold level slightly higher than 1.0×10^{-10}mol/cm^2/min), it is observed that the threshold NO level needed to kill breast cancer cell line MDA-MB-231 was greater than an order of magnitude (10×10^{-10}mol/cm^2/min). The devices developed in this work will probe the roles NO plays in tumors and potentials on how to use NO to achieve localized cytotoxicity for cancer therapy.

6.3.1 Measuring NO from tumor tissues

NOS gene expression has been reported in a variety of tumor tissues [214]. Many gene therapy models have been established to overexpress exogenous iNOS in cancer cells. But the treatment results seem paradoxical. For example, Jenkins et al. [215] reported that a transfection of iNOS cDNA cassette into murine tumor cells, instead of killing cancer cells, promoted tumor growth (human colon cancer DLD-1 cells generating 20 pmol/min/mg NOS protein), while iNOS microencapsulated cells (producing up to 300±40 pmol/min/mg NOS activity) achieves almost 100% killing of SKOV-3 ovarian tumor and half of DLD-1 tumor [214]. Meanwhile tumor cells' genetic background may complicate this question. One example would be NO's cytotoxicity was reported as p53-dependent. In wild-type p53 cells, NO, as an anti-tumor drug, induces p53 phosphorylation, eventually causing apoptosis. However, in p53 mutant tumor cells favors NO for its VEGF inducing effect, which promotes tumor angiogenesis. In addition, incorrect levels of NO can even potentially create a selection pressure for mutant p53 cells, making the mutants more NO resistant, worsening the cases (reviewed by Xu et al. [22]).

Since NO's effect in tumor tissue is always controversial, many studies evaluated the correlation between NO and the tumor tissue development. For example, in human ovarian cells, iNOS was only observed in tumor cells not normal ones [216]. Data also

suggested that NO level is strongly correlated with breast tumor development stages. Compared with non tumorigenic cells NO levels were found significantly higher in cancer cells, especially in the more invasive grade III cells [217]. Besides cancer cells themselves, tumor associated macrophages (TAMs) is another important source of NO in the cancer tissues, whose status is closely related to cancer prognosis [218]. It has been shown that the present of iNOS in TAMs in the stroma of breast carcinomas also promotes tumor growth [219].

To fully explain these contradictions, it is pointed out that all the NO experiments need better control in terms of the real NO status within the biological environment created by NO donors or iNOS expression systems. Some control examples would be Thomas et al. [154] showed MCF-7 cells exposed to different time spans and concentrations of NO resulted in totally different cell fates. And Hickok and Thomas [220] showed totally different HIF-α accumulation patterns in MCF-7 cells because of using different NO donors. However, in these experimental designs the NO measurement method itself was still rough in terms of time resolution and NO delivery control was not achieved.

Considering NO's biological functions, such as angiogenic property and the potential to activate matrix metalloproteinase, NO levels in a complex tumors can be variant due to different tumor nutrients and metastasis. Meanwhile NO from macrophages showed tumoricidal activity too [221]. The hypothesis is that there are NO thresholds,

above which NO will perform as a tumor inhibitor otherwise as the cancer protector or promoting signaling for angiogenesis. So that by measuring NO level not only cancer cells might be correctly staged, more importantly cancer cells' local environment, such as blood supply status, oxidative states, potential chemo/radio resistance pathways, and immune activity, can be more precisely understood.

Many studies have been done to add new data and knowledge on how NO's level and temporal status affect the cell fate (Reviewed in [65]). But there is no research that has been done to systematically study this important biological event largely due to the lack of a good study tools. The two-chamber NO measurement device with the NOA real-time measurement may have great potential here. Different from the traditional semi-quantitative measuring methods, the device developed has achieved direct absolute NO surface flux quantification, without influencing the cell's normal growth. So that the same cells that were used in NO measurement experiments can also be used for other biological assays if needed. In this case it achieved that every single biological sample can have its own NO profile data and be analyzed even more comprehensively by other biological assays.

A preliminary study on measuring NO from tissues was completed. Though simulation of NO flux from a solid tissue is missing now, the work here circumvented this difficulty by preparing a PEG-based SNAP grafted NO generating hydrogel. SNAP was covalently linked to PEG hydrogel. NO generation was enhanced by shining light

onto the gel. A 6 mm diameter 4 mm high hydrogel was attached onto our device membrane. NO flux from the bottom can be measured as shown in Fig. 6.4. The NO profile shows good time resolution upon the light stimulation. And according to the simulation and the previous NO releasing polymer biocompatibility test, which shows endothelial cell layer has an NO surface flux of about 1×10^{-10}mol/cm^2/min magnitude [113], the data presented here shows the device might be applicable to process cancer studies on biologically relevant NO levels if tissue culture can be correctly processed in the device.

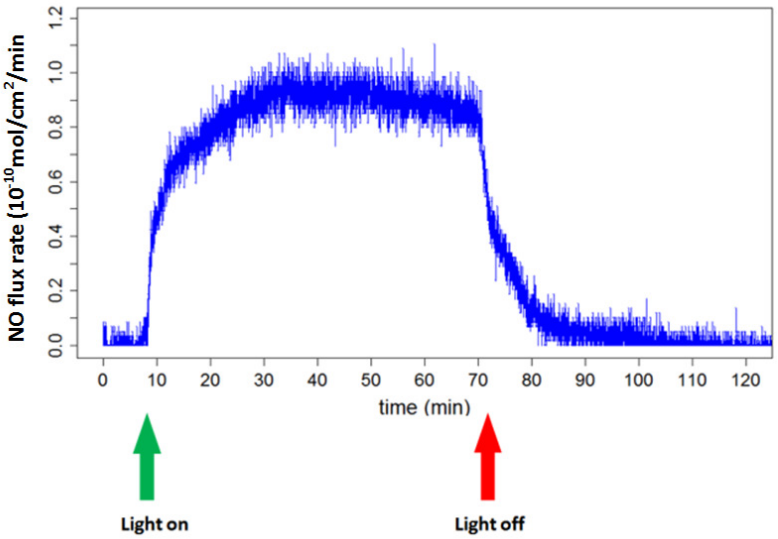

Figure 6.4: NO flux measured from the light-initiated NO releasing PEG-SNAP hydrogel. PEG-SNAP hydrogel was applied to the NO measurement device and soaked within PBS; constant light intensity from an LED bulb was applied to the material to initiate high NO dose releasing. Green arrow indicates light on; red, off.

Since within many cancers, one major source of NO could be TAMs, which can be

strongly correlated with a poor prognosis [218], macrophage RAW264.7 cells were cultured on a 18 mm × 18 mm glass cover slip and stimulated with 100 ng/ml LPS to mimic a cancer tissue with TAMs that releases NO. RAW264.7 cells were seeded at a starting density of 80,000 cell/cm^2 and cultured for overnight. Then cells were stimulated with LPS. 12 h after LPS was added, the cover-slip was applied to the NO measurement device for NO measurement. Figure 6.5 shows once cover-slip was cell-side-down mounted to the measurement device, the NO signal was detected almost immediately, suggesting good time resolution of the device and applicability for measuring NO level associated with cancer tissues. Combing with the hydrogel data, it is suggested by normal cancer cell and tissue culture the device may be able to quantify tissue NO levels of interest.

Since real-time NO data will potentially indicate specific cancer stages very quickly, the measurement device will definitely support the traditional assay data and make pathological assays more accurate and quick to guide the diagnosis and treatment. The future work can be focusing on measuring NO level in the cultured cancer cells and tissues in real-time by using tissue culture standard protocols. Tumor microenvironment might be different from the normal tissue, which may influence the activity of the NOSs and the efficacy of the anti-tumor drugs. Recent study has shown that antineoplastic pro-drug Banoxantrone (AQ4N) can only be activated by NO generating macrophages under hypoxic conditions [222], suggesting that the importance of understanding NO and oxidative status when studying the drug-tumor interaction.

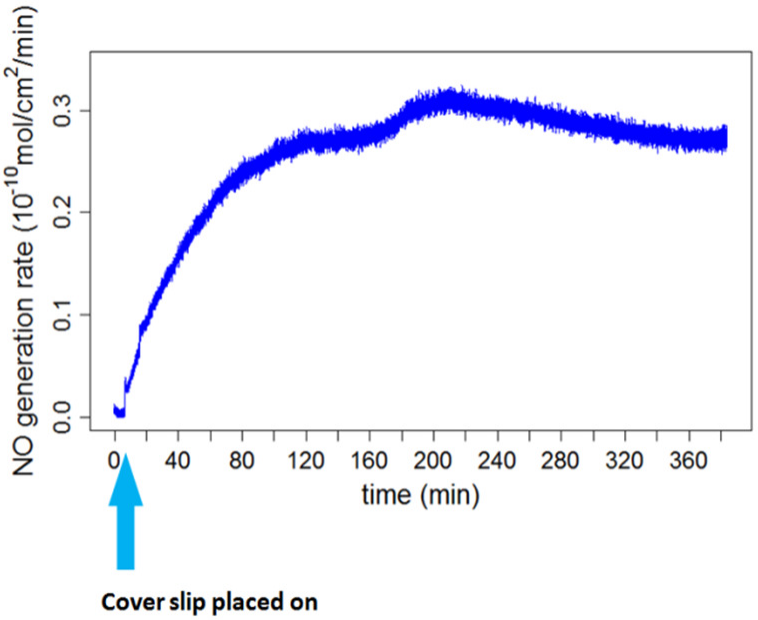

Figure 6.5: NO flux measurement of the macrophages (RAW264.7) cultured on the cover-slip. Blue arrow indicates when the sample was placed on the device.

The two-chamber system provides real-time NO information relatively independent to cell culture and treatment processes. In this case the potency of each factors that may affect cancer and NO behavior can be evaluated by using this device. For example to study how NO determines cancer cell fate under normal, hyperoxic and hypoxic conditions and environment with different reactive oxygen species (such as superoxide and peroxide), it is simply needed to culture the cells in the device under different conditions and apply the measurement methods.

6.3.2 Localized delivery of NO to the breast cancer cell line in a controllable manner

NO has almost all the good properties of an ideal anticancer molecule, including small cytotoxicity effective distance, short acting time, and relatively safe ultimate products. NO may be an active chemosensitizing regulator in hypoxic tumor cells [223, 224]. NO donor, conjugated with other anti-cancer drugs, showed an enhancement of drug efficiencies [225, 226]. NO was also used alone to inhibit cancer growth by gene therapy methods [227]. Whether working synergistically with other drugs or alone, a correct NO level is critical, where NO will not exert its other functions for instance cytoprotection, angiogensis, or metastasis. If not, paradoxical results might appear such as iNOS's cancer promoting effect observed by Jeckins et al. [215] vs cancer inhibition effect claimed by Xu et al. [214]. Although the control over the dose and temporal variables of NO used for cell treatment has been emphasized for years, in fact NO experimental procedures are still not well controlled. Quantitative work was largely dependent on the experience of the operators or the estimation from the kinetic equations.

It has been shown that the NO delivery device can be successfully used to inhibit the proliferation of SMC cell line MOVAS cell by using NO releasing polymer for localized NO delivery (As shown in Figure 5.3 and 5.10). Due to NO's high reactivity,

NO's effective distance is only within then hundreds of micrometers range, where it functions and also loses its functions. This will confine its effective range and minimize the potential side-effect. By using the same principle, optimized therapeutic NO level for killing or inhibiting cancer cells can be examined. To evaluate the feasibility, breast cancer cell line MDA-MB-231 were applied for the NO delivery examination.

Cells were seeded into the NO delivery device at a starting density of 40,000 cell/cm^2 and after overnight recovery the lethal NO level determined in 5.4 ($1 - 2 \times 10^{-10}$mol/cm^2/min) was applied. Data showed this cancer cell line is more NO resistant compared with the smooth muscle cell line (Fig. 6.6 A and C).

According to the previous reports, an initial high level of NO treatment for a relatively short time is advised for cancer treatment [22, 214], but there is no quantitative statement yet that defined how high and short this burst treatment should be. High flux of NO (average $13.8 \pm 2.1 \times 10^{-10}$mol/cm^2/min) was delivered to MDA cells for only 30 min. Twenty-four hours after treatment, live-dead assay also shows MDA cells survived such an NO treatment (Fig. 6.6 B and D).

Their corresponding real-time NO delivery patterns were shown in Fig. 6.7, respectively. It suggests that a beneficial NO level for cancer-toxicity might be very high (even higher than around 15×10^{-10}mol/cm^2/min, which is normally very toxic to MOVAS cells), or there might be certain scavenging pathways within MDA cells to suppress the effective NO level that was actually experienced by the MDA cells.

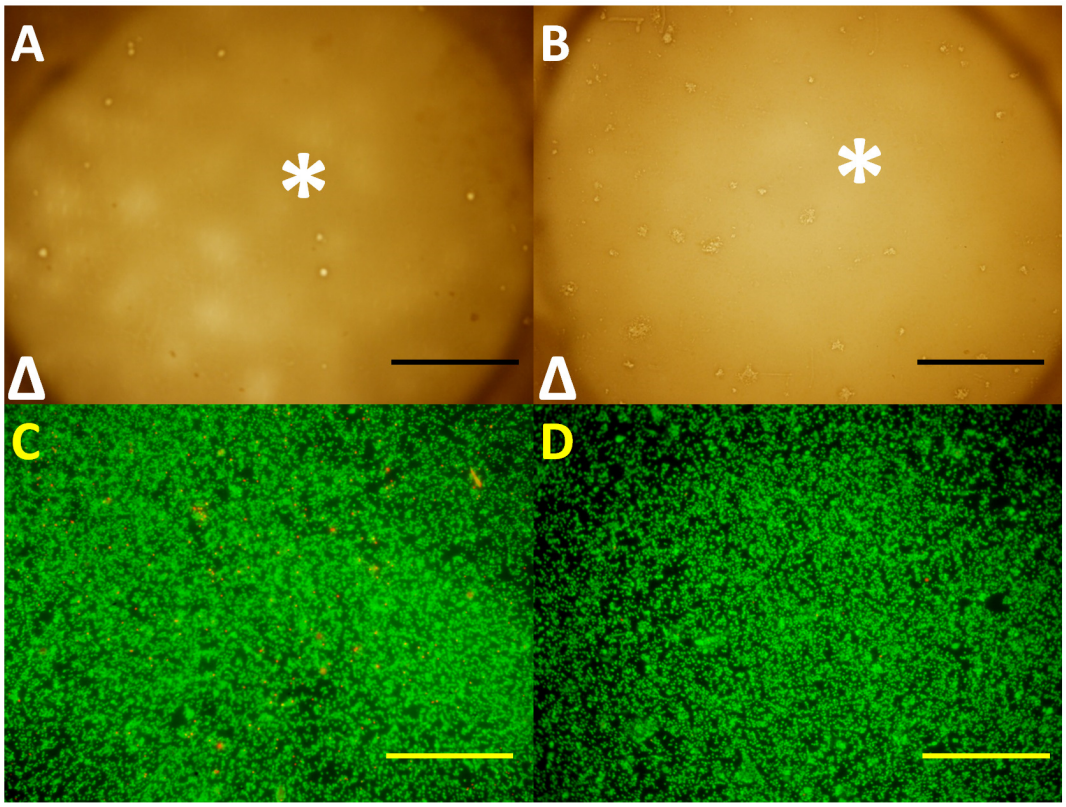

Figure 6.6: Controllable NO delivery to MDA-MB-231 cells. (A) and (B) show where the NO releasing region is indicated by $*$ and regions without NO by Δ. (C) and (D) show cell growth on the membrane corresponding to (A) and (B), respectively.

Further increase of NO flux to up to 30×10^{-10}mol/cm^2/min for the first 20 min achieved killing MDA cells (Fig. 6.8), showing the cyto-toxicity of NO to MDA and this effect is also very local.

These results are interesting. The NO threshold that can kill MDA cells is very different from the threshold for MOVAS cells, which directly proves the tissue specificity of NO's effect. Currently many NO studies use relatively complex models. Though many results are intriguing and significant for medical applications, it might not be

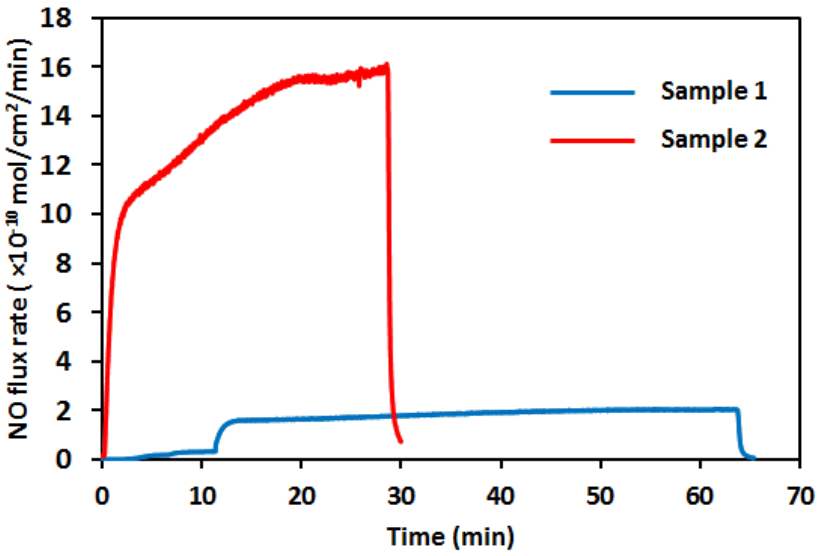

Figure 6.7: NO delivery to MDA-MB-231 cells. Sample 1 corresponds to cells shown in Fig. 6.6 (A) and (C), while Sample 2 corresponds to Fig. 6.6 (B) and (D).

very helpful for elucidating the detailed underlying mechanisms since the variable control is very difficult to achieve in such conditions. Separating factors and understanding the weight of each factor rely on the in depth NO quantitative investigation in different simpler and controllable biological systems. By using the method presented here as an example, hopefully more fundamental researches can be carried-out to unveil NO's level, temporal, spacial and tissue-dependent nature.

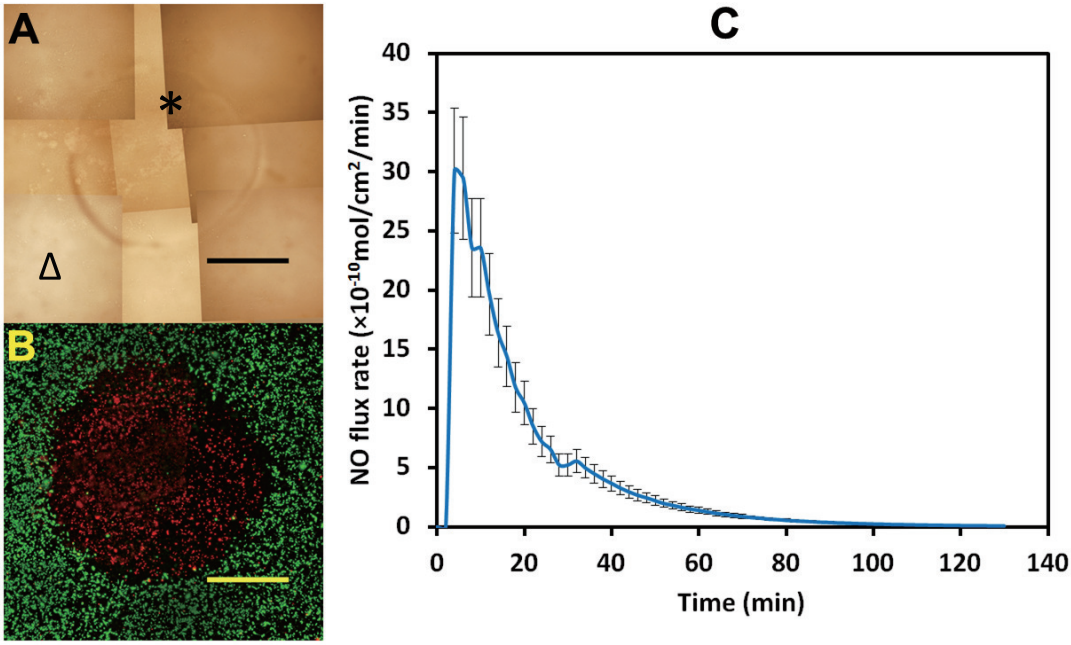

Figure 6.8: NO delivery to MDA-MB-231 cells to kill MDA-MB-231 cells. (A) indicates where SNAP-PDMS was placed; the NO releasing region is indicated by $*$ and regions without NO is indicated by Δ; (B) cell growth on the membranes, green indicates living cells stained by calcein; red, dead cells by EthBr; (C) shows real-time NO flux delivered to the designated cells. Scale bar, 2 mm. The curve is the average NO flux pattern of the triplicate; error bar represent standard deviation. Scale bar 2 mm.

6.4 Conclusions

Current biomedical research methods, especially chemistry and biology based experimental assays, have many problems, such as they are hard to apply for in depth quantitative analysis, not representative enough to the actual biological status, and inevitably invasive. Studying the dose, temporal and spacial aspect of NO's effect is essential to precisely understanding the biological functions of NO and developing

the related biomedical applications. Due to the high reactivity and diffusivity of NO, this work has been challenging and poorly done for long. The design and application of tools for NO quantitative study can push our understanding of the effects of NO forward, leading to developments that will allow therapeutic interventions to be utilized to help solve complex issues of biocompatibility and tissue regeneration.

By combining well understood materials, we were able to obtain a composite selective membrane that achieves the specific requirements for both the NO measurement system and NO cross-membrane delivery system. The design of the two-chamber system is fully compatible with the current in vitro cell culture experimental protocols and achieved real-time NO monitoring (in biological environment), which will not affect the normal cell growth and other experimental procedures. These devices have the potential to greatly increase our understanding of the temporal parameters of NO generation, which were emphasized by various discussions but lacks the actual real-time data for support, let alone the analysis method or statistical algorithms.

Superior to the conventional soluble NO releasing chemicals used in NO research, the use of the novel NO releasing polymer SNAP-PDMS to deliver NO also makes control over temporal NO parameters and absolute quantification of NO experienced by cells possible. Hopefully by applying this device to additional biological models (such as cancer cell lines and in vitro biological molecule reaction systems shown in this chapter), more practical and standard methods can be developed. The big

advantage of these two devices is that calibration is not affected by the complexity of the biological system. So that calibration is much easier and more reliable compared with the NO electrochemical probes. However, change of the parameters such as composition of sweep gas, size of trap and membrane characters can have substantial effect on the final calculation, which should be well controlled and clearly stated.

The measurement device can be used to understand the physiological NO level or cellular NO level under different conditions, while the delivery system investigates the effect of different exogenous NO level to cells, which can also mimic the cases measured by the NO measurement device to validate each other. More specifically, the NO generation profiles from the macrophage cell-line RAW264.7 stimulated by 100 ng/ml LPS and/or 10 ng/ml IFN-γ were recorded by the NO measurement device. The factors that may potentially influence NO generation from the cells were studied and discussed in detail, directly showing dependent natural factors that affect NO generation from cells can be. The conventional report of an average flux or maximum flux is not sufficient to represent the highly dynamic and reactive properties of NO and not helpful for understanding NO's dose and temporal dependent effects. LPS and IFN-γ's synergetic effect to RAW264.7 NO generation was also directly shown and quantitatively analyzed by the device. The rate variation and response time of RAW264.7 NO generation due to the exposure to extra L-arginine, nor-NOHA and L-NAME were also studied by the device, especially the different potencies when the same concentration of L-arginine was applied at different time points.

Examples were also given to show the utility of the NO delivery device. To validate the device, the well understood SMC–NO interaction was used as a model, and the current data indicates that the device was able to deliver physiologically relevant level of NO in a controllable manner (NO flux rate, release duration and spacial distribution). Cell data supports the idea that NO flux rate determines the cell fate. Systematically manipulating NO levels that cultured cells experience by using the NO delivery device showed that $> 1.0 \times 10^{-10}$mol/cm^2/min NO flux can be fatal for MOVAS cell; around 0.7×10^{-10}mol/cm^2/min was associated with inhibition of MOVAS proliferation without observable cytotoxic effect; $< 0.4 \times 10^{-10}$mol/cm^2/min was not sufficient to inhibit MOVAS proliferation. And these effective NO levels were also directly proved to be time-dependent by using the novel NO delivery device. For example, the MOVAS cytotoxicity was shown to require over 1 h exposure of a little over 1.0×10^{-10}mol/cm^2/min NO flux, and less than this duration did not induce permanently damage to MOVAS cells. However, a very high NO flux (an average of 50×10^{-10}mol/cm^2/min, up to 200×10^{-10}mol/cm^2/min) caused permanent cell damage with 10 min treatment, directly showing the importance of precisely controlling NO release profiles when using NO releasing biomaterials and chemicals. Moreover, the local effect of NO was studied and localized NO delivery was achieved by using this delivery system. This property is important for NO's pharmaceutical application, because unlike the conventional drugs, the effective distance of NO is highly limited (NO flux decreased to less than its half after 20 μm diffusion in DMEM

from the data shown in Fig. 5.1), so that the surrounding health tissue is not likely to be exposed to a potentially cytotoxic NO environment.

Some practical biomedical applications were also accomplished to further show the usefulness and potentially wide applications of these two devices. To restore the correct NO level, using NO donor is still a widely used method. But currently it is still unclear about the different potencies of different NO donors and difficult to predict the NO level that cells actually experience when using those donors. To overcome these problems, the NO generation profiles of different soluble NO donors in different solutions (in both PBS buffer and cell culture media, and these NO levels directly represent NO that cells experience in cell culture) were studied by the real-time NO measurement device, including CysNO SNAP, GSNO and DETA NONOate, proving that NO release profiles of all NO donors were very condition dependent. The factors that potentially affect the ultimate NO that cells experience were studied, including pH, transition metal irons, redox level, free thiol and media relative volume. By using MOVAS interaction with NO as a model, it is directly proved that different NO donors (with the same effective concentration) inhibited MOVAS proliferation in different degrees, and this inhibition was not consistent with the so-called stability of NO donors, which is directly related to the $t_{1/2}$ of the specific donors measured in vitro in PBS, but was consistent with the actual NO generation profiles measured when NO donors were actually applied to the cultured cells. This data indicates that understanding the NO profiles of every single experiment is the key to understanding

NO's actual effect, and tracking individual NO profiles in different experiments is the only way to avoid generating confusing data.

For future direction, it has been shown how the measurement device can be potentially used to study the reaction kinetics of NO with other species such as ascorbic acid, understand NO levels in different cell types and solid tissues if possible. Specifically, NO releasing hydrogel and NO generating cells cultured on glass cover-slip were used to mimic tissues that generate NO, hoping that if the correct tissue culture and device calibration can be applied, NO generation from different healthy and pathological tissues can be directly studied. Controllable delivery device was used to show that the breast cancer cell line MDA-MB-231 was significantly more NO resistant than MOVAS cells, which would be a good example for investigating the tissue specificity of NO.

Currently, these methods have their own problems too. The systems are only compatible with in vitro cell culture models. Also, when discussing NO behaviors in a subcellular level, those systems are not mature yet. Just like all the other instruments, every one of them has its own application scope and limitations. But by correct adjustment and modification for specific uses problems are expected to be solved or bypassed, which is the same as the case where the modification to the dimension and surface of the old NO electrochemical probes solved the spacial resolution, sensitivity and selectivity problems associated with the electrochemical probe.

However, such development cannot be accomplished in one day. With further study, the NO quantification tools that I introduced may have even wider and more mature applications.

References

[1] Priestly, J. *Experiments and Observations on Different Kinds of Air*, Vol. 1; London, 1775.

[2] Prout, W. *Medico-chirurgical transactions* **1818**, *9*(Pt 2), 472.

[3] Mitchell, H.; Shonle, H.; Grindley, H. *Journal of Biological Chemistry* **1916**, *24*(4), 461–490.

[4] Green, L. C.; De Luzuriaga, K. R.; Wagner, D. A.; Rand, W.; Istfan, N.; Young, V. R.; Tannenbaum, S. R. *Proceedings of the National Academy of Sciences* **1981**, *78*(12), 7764–7768.

[5] Green, L. C.; Goldman, P.; others. *Science* **1981**, *212*(4490), 56–58.

[6] Stuehr, D. J.; Marletta, M. A. *Proceedings of the National Academy of Sciences* **1985**, *82*(22), 7738–7742.

[7] Furchgott, R. F.; Bhadrakom, S. *Journal of Pharmacology and Experimental Therapeutics* **1953**, *108*(2), 129–143.

[8] Furchgott, R. F. *Journal of Pharmacology and Experimental Therapeutics* **1954**, *111*(3), 265–284.

[9] Furchgott, R. F.; Zawadzki, J. V.; others. *Nature* **1980**, *288*(5789), 373–376.

[10] Hibbs, J. B.; Taintor, R. R.; Vavrin, Z. *Science* **1987**, *235*(4787), 473–476.

[11] Palmer, R. M.; Ferrige, A.; Moncada, S. *Nature* **1987**, *327*.

[12] Ignarro, L. J.; Buga, G. M.; Wood, K. S.; Byrns, R. E.; Chaudhuri, G. *Proceedings of the National Academy of Sciences* **1987**, *84*(24), 9265–9269.

[13] Furchgott, R. F. *Angewandte Chemie International Edition* **1999**, *38*(13-14), 1870–1880.

[14] Murad, F. *Angewandte Chemie International Edition* **1999**, *38*(13-14), 1856–1868.

[15] Ignarro, L. J. *Angewandte Chemie International Edition* **1999**, *38*(13-14), 1882–1892.

[16] Loscalzo, J.; Welch, G. *Progress in cardiovascular diseases* **1995**, *38*(2), 87–104.

[17] Radomski, M.; Palmer, R.; Moncada, S. *The Lancet* **1987**, *330*(8567), 1057–1058.

[18] Moncada, S.; Radomski, M. W.; Palmer, R. M. *Biochemical pharmacology* **1988**, *37*(13), 2495–2501.

[19] Schuman, E. M.; Madison, D. V. *Annual review of neuroscience* **1994**, *17*, 153–183.

[20] Lo, H.; Hung, M. *British journal of cancer* **2006**, *94*(2), 184–188.

[21] Correa-Aragunde, N.; Graziano, M.; Chevalier, C.; Lamattina, L. *Journal of Experimental Botany* **2006**, *57*(3), 581–588.

[22] Xu, W.; Liu, L. Z.; Loizidou, M.; Ahmed, M.; Charles, I. G. *Cell research* **2002**, *12*(5), 311–320.

[23] Ziche, M.; Morbidelli, L. *Journal of neuro-oncology* **2000**, *50*(1-2), 139–148.

[24] Bogdan, C. *Nature immunology* **2001**, *2*(10), 907–916.

[25] Chen, B.; Keshive, M.; Deen, W. M. *Biophysical journal* **1998**, *75*(2), 745–754.

[26] Thomas, D. D.; Miranda, K. M.; Colton, C. A.; Citrin, D.; Espey, M. G.; Wink, D. A. *Antioxidants and Redox Signaling* **2003**, *5*(3), 307–317.

[27] Radi, R.; Beckman, J. S.; Bush, K. M.; Freeman, B. A. *Journal of Biological Chemistry* **1991**, *266*(7), 4244–4250.

[28] Nalwaya, N.; Deen, W. M. *Chemical research in toxicology* **2005**, *18*(3), 486–493.

[29] Chin, M. P.; Schauer, D. B.; Deen, W. M. *Chemical research in toxicology* **2010**, *23*(4), 778–787.

[30] Radi, R.; Beckman, J. S.; Bush, K. M.; Freeman, B. A. *Archives of biochemistry and biophysics* **1991**, *288*(2), 481–487.

[31] Palmer, R. M.; Ashton, D.; Moncada, S. *Nature* **1988**, *333*(6174), 664–666.

[32] Nathan, C.; Xie, Q.-w. *Cell* **1994**, *78*(6), 915–918.

[33] Bredt, D. S.; Snyder, S. H. *Proceedings of the National Academy of Sciences* **1990**, *87*(2), 682–685.

[34] Yui, Y.; Hattori, R.; Kosuga, K.; Eizawa, H.; Hiki, K.; Kawai, C. *Journal of Biological Chemistry* **1991**, *266*(19), 12544–12547.

[35] Pollock, J. S.; Förstermann, U.; Mitchell, J. A.; Warner, T. D.; Schmidt, H.; Nakane, M.; Murad, F. *Proceedings of the National Academy of Sciences* **1991**, *88*(23), 10480–10484.

[36] Groves, J. T.; Wang, C. C. *Current opinion in chemical biology* **2000**, *4*(6), 687–695.

[37] Billiar, T. R. *Annals of surgery* **1995**, *221*(4), 339.

[38] MacMicking, J.; Xie, Q.-w.; Nathan, C. *Annual review of immunology* **1997**, *15*(1), 323–350.

[39] Förstermann, U.; Gath, I.; Schwarz, P.; Closs, E. I.; Kleinert, H. *Biochemical pharmacology* **1995**, *50*(9), 1321–1332.

[40] Garthwaite, J.; Boulton, C. *Annual review of physiology* **1995**, *57*(1), 683–706.

[41] Prast, H.; Philippu, A. *Progress in neurobiology* **2001**, *64*(1), 51–68.

[42] Barouch, L. A.; Harrison, R. W.; Skaf, M. W.; Rosas, G. O.; Cappola, T. P.; Kobeissi, Z. A.; Hobai, I. A.; Lemmon, C. A.; Burnett, A. L.; O'Rourke, B.; others. *Nature* **2002**, *416*(6878), 337–339.

[43] Fukumura, D.; Gohongi, T.; Kadambi, A.; Izumi, Y.; Ang, J.; Yun, C.-O.; Buerk, D. G.; Huang, P. L.; Jain, R. K. *Proceedings of the National Academy of Sciences* **2001**, *98*(5), 2604–2609.

[44] Cai, H.; Li, Z.; Goette, A.; Mera, F.; Honeycutt, C.; Feterik, K.; Wilcox, J. N.; Dudley, S. C.; Harrison, D. G.; Langberg, J. J. *Circulation* **2002**, *106*(22), 2854–2858.

[45] Wheeler, M. A.; Smith, S. D.; García-Cardeña, G.; Nathan, C. F.; Weiss, R. M.; Sessa, W. C. *Journal of Clinical Investigation* **1997**, *99*(1), 110.

[46] Melillo, G.; Musso, T.; Sica, A.; Taylor, L. S.; Cox, G. W.; Varesio, L. *The Journal of experimental medicine* **1995**, *182*(6), 1683–1693.

[47] Iadecola, C.; Zhang, F.; Xu, X. *American Journal of Physiology-Regulatory, Integrative and Comparative Physiology* **1995**, *268*(1), R286–R292.

[48] Iadecola, C.; Zhang, F.; Casey, R.; Clark, H. B.; Ross, M. E. *Stroke* **1996**, *27*(8), 1373–1380.

[49] Weinberg, J.; Misukonis, M.; Shami, P.; Mason, S.; Sauls, D.; Dittman, W.; Wood, E.; Smith, G.; McDonald, B.; Bachus, K. *Blood* **1995**, *86*(3), 1184–1195.

[50] Pervin, S.; Singh, R.; Sen, S.; Chaudhuri, G. In *Nitric Oxide (NO) and Cancer;* Springer, 2010; pages 39–57.

[51] Nagy, G.; Clark, J. M.; Buzás, E. I.; Gorman, C. L.; Cope, A. P. *Immunology letters* **2007**, *111*(1), 1–5.

[52] Böhme, G. A.; Bon, C.; Stutzmann, J.-M.; Doble, A.; Blanchard, J.-C. *European journal of pharmacology* **1991**, *199*(3), 379–381.

[53] Togashi, H.; Sakuma, I.; Yoshioka, M.; Kobayashi, T.; Yasuda, H.; Kitabatake, A.; Saito, H.; Gross, S.; Levi, R. *Journal of Pharmacology and Experimental Therapeutics* **1992**, *262*(1), 343–347.

[54] Ling, L.; Karius, D. R.; Fiscus, R. R.; Speck, D. F. *Journal of neurophysiology* **1992**, *68*(5), 1910–1912.

[55] Meller, S.; Gebhart, G. *Pain* **1993**, *52*(2), 127–136.

[56] Huerta-Yepez, S.; Vega, M.; Jazirehi, A.; Garban, H.; Hongo, F.; Cheng, G.; Bonavida, B. *Oncogene* **2004**, *23*(29), 4993–5003.

[57] Mitchell, J. B.; Wink, D. A.; DeGraff, W.; Gamson, J.; Keefer, L. K.; Krishna, M. C. *Cancer research* **1993**, *53*(24), 5845–5848.

[58] Zhang, X.; Xu, Q. *Melanoma research* **2001**, *11*(6), 559–567.

[59] Greenblatt, M.; Philippe, S. K. *Journal of the National Cancer Institute* **1968**, *41*(1), 111–124.

[60] Eu, J. P.; Liu, L.; Zeng, M.; Stamler, J. S. *Biochemistry* **2000**, *39*(5), 1040–1047.

[61] Ischiropoulos, H.; Al-Mehdi, A. B. *FEBS letters* **1995**, *364*(3), 279–282.

[62] Schopfer, F. J.; Baker, P. R.; Freeman, B. A. *Trends in biochemical sciences* **2003**, *28*(12), 646–654.

[63] Wink, D. A.; Kasprzak, K. S.; others. *Science* **1991**, *254*(5034), 1001.

[64] Nguyen, T.; Brunson, D.; Crespi, C.; Penman, B.; Wishnok, J.; Tannenbaum, S. *Proceedings of the National Academy of Sciences* **1992**, *89*(7), 3030–3034.

[65] Thomas, D. D.; Ridnour, L. A.; Isenberg, J. S.; Flores-Santana, W.; Switzer, C. H.; Donzelli, S.; Hussain, P.; Vecoli, C.; Paolocci, N.; Ambs, S.; Coltonf, C. A.; Harrisd, C. C.; . Robertsc, D. D.; Wink, D. A. *Free Radical Biology and Medicine* **2008**, *45*(1), 18–31.

[66] Wink, D. A.; Miranda, K. M.; Espey, M. G.; Pluta, R. M.; Hewett, S. J.; Colton, C.; Vitek, M.; Feelisch, M.; Grisham, M. B. *Antioxidants and Redox Signaling* **2001**, *3*(2), 203–213.

[67] Kröncke, K.; Fehsel, K.; Kolb-Bachofen, V. *Clinical and experimental immunology* **1998**, *113*, 147–156.

[68] Lipton, S.; Stamler, J. *Neuropharmacology* **1994**, *33*(11), 1229–1233.

[69] Colton, C.; Gbadegesin, M.; Wink, D.; Miranda, K.; Espey, M.; Vicini, S. *Journal of neurochemistry* **2001**, *78*(5), 1126–1134.

[70] Christopherson, K. S.; Bredt, D. S. *Journal of Clinical Investigation* **1997**, *100*(10), 2424.

[71] Heales, S. J.; Bolaños, J. P.; Stewart, V. C.; Brookes, P. S.; Land, J. M.; Clark, J. B. *Biochimica et Biophysica Acta (BBA)-Bioenergetics* **1999**, *1410*(2), 215–228.

[72] Knott, A. B.; Bossy-Wetzel, E. *Antioxidants & redox signaling* **2009**, *11*(3), 541–553.

[73] Hetrick, E. M.; Schoenfisch, M. H. *Annual review of analytical chemistry (Palo Alto, Calif.)* **2009**, *2*, 409.

[74] Coneski, P. N.; Schoenfisch, M. H. *Chemical Society Reviews* **2012**, *41*(10), 3753–3758.

[75] Cooke, MD, J. P.; Dzau, MD, V. J. *Annual review of medicine* **1997**, *48*(1), 489–509.

[76] Lancaster, J. R. *Nitric Oxide* **1997**, *1*(1), 18–30.

[77] Lancaster, J. R. *Proceedings of the National Academy of Sciences* **1994**, *91*(17), 8137–8141.

[78] Sun, J.; Zhang, X.; Broderick, M.; Fein, H. *Sensors* **2003**, *3*(8), 276–284.

[79] Higuchi, K.; Motomizu, S. *Analytical sciences* **1999**, *15*(2), 129–134.

[80] Toda, K.; Hato, Y.; Ohira, S.-I.; Namihira, T. *Analytica chimica acta* **2007**, *603*(1), 60–66.

[81] Noack, E.; Kubitzek, D.; Kojda, G. *Neuroprotocols* **1992**, *1*(2), 133–139.

[82] Kleschyov, A. L.; Mollnau, H.; Oelze, M.; Meinertz, T.; Huang, Y.; Harrison, D. G.; Munzel, T. *Biochemical and biophysical research communications* **2000**, *275*(2), 672–677.

[83] Kojima, H.; Nakatsubo, N.; Kikuchi, K.; Kawahara, S.; Kirino, Y.; Nagoshi, H.; Hirata, Y.; Nagano, T. *Analytical chemistry* **1998**, *70*(13), 2446–2453.

[84] Davies, I. R.; Zhang, X. *Methods in enzymology* **2008**, *436*, 63–95.

[85] Liu, X.; Liu, Q.; Gupta, E.; Zorko, N.; Brownlee, E.; Zweier, J. L. *Nitric Oxide* **2005**, *13*(1), 68–77.

[86] Malinski, T.; Taha, Z. *Nature* **1992**, *358*(6388), 676–678.

[87] Sievers nitric oxide analyzer NOA280i operation and maintenance manual. GE Analytical Instruments, **2006**.

[88] Kikuchi, K.; Nagano, T.; Hayakawa, H.; Hirata, Y.; Hirobe, M. *Analytical chemistry* **1993**, *65*(13), 1794–1799.

[89] Lancaster, J. R.; Langrehr, J.; Bergonia, H.; Murase, N.; Simmons, R.; Hoffman, R. *Journal of Biological Chemistry* **1992**, *267*(16), 10994–10998.

[90] Zweier, J. L.; Wang, P.; Kuppusamy, P. *Journal of Biological Chemistry* **1995**, *270*(1), 304–307.

[91] Hobbs, A. J.; Higgs, A.; Moncada, S. *Annual Review of Pharmacology and Toxicology* **1999**, *39*(1), 191–220.

[92] Bennett, B. M.; Leitman, D. C.; Schröder, H.; Kawamoto, J. H.; Nakatsu, K.; Murad, F. *Journal of Pharmacology and Experimental Therapeutics* **1989**, *250*(1), 316–323.

[93] Miller, M.; Megson, I. *British journal of pharmacology* **2007**, *151*(3), 305–321.

[94] Chen, Z.; Zhang, J.; Stamler, J. S. *Proceedings of the National Academy of Sciences* **2002**, *99*(12), 8306–8311.

[95] Williams, D. L. H. *Accounts of chemical research* **1999**, *32*(10), 869–876.

[96] Napoli, C.; Ignarro, L. J. *Annual review of pharmacology and toxicology* **2003**, *43*(1), 97–123.

[97] Smith, D. J.; Chakravarthy, D.; Pulfer, S.; Simmons, M. L.; Hrabie, J. A.; Citro, M. L.; Saavedra, J. E.; Davies, K. M.; Hutsell, T. C.; Mooradian, D. L.; others. *Journal of medicinal chemistry* **1996**, *39*(5), 1148–1156.

[98] Tierney, T. S.; Clatterbuck, R. E.; Lawson, C.; Thai, Q.-A.; Rhines, L. D.; Tamargo, R. J. *Neurosurgery* **2001**, *49*(4), 945–953.

[99] Chaux, A.; Ruan, X. M.; Fishbein, M. C.; Ouyang, Y.; Kaul, S.; Pass, J. A.; Matloff, J. M. *The Journal of Thoracic and Cardiovascular Surgery* **1998**, *115*(3), 604–614.

[100] Shishido, S. M.; Oliveira, M. G. *Photochemistry and photobiology* **2000**, *71*(3), 273–280.

[101] Shishido, S. M.; Seabra, A. B.; Loh, W.; de Oliveira, M. G. *Biomaterials* **2003**, *24*(20), 3543–3553.

[102] Frost, M. C.; Reynolds, M. M.; Meyerhoff, M. E. *Biomaterials* **2005**, *26*(14), 1685–1693.

[103] Mowery, K. A.; Schoenfisch, M. H.; Saavedra, J. E.; Keefer, L. K.; Meyerhoff, M. E. *Biomaterials* **2000**, *21*(1), 9–21.

[104] Frost, M. C.; Meyerhoff, M. E. *Journal of the American Chemical Society* **2004**, *126*(5), 1348–1349.

[105] Pulfer, S. K.; Ott, D.; Smith, D. J. *Journal of biomedical materials research* **1997**, *37*(2), 182–189.

[106] Zhang, H.; Annich, G. M.; Miskulin, J.; Stankiewicz, K.; Osterholzer, K.; Merz, S. I.; Bartlett, R. H.; Meyerhoff, M. E. *Journal of the American Chemical Society* **2003**, *125*(17), 5015–5024.

[107] Riccio, D. A.; Schoenfisch, M. H. *Chemical Society Reviews* **2012**, *41*(10), 3731–3741.

[108] Frost, M. C.; Meyerhoff, M. E. *Journal of Biomedical Materials Research Part A* **2005**, *72*(4), 409–419.

[109] Stasko, N. A.; Schoenfisch, M. H. *Journal of the American Chemical Society* **2006**, *128*(25), 8265–8271.

[110] Frost, M. C.; Rudich, S. M.; Zhang, H.; Maraschio, M. A.; Meyerhoff, M. E. *Analytical chemistry* **2002**, *74*(23), 5942–5947.

[111] Boyden, S. *The Journal of experimental medicine* **1962**, *115*(3), 453–466.

[112] Mowery, K.; Meyerhoff, M. *Polymer* **1999**, *40*(22), 6203–6207.

[113] Vaughn, M. W.; Kuo, L.; Liao, J. C. *American Journal of Physiology-Heart and Circulatory Physiology* **1998**, *274*(6), H2163–H2176.

[114] Laurent, M.; Lepoivre, M.; Tenu, J. *Biochem. J* **1996**, *314*, 109–113.

[115] Möller, M.; Botti, H.; Batthyany, C.; Rubbo, H.; Radi, R.; Denicola, A. *Journal of Biological Chemistry* **2005**, *280*(10), 8850–8854.

[116] Malinski, T.; Taha, Z.; Grunfeld, S.; Patton, S.; Kapturczak, M.; Tomboulian, P. *Biochemical and biophysical research communications* **1993**, *193*(3), 1076–1082.

[117] Wise, D.; Houghton, G. *Chemical Engineering Science* **1968**, *23*(10), 1211–1216.

[118] Cussler, E. L. *Diffusion: mass transfer in fluid systems;* Cambridge university press, 2009.

[119] Wink, D. A.; Darbyshire, J. F.; Nims, R. W.; Saavedra, J. E.; Ford, P. C. *Chemical research in toxicology* **1993**, *6*(1), 23–27.

[120] Kharitonov, V. G.; Sundquist, A. R.; Sharma, V. S. *Journal of Biological Chemistry* **1995**, *270*(47), 28158–28164.

[121] Schmidt, K.; Desch, W.; Klatt, P.; Kukovetz, W. R.; Mayer, B. *Naunyn-Schmiedeberg's archives of pharmacology* **1997**, *355*(4), 457–462.

[122] Feelisch, M. *Naunyn-Schmiedeberg's archives of pharmacology* **1998**, *358*(1), 113–122.

[123] Feelisch, M.; Stamler, J. S. *Methods in nitric oxide research;* Wiley, 1996.

[124] Wali, M. A.; Suleiman, S. A.; Kadoumi, O. F.; Nasr, M. *Annals of thoracic and cardiovascular surgery: official journal of the Association of Thoracic and Cardiovascular Surgeons of Asia* **2002**, *8*(5), 286–290.

[125] Rocic, P.; Kolz, C.; Reed, R.; Potter, B.; Chilian, W. M. *American Journal of Physiology-Heart and Circulatory Physiology* **2007**, *292*(6), H2729–H2736.

[126] Mesároš, Š.; Vaňková, Ž.; Mesárošová, A.; Tomčık, P.; Grunfeld, S. *Bioelectrochemistry and bioenergetics* **1998**, *46*(1), 33–37.

[127] Marxer, S. M.; Rothrock, A. R.; Nablo, B. J.; Robbins, M. E.; Schoenfisch, M. H. *Chemistry of materials* **2003**, *15*(22), 4193–4199.

[128] Amadeu, T. P.; Seabra, A. B.; De Oliveira, M. G.; Costa, A. M. *Journal of the European Academy of Dermatology and Venereology* **2007**, *21*(5), 629–637.

[129] Amadeu, T. P.; Seabra, A. B.; de Oliveira, M. G.; Monte-Alto-Costa, A. *Journal of Surgical Research* **2008**, *149*(1), 84–93.

[130] Tarr, H. *Nature* **1941**, *147*(3727), 417–418.

[131] Liew, F.; Millott, S.; Parkinson, C.; Palmer, R.; Moncada, S. *The Journal of Immunology* **1990**, *144*(12), 4794–4797.

[132] Denis, M. *Journal of Leukocyte Biology* **1991**, *49*(4), 380–387.

[133] Vogt, C.; Xing, Q.; He, W.; Li, B.; Frost, M. C.; Zhao, F. *Biomacromolecules* **2013**, *14*(8), 2521–2530.

[134] Friedman, A. J.; Han, G.; Navati, M. S.; Chacko, M.; Gunther, L.; Alfieri, A.; Friedman, J. M. *Nitric Oxide* **2008**, *19*(1), 12–20.

[135] Han, G.; Martinez, L. R.; Mihu, M. R.; Friedman, A. J.; Friedman, J. M.; Nosanchuk, J. D. *PLoS One* **2009**, *4*(11), e7804.

[136] Parzuchowski, P. G.; Frost, M. C.; Meyerhoff, M. E. *Journal of the American Chemical Society* **2002**, *124*(41), 12182–12191.

[137] Romanowicz, G. E.; Nielsen, M.; Frost, M. C. *Science and Technology of Advanced Materials* **2011**, *12*(5), 055007.

[138] Moynihan, H. A.; Roberts, S. M. *J. Chem. Soc., Perkin Trans. 1* **1994**, (7), 797–805.

[139] Zhou, J.; Ellis, A. V.; Voelcker, N. H. *Electrophoresis* **2010**, *31*(1), 2–16.

[140] Lee, H.; Dellatore, S. M.; Miller, W. M.; Messersmith, P. B. *Science* **2007**, *318*(5849), 426–430.

[141] Yin, X.; Liu, D. *Journal of Chromatography A* **2008**, *1212*(1), 130–136.

[142] Archer, S. *The FASEB journal* **1993**, *7*(2), 349–360.

[143] Taha, Z. H. *Talanta* **2003**, *61*(1), 3–10.

[144] Gladwin, M. T.; Ognibene, F. P.; Pannell, L. K.; Nichols, J. S.; Pease-Fye, M. E.; Shelhamer, J. H.; Schechter, A. N. *Proceedings of the National Academy of Sciences* **2000**, *97*(18), 9943–9948.

[145] Owusu, B. Y.; Stapley, R.; Patel, R. P. *The Journal of physiology* **2012**, *590*(20), 4993–5000.

[146] Hunter, R. A.; Storm, W. L.; Coneski, P. N.; Schoenfisch, M. H. *Analytical chemistry* **2013**, *85*(3), 1957–1963.

[147] Bedioui, F.; Villeneuve, N. *Electroanalysis* **2003**, *15*(1), 5–18.

[148] Allen, B. W.; Liu, J.; Piantadosi, C. A. *Methods in enzymology* **2005**, *396*, 68–77.

[149] Bates, J. N. *Neuroprotocols* **1992**, *1*(2), 141–149.

[150] Privett, B. J.; Shin, J. H.; Schoenfisch, M. H. *Chemical Society Reviews* **2010**, *39*(6), 1925–1935.

[151] Lee, Y.; Yang, J.; Rudich, S. M.; Schreiner, R. J.; Meyerhoff, M. E. *Analytical Chemistry* **2004**, *76*(3), 545–551.

[152] Fontijn, A.; Sabadell, A. J.; Ronco, R. J. *Analytical Chemistry* **1970**, *42*(6), 575–579.

[153] Dunham, A. J.; Barkley, R. M.; Sievers, R. E. *Analytical chemistry* **1995**, *67*(1), 220–224.

[154] Thomas, D. D.; Espey, M. G.; Ridnour, L. A.; Hofseth, L. J.; Mancardi, D.; Harris, C. C.; Wink, D. A. *Proceedings of the National Academy of Sciences of the United States of America* **2004**, *101*(24), 8894–8899.

[155] Schmidt, H. H.; Warner, T. D.; Nakane, M.; Förstermann, U.; Murad, F. *Molecular pharmacology* **1992**, *41*(4), 615–624.

[156] Noda, T.; Amano, F. *Journal of biochemistry* **1997**, *121*(1), 38–46.

[157] Lee, H.; Dellatore, S. M.; Miller, W. M.; Messersmith, P. B. *science* **2007**, *318*(5849), 426–430.

[158] Xu, C.; Yang, F.; Wang, S.; Ramakrishna, S. *Journal of Biomedical Materials Research Part A* **2004**, *71*(1), 154–161.

[159] Pelham, R. J.; Wang, Y. *Proceedings of the National Academy of Sciences* **1997**, *94*(25), 13661–13665.

[160] Peyton, S. R.; Raub, C. B.; Keschrumrus, V. P.; Putnam, A. J. *Biomaterials* **2006**, *27*(28), 4881–4893.

[161] Palchesko, R. N.; Zhang, L.; Sun, Y.; Feinberg, A. W. *PLoS ONE* **2012**, *7*(12).

[162] Kojima, H.; Urano, Y.; Kikuchi, K.; Higuchi, T.; Hirata, Y.; Nagano, T. *Angewandte Chemie International Edition* **1999**, *38*(21), 3209–3212.

[163] Morris Jr, S. M. *Annual review of nutrition* **2002**, *22*(1), 87–105.

[164] Mehibel, M.; Singh, S.; Chinje, E. C.; Cowen, R. L.; Stratford, I. J. *Molecular cancer therapeutics* **2009**, *8*(5), 1261–1269.

[165] Wang, C.; Deen, W. M. *Annals of biomedical engineering* **2003**, *31*(1), 65–79.

[166] Langford, E.; Wainwright, R.; Martin, J. *Arteriosclerosis, thrombosis, and vascular biology* **1996**, *16*(1), 51–55.

[167] Megson, I.; Greig, I.; Gray, G.; Webb, D.; Butler, A. *British journal of pharmacology* **1997**, *122*(8), 1617–1624.

[168] Megson, I.; Morton, S.; Greig, I.; Mazzei, F.; Field, R.; Butler, A.; Caron, G.; Gasco, A.; Fruttero, R.; Webb, D. *British journal of pharmacology* **1999**, *126*(3), 639–648.

[169] Mathews, W. R.; Kerr, S. W. *Journal of Pharmacology and Experimental Therapeutics* **1993**, *267*(3), 1529–1537.

[170] Singh, R. J.; Hogg, N.; Joseph, J.; Kalyanaraman, B. *Journal of Biological Chemistry* **1996**, *271*(31), 18596–18603.

[171] Beckman, J. S.; Koppenol, W. H. *American Journal of Physiology-Cell Physiology* **1996**, *271*(5), C1424–C1437.

[172] Maragos, C. M.; Morley, D.; Wink, D. A.; Dunams, T. M.; Saavedra, J. E.; Hoffman, A.; Bove, A. A.; Isaac, L.; Hrabie, J. A.; Keefer, L. K. *Journal of medicinal chemistry* **1991**, *34*(11), 3242–3247.

[173] Mooradian, D. L.; Hutsell, T. C.; Keefer, L. K. *Journal of cardiovascular pharmacology* **1995**, *25*(4), 674–678.

[174] Stamler, J. S.; Simon, D. I.; Osborne, J. A.; Mullins, M. E.; Jaraki, O.; Michel, T.; Singel, D. J.; Loscalzo, J. *Proceedings of the National Academy of Sciences* **1992**, *89*(1), 444–448.

[175] Wike-Hooley, J.; Haveman, J.; Reinhold, H. *Radiotherapy and Oncology* **1984**, *2*(4), 343–366.

[176] Tannock, I. F.; Rotin, D. *Cancer research* **1989**, *49*(16), 4373–4384.

[177] Hansen, T.; Croisy, A.; Keefer, L. *IARC scientific publications* **1981**, (41), 21–29.

[178] Hrabie, J. A.; Keefer, L. K. *Chemical reviews* **2002**, *102*(4), 1135–1154.

[179] Keefer, L. K. *Annual review of pharmacology and toxicology* **2003**, *43*(1), 585–607.

[180] Davies, K. M.; Wink, D. A.; Saavedra, J. E.; Keefer, L. K. *Journal Of the American Chemical Society* **2001**, *123*(23), 5473–5481.

[181] Wang, P. G.; Xian, M.; Tang, X.; Wu, X.; Wen, Z.; Cai, T.; Janczuk, A. J. *Chemical Reviews* **2002**, *102*(4), 1091–1134.

[182] Wink, D. A.; Hanbauer, I.; Krishna, M. C.; DeGraff, W.; Gamson, J.; Mitchell, J. B. *Proceedings Of the National Academy Of Sciences* **1993**, *90*(21), 9813–9817.

[183] Wink, D. A.; Cook, J. A.; Pacelli, R.; Liebmann, J.; Krishna, M. C.; Mitchell, J. B. *Toxicology letters* **1995**, *82*, 221–226.

[184] Sawa, T.; Akaike, T.; Maeda, H. *Journal of Biological Chemistry* **2000**, *275*(42), 32467–32474.

[185] Garg, U. C.; Hassid, A. *Journal of Clinical Investigation* **1989**, *83*(5), 1774.

[186] Kariya, K.-i.; Kawahara, Y.; Araki, S.-i.; Fukuzaki, H.; Takai, Y. *Atherosclerosis* **1989**, *80*(2), 143–147.

[187] Tanner, F. C.; Meier, P.; Greutert, H.; Champion, C.; Nabel, E. G.; Lüscher, T. F. *Circulation* **2000**, *101*(16), 1982–1989.

[188] Wink, D. A.; Cook, J. A.; Pacelli, R.; DeGraff, W.; Gamson, J.; Liebmann, J.; Krishna, M. C.; Mitchell, J. B. *Archives of biochemistry and biophysics* **1996**, *331*(2), 241–248.

[189] Trujillo, M.; Alvarez, M. N.; Peluffo, G.; Freeman, B. A.; Radi, R. *Journal of Biological Chemistry* **1998**, *273*(14), 7828–7834.

[190] Campbell, J. M.; McCrae, F.; Reglinski, J.; Wilson, R.; Smith, W. E.; Sturrock, R. D. *Biochimica et Biophysica Acta (BBA)-General Subjects* **1993**, *1156*(3), 327–333.

[191] Gergel, D.; Misik, V.; Ondrias, K.; Cederbaum, A. I. *The Journal of biological chemistry* **1995**, *270*(36), 20922–20929.

[192] Farias-Eisner, R.; Chaudhuri, G.; Aeberhard, E.; Fukuto, J. M. *Journal of Biological Chemistry* **1996**, *271*(11), 6144–6151.

[193] Starrett, M. A.; Nielsen, M.; Smeenge, D. M.; Romanowicz, G. E.; Frost, M. C. *Nitric Oxide* **2012**, *27*(4), 228–234.

[194] Romanowicz, G. E.; He, W.; Nielsen, M.; Frost, M. C. *Redox biology* **2013**, *1*(1), 332–339.

[195] Stamler, J. S. *Cell* **1994**, *78*(6), 931–936.

[196] Radi, R. *Proceedings of the National Academy of Sciences* **2004**, *101*(12), 4003–4008.

[197] Hu, T.-M.; Chou, T.-C. *The AAPS journal* **2006**, *8*(3), E485–E492.

[198] Morakinyo, M. K. **2010**.

[199] Torfgård, K. E.; Ahlner, J. In *Nitrates Updated;* Springer, 1997; pages 21–56.

[200] Yang, B. K.; Vivas, E. X.; Reiter, C. D.; Gladwin, M. T. *Free radical research* **2003**, *37*(1), 1–10.

[201] Reynolds, M. M.; Frost, M. C.; Meyerhoff, M. E. *Free Radical Biology and Medicine* **2004**, *37*(7), 926–936.

[202] Carpenter, A. W.; Schoenfisch, M. H. *Chemical Society Reviews* **2012**, *41*(10), 3742–3752.

[203] Xing, Q.; Yates, K.; Bailey, A.; Vogt, C.; He, W.; Frost, M. C.; Zhao, F. *Surface Innovations* **2013**, *1*(4), 224–232.

[204] Nablo, B. J.; Rothrock, A. R.; Schoenfisch, M. H. *Biomaterials* **2005**, *26*(8), 917–924.

[205] Nablo, B. J.; Schoenfisch, M. H. *Biomaterials* **2005**, *26*(21), 4405–4415.

[206] Cai, H.; Harrison, D. G. *Circulation research* **2000**, *87*(10), 840–844.

[207] Isenberg, J. S.; Ridnour, L. A.; Perruccio, E. M.; Espey, M. G.; Wink, D. A.; Roberts, D. D. *Proceedings of the National Academy of Sciences of the United States of America* **2005**, *102*(37), 13141–13146.

[208] Ridnour, L. A.; Windhausen, A. N.; Isenberg, J. S.; Yeung, N.; Thomas, D. D.; Vitek, M. P.; Roberts, D. D.; Wink, D. A. *Proceedings of the National Academy of Sciences* **2007**, *104*(43), 16898–16903.

[209] Szomor, Z.; Appleyard, R.; Murrell, G. *Journal of orthopaedic research* **2006**, *24*(1), 80–86.

[210] Sharma, P.; Maffulli, N. *Journal of Musculoskeletal and Neuronal Interactions* **2006**, *6*(2), 181.

[211] Niki, E. *The American journal of clinical nutrition* **1991**, *54*(6), 1119S–1124S.

[212] Thomas, D. D.; Ridnour, L. A.; Espey, M. G.; Donzelli, S.; Ambs, S.; Hussain, S. P.; Harris, C. C.; DeGraff, W.; Roberts, D. D.; Mitchell, J. B.; others. *Journal of Biological Chemistry* **2006**, *281*(36), 25984–25993.

[213] Jackson, T. S.; Xu, A.; Vita, J. A.; Keaney, J. F. *Circulation research* **1998**, *83*(9), 916–922.

[214] Xu, W.; Liu, L.; Charles, I. G. *The FASEB Journal* **2002**, *16*(2), 213–215.

[215] Jenkins, D.; Charles, I.; Thomsen, L. L.; Moss, D.; Holmes, L.; Baylis, S.; Rhodes, P.; Westmore, K.; Emson, P.; Moncada, S. *Proceedings of the National Academy of Sciences* **1995**, *92*(10), 4392–4396.

[216] Thomsen, L. L.; Lawton, F. G.; Knowles, R. G.; Beesley, J. E.; Riveros-Moreno, V.; Moncada, S. *Cancer Research* **1994**, *54*(5), 1352–1354.

[217] Thomsen, L.; Miles, D.; Happerfield, L.; Bobrow, L.; Knowles, R.; Moncada, S. *British Journal of Cancer* **1995**, *72*(1), 41.

[218] Bingle, L.; Brown, N.; Lewis, C. *The Journal of pathology* **2002**, *196*(3), 254–265.

[219] Pollard, J. W. *Nature Reviews Cancer* **2004**, *4*(1), 71–78.

[220] Hickok, J. R.; Thomas, D. D. *Current pharmaceutical design* **2010**, *16*(4), 381.

[221] Keller, R.; Geiges, M.; Keist, R. *Cancer research* **1990**, *50*(5), 1421–1425.

[222] Mehibel, M.; Singh, S.; Chinje, E. C.; Cowen, R. L.; Stratford, I. J. *Molecular cancer therapeutics* **2009**, *8*(5), 1261–1269.

[223] Matthews, N. E.; Adams, M. A.; Maxwell, L. R.; Gofton, T. E.; Graham, C. H. *Journal of the National Cancer Institute* **2001**, *93*(24), 1879–1885.

[224] Frederiksen, L. J.; Sullivan, R.; Maxwell, L. R.; Macdonald-Goodfellow, S. K.; Adams, M. A.; Bennett, B. M.; Siemens, D. R.; Graham, C. H. *Clinical cancer research* **2007**, *13*(7), 2199–2206.

[225] Williams, J. L.; Borgo, S.; Hasan, I.; Castillo, E.; Traganos, F.; Rigas, B. *Cancer Research* **2001**, *61*(8), 3285–3289.

[226] Rao, C. V.; Reddy, B. S.; Steele, V. E.; Wang, C.; Liu, X.; Ouyang, N.; Patlolla, J. M.; Simi, B.; Kopelovich, L.; Rigas, B. *Molecular cancer therapeutics* **2006**, *5*(6), 1530–1538.

[227] Juang, S.-H.; Xie, K.; Xu, L.; Shi, Q.; Wang, Y.; Yoneda, J.; Fidler, I. J. *Human gene therapy* **1998**, *9*(6), 845–854.

[228] Campbell, N. A.; Reece, J. B.; Mitchell, L. G.; Taylor, M. R. *Biology: Concepts and Connections 4th Edition;* Benjamine Cummings, 2002.

[229] Knowles, R. G.; Moncada, S. *Biochemical Journal* **1994**, *298*(Pt 2), 249.

[230] Wink, D. A.; Ridnour, L. A.; Hussain, S. P.; Harris, C. C. *Nitric oxide: biology and chemistry/official journal of the Nitric Oxide Society* **2008**, *19*(2), 65.

[231] Stasko, N. A.; Fischer, T. H.; Schoenfisch, M. H. *Biomacromolecules* **2008**, *9*(3), 834–841.

[232] Kjeldahl, J. *Fresenius' Journal of Analytical Chemistry* **1883**, *22*(1), 366–382.

[233] Murdaugh, L.; Wang, Z.; Del Priore, L.; Dillon, J.; Gaillard, E. *Experimental eye research* **2010**, *90*(5), 564–571.

[234] Zhang, R.; Hrushesky, W. J.; Wood, P. A.; Lee, S. H.; Hunt, R. C.; Jahng, W. J. *International journal of biological macromolecules* **2010**, *47*(2), 255–260.

[235] Crow, J. P.; Beckman, J. S. *Methods* **1995**, *7*(1), 116–120.

[236] Reed, J. W.; Ho, H. H.; Jolly, W. L. *Journal of the American Chemical Society* **1974**, *96*(4), 1248–1249.

[237] Jiao, K.; Mandapati, S.; Skipper, P. L.; Tannenbaum, S. R.; Wishnok, J. S. *Analytical biochemistry* **2001**, *293*(1), 43–52.

[238] Hui, Y.; Wong, M.; Zhao, S. S.; Love, J. A.; Ansley, D. M.; Chen, D. D. *Electrophoresis* **2012**, *33*(4), 697–704.

[239] Sripathi, S. R.; He, W.; Um, J.-Y.; Moser, T.; Dehnbostel, S.; Kindt, K.; Goldman, J.; Frost, M. C.; Jahng, W. J. *Advances in Bioscience and Biotechnology* **2012**, *3*(8).

[240] Antony, R.; Lukiw, W. J.; Bazan, N. G. *Journal of Biological Chemistry* **2010**, *285*(24), 18301–18308.

[241] Duncan, M. *Amino acids* **2003**, *25*(3-4), 351–361.

Appendix A

Sample Code

This part shows the code that I used to simulate NO concentration and NO flux change with time and distance by using FlexPDE6s. Both auto-oxidations of NO by O_2 and superoxide are considered.

```
title
'Diffusion'
variables

u(threshold=0.1)

definitions

D = 4.8e-9
v=1.7e-5
k=1.32
p=5
M = sqrt(v/k)*((exp(2*sqrt(k*v)*t)-1)/(exp(2*sqrt(k*v)*t)+1))
s=5e-8
ros=0.07

initial values

u = 0

equations
 u : div(D*grad(u)) - k*u^2-p*ros*u= dt(u)

boundaries
region 1

start(0,0)
natural(u) = 0 line to (0.0005,0)
value(u) = 0 line to (0.0005,0.0005)
natural(u) = 0  line to (0,0.0005)
natural(u) = s line to close

time 0 to 120 by 0.01

plots
for t=0 by 0.5 to endtime
  contour(u)
  surface(u)
  elevation(u) from (0,0.0005) to (0.0005,0.0005)
histories

history(u) at (0,0.0001) (0.0001,0.0001) (0.0002,0.0001) (0.0003,0.0001) (0.0004,0.0001) (0.0005,0.0001)

History(-D*grad(u)) at (0,0.0001) (0.0001,0.0001) (0.0002,0.0001) (0.0003,0.0001) (0.0004,0.0001) (0.0005,0.0001) as "NO flux rate" print

end
```

Appendix B

Characterization of the NO Biological Products

B.1 Nitrotyrosine detection by HPLC

Protein tyrosine kinase, one major type of cell membrane signaling molecules, binds ligands from outside of the membrane and passes this signaling into the cells to make cells respond appropriately to the outside chemical environment. Specific tyrosine residues within the protein tyrosine kinase undergo autophoshorylation once their ligands are bound to its extra-membrane domain, which causes protein configuration changes and activation/deactivation. Then the activated protein tyrosine

kinase can bind to SH2 (Src Homology 2) domain-containing protein, which further delivers the ligand information to the inside of the cell [228]. Tyrosine nitration on phenyl groups at position 3 generates greater steric hindrance, which inhibits the phosphorylation process, leading to failure of functional modulation of the protein kinase. In vivo, the production of nitrotyrosine (NO_2Tyr) is from reactive nitrogen species (RNS), with a MW of 226.19 Da. Similar to reactive oxygen species (ROS), RNS can initiate many free radical reactions including inducing the formation of tyrosyl group free radicals. The eventual reaction occurs between tyrosyl group free radicals and $NO_2\bullet$, forming NO_2Tyr. The most important source of $NO_2\bullet$ is $NO\bullet$, which can be innately generated by the body at very high production rates (estimation of $1 - 4 \times 10^{-10}$mol/cm^2/min by blood vessel endothelium [113] and up to 9 pmol/10^6cell/sec from our data 3.6). NO is a free radical, which can be oxidized easily by O_2, O_2^-, forming NO_2^-, $NO_2\bullet$ and $ONOO^-$. $ONOO^-$ will produce $NO_2\bullet$ while pH is lower than 6.8 and CO_2 is presenting [62]. Under pathological conditions, because of inflammation, oxidative stress is generated either locally or within the whole body, producing more O_2^-, which make this reaction more likely to occur.

People have noted that huge increases of basal level of NO_2Tyr in blood plasma in rheumatoid arthritis, renal failure, and septic shock patients and aging models. Murdaugh et al. [233] reported the accumulation of 3-nitrotyrosine and other nitro group derived products within AMD sample. Zhang et al. [234] identified PP2A-a tyrosine nitration under prolonged light stress within mouse retina. To understand the

role NO plays in terms of concentration and tempo in PP2A tyrosine nitration process and AMD development, it is needed to quantify NO_2Tyr levels, examine specific protein tyrosine sites and investigate the relationships between those quantitative data and the NO levels and duration in the retina.

There are different assays which can be used to either qualitatively and/or quantitatively analyze NO_2Tyr. NO_2Tyr monoclonal antibodies are able to recognize NO_2Tyr residues within proteins with high specificity, where NO_2Tyr signal quantity is directly used to represent the change of the activity of the enzyme under investigation. However, the quality of those assays is highly dependent on antibody quantity. The related assays which we are able to perform based on antibody techniques include Western blotting, ELISA (Enzyme-linked immuno sorbent assay), even immunohistochemical assay etc (reviewed in [241]). Their limitation is that they reveal neither site specific information nor achieve absolute quantification.

According to the protocol from Crow et al. [235] with minor modification, phenyl-derivatized reverse phase column with a mobile phase of 80% 50 mM ammonium formate buffer, pH=3.5 and 20% acetonitrile was used to determine nitrotyrosine content in a Perkin Elmer Series 200 HPLC-UV/Vis system. The phenol ring of both tyrosine and nitrotyrosine contains an absorbance peak at 274 nm, however nitrotyrosine displays another peak at 359 nm. The products are detected by Perkin Elmer Series 200EP diode array detector.

In preliminary experiments, a mixture of tyrosine and 3-nitrotyrosine solution was injected to HPLC for method validation. As controls, tyrosine and nitrotyrosine standards were applied to HPLC and they were clearly distinguished according to the retention time (Fig. B.1 A upper panel, where t_R for Tyr was shown to be 3.5 min and t_R for nitrotyrosine 7.6 min). By using the area under the peak, a calibration curve was established and the detection limit was found to be 0.1-0.2 μM in the specified system (Fig. B.1 B). To validate the nitration system, $ONOO^-$ was used to nitrate whole cell protein, where whole cell protein was extracted by using RIPA lysis buffer, hoping to obtain the nitration products. $ONOO^-$ stock solution was added into the protein samples directly, making the final $ONOO^-$ concentration of 1mM. Then the nitrated protein was applied to 6 M concentrated HCl for total hydrolyzation, at 110 °C for 16 h [235]. The ultimate products were redissolved in phosphate buffer and injected to the HPLC. Both 274 nm and 359 nm were used for signal test. Fig. B.1 A lower panel shows the chromatography result of HPLC UV/Vis. In both standard and real reaction system, nitrotyrosine peak was shown in $t_R = 7.6$ min.

To quantitatively understand the reaction between NO and tyrosine, the reaction between tyrosine and NO was investigated. The reaction between tyrosine and peroxynitrite $ONOO^-$ [184] was used as the positive control. The reaction system was 100 μM tyrosine in 0.1 M sodium phosphate buffer (pH 7.0, containing 0.1 mM DTPA) with different final concentrations of $ONOO^-$ (0.05-3.0 mM); the reaction time was set as 2 min [184]. $ONOO^-$ preparation and quantification were completed according

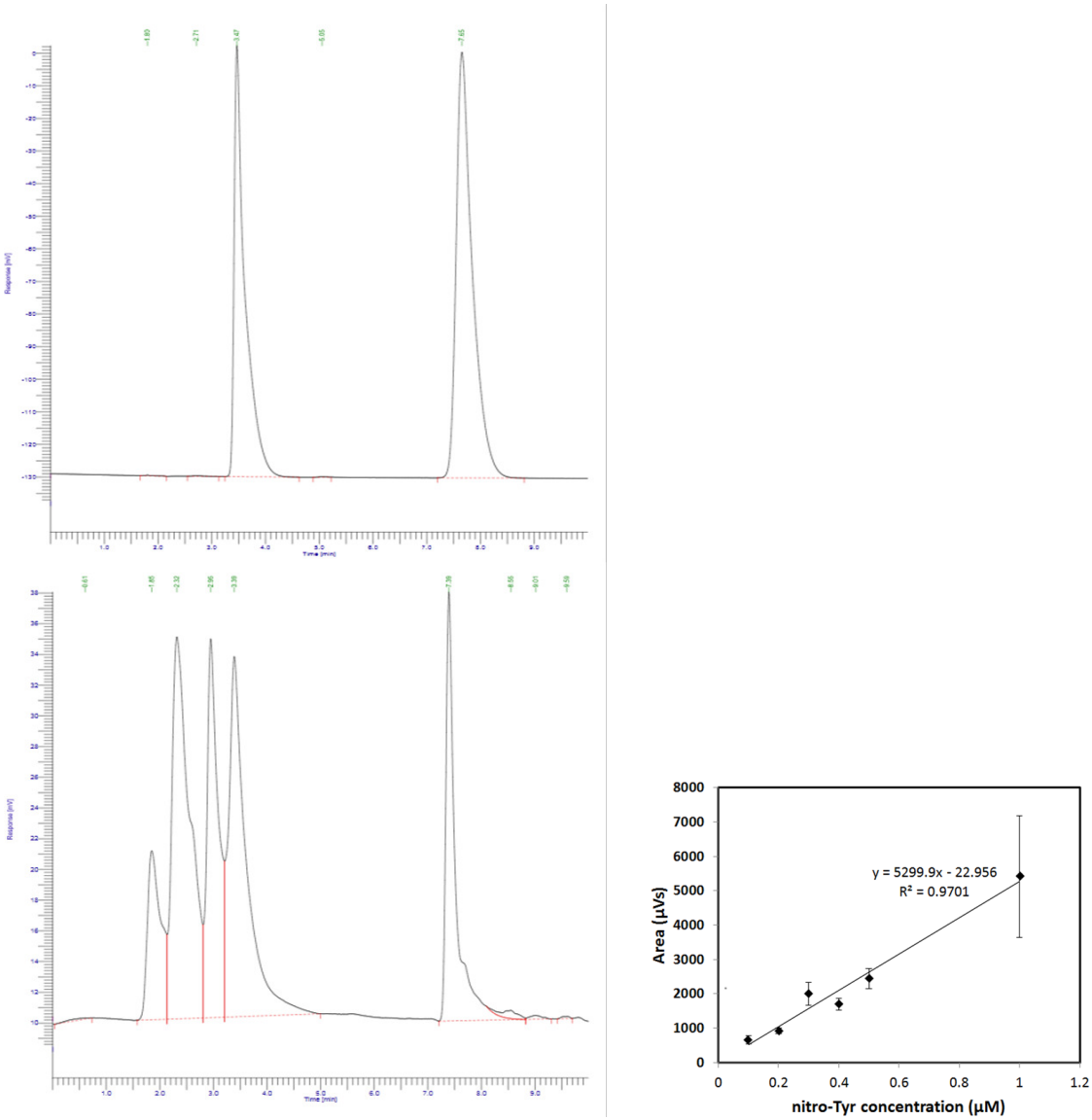

(A) (B)

Figure B.1: Identifying nitro-tyrosine by using HPLC. (A) The upper panel shows the standards of tyrosine and nitro-tyrosine, and the lower panel represents result from HCl hydrolyzed nitrated proteins; (B) relationship of the nitro-tyrosine standard and the signal strength.

to Reed et al. [236]. The HPLC successfully separated 3-nitrotyrosine from the reaction system and data illustrated that the increase of $ONOO^-$ concentration resulted in the increase of product nitrotyrosine shown in Fig. B.2 with a regression line of

$y = 10.417x - 91.37$ and $R^2 = 0.9717$ (note that the overall trend of this plot is quite similar to the published data by Sawa et al. [184]).

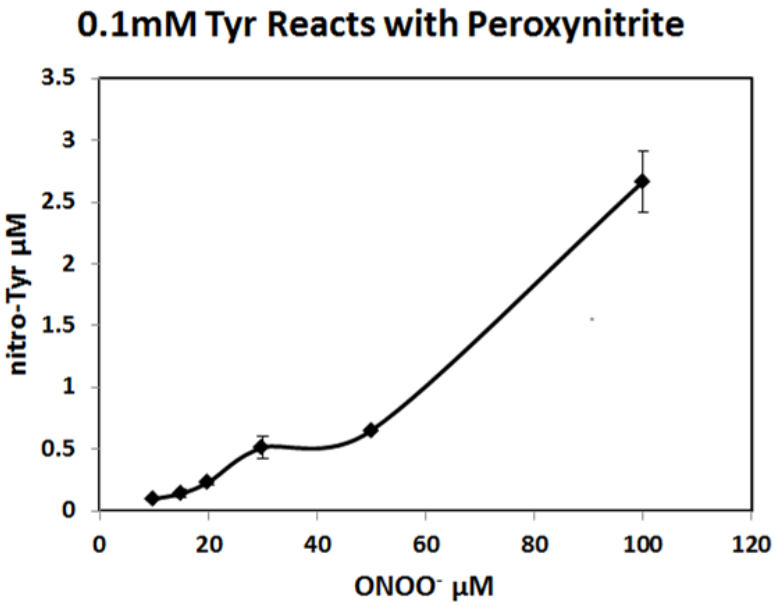

Figure B.2: The reaction of $ONOO^-$ and tyrosine examined by HPLC system. Error bar stands for standard errors.

The tyrosine reaction with NO and superoxide was carried out using a SNAP-PDMS-HX-XO system. Tyrosine solution (0.1 mM) with superoxide generator HX-XO was applied to SNAP-PDMS with strong light, where Tyr is expected to be converted to 3-nitrotyrosine [184]. However, by using this system, no 3-nitrotyrosine signal was observed even when the very high concentration of all reactants were used (2 mM HX and 50 mU/ml OX). This might be because that the yield of nitrotyrosine through the reaction of Tyr with NO and superoxide is too low so that the product concentration is even smaller than the detection limit of the HPLC system used in this study(1-2

μM for our system and less than 200 nM for Sawa et al.'s set-up [184]).

B.2 Tyrosine residue nitration detection by MS

Some HPLC systems with more sensitive UV detectors have very good limit of detection, which are very useful for 3-nitrotyrosine chemistry study. But since the chromatography provides indirect evidences, only according to the correct retention time and comparison with standards, there might be large false signals from complex biological samples. Other researchers managed to use LC-MS/MS of better LOD and LOQ to measure NO_2Tyr level of plasma or other tissue source. Hui et al. [238] reported very inspiring results with plasma NO_2Tyr level from patients receiving on-pump coronary artery bypass grafting surgery by using Varian 1200L LC-MS/MS system (Agilent Technologies). The claimed LOD, LOQ, and LLOQ (low limit of quantification, a concentration at which the analyte peak is identifiable, discrete, and reproducible with a precision of 20% and accuracy of 80120%) are 0.034 nM, 0.112 nM, and 0.625 nM, respectively. And their result was 1.494 $\pm$ 0.1065 and 2.167 $\pm$ 0.1770 nM for before and after the surgery. An MS method was also used to identify site-specific nitrotyrosine.

Two interesting questions that can be addressed by MS are how much tyrosine will be nitrated at different specific NO levels and whether there are specific NO sensitive

tyrosine sites that are prone to be nitrated, which makes nitration a specific process (important for cell signaling). The following MALDI-TOF work is to target the second question.

Jiao et al. studied the site specific effect of peroxynitrite to human serum albumin by using HPLC and CID (collision-induced decomposition), showing that though total of 18 tyrosine residues are present in the entire HAS (human albumin serum) molecule, only 2 nitro-tyrosine sites were detected. They were Y411 (in YTK fragment, $[M + H^+]^+$=411.0 m/z) and Y140 (the second Y in YLYEIAR fragment, $[M + H^+]^+$=927.5 m/z). To examine whether NO's nitration is also site-specific, bovine serum albumin (BSA) was selected as the standard and control. Albumin nitration by $ONOO^-$ was carried out according to Jiao et al. [237]. 0.3 mM albumin in 150 mM potassium phosphate/ 25 mM sodium bicarbonate buffer at pH 7.2 reacts with 1 μM $ONOO^-$. The product was then collected and applied to dialysis for 24 h (molecular wright cut-off 12,000 Da). The NO releasing polymer SNAP-PDMS with HX-XO (NO flux was up to 15×10^{-10} mol/cm^2/min, the concentration of HX was 1 mM, and 20mU/ml XO was used [184].) was used to nitrate BSA to mimic the nitration of proteins in vivo in the inflammation site. Then the product proteins were dialyzed and subject to trypsin for complete digestion in a 40:1 ratio (wt/wt) for 5 h at 37 °C [237]. Matrix alpha-Cyano-4-hydroxycinnamic acid (CHCA) was used and samples were loaded with overlayer preparation method to MALDI-TOF sample plate.

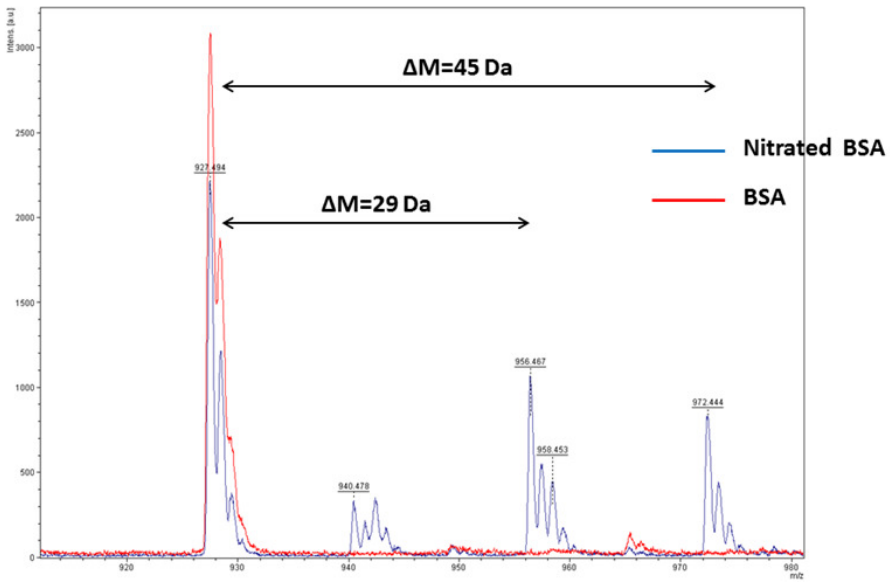

Figure B.3: MALDI-TOF of trypsonized nitrated BSA.

From the MALDI-TOF data, one nitro-tyrosine residue site in YLYEIAR was clearly observed, $[M + H^+]^+$=972.5 m/z. Data also shows its fragmentation at 956.5 m/z, where one oxygen atom was missing(Fig. B.3). Other nitrated fragments were not detected, indicating that nitration of tyrosine was indeed site-specific. However, no nitrotyrosine containing fragment was found in BSA treated by SNAP-PDMS/HX-OX, indicating tyrosine nitration may not be easy to occur and the yield was low.

Post-transcription modification of PP2A-a is crucial for its normal function. Since it has been approved that NO is associated with RPE cell death [239, 240], understanding how NO level and duration will regulate the apoptotic pathways will help us protect RPE from damaging and retina from degeneration. Future direction

can be using more sensitive detection methods to identify and quantitate the post-translation modification. Or considering the low amount of nitrotyrosine, examining the reversible nitrosation of those molecules is more biological relevant.

Appendix C

Letters of Permission

This part shows the permission that I obtained from the publishers showing I have the right to use the related materials.

This letter shows I have the right to use the related materials for Fig. 2.6

SPRINGER LICENSE
TERMS AND CONDITIONS

Oct 18, 2015

This is a License Agreement between Weilue He ("You") and Springer ("Springer") provided by Copyright Clearance Center ("CCC"). The license consists of your order details, the terms and conditions provided by Springer, and the payment terms and conditions.

All payments must be made in full to CCC. For payment instructions, please see information listed at the bottom of this form.

License Number	3731700621410
License date	Oct 17, 2015
Licensed content publisher	Springer
Licensed content publication	Naunyn-Schmiedeberg's Archives of Pharmacology
Licensed content title	Release of nitric oxide from donors with known half-life: a mathematical model for calculating nitric oxide concentrations in aerobic solutions
Licensed content author	K. Schmidt
Licensed content date	Jan 1, 1997
Volume number	355
Issue number	4
Type of Use	Thesis/Dissertation
Portion	Figures/tables/illustrations
Number of figures/tables/illustrations	1
Author of this Springer article	No
Order reference number	None
Original figure numbers	Figure 1
Title of your thesis / dissertation	Systematic Study of the Biological Effects of Nitric Oxide using Innovative NO Measurement and Delivery Systems
Expected completion date	Nov 2015
Estimated size(pages)	260
Total	0.00 USD
Terms and Conditions	

Introduction
The publisher for this copyrighted material is Springer Science + Business Media. By clicking "accept" in connection with completing this licensing transaction, you agree that the following terms and conditions apply to this transaction (along with the Billing and Payment terms and conditions established by Copyright Clearance Center, Inc. ("CCC"), at the time that you opened your Rightslink account and that are available at any time at http://myaccount.copyright.com).

Limited License

With reference to your request to reprint in your thesis material on which Springer Science and Business Media control the copyright, permission is granted, free of charge, for the use indicated in your enquiry.

Licenses are for one-time use only with a maximum distribution equal to the number that you identified in the licensing process.

This License includes use in an electronic form, provided its password protected or on the university's intranet or repository, including UMI (according to the definition at the Sherpa website: http://www.sherpa.ac.uk/romeo/). For any other electronic use, please contact Springer at (permissions.dordrecht@springer.com or permissions.heidelberg@springer.com).

The material can only be used for the purpose of defending your thesis limited to university-use only. If the thesis is going to be published, permission needs to be re-obtained (selecting "book/textbook" as the type of use).

Although Springer holds copyright to the material and is entitled to negotiate on rights, this license is only valid, subject to a courtesy information to the author (address is given with the article/chapter) and provided it concerns original material which does not carry references to other sources (if material in question appears with credit to another source, authorization from that source is required as well).

Permission free of charge on this occasion does not prejudice any rights we might have to charge for reproduction of our copyrighted material in the future.

Altering/Modifying Material: Not Permitted

You may not alter or modify the material in any manner. Abbreviations, additions, deletions and/or any other alterations shall be made only with prior written authorization of the author(s) and/or Springer Science + Business Media. (Please contact Springer at (permissions.dordrecht@springer.com or permissions.heidelberg@springer.com)

Reservation of Rights

Springer Science + Business Media reserves all rights not specifically granted in the combination of (i) the license details provided by you and accepted in the course of this licensing transaction, (ii) these terms and conditions and (iii) CCC's Billing and Payment terms and conditions.

Copyright Notice:Disclaimer

You must include the following copyright and permission notice in connection with any reproduction of the licensed material: "Springer and the original publisher /journal title, volume, year of publication, page, chapter/article title, name(s) of author(s), figure number(s), original copyright notice) is given to the publication in which the material was originally published, by adding; with kind permission from Springer Science and Business Media"

Warranties: None

Example 1: Springer Science + Business Media makes no representations or warranties with respect to the licensed material.

Example 2: Springer Science + Business Media makes no representations or warranties with respect to the licensed material and adopts on its own behalf the limitations and disclaimers established by CCC on its behalf in its Billing and Payment terms and conditions for this licensing transaction.

Indemnity

You hereby indemnify and agree to hold harmless Springer Science + Business Media and CCC, and their respective officers, directors, employees and agents, from and against any and all claims arising out of your use of the licensed material other than as specifically authorized pursuant to this license.

No Transfer of License
This license is personal to you and may not be sublicensed, assigned, or transferred by you to any other person without Springer Science + Business Media's written permission.
No Amendment Except in Writing
This license may not be amended except in a writing signed by both parties (or, in the case of Springer Science + Business Media, by CCC on Springer Science + Business Media's behalf).
Objection to Contrary Terms
Springer Science + Business Media hereby objects to any terms contained in any purchase order, acknowledgment, check endorsement or other writing prepared by you, which terms are inconsistent with these terms and conditions or CCC's Billing and Payment terms and conditions. These terms and conditions, together with CCC's Billing and Payment terms and conditions (which are incorporated herein), comprise the entire agreement between you and Springer Science + Business Media (and CCC) concerning this licensing transaction. In the event of any conflict between your obligations established by these terms and conditions and those established by CCC's Billing and Payment terms and conditions, these terms and conditions shall control.
Jurisdiction
All disputes that may arise in connection with this present License, or the breach thereof, shall be settled exclusively by arbitration, to be held in The Netherlands, in accordance with Dutch law, and to be conducted under the Rules of the 'Netherlands Arbitrage Instituut' (Netherlands Institute of Arbitration).***OR:***
All disputes that may arise in connection with this present License, or the breach thereof, shall be settled exclusively by arbitration, to be held in the Federal Republic of Germany, in accordance with German law.
Other terms and conditions:
v1.3

Questions? customercare@copyright.com or +1-855-239-3415 (toll free in the US) or +1-978-646-2777.

This letter shows I have the right to use the related materials for Fig. 2.9

Copyright Clearance Center

Confirmation Number: 11469577
Order Date: 10/18/2015

Customer Information

Customer: Weilue He
Account Number: 3000966712
Organization: Weilue He
Email: weilueh@mtu.edu
Phone: +1 (906)2312979
Payment Method: Invoice

This is not an invoice

Order Details

Science and Technology of Advanced Materials

Billing Status: **N/A**

Order detail ID: 68683146
ISSN: 1468-6996
Publication Type: Journal
Volume:
Issue:
Start page:
Publisher: IOP Publishing

Permission Status: **Granted**
Permission type: Republish or display content
Type of use: Thesis/Dissertation
Order License Id: 3731710988503

Requestor type	Academic institution
Format	Print, Electronic
Portion	chart/graph/table/figure
Number of charts/graphs/tables/figures	2
Title or numeric reference of the portion(s)	Figure 1 and Figure 3
Title of the article or chapter the portion is from	S-Nitroso-N-acetyl-D-penicillamine covalently linked to polydimethylsiloxane (SNAPâPDMS) for use as a controlled photoinitiated nitric oxide release polymer
Editor of portion(s)	N/A
Author of portion(s)	N/A
Volume of serial or monograph	N/A
Page range of portion	2
Publication date of portion	23 September 2011
Rights for	Main product
Duration of use	Life of current edition
Creation of copies for the disabled	no
With minor editing privileges	yes
For distribution to	Worldwide
In the following language(s)	Original language of publication

With incidental promotional use	no
Lifetime unit quantity of new product	Up to 499
Made available in the following markets	education and professional
The requesting person/organization	Weilue He, Michigan Technological University
Order reference number	
Author/Editor	Weilue He
The standard identifier	N/A
Title	Systematic Study of the Biological Effects of Nitric Oxide using Innovative NO Measurement and Delivery Systems
Publisher	N/A
Expected publication date	May 2016
Estimated size (pages)	260

Note: This item was invoiced separately through our **RightsLink service.** More info **$ 0.00**

Total order items: 1 **Order Total: $0.00**